

USE OF DISTINCT ELEMENT METHOD IN THE ASSESSMENT OF  
EARTHQUAKE BEHAVIOR OF MASONRY STRUCTURES

by

Özden Saygılı

B.S., Civil Engineering, Yıldız Technical University, 2008

M.S., IT Based Construction Management, Istanbul Technical University, 2009

Submitted to the Institute for Graduate Studies in  
Science and Engineering in partial fulfillment of  
the requirements for the degree of  
Doctor of Philosophy

Graduate Program in Earthquake Engineering  
Boğaziçi University

2014

## ACKNOWLEDGEMENTS

The present work was developed with the support and assistance of many people. I would like to thank all those who have contributed to this research work. First of all, my sincere thanks go to my supervisor Prof. Eser Çaktı for her continuous guidance and support at each step of this study. A great acknowledgment is due to Dr. José Antero Senra Vieira de Lemos and Prof. Carlos Sousa Oliveira for their precious collaboration and suggestions in numerical investigations for improving the quality of work. This work has benefited from their valuable reviews and comments.

I also appreciate the support provided by ITASCA for the access to 3DEC®. A special thanks is extended to Dr. Maria Luísa Braga Farinha and her great family for their friendship and help during my research visit to Lisbon. I am grateful to Dr. Sérgio Bruno Martins de Oliveira for his help in MATLAB programming.

I am grateful to the staff of the Shake Table Laboratory of the Department of Earthquake Engineering of Kandilli Observatory and Earthquake Research Institute of Boğaziçi University and the Materials Laboratory of the Department of Civil Engineering of Boğaziçi University. I want to acknowledge Prof. Mustafa Erdik for providing the base isolators. I wish to offer my thanks to the Mr. Talat Sivrioğlu, BASF Yapı Kimyasalları San. A.Ş., for providing the FRPs used in strengthening of the model and Mr. Eren Kalafat and Mr. Korhan Oral for the construction of the model.

Additionally, I am pleased to acknowledge Prof. Lidija Krstevska and Prof. Ljubomir Tashkov of University of Ss. Cyril and Methodius, Skopje, for their guidance and discussion during the construction of scaled model. I would like to thank Ms. Esra Zengin for providing stochastically simulated ground motion time histories and Mr. Serkan Görk for his assistance with the ultrasonic tests in the minaret of the Mihrimah Sultan Mosque.

Last but not least I would like to thank my family for their love and support during my Ph.D. studies.

## **ABSTRACT**

### **USE OF DISTINCT ELEMENT METHOD IN THE ASSESSMENT OF EARTHQUAKE BEHAVIOR OF MASONRY STRUCTURES**

There are a number of masonry structures in Istanbul and in other cities of Turkey that suffered severe damage from earthquakes. As they will continue to get affected by the earthquakes, more research is needed to assess their seismic dynamic behavior particularly in the states of large deformations/damage and collapse. This still remains as a challenge in spite of significant developments in understanding factors affecting the seismic resistance of masonry structures. The present thesis deals with non-linear dynamic analysis of masonry structures modelled through distinct element methodology. First, a masonry mosque has been built at 1:10 reduced scale and tested by subjecting it to a sequence of earthquake excitations on the shake table in three phases: test of the base-isolated model, of the model as it is and that of the strengthened model. The results of these three phases were used in the calibration/validation of the numerical model developed by distinct element approach. It has been concluded that the methodology and the elements developed in this stage are good enough to be employed in the investigation of real masonry structures. In the second stage, three masonry minarets in Istanbul were studied under sine waves (velocity amplitude range: 10 cm/s – 100 cm/s; frequency range: 0.1 Hz – 13 Hz) and under real and simulated earthquake ground motion. The deformation levels and patterns induced in the minarets and the energy balance in the system are investigated to analyze the damage processes.

## ÖZET

### YIĞMA YAPILARIN YAPISAL DAVRANIŞININ İNCELENMESİNDE AYRIK ELEMENLAR METODUNUN KULLANILMASI

İstanbul’ da ve Türkiye’ nin birçok yerinde depremlerden önemli oranda etkilenmiş çok sayıda yığma yapı bulunmaktadır. Yığma yapıların deprem davranışlarının incelenmesi, özellikle hasar, kalıcı deformasyon ve göçme durumlarının ayrıntılı olarak anlaşılması için daha fazla araştırmaya ihtiyaç vardır. Her ne kadar, bu tip yapıların deprem dayanımını anlamaya yönelik önemli gelişmeler kaydedilse de, yüksek deformasyon ve göçme seviyelerindeki davranış özellikleri üzerine yapılan araştırmalar yeterli değildir. Bu tez çalışması, ayrik elemanlar yöntemi ile modellenmiş yığma yapıların doğrusal olmayan dinamik analizi ile ilgilidir. Öncelikle, 1:10 ölçeğinde yığma bir cami modeli inşa edilmiş ve model üç aşamalı bir program kapsamında, sarsma masası üzerinde test edilmiştir: sismik izolatör uygulaması yapılmış modelin testleri, modelin kendisinin test edilmesi ve güçlendirilmiş modelin testleri.. Bu üç aşamanın sonuçları ayrik elemanlar yöntemi ile oluşturulan nümerik modellerin kalibrasyonunda kullanılmıştır. Ayrik elemanlar yöntemi ile oluşturulan ve üç farklı durum için doğrulanan nümerik modellerin gerçek yığma yapıların incelenmesi için yeterince iyi olduğu sonucuna varılmıştır. İkinci aşamada, İstanbul'daki üç adet yığma minarenin dinamik davranışları sinüs dalgaları (hız genlik aralığı: 10 cm/s – 100 cm/s; frekans aralığı: 0.1 Hz – 13 Hz) ile gerçek ve simüle edilmiş deprem hareketleri altında incelenmiştir. Yapısal hasar oluşumlarının analizi için minarelerde oluşan deformasyonlar, ve yapısal sistemdeki enerji dengesi incelenmiştir.

## TABLE OF CONTENTS

ACKNOWLEDGEMENTS.....	ii
ABSTRACT.....	iii
ÖZET.....	iv
TABLE OF CONTENTS.....	v
LIST OF FIGURES.....	ix
LIST OF TABLES.....	xxvi
LIST OF SYMBOLS /ABBREVIATIONS.....	xxviii
1. INTRODUCTION.....	1
1.1. Aim and Objectives of the Research.....	1
1.2. Outline of Thesis.....	2
2. METHODS USED IN EARTHQUAKE PERFORMANCE ASSESSMENT OF MASONRY STRUCTURES.....	3
2.1. Mechanical Characteristics of Masonry Structures.....	3
2.1.1. Mortar.....	3
2.1.2. Brick.....	4
2.1.3. Stone.....	5
2.1.4. Bond.....	6
2.2. Damages and Failure Mechanisms of Masonry Structures.....	7
2.3. Mechanical Tests.....	10
2.3.1. Destructive Testing Methods.....	10
2.3.2. Minor Destructive Testing Methods.....	11
2.3.3. Non Destructive Testing Methods.....	12
2.4. Shaking Table and Pseudo Dynamic Tests.....	105
2.4.1. Quasi-static Tests.....	15
2.4.2. Pseudo Dynamic Tests.....	16

2.4.3. Shaking Table Tests.....	19
2.5. Strengthening Methods in Masonry Structures.....	20
2.6. Physical Modeling.....	23
2.6.1. Dimensional Analysis.....	24
2.6.2. Similitude Theory.....	24
2.6.3. Geometric Similarity.....	24
2.6.4. Kinematic Similarity.....	25
2.6.5. Dynamic Similarity.....	25
2.7. Analytical (Numerical) Modeling.....	29
2.7.1. Fundamentals of Analytical Modeling.....	29
2.7.2. Idealization of the Geometry and Material.....	29
2.7.2.1. Idealization of the Geometry.....	31
2.7.2.2. Detailed Micro Modeling.....	32
2.7.2.3. Simplified Micro Modeling.....	33
2.7.2.4. Macro Modeling.....	33
2.7.3. Idealization of the Behavior.....	35
2.7.3.1. Elastic (Linear) Behavior.....	35
2.7.3.2. Plastic Behavior.....	35
2.7.3.3. Inelastic (Non-linear) Behavior.....	35
2.8. Analysis.....	36
2.8.1. Structural Analysis Methods.....	36
2.8.1.1. Linear Analysis.....	36
2.8.1.2. Nonlinear Analysis.....	37
2.8.1.3. Limit Analysis.....	38
3. MODELING MUSTAFA PAŞA MOSQUE IN SKOPJE.....	40
3.1. Introduction.....	40
3.2. Development of Test Structure.....	42

3.2.1. Construction of the Shake Table Model.....	42
3.2.2. Material Testing.....	45
3.2.2.1. Mortar Test.....	46
3.2.2.2. Compression Tests.....	48
3.2.2.3. Diagonal Tension (Shear) Tests.....	49
3.3. Shake Table Testing.....	51
3.3.1. Description of the DEE-KOERI Shake Table.....	51
3.3.2. Instrumentation of the Model.....	52
3.3.3. Preparation of Input Motion.....	56
3.3.4. Testing Program and Results.....	57
3.4. Development of the Distinct Element Model.....	66
3.4.1. Modeling Assumptions and Contacts.....	67
3.5. Numerical Investigation of the Distinct Element Model with Base Isolation and Comparison with Experimental Data.....	74
3.6. Numerical Investigation of the Distinct Element Model and Comparison with Experimental Data.....	84
3.6.1. Analytical Model Predictions and Comparison with Experimental Results.....	85
3.7. Numerical Investigation of the Distinct Element Model with FRP Strengthening and Comparison with Experimental Data.....	107
3.7.1. Analytical Model Predictions and Comparison with Experimental Results.....	108
3.8. Discussion and Conclusions.....	115
4. BEHAVIOR ANALYSIS OF MASONRY MINARETS.....	116
4.1. Introduction.....	116
4.1.1. Previous Studies.....	117
4.2. General Description of Minarets Selected for Analysis.....	118
4.2.1. The Minaret of the Mihrimah Sultan Mosque.....	118

4.2.2. The Minaret of the Hagia Sophia Museum.....	120
4.2.3. The Minaret of the Süleymaniye Mosque.....	120
4.3. Ultrasonic Testing of the Mihrimah Minaret.....	121
4.4. Analytical Modeling and Assumptions.....	124
4.5. Comparative Analyses Using Sine Waves.....	127
4.5.1. Patterns of Deformation and Collapse.....	131
4.5.2. Assessment of Absolute Top and Relative Drum Deformations.....	134
4.5.3. Energy Parameters.....	142
4.6. Employment of Real Earthquakes and Broadband Simulations in the Assessment of Minaret Models.....	154
4.6.1. Assessment of Earthquake Behavior.....	155
4.6.2. Assessment of Collapse Mechanisms.....	163
4.7. Conclusion and Discussions.....	168
5. CONCLUSIONS.....	170
REFERENCES.....	174

## LIST OF FIGURES

Figure 2.1.	Masonry failure modes.....	9
Figure 2.2.	Images of shear, sliding and rocking failures.....	9
Figure 2.3.	An experimental study method for investigating masonry structure.	28
Figure 2.4.	(a) Detailed micro modeling; (b) Simplified micro modeling; (c) Macro modeling (Lourenço, 1996).....	31
Figure 2.5.	Coulomb slip model with residual strength (shear and normal behavior) ( Al-Heib, 2012).....	32
Figure 3.1.	Image of Mustafa Paşa Mosque in Skopje, Macedonia (Tashkov <i>et al.</i> , 2012).....	40
Figure 3.2.	Images of 1:10 scale model of the Mustafa Paşa Mosque during its construction (a,b,c,d).....	43
Figure 3.3.	Images of 1:10 scale model of the Mustafa Paşa Mosque during its transfer on to the shake table.....	44
Figure 3.4.	Test set up for mortar testing (a, b), the control software (c) and the mortar specimen in failure (d) at the Materials Laboratory of Department of Civil Engineering, Boğaziçi University.....	47
Figure 3.5.	Compression (a, b) and shear test setup (c), and failure mode of a specimen during shear test (d). Images taken during testing at the Materials Laboratory of Department of Civil Engineering of Boğaziçi University.....	50

Figure 3.6.	Image of shake table at the Department of Earthquake Engineering of Kandilli Observatory and Earthquake Research Institute of Boğaziçi University.....	52
Figure 3.7.	Accelerometer installation and displacement transducer set up (1)...	53
Figure 3.8.	Accelerometer installation and displacement transducer set up (2)...	54
Figure 3.9.	Accelerometer installation and displacement transducer set up (3)...	55
Figure 3.10.	Supporting the test structure with four isolators.....	58
Figure 3.11.	Time domain shake table output observed during stage one (base-isolated model). Left: 50 % Montenegro Earthquake. Right: 100 % Montenegro Earthquake.....	59
Figure 3.12.	Time domain shake table output observed during stage two (model as it is). Left: 10 % Montenegro Earthquake. Right: 250 % Montenegro Earthquake.....	60
Figure 3.13.	Image of the first crack in the minaret right after 155 % Montenegro input.....	61
Figure 3.14.	Displacement time histories observed during stage two (model as it is). Top: 10 % Montenegro Earthquake. Bottom: 250 % Montenegro Earthquake.....	61
Figure 3.15.	Damage to the drum, walls and dome.....	62
Figure 3.16.	Damage to the experimental model, details from the windows and the dome base.....	63
Figure 3.17.	Images from FRP application (upper two images) and the strengthened model.....	64

Figure 3.18.	Time domain shake table output observed during stage three (strengthened model.) left: 20 % Montenegro Earthquake, right: 250 % Montenegro Earthquake.....	65
Figure 3.19.	Damage to the strengthened model, details from the windows and the dome base.....	65
Figure 3. 20.	Numerical model developed using 3DEC.....	66
Figure 3.21.	Interface model (Idris <i>et al.</i> , 2009).....	70
Figure 3.22.	Elasto-plastic Mohr-Coulomb joint model (Itasca, 2000).....	71
Figure 3. 23.	Variation of normalized critical damping ratio with angular frequency (Itasca, 2013).....	73
Figure 3.24.	Numerical model with elements representing isolators.....	75
Figure 3.25.	Velocity time history comparisons between isolated experimental and numerical model under 50 % Montenegro Earthquake. The input to the numerical model is applied under the four isolators. Comparisons are provided at four locations: at the isolation level and at the three corners of the foundation.....	77
Figure 3.26.	FAS comparisons between isolated experimental and numerical model under 50 % Montenegro Earthquake. The input to the numerical model is applied under the four isolators. Comparisons are provided at four locations: at the isolation level and at the three corners of the foundation.....	78

- Figure 3.27. Velocity time history comparisons between isolated experimental and numerical model under 70 % Montenegro Earthquake. The input to the numerical model is applied under the four isolators. Comparisons are provided at four locations: at the isolation level and at the three corners of the foundation..... 79
- Figure 3.28. FAS comparisons between isolated experimental and numerical model under 70 % Montenegro Earthquake. The input to the numerical model is applied under the four isolators. Comparisons are provided at four locations: at the isolation level and at the three corners of the foundation..... 80
- Figure 3.29. Velocity time history comparisons between isolated experimental and numerical model under 100 % Montenegro Earthquake. The input to the numerical model is applied under the four isolators. Comparisons are provided at four locations: at the isolation level and at the three corners of the foundation..... 81
- Figure 3.30. FAS comparisons between isolated experimental and numerical model under 100 % Montenegro Earthquake. The input to the numerical model is applied under the four isolators. Comparisons are provided at four locations: at the isolation level and at the three corners of the foundation..... 82

Figure 3.31.	The variation of peak experimental and analytical velocities at the instrument 1. Refer to Figure 3.34 for the instrumentation on the foundation of the shake table model and corresponding point on the numerical model. Top x axis of the figure displays the peak velocities equaled to % earthquake loading.....	83
Figure 3.32.	The variation of peak experimental and analytical FAS with respect to the change in the amplitude of input motion.....	83
Figure 3.33.	Measurement locations on the minaret of the shake table model and corresponding points on the numerical model.....	86
Figure 3.34.	Measurement locations on the body of the shake table model and corresponding points on the numerical model.....	86
Figure 3.35.	Comparisons of experimental and analytical velocities along the minaret under 100 % Montenegro Earthquake loading. 1, 2, 3, 4, 5 indicate the measurement locations. Refer to Figure 3.33 for the measurement locations on the minaret and corresponding points on the numerical model.....	87
Figure 3.36.	Comparisons of experimental and numerical FAS amplitude along the minaret under 10 % Montenegro Earthquake loading. 1, 2, 3, 4, 5 indicate the measurement locations. Refer to Figure 3.33 for the measurement locations on the minaret and corresponding points on the numerical model.....	88

Figure 3.37.	Comparisons of experimental and analytical velocities along the minaret under 100 % Montenegro Earthquake loading. 1, 2, 3, 4, 5 indicate the measurement locations. Refer to Figure 3.33 for the measurement locations on the minaret and corresponding points on the numerical model.....	89
Figure 3.38.	Comparisons of experimental and numerical FAS amplitude along the minaret under 100 % Montenegro Earthquake loading. 1, 2, 3, 4, 5 indicate the measurement locations. Refer to Figure 3.33 for the measurement locations on the minaret and corresponding points on the numerical model.....	90
Figure 3.39.	Comparisons of experimental and analytical velocities along the minaret under 250 % Montenegro Earthquake loading. 1, 2, 3, 4, 5 indicate the measurement locations. Refer to Figure 3.33 for the measurement locations on the minaret and corresponding points on the numerical model.....	91
Figure 3.40.	Comparisons of experimental and numerical FAS amplitude along the minaret under 250 % Montenegro Earthquake loading. 1, 2, 3, 4, 5 indicate the measurement locations. Refer to Figure 3.33 for the measurement locations on the minaret and corresponding points on the numerical model.....	92

Figure 3.41. Comparisons of experimental and analytical velocities on the body of mosque model under 10 % Montenegro Earthquake loading. 10, 9, 8, 7 and 6 indicate the locations of accelerometers on the top of the dome and 4 at the four top corners of the body respectively. Refer to Figure 3.34 for the on the body of the shake table model and corresponding points on the numerical model..... 93

Figure 3.42. Comparisons of experimental and numerical FAS amplitude on the body of mosque under 10 % Montenegro Earthquake loading. 10, 9, 8, 7 and 6 indicate the locations of accelerometers on the top of the dome and 4 at the four top corners of the body respectively. Refer to Figure 3.34 for the on the body of the shake table model and corresponding points on the numerical model..... 94

Figure 3.43. Comparisons of experimental and analytical velocities on the body of mosque model under 100 % Montenegro Earthquake loading. 10, 9, 8, 7 and 6 indicate the locations of accelerometers on the top of the dome and 4 at the four top corners of the body respectively. Refer to Figure 3.34 for the on the body of the shake table model and corresponding points on the numerical model..... 95

Figure 3. 44. Comparisons of experimental and numerical FAS amplitude on the body of mosque under 100 % Montenegro Earthquake loading. 10, 9, 8, 7 and 6 indicate the locations of accelerometers on the top of the dome and 4 at the four top corners of the body respectively. Refer to Figure 3.34 for the on the body of the shake table model and corresponding points on the numerical model..... 96

- Figure 3.45. Comparisons of experimental and analytical velocities on the body of mosque model under 250 % Montenegro Earthquake loading. 10, 9, 8, 7 and 6 indicate the locations of accelerometers on the top of the dome and 4 at the four top corners of the body respectively. Refer to Figure 3.34 for the on the body of the shake table model and corresponding points on the numerical model..... 97
- Figure 3.46. Comparisons of experimental and numerical FAS amplitude on the body of mosque under 250 % Montenegro Earthquake loading. 10, 9, 8, 7 and 6 indicate the locations of accelerometers on the top of the dome and 4 at the four top corners of the body respectively. Refer to Figure 3.34 for the on the body of the shake table model and corresponding points on the numerical model..... 98
- Figure 3.47. Comparison of numerical model and experimental results of test structure under 160 % Montenegro Earthquake..... 98
- Figure 3.48. Comparison of numerical shear displacement and shear stresses at the joints under 250 % Montenegro Earthquake with damages that took place on the experimental model under the same level input motion..... 99
- Figure 3.49. Experimental and numerical transfer function amplitude for levels of 2, 3, 4 and 5 respectively at 1.75 m, 2.45 m, 3.25 m and 3.90 m of minaret under 10 %, 30 % and 50 % earthquake loading..... 101
- Figure 3.50. Experimental and numerical transfer function amplitude for levels of 2, 3, 4 and 5 respectively at 1.75 m, 2.45 m, 3.25 m and 3.90 m of minaret under 70 %, 100 % and 130 % earthquake loading..... 102

Figure 3.51.	Experimental and numerical transfer function amplitude for levels of 2, 3, 4 and 5 respectively at 1.75 m, 2.45 m, 3.25 m and 3.90 m of minaret under 150 %, 160 % and 220 % earthquake loading.....	103
Figure 3.52.	Experimental and numerical transfer function amplitude for levels of 2, 3, 4 and 5 respectively at 1.75 m, 2.45 m, 3.25 m and 3.90 m of minaret under 250 % earthquake loading.....	104
Figure 3.53.	Time domain comparisons of experimental and numerical displacement under 10 %, 30 %, 50 %, 70 %, 100 %, 130 % and 150 % earthquake loading.....	105
Figure 3.54.	Time domain comparisons of experimental and numerical displacement under 160 %, 220 % and 250 % earthquake loading...	106
Figure 3.55.	Displacement vectors under 220 % (left), and 250 % (right) Montenegro Earthquake.....	106
Figure 3.56.	Images of experimental and analytical strengthened models.....	107
Figure 3.57.	FRP-strengthened experimental and numerical transfer function amplitude for levels of 2, 3, 4 and 5 respectively at 1.75 m, 2.45 m, 3.25 m and 3.90 m of minaret under 60 % and 160 % earthquake loading.....	109
Figure 3.58.	FRP-strengthened experimental and numerical transfer function amplitude for levels of 2, 3, 4 and 5 respectively at 1.75 m, 2.45 m, 3.25 m and 3.90 m of minaret under 190 % 210 % and 230 % earthquake loading.....	110

Figure 3.59.	FRP-strengthened experimental and numerical transfer function amplitude for levels of 2, 3, 4 and 5 respectively at 1.75 m, 2.45 m, 3.25 m and 3.90 m of minaret under 250 % and 325 % earthquake loading.....	111
Figure 3.60.	Transfer function amplitude of FRP-strengthened and un-strengthened models for levels of 2, 3, 4 and 5 respectively at 1.75 m, 2.45 m, 3.25 m and 3.90 m of minaret under 160 % earthquake loading.....	112
Figure 3.61.	Comparisons of experimental and numerical fundamental frequencies of un-strengthened (a) and FRP- strengthened (b) models under sequential loadings. Top x axes of the figures display the peak velocities corresponding % earthquake loading...	113
Figure 3.62.	Variation of experimental and numerical fundamental frequencies of un-strengthened and FRP- strengthened models under sequential loadings.....	114
Figure 4.1.	Minaret component description of a typical Ottoman minaret (Oliveira <i>et al.</i> , 2012).....	116
Figure 4.2.	Images of the Mihrimah Sultan Mosque (left), its minaret before its disassemblage (center), cross-section of the minaret (right).....	119
Figure 4.3.	Image of the Mihrimah Sultan Mosque with the minaret that collapsed in the 1894 earthquake. Image taken sometime between 1894 and 1907 (Gurlitt, 1999).....	119
Figure 4.4.	The Hagia Sophia Mosque (left), study case minaret (right).....	120
Figure 4.5.	View of the Süleymaniye Complex (Ediz and Ostwald, 2012).....	121

Figure 4.6.	Schematic views direct (right), semi-direct (center) and indirect (left) methods of ultrasonic measurements.....	122
Figure 4.7.	Summary of results of ultrasonic testing in the Mihrimah minaret. In the upper row velocity readings are shown. Lower row includes shear modulus G, Poisson's ratio and modulus of elasticity E estimated from the velocities (Çaktı <i>et al.</i> , 2014).....	123
Figure 4.8.	Model of the Mihrimah (a), Hagia Sophia (b) and Süleymaniye minarets (c), general view and cross-section.....	125
Figure 4.9.	The example of plot of the 1.20Hz sine-waves for the dynamic analysis of the Hagia Sophia.....	130
Figure 4.10.	Heavy damage patterns for the Mihrimah minaret during the combination of $f=7$ Hz & 60 cm/s (1), $f=6$ Hz & 70 cm/s (2), $f=4$ Hz & 90 cm/s (3) and collapse patterns during the combination of $f=9$ Hz & 60 cm/s (4), $f=4$ Hz & 70 cm/s (5), $f=5$ Hz & 80 cm/s (6), $f=0.9$ Hz & 90 cm/s (7), $f=9$ Hz & 90 cm/s (8), $f=0.5$ Hz & 100 cm/s (9) and $f=0.7$ Hz & 100 cm/s (10).....	132
Figure 4.11.	Damage patterns for the Hagia Sophia minaret during the combination of $f=3$ Hz & 60 cm/s (1), $f=3$ Hz & 70 cm/s (2), $f=3$ Hz & 80 cm/s (3), $f=3$ Hz & 90 cm/s (4), $f=8$ Hz & 90 cm/s (5), $f=13$ Hz & 90 cm/s (6), $f=2$ Hz & 100 cm/s (7), $f=4$ Hz & 100 cm/s (8), $f=6$ Hz & 100 cm/s (9) and $f=11$ Hz & 100 cm/s (10).....	133

Figure 4.12. Heavy damage patterns for the Süleymaniye minaret during the combination of  $f=8$  Hz & 70 cm/s (1),  $f=2$  Hz & 80 cm/s (2),  $f=6$  Hz & 80 cm/s (3) and collapse patterns during the combination of  $f=6$  Hz & 60 cm/s (4),  $f=7$ Hz & 90 cm/s (5),  $f=8$  Hz & 90 cm/s (6),  $f=2$  Hz & 100 cm/s (7),  $f=8$  Hz & 100 cm/s (8),  $f=4$  Hz & 100 cm/s (9) and  $f=0.95$  Hz & 100 cm/s (10)..... 133

Figure 4.13. Scatter plot of maximum normalized relative displacement versus normalized maximum top displacement in terms of amplitude for minaret of the Mihrimah (a), Hagia Sophia (b) and Süleymaniye (c). Note that for the minaret of Mihrimah at the collapse cases assumed as  $u_{top} = 1$  and  $u_d = 0.24$  and for the minaret of Süleymaniye at the collapse cases assumed as  $u_{top} = 0.6$  and  $u_d = 0.35$ ..... 136

Figure 4.14. Scatter plot of maximum normalized relative displacement versus normalized top displacement in terms of frequency for minaret of the Mihrimah (a), Hagia Sophia (b) and Süleymaniye (c) Refer to the Table 4.7 for the first dominant frequency of the minarets. Note that for the minaret of Mihrimah at the collapse cases assumed as  $u_{top} = 1$  and  $u_d = 0.24$  and for the minaret of Süleymaniye at the collapse cases assumed as  $u_{top} = 0.6$  and  $u_d = 0.35$ ..... 137

- Figure 4.15. Variation of maximum normalized relative displacement with sine wave amplitude for the case of Mihrimah (a), Hagia Sophia (b) and Süleymaniye (c). Refer to the Table 4.7 for the first dominant frequency of the minarets. Note that for the minaret of Mihrimah at the collapse cases assumed as  $u_{top} = 1$  and  $u_d = 0.24$  and for the minaret of Süleymaniye at the collapse cases assumed as  $u_{top} = 0.6$  and  $u_d = 0.35$ ..... 138
- Figure 4.16. Variation of maximum normalized relative displacement with frequency for the case of Mihrimah (a), Hagia Sophia (b) and Süleymaniye (c) minaret. Refer to the Table 4.7 for the first dominant frequency of the minarets. Note that for the minaret of Mihrimah at the collapse cases assumed as  $u_{top} = 1$  and  $u_d = 0.24$  and for the minaret of Süleymaniye at the collapse cases assumed as  $u_{top} = 0.6$  and  $u_d = 0.35$ ..... 139
- Figure 4.17. Variation of maximum normalized top displacement with sine wave amplitude for the case of Mihrimah (a), Hagia Sophia (b) and Süleymaniye (c) minaret. Refer to the Table 4.7 for the first dominant frequency of the minarets. Note that for the minaret of Mihrimah at the collapse cases assumed as  $u_{top} = 1$  and  $u_d = 0.24$  and for the minaret of Süleymaniye at the collapse cases assumed as  $u_{top} = 0.6$  and  $u_d = 0.35$ ..... 140

Figure 4.18.	Variation of maximum normalized top displacement with frequency for the case of Mihrimah (a), Hagia Sophia (b) and Süleymaniye (c) minaret. Refer to the Table 4.7 for the first dominant frequency of the minarets. Note that for the minaret of Mihrimah at the collapse cases assumed as $u_{top} = 1$ and $u_d = 0.24$ and for the minaret of Süleymaniye at the collapse cases assumed as $u_{top} = 0.6$ and $u_d = 0.35$ .....	141
Figure 4.19.	Total energy stored in compression and tension for the Mihrimah minaret under sine wave amplitude of 0.6 m/s. Note that the case with collapse, frequency of 9 Hz, is not included.....	146
Figure 4.20.	Total energy stored in shear and total released energy for the Mihrimah minaret under sine wave amplitude of 0.6 m/s. Note that the case with collapse, frequency of 9 Hz, is not included.....	147
Figure 4.21.	Total energy stored in compression and tension for the Hagia Sophia minaret under sine wave amplitude of 0.6 m/s.....	148
Figure 4.22.	Total energy stored in shear and total released energy for the Hagia Sophia minaret under sine wave amplitude of 0.6 m/s.....	149
Figure 4.23.	Total energy stored in compression and tension for the Süleymaniye minaret under sine wave amplitude of 0.6 m/s. Note that the case with collapse, frequency of 6 Hz, is not included.....	150
Figure 4.24.	Total energy stored in shear and total released energy for the Süleymaniye minaret under sine wave amplitude of 0.6 m/s. Note that the case with collapse, frequency of 6 Hz, is not included.....	151

Figure 4.25.	Total released energy of the (a) Mihrimah and (b) Hagia Sophia minarets. Note that for the Mihrimah minaret the cases with collapse are not included.....	152
Figure 4.26.	Total released energy of the Süleymaniye minaret. Note that the cases with collapse are not included.....	153
Figure 4.27.	Response spectra of simulated and recorded ground motions used in non-linear dynamic analyses (left: NS components, right: EW components). Note that EXSIM simulates the random component. Therefore three stochastic simulations are shown in both plots (Çaktı <i>et al.</i> , 2013).....	154
Figure 4.28.	Response of the Mihrimah minaret under Yarımca record from the Kocaeli Earthquake, from left to right: residual block displacements, maximum joint shear displacements, maximum joint normal stresses and maximum joint normal displacements.....	158
Figure 4.29.	Response of the Hagia Sophia minaret under Yarımca record from the Kocaeli Earthquake, from left to right: residual block displacements, maximum joint shear displacements, maximum joint normal stresses and maximum joint normal displacements....	158
Figure 4.30.	Response of the Süleymaniye minaret under Yarımca record from the Kocaeli Earthquake, from left to right: residual block displacements, maximum joint shear displacements, maximum joint normal stresses and maximum joint normal displacements....	159

Figure 4.31.	Magnitude of displacement of the Mihrimah minaret at end of the record. (a): self-weight static analysis under gravitational loads, (b)-(f) Broadband simulations, (g)-(i)EXSIM simulations, (j):Fatih record, (k):Yarımca record.....	160
Figure 4.32.	Joint normal displacement vectors of the Mihrimah minaret at end of the record for the minaret of Mihrimah. (a): self-weight static analysis under gravitational loads, (b)-(f) Broadband simulations, (g)-(i) EXSIM simulations, (j):Fatih record, (k):Yarımca record....	160
Figure 4.33.	Magnitude of displacement of the Hagia Sophia minaret at end of the record. (a): self-weight static analysis under gravitational loads, (b)-(f) Broadband simulations, (g)-(i)EXSIM simulations, (j):Fatih record, (k):Yarımca record.....	161
Figure 4.34.	Joint normal displacement vectors of the Hagia Sophia minaret at end of the record. (a): self-weight static analysis under gravitational loads, (b)-(f) Broadband simulations, (g)-(i)EXSIM simulations, (j):Fatih record, (k):Yarımca record.....	161
Figure 4.35.	Magnitude of displacement of the Süleymaniye minaret at end of the record. (a): self-weight static analysis under gravitational loads, (b)-(f) Broadband simulations, (g)-(i)EXSIM simulations, (j):Fatih record, (k):Yarımca record.....	162
Figure 4.36.	Joint normal displacement vectors of the Süleymaniye minaret at end of the record. (a): self-weight static analysis under gravitational loads, (b)-(f) Broadband simulations, (g)-(i)EXSIM simulations, (j):Fatih record, (k):Yarımca record.....	162

Figure 4.37.	Collapse mechanisms of the Mihrimah minaret under eight scaled earthquake inputs.....	165
Figure 4.38.	Collapse mechanisms of the Hagia Sophia minaret under six scaled earthquake inputs.....	166
Figure 4.39.	Collapse mechanisms of the Süleymaniye minaret under six scaled earthquake inputs.....	167

## LIST OF TABLES

Table 2.1.	General properties of bricks (Ünay, 2002).....	5
Table 2.2.	General properties of stones (Ünay, 2002).....	6
Table 2.3.	Strengthening Methods in Masonry Structures.....	23
Table 2.4.	Summary of scale factors for reinforced masonry structural materials (Schriever, 1980).....	27
Table 2.5.	Scale factors of the Cauchy and Froude similitude law.....	27
Table 3.1.	Mortar Mixture Combinations.....	47
Table 3.2.	Compression and tension strength results for mortar samples.....	48
Table 3.3.	Diagonal shear test results for masonry specimens.....	50
Table 3.4.	Similitude laws for the model (Tashkov <i>et al.</i> , 2012).....	56
Table 3.5.	Nonlinear material properties.....	74
Table 3.6.	Mechanical properties of base isolators (Erdik, 2012).....	75
Table 3.7.	FRP properties used in the numerical and experimental analysis.....	108
Table 4.1.	Geometrical properties of the Mihrimah minaret model.....	125
Table 4.2.	Geometrical properties of the Hagia Sophia minaret model.....	125
Table 4.3.	Geometrical properties of the Süleymaniye minaret model.....	126
Table 4.4.	Modeling parameters for the Mihrimah minaret.....	126
Table 4.5.	Modeling parameters for the Hagia Sophia minaret.....	126
Table 4.6.	Modeling parameters for the Süleymaniye minaret.....	127
Table 4.7.	Covered frequency ranges for three minarets.....	129
Table 4.8.	Experimental and analytical frequencies of vibration.....	129
Table 4.9.	PGAs and PGVs of all records employed in the analyses.....	155

Table 4.10.	Residual block displacements, peak shear displacements, peak normal stresses and peak normal displacements during seismic loading.....	157
-------------	--	-----

## LIST OF SYMBOLS /ABBREVIATIONS

$A_n$	Net area
$c$	Joint cohesion
$D_i$	Drum diameter
$D_{drum}$	Diameter of the top drum of minaret
$E_k$	Kinetic energy in the system
$E_m$	Total stored strain energy
$E_b$	Young's modulus of the brick
$f$	Natural frequency of the system
$f_n$	Normal force at a contact
$f_s$	Shear force at a contact
$f'_n$	Previous normal force at a contact
$f'_s$	Previous shear force at a contact
$f_{smax}$	Shear stress at which the Coulomb slip condition is met
$F_d$	Damping force
$g_i$	Gravity acceleration vector
$h$	Height of specimen
$I_1, I_2, I_3$	Principal moments of inertia of the block
L	Dimension in the prototype or model
$m$	Block mass
$M_1, M_2, M_3$	Components of torque applied to the block
$n$	Percent of the cross area of the unit that is solid
$P$	Applied load
$resu_i$	Relative drum dislocations
$t_b$	Thickness of brick
$t_m$	Thickness of mortar bed joint
UDEC	Universal distinct element code
$u_{top}$	Maximum top displacement
$u_n$	Incremental normal displacements at the contact
$u_s$	Incremental shear displacements at the contact

$w$	Width of specimen
$W_r$	Difference between the works done at the boundary of the model
$W_\xi$	Total mass damping work
$W_v$	Total viscous (non-reflecting) boundaries work
$\dot{W}_d$	Rate of damped energy change at a block
$\dot{\omega}_1, \dot{\omega}_2, \dot{\omega}_3$	Angular accelerations about the principal axes
$\omega_1, \omega_2, \omega_3$	Angular velocities about the principal axes
$\ddot{x}_t$	Acceleration of the block centroid
$\dot{x}_t$	Velocity of the block centroid
$\alpha$	Viscous (mass-proportional) damping constant
$\phi$	Friction angle
$\alpha$	Mass proportional damping constant
$\beta$	Stiffness proportional damping constant
$\dot{u}$	Velocity of a block of mass
$\sum F$	Force sum at the block
$\gamma$	Fraction of critical damping
$\tau$	Shear stress
3DEC	Three dimensional distinct element codes
$\Delta\sigma_{xb}$	Increment of lateral stress in the brick
$\Delta\sigma_y$	Increment of vertical stress on prism
$\nu_b$	Poisson's ratio of the brick

# 1. INTRODUCTION

## 1.1. Aim and Objectives of the Research

The masonry building stock in Istanbul and in other cities of Turkey are exposed to significant earthquake hazard. Many of them received earthquake damage in the past. There is an expectation of a large Istanbul earthquake in the near future that will most probably affect them as well. Determination of the safety of masonry structures against earthquakes is a complex challenge. Several investigations have been completed in recent years, concerning masonry structures geared towards their earthquake safety assessment. (Doğangün *et al.*, 2008; Bayraktar *et al.*, 2010; Pena *et al.*, 2010; Russo *et al.*, 2010; Gesualdo and Monaco, 2011; Pineda *et al.*, 2011; Kouris and Weber, 2011; Quiroz, 2011; Romaro, 2011; D'Ambrisi *et al.*, 2012; Cagnan, 2012; Tabeshpour, 2012; Oliveira *et al.*, 2012; Foti *et al.*, 2012; Atamtürktür, and Sevim, 2012; Nazir and Dhanasekar, 2013; Bartoli *et al.*, 2013; Casolo *et al.*, 2013). As they will continue to get affected by the earthquakes, more research is needed to assess their earthquake performance. Improvements of codes and guidelines concerning their maintenance and preservation, and the construction of new ones are also essential.

In dealing with the problem of global analysis of masonry structures, linear and non-linear methods are used in common practice. Regarding the modeling, finite element method is the most well-known methodology based on elements that behave rather connected under static and dynamic loading conditions. However, masonry structures have a natural complexity due to the heterogeneity of materials (stone, brick, mortar), discontinuities and different elastic plastic behavior characteristics of stone, brick and mortar under static and seismic loading. In order to create effective and practical methods of dynamic analysis, many research programs are being conducted to better understand masonry structures.

The ultimate aim of this PhD research is to enhance our modeling and structural analysis capabilities of historical masonry structures, which display a highly complex behavior due to their material characteristics, structural and architectural configuration and damage history.

## 1.2. Outline of Thesis

The present thesis deals with experimental tests and non-linear dynamic analysis of masonry structures modeled through discrete element method. The work that has been conducted is organized as in the following:

The objective and the outline are described in the 1st chapter, which the present one.

In the 2nd chapter, a brief review of important approaches and methods used in earthquake performance assessment of masonry structures will be reported, along with the modeling and analysis techniques.

The 3rd chapter of the thesis is summarized as follows: Construction of the 1:10 scale model of Mustafa Paşa Mosque and the data obtained from the sensors on it during its testing on the shake table is the starting point of the 3rd chapter. Elements of 3D distinct element models will be developed that represent the linear and nonlinear behavior of the shake table model of the Mustafa Paşa Mosque as closely as possible during all three stages of testing: base-isolated model, the model as it is and strengthened model.

In the 4th chapter, three masonry minarets in Istanbul with different heights will be studied under sine waves, and under ten real and simulated earthquakes to investigate how their seismic response is influenced by structural geometry and input motion. By using the discrete element technique, 3D models of the minarets will be created and calibrated. Two parameters will be defined for the characterization of damage. Time histories at given locations, the distribution of peak values of joint displacements and stresses, and energy balance in the system will be evaluated to analyze the damage and collapse in masonry minarets.

The final chapter will summarize and discuss the findings of the study.

## **2. METHODS USED IN EARTHQUAKE PERFORMANCE ASSESSMENT OF MASONRY STRUCTURES**

In this chapter an attempt has been made to present the seismic responses of masonry structures under seismic actions that show objective difficulties because of the geometrical and morphological characteristics and the nonlinear behavior of the material. A panoramic view of investigations and different approaches adopted in the study of masonry structures is illustrated in this chapter, dealing.

### **2.1. Mechanical Characteristics of Masonry Structures**

In the investigation of the structural behavior of masonry structures, the study of the mechanical behavior of the constituent materials of masonry is a considerably important first step. The mechanics of mortar, brick, stone and bond and their interaction with brief explanations are given below.

#### **2.1.1. Mortar**

Sludge is the oldest mortar used by man, but it has not got sufficient strength for a heavy wall. Mortar is comprised of cement, lime and sand and has been used in masonry construction such as vaults, domes and arches since the Roman period (Çamlıbel, 2000). Mortar has strength and binding characteristics and exhibits non-linear, time-dependent, stress-strain characteristics because this material suffers from time effects more than other materials (Page, 1978). Elastic properties of mortar are defined using experimental methods but it is difficult to find a proper estimation of the Poisson's ratio. Modulus of elasticity of masonry materials depends on the modulus of elasticity of the mortar which may be determined by investigation of the stress-strain curve. In general, mortar shows a softer behavior when compared to brick or stone units. Under uniaxial compressive loading, the mortar tries to expand laterally more than the stone or brick units. Because mortar and brick are bonded together chemically and mechanically, the mortar is confined laterally by the brick.

Because of the continuity between the units and the mortar, combined by cohesion and friction, the mortar is confined laterally by the units. Shear stresses at the brick-mortar interface result in an internal state of stress which consists of triaxial compression in the mortar and bilateral tension coupled with axial compression in the brick (Oliveira, 2000).

### 2.1.2. Brick

Brick is one of the most important materials that have been used in masonry construction since before the Roman period. Brick was once composed of clay and was generally produced by using ruins of sand accumulated on the surface of stream beds. This traditional technique was replaced by machinery during the Industrial Revolution (Lourenço, 1996). In the absence of oven machinery procedures, bricks are produced using heat from the sun (Ünay, 2002). Commonly bricks have elastic-brittle behavior under seismic activity.

In general, the tensile strength of brick is 8 % of the compressive strength of the brick and the shear strength is 30 % of the compressive strength of the brick. However with respect to stones, bricks are stronger because of their ductility. Ductility causes the bricks to absorb stress concentrations much more easily than stones (Ünay, 1997). Approximate mechanical properties of bricks such as elastic modulus, compression, tension and shear strength are given in Table 2.1.

Table 2.1. General properties of bricks (Ünay, 2002).

Elasticity Modulus (kPa)	Compression Strength (kPa)	Tensile Strength (kPa)	Shear Strength (kPa)
150.000 - 300.000	10.000 - 30.000	2.700 - 5.000	10.000 - 20.000

According to the theory proposed by Atkinson (1983), the lateral stress in the brick can be expressed as;

$$\Delta \sigma_{xb} = \frac{\Delta \sigma_y \left[ \nu_b - \frac{E_b}{E_m(\sigma_1, \sigma_3)} \nu_m(\sigma_1, \sigma_3) \right]}{1 + \frac{E_b}{E_m(\sigma_1, \sigma_3)} \frac{t_b}{t_m} - \nu_b - \frac{E_b}{E_m(\sigma_1, \sigma_3)} \frac{t_b}{t_m} \nu_m(\sigma_1, \sigma_3)} \quad (2.1)$$

where

$\Delta \sigma_{xb}$  = increment of lateral stress in the brick;

$\Delta \sigma_y$  = increment of vertical stress on prism;

$\nu_b$  = Poisson's ratio of the brick;

$E_b$  = Young's modulus of the brick;

$\nu_m(\sigma_1, \sigma_3)$  = Poisson's ratio of the mortar as a function of principal stresses;

$E_m(\sigma_1, \sigma_3)$  = Young's modulus of the mortar as a function of principal stresses;

$t_b$  - thickness (height) of brick;

$t_m$  = thickness of mortar bed joint.

This equation describes the increment of lateral stress in the brick,  $\Delta \sigma_{xb}$ , resulting from an increment of compressive stress,  $\Delta \sigma_y$ . The lateral stress in the brick is a function of the material properties of the brick and mortar. Poisson's ratio,  $\nu_m$ , and Young's modulus,  $E_m$ , of the mortar are expressed as a function of the vertical stress,  $\sigma_1$ , and the lateral stress,  $\sigma_3$ . This accounts for the nonlinear properties of the mortar with respect to the existing state of stress. The properties of the brick are assumed to be constant under all stress states.

### 2.1.3. Stone

In general, because of better availability than other materials, stone is the most used material by man in masonry construction. Stone is suitable material for masonry construction of large openings, arches, vaults, domes and compression walls and it is strong in compression but very weak in tension. The tensile strength of stone is approximately 10 % of its compressive strength, and the shear strength of stone is 25 % of its compressive strength. Approximate mechanical properties of some types of stones such as elastic modulus, compression, tension and shear strength are given in Table 2.2.

Table 2.2. General properties of stones (Ünay, 2002).

Type of Stone	Elasticity Modulus (kPa)	Compression Strength (kPa)	Tensile Strength (kPa)	Shear Strength (kPa)
Granite	$30 \times 10^6$ - $55 \times 10^6$	30.000-70.000	4.000-7.000	14.000-33.000
Limestone	$10 \times 10^6$ - $55 \times 10^6$	18.000-35.000	2.000-6.000	6.000-20.000
Marble	$25 \times 10^6$ - $70 \times 10^6$	25.000-65.000	1.000-15.000	9.000-45.000
Sandstone	$13 \times 10^6$ - $50 \times 10^6$	5.000-30.000	2.000-4.000	2.000-10.000
Serpentine	$23 \times 10^6$ - $45 \times 10^6$	7.000-30.000	6.000-11.000	2.000-10.000
Quartz	$15 \times 10^6$ - $55 \times 10^6$	10.000-30.000	3.000-4.000	3.000-10.000

#### 2.1.4. Bond

Bond is associated with the tensile strength of masonry structures since it is usually equal to the tensile bond strength between the joint and the unit. The presence of asperities or a thin hydrated layer affects the bond properties. In case the tensile bond strength is higher than that of the unit, the tensile strength of masonry is equal to the tensile strength of units. Tensile bond strength is very low in masonry structures and even in some studies no tensile is assumed. However, tensile bond strength of the unit-mortar interface is a very important mechanical property of the masonry construction since most of the times non-linear behavior is originated by cracking in the mortar joints. Figure 2.1 shows some masonry failure modes (Sutcliffe *et al.*, 2001). Anthoine proposed a test to define the bond properties. In that test, bond is assumed to show brittle-elastic behavior to modeling of tensile behavior (Anthoine, 1992). Sugo proposed a systematic quantification of a number of factors that detract from bond, such as air entraining agents, and completed a scanning electron microscopy study that explains the characteristics of good and poor bond (Sugo *et al.*, 1996).

## 2.2. Damages and Failure Mechanisms of Masonry Structures

Masonry buildings show several sources of seismic vulnerability since they have different construction types and more relative stiffness of lateral load resisting elements than other types of structures.

The high vulnerability of historical masonry buildings to seismic actions is mostly due to the structural elements, with inadequate connections between several parts of the structure which are interconnected orthogonally to each other with relatively flexible diaphragms. Generally, in the case of masonry structures, elements are supposed to resist seismic, horizontal action besides the vertical loads which may induce partial collapse or drive the whole structure. Limit stress state of strength is also important for vulnerability dynamic action. However these possible collapses or damages are generally resulting from the equilibrium loss of some structural parts. During a seismic activity, masonry buildings such as mosques show the absence of box behavior which may induce a collapse of a portion of the structure.

During a seismic action, structural damage that may occur on masonry structures can be classified according to the possible inferred causes, called failure mechanisms. Failure mechanisms are assembled into two main groups as out-of plane and in-plane failures. In-plane failures occur in the longitudinal plane of individual masonry walls during an earthquake, since ground forces from the foundation of a masonry structure are transformed to the in-plane walls.

Failures mechanisms substantially differ according to the loading case such as the axial stress, height to width ratio, material strength and boundary conditions. Failure mechanisms occur in the longitudinal plane of individual walls, generally common subjects of seismic analysis and resistance of masonry structures. Global response of the whole masonry structure causes the in-plane wall failures. These failure mechanisms differ from local collapse failures which may occur with respect to the insufficient vulnerability of the elements or improper construction.

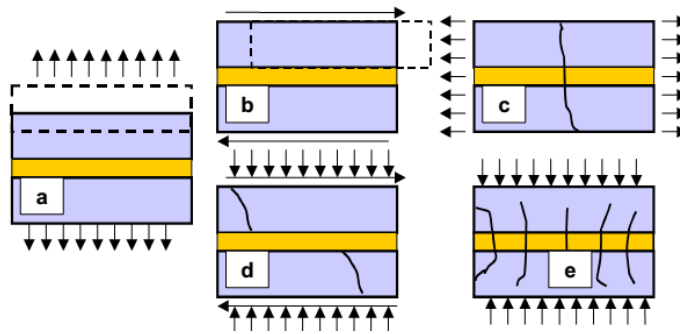


Figure 2.1. Masonry failure modes.

Masonry failure modes are illustrated in Figure 2.1 as; direct tensile cracking of joint in Figure 2.1a; sliding along joint cracking of unit and joint in Figure 2.1b; diagonal tensile cracking of units in Figure 2.1c; compressive failure due to mortar mortality in Figure 2.1d by Idris *et al.* (2009). Axial forces at the wall toes result in crushing cracks and also tensile cracks occurring orthogonal to the axial forces. In the case of low vertical stresses and poor quality of materials, sliding shear cracking arises along a mortar bed joint and tension shear cracking occurs, which consists of diagonal cracking and begins at the wall center and propagates along the diagonal toward the toes. When vertical compression combines with horizontal tension, this causes vertical cracking with failure of bricks. When the horizontal shear stresses exceed the joint shear strength of the masonry this leads to sliding failure (Figure 2.2).

Diagonal shear failure occurs where the principal tensile stresses exceed the tensile strength of the masonry as shown in Figure 2.2. Unit and mortar joints have different deformation characteristics which lead to failures in compression. The difference of the elastic properties of the component materials strongly influences the failure mode which can cause either tension cracks parallel to the direction of loading or a kind of shear failure along some lines of weakness (Hendry, 1998). Vertical loads may cause collapse if mortar is poor and the thickness of the joints is high. In the event of stress concentration, irregularly composed stone elements may also lead to failures. Furthermore, when structural walls have inadequate thickness with respect to the inertial core, this again may result with collapse or horizontal inertial forces may provoke the loss of equilibrium.

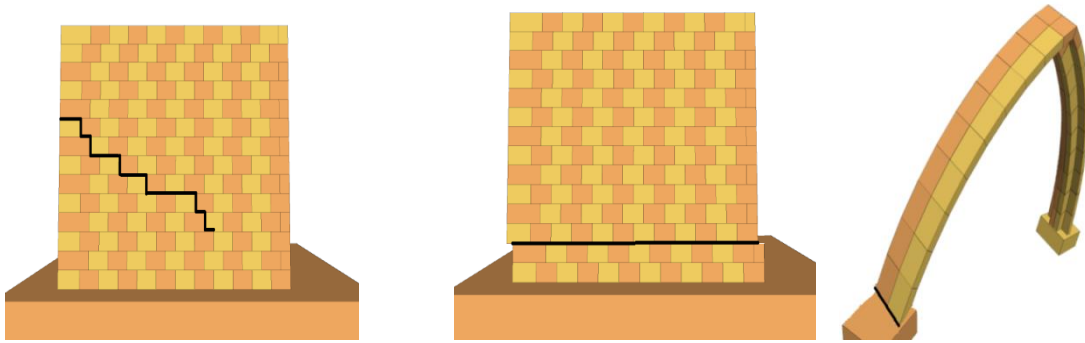


Figure 2.2. Images of shear, sliding and rocking failures.

Masonry structures usually have an inadequate resistance to horizontal actions and this leads to overturning collapses of the perimeter walls under seismic loads and combined in- and out-of-plane failures. In the event of large flexure moment and improved shear resistance, this leads to horizontal cracks at the top and bottom resulting in a rigid body subject to rotation, called rocking failure (Figure 2.2). When in-plane walls have suitable and correct connections with the diaphragm, forces are transferred to the orthogonal walls and these in-plane walls transfer the forces to the attached walls in the out-of-plane direction. Consequently, the diaphragm shows deep beam behavior, simply supported at the ends. Transmissions of inertial forces give rise to deflection of diaphragms in an amount which depends on the in-plane stiffness of the diaphragm. Masonry structures may resist the seismic activity on the condition that structural elements have proper connections between the walls and the floors that can exploit the in-plane resistance of walls. Structural damage based on this kind of response is mostly related to the in-plane response of masonry walls. Structural damages also may occur on specific portions of masonry structures such as masonry piers associated with the openings. Geometry of the structure, division of openings, poor construction and location of the walls are important factors to the seismic response of masonry buildings. Out of plane failures occur if the units of the masonry walls do not have the adequate connections. When there are no proper connections between floors and walls and absence of the out of plane restraints, these result with the out-of-plane overturning of single walls. For each of these failures, the allowable lateral force depends upon the given axial force, boundary conditions, length-to-width ratio, and mechanical properties of masonry structures (Romano, 2005; Şen, 2006; Javed, 2009; Parisi, 2010).

### 2.3. Mechanical Tests

Since historical masonry buildings have several parts with different material characteristics and mechanical properties they should be evaluated using a correct method. The meaningful characterization of existing materials and the current condition of the structures are generally identified by site and laboratory tests. Several techniques such as non-destructive, minor destructive and destructive tests, laboratory tests and on-site test experimental investigation are used to investigate the correct structural condition or determine the composition of the masonry structure.

The knowledge of typology and damage of historic masonry structures in seismic locations is fundamental for the selection of a proper and technically effective method. Like all other buildings materials, masonry structures suffer from the accumulated effects of material degradation, aging, overloading and foundation settlements. These changes in environmental condition affect the accurate information on material properties and mechanical characteristics of masonry structures. During the last decade, the technology for the rehabilitation and the maintenance of existing masonry structures has been significantly improved and extensively used. In literature, there are a number of studies concerning the development of new restoration technologies and maintenance of existing building (Drysdale *et al.*, 1994; Macchi, 1997; Lourenco, 1998b; Olivito and Stumpo, 2001; Pietruszczak and Ushaksaraei, 2003; Milani *et al.*, 2006; Petrova *et al.*, 2011; Asteris *et al.*, 2012; Asteris and Giannopoulos, 2012; Laska *et al.*, 2013). Common non-destructive, minor destructive and destructive testing methods are briefly described below:

#### 2.3.1. Destructive Testing Methods

Most of the structural analyses and assessment techniques require masonry strength and other mechanical properties. Destructive testing methods such as mechanical, physical, and chemical tests are used for characterizing these properties of masonry materials. This methodology is based on testing cored samples in laboratories, or the removal of masonry at a probe hole for visual examination.

Generally these tests are affected by proper uncertainties and provide localized information on the cored sample. However results can be extended to the whole masonry structure to estimate its composition or determine the whole material property if the selected technique gives reliable and proper results.

### **2.3.2. Minor Destructive Testing Methods**

Minor destructive testing methods assess the mechanical properties of masonry structures by slightly and temporarily damaging the structure, and after the test these damages easily can be repaired.

These testing methods provide qualitative information on the masonry condition of the structure and are generally used for preliminary investigations. Some of the minor destructive testing methods with brief explanations are given below.

**Borescope:** Materials are identified mechanically with a small camera which is inserted into boreholes. These small diameter holes are drilled in the structure and into mortar allowing a detailed study on anomalies and defects. These boreholes are also used for identifying the existence of internal cavities and cracks. This technique gives reliable results but provides only localized information about anomalies and defects (Gentry, 2012; Nacheman and Badheka, 2012).

**Flat-jack Testing Methods:** A flat-jack is a thin steel envelope that hydraulically pressurizes and applies stress to the surrounding masonry structure. This technique is temporarily destructive since a portion of the mortar is removed to manage the test and after finishing the test mortar can be repointing into the joint, so this technique is assumed as one minor destructive test. This methodology is suitable in identifying the in-situ stress, compression modulus, and compression strength under uniaxial compression. It is also used for determining the deformability properties such as shear strength along the mortar joints for structural evaluation (Candela *et al.*, 2012; Almeida *et al.*, 2012; Lombillo *et al.*, 2013; Casarin *et al.*, 2013).

### 2.3.3. Non Destructive Testing Methods

Non Destructive Testing methods are used to evaluate the relative quality of the material of a masonry structure without causing permanent damages, because sometimes sampling from important historic monuments is not allowed. However these techniques do not determine the direct measurements of the engineering properties of a masonry structure.

**Impact-Echo:** ‘Impact echo technique’ is used to determine the discontinuities and variations in the masonry by analysis of wave echoes. Sansalone and Streett (1997), McCann (2001) and Sadri (2003) used ‘Impact echo technique’ to identify the internal discontinuities. Lombillo *et al.* (2013) carried out impact-echo tests on rubble stone masonry walls for the morphological identification of the Riva–Herrera palace. Dawood *et al.* (2013) used the ‘impact-echo test’ to measure the depth of the different cracks of a Jetty bridge structure.

**Infrared Thermography Testing:** Infrared thermography testing is used to determine the wet location, voids, cracks that occurred at the subsurface of masonry, internal anomalies, and variations in insulation. This technique is effective in large areas for surviving quickly and efficiently, but this method is susceptible to surface conditions such as a few centimeters below the surface (Clark *et al.*, 2003; Michael and Schuller, 2003; Avdelidis and Moropoulou, 2004; Meola, 2007; Tavukçuoğlu *et al.*, 2010; Cerdeira *et al.*, 2011; Largo and Angiuli, 2013).

**Metal Location:** Metal location approach is used to determine the structural steels that are embedded in a masonry structure.

**Rebound Hammer:** Rebound hammer technique is used to evaluate the surface hardness and variations in masonry structure such as variations in material.

**Stress Wave Transmission:** Stress wave transmission approach evaluates the internal part of masonry as determines the void locations in masonry structures by transmission of pulses.

**Ground Penetrating Radar Testing:** Surface penetrating radar technique uses high frequency wave energy to provide valuable information about structural anomalies. This testing method is effective at identifying the voids, hidden layers of the structure, the presence of other materials such as metal inclusions, the thickness of the element, internal damage or deterioration in walls, moisture content and the locations of the internal defects in masonry (Lubowiecka *et al.*, 2009; Solla *et al.*, 2011; Hamrouche *et al.*, 2012; Solla *et al.*, 2012; Solla *et al.*, 2014).

**Tomographic Imaging Testing:** Tomographic imaging testing is used to image defects within masonry and determine the general type of internal feature and anomalies, voids, cracks and deteriorations by using a large number of ultrasonic stress wave velocity measurements (Concu *et al.*, 2009; Bosiljkov *et al.*, 2010; Raffaele *et al.*, 2010).

**Ultrasonic Velocity Testing:** Ultrasonic velocity testing approach uses ultrasonic impulses to determine the discontinuities void location and internal masonry damages. The sonic waves are generated and transmitted through the masonry structure and the time that it takes to reach the receiver is measured, because the stress wave velocity depends on the density in masonry. This time is evaluated for determining the asperities or void locations. This technique is slower than other nondestructive testing methods and requires a specialist for calibration and interpretation. In literature there are a number of case studies that use Ultrasonic velocity testing approach to identify the void location and internal damages (Abbateo *et al.*, 1995; Rossi *et al.*, 1996; Krause *et al.*, 2003; Faella *et al.*, 2012).

Some references in the literature are related with destructive and/or nondestructive testing methods. Mechanical properties such as shear strength of mortar and compressive strength of units are generally assessed using experimental tests (Lourenço, 1994; Almeida *et al.*, 2012; Candela *et al.*, 2012; Casarin *et al.*, 2013; Lombillo *et al.*, 2013). Civic Tower in Pavia was evaluated using mortar samples to define the role of degradation of mortar quality on the collapse (Baronio and Binda, 1995). Colla *et al.* (1997) assessed and discussed masonry arch bridges using the non-destructive techniques of radar and sonic methods. They concluded that sonic methods require attention about correct grid density to get good results and these techniques are effective and that tomographic plots aid the interpretation of data.

Materials used at the masonry structures in Catalonia were examined using experimental tests on specimen (Oliveira, 2000). Experimental tests were conducted to define the mortar effect on load bearing capacity of historical masonry structures (Papayianni and Stefanidou, 2001). The structural behavior of Noto Cathedral was evaluated, and the effects of the used materials were examined (Baronio *et al.*, 2003). Mechanical properties of material used at the Frauenkirche were evaluated using destructive tests (Pohle and Jager, 2003). The role of the materials used at the masonry structures located at Toledo was investigated (Lopez- Arce *et al.*, 2003).

Mechanical properties of masonry structures were examined through hammer tests (Brencich and Sterpi, 2006). Orbána and Gutermann (2009) also assessed the masonry arch railway bridge and concluded that destructive testing methods focus mainly on the mechanical characteristics of the materials, however non-destructive testing methods can provide an overall qualitative review of the condition of the bridge or additional information on its internal geometry. Mechanical properties of Akaretler Row Houses located in İstanbul were examined using destructive and nondestructive testing methods (İspir *et al.*, 2010). Tavukçuoğlu *et al.* (2010) performed ultrasonic testing on a sixteenth century monument, and concluded the behavior and ultrasonic characteristics of cracks in relation to depth and moisture content. Miranda *et al.* (2013) applied sonic tests to study the propagation of sonic waves through stone masonry walls. The results allowed a better understanding of the influence of the stones characteristics and the samples geometries, to the global response of the masonry to the propagation of sonic waves. Bartoli *et al.* (2012) performed Ultrasonic and dynamic tests to evaluate the modal properties of a stone colonnade of the Dome of the Siena Cathedral in Italy. Tests were aimed at both measuring the fundamental natural frequency of stone columns and identifying their boundary conditions. Solla *et al.* (2014) performed of ground-penetrating radar, photogrammetry and infrared thermography for the analysis of moisture in the masonry arch bridge of Lubians in Spain. They concluded that the detection and analysis of moisture in the bridge can be useful information to decide subsequent conservation actions.

## **2.4. Shaking Table and Pseudo Dynamic Tests**

The decision about selecting the proper method to examine the earthquake performance on structures is of high importance due to the required information, technical problems and results and also the budget of the research. Experimental methods are the best ways for simulating earthquake effects on structures and are able to reflect the actual behavior of the structure. There is an increasing demand for the conducting of experimental tests to evaluate the seismic behavior of a structure or structural elements. However studies on full scale masonry structures are still challenging, even in testing techniques or in analytical modeling.

Natural frequencies, damping ratio, vibration modes of structures and inelastic behavior of structure are evaluated by seismic simulation tests that apply on physical models. Seismic responses of acceleration, displacement, strain of structure, collapse style and failure mechanisms can also be predicted by using experimental testing methods. Seismic simulation tests give more reliable results with respect to the analytical models because the stresses, deformations and modal shapes that are estimated by analytical models are generally based on the simplified modeling techniques and nonlinear of material. Shaking table researches also provide valuable information about liquefaction, post-earthquake settlement, foundation response and lateral earth pressure problems. Hence, they are closely related to the modern trends in geotechnical earthquake engineering which recognize the strong influence of the local site effects on the intensity and on the frequency content of the input motions on structures.

### **2.4.1. Quasi-static Tests**

The quasi-static testing method is performed to evaluate the progress of damage evolution and the seismic behavior of masonry structures. In quasi-static tests, there is no limits on the size of the structure for assessing the seismic performance of the structure and these tests are relatively inexpensive, and do not require very special types of apparatus. However, since the loads and displacements are applied at slow rates, acceleration-dependent inertial forces and velocity-dependent damping forces effects are eliminated. Displacement and force histories are defined before and then used for conducting the test.

The quasi-static testing method uses lumped masses of inertial forces that are with respect to mass on the structure and this is one the disadvantages of this method for structures possessing distributed mass. The elimination of the rate and pattern of used displacement history is also another disadvantage of this technique. Some researches in literature conducted quasi-static testing method and this contributed to the effects of earthquakes on masonry structures (Rots, 1997; Wei *et al.*, 1999; Indirli *et al.*, 2000; Burnett *et al.*, 2007; Klingner *et al.*, 2011; Beyer and Dazio, 2012; Salmanpour *et al.*, 2013)

#### **2.4.2. Pseudo Dynamic Tests**

The method of the Pseudo dynamic test was introduced by Takanashi (1974) in Japan, for investigating large structures under seismic ground motions. The pseudo dynamic testing method is one of the experimental methods that use computer and quasi-static loads to reproduce the dynamic effects that results in the form of inertial forces. This method is composed of computational and experimental parts to simulate the seismic behavior structures with respect to the time domain. In this technique, the dynamic response of a structure is computed using the experimental result in each time step. The computational part can be performed by the computer; the structural response as displacement is calculated in a time step. Inertial and damping forces that are required during the analysis process are modeled analytically to solve the equations of motion. The computer, after calculating structural displacement at a specific time step, electronically provides this result to the actuator system. In the experimental process, the computed displacements are imposed to a real system or to convenient structural component by means of hydraulic actuators which then measure and return the restoring force, to the computer. By using the measured data, the computer can calculate the response in the next time step (Javed, 2009). Therefore, in this method, the equation of motion is solved based on the restoring force which is measured on the structure. Also at every time step the stiffness matrix is assembled.

The experimental model is based on a control system able to impose displacements and to measure the required forces on the specimen structure working at a quasi-static loading rate and the loading rate is transformed from frequencies in the order of a few Hertz, which correspond to the prototype earthquake, to frequencies hundreds or even thousands of times lower, while keeping the original amplitude of the displacements. The flow of computational procedure is as follows (Kim, 1995);

In the numerical process,

1. Calculation of the initial condition using equation;

$$\ddot{x}_0 = M^{-1}(F_0^e - F_0^i) \quad (2.2)$$

2. Evaluation of the displacement using the equation;

$$x_{n+1} = x_n + \Delta t \dot{x}_n + \frac{\Delta t^2}{2} \ddot{x}_n \quad (2.3)$$

In the experimental process,

3. Imposing the displacement  $x_{n+1}$  on real system or to convenient structural component to be tested.
4. Measurement of the restoring force  $R_{n+1}$  at the designated points of structure.

In the numerical process,

5. Correction of the restoring force.
6. Computation of the acceleration and the corresponding using the equations

$$\ddot{x}_{n+1} = \left( M + \frac{\Delta t}{2} C \right)^{-1} \cdot \left( F_{n+1} + R_{n+1} - C \dot{x}_{n+1} - \frac{\Delta t}{2} C \ddot{x}_n \right), \quad x_{n+1} = x_n + \frac{\Delta t}{2} \left( \ddot{x}_{n+1} + \ddot{x}_n \right) \quad (2.4)$$

7. If the step  $n$  is less than the total number of steps  $N$ , return to 2 after setting  $n = n + 1$ .  
Otherwise stop.

The pseudo dynamic testing method is a relatively inexpensive method and applicable to simulate the seismic response for large scale structures that overcomes the limit problem since this method is a dynamic testing method with a static device. This method is not a real time scale test since in this method inertia forces are not experimentally produced. Rather, they are modeled numerically and are replaced by equivalent pseudo-static loads. The main feature of pseudo-dynamic test is testing the structural elements whose mechanical properties are not well defined and modeling the remaining structural elements numerically. The mechanical properties of elements numerically modeled are considered to be well defined rather than the elements subjected to the actual forces.

A part of the structure can only be tested while the rest of the structure can be modeled analytically. This is advantageous in that it simplifies the equipment needed and it allows for inspection of the test structure between load steps. A major potential drawback, however, is that any time-dependent behavior in the test specimen is not included. The method has difficulty in consuming a lot of time to conduct the test because of the solution of equation of motion for determining the displacements by computers. The results of the experiment are not always sensitive since the simulation of an earthquake may take hours of time. This technique relies on the appropriate assignment of damping properties. Using a constant damping matrix based on the elastic properties of the system may cause unpredictable results (Shing and Mahin, 1985). Kumar *et al.* (1997) used pilot tests to clarify the scale factors for pseudo dynamic tests and classify the possible similitude relations. This classification helps to select the most suitable procedure and similitude relationships for pseudo dynamic testing using available equipment.

The experimental results are available in literature obtained during the pseudo dynamic tests. Almost all of them include the comparison of numerical results with experimental results (Kumar *et al.*, 1997; Giordano *et al.*, 2002; Paquette and Bruneau, 2004; Yang, 2010). Paquette and Bruneau (2004) performed pseudo-dynamic testing on a full-scale one-story unreinforced brick masonry specimen having a wood diaphragm. The specimen was subjected to earthquake excitations to understand the flexible-floor/rigid-wall interaction, the impact of wall continuity at the building corners and the effect of a relatively weak diaphragm on the expected seismic behavior.

Tan and Wu (2011) investigated the seismic behavior of a single-story ten-bay confined masonry structure using substructure pseudo-dynamic tests. They conclude that prototypes of the tested type exhibited satisfactory seismic performance. An *et al.* (2012) performed pseudo dynamic tests to estimate the deformability and ultimate bearing capacity of confined masonry with tie-column and ring-beam. These tests verify that the tie-column and ring-beam system is an effective seismic requirement to enhance the seismic performance of a masonry structure. Then An *et al.* (2013) carried on a study using pseudo dynamic tests in order to assess the hysteretic behavior and deformation under horizontal artificial earthquake motion and strong motion recording.

### **2.4.3. Shaking Table Tests**

Shaking tables were first used for simulating seismic loads on structures in the 1940s and their usage has been widespread since the 1960s. By this technique dynamic behavior of the structure can be monitored, measured and the results match very well to reality. The intended model of structure is constructed on a stiff platform according to the shaking table size and load capacity. The correct inertia forces are then generated throughout the structure and the response of dynamic motion within the capacities of force, velocity, displacement, and frequency of the system can be measured. Dynamic motion is generated by a computer with respect to the degrees of freedom of the table, and then imposed on the actuators of the shaking table. The main elements of the table system are the hydraulic actuators and the platform that can be shaken along one or more axes.

Shaking table tests have more advantages with respect to the quasi-static test such as that the forces and relative displacements in the building are generated by the dynamic response of the structure. Structures do not have to be modeled as an equivalent lumped mass as in quasi static tests. Shaking table tests are useful to understand the nonlinear dynamic behavior of structures under earthquakes of different intensities and verify the reliability of earthquake response predication by means of inelastic dynamic response analysis.

Some researchers in literature carried on a study of using the shaking table test to reproduce the dynamic behavior of the structure and its damage style under earthquake motion (Blondet *et al.*, 1980; Takanashi and Nakashima, 1987; Mahin and Shing, 1989; Iliba *et al.*, 1996; Lu *et al.*, 1996; Zhang, 1997; Juha'sova' *et al.*, 2002; Elwood and Moehle, 2003; Xianguo *et al.*, 2004; Li *et al.*, 2006; Rezaifar *et al.*, 2009; Yang, 2010; Tomaževic and Gams, 2012; Mendes *et al.*, 2014). There are a number of researches that contributed to the development and verification of the ability of the shaking table testing method. Candeias *et al.* (2004) performed tests in the LNEC 3D shaking table on 1:3 reduced scale models of 4 story unreinforced masonry buildings with masonry shear walls and wood-framed floors to determine the weak points.

Krstevska *et al.* (2009) performed shaking table test of a Mustafa Paşa Mosque large scale model. They used a model that was designed and constructed to a length scale of 1:6 using the same materials as for the prototype structure with stone and brick in lime mortar. They evaluated the seismic stability of the monument after applying a reversible technology for strengthening. The obtained results gave valuable information about the effectiveness of the proposed strengthening technique. Liu *et al.* (2011) conducted the shaking table tests, with 1:3 scale walls of two-story model subjected to horizontal earthquake loads to investigate the out-of-plane behaviors with different connections between walls and beams. The test results show that the connection methods employed between walls and beams have a significant effect on the out-of-plane stability of infill walls. Nakagawa *et al.* (2012) carried on a study of using a shaking table in order to analyze and simulate seismic performance of the masonry structures. Mendes *et al.* (2014) carried out shaking table tests to assess the seismic performance of an existing masonry building and to validate the efficiency of a strengthening technique.

## **2.5. Strengthening Methods in Masonry Structures**

The problem of the seismic reliability assessment and strengthening of masonry structures is of great practical concern. In Europe today, especially in Turkey, there is significantly grown need for strengthening of masonry structures.

Increased loading on the structure due to change in use, structural element with poor quality connection, original design errors that underestimated the actual loading on the structural members, load bearing structures with stability problems, improvements in analytical tools and codes that demonstrate the inadequate strength of the member as it was originally designed and constructed require strengthening. While various codes do provide detailed guidelines for design of new masonry structures, few provisions are available for strengthening existing masonry structural members. The applications generally used in the field of strengthening of masonry structures are briefly summarized in Table 2.3 (Jeffs, 2000; Trujilio Leon, 2007; Islam, 2008; Vinzileou, *et al.*, 2011). In the last decades the use of innovative materials, such as composites, received great interest because of their possible advantages in terms of low weight, simplicity of application, high strength in the fibers direction, immunity of corrosion and quite reduced invasiveness.

The use of Fiber reinforced polymers (FRP), high strength composite materials characterized by the combination of strong fibers and a matrix, is growing in the field of structural repair of both recent and historical masonry buildings.

Fiber reinforced polymers (FRPs) are composite materials constituted by polymeric matrix and high-strength fibers. Long and continuous fibers bonded to the exterior surface of the structural element. The FRP serve as supplementary steel reinforcement for flexure, shear or confinement to obtain high mechanical resistance, tensile strength and flexibility in unreinforced masonry (URM) structures. Depending on the structure it is possible to obtain different fabric geometry and strength of FRP. The cross-sectional dimensions of the wall, dome or minaret do not increase and the mass of the dome and minaret do not increase, which means that the seismic action on the structure remains unchanged. By this way, masonry structures strengthened with FRPs can resist substantial flexural stresses and generally behave linearly elastic to failure at large strain.

Table 2.3. Strengthening Methods in Masonry Structures.

Strengthening Methods in Masonry Structures	
Foundations Beneath the foundation	Application of micro piling, jet grouting to the foundations, existing on not consolidated soil, to transfer the load and improve soil properties.
Foundations Direct interventions	Widening, connecting, repairing and reinforcing the damaged, poorly dimensioned foundations to get better load distribution and improvement.
Injecting	Injecting the mortar to the existing cavities and internal voids for bonding the missing parts and sealing cracks
Jacketing	Application of self-supporting reinforced concrete cover to the parts that subjected to high compression stresses and lateral deformation, to improve the strength and provide additional strength to seismic loads.
Local tying	Fastening of confining parts on poor connected elements to develop a micro continuity in the structure.
Pre-compression	Providing counteracting compressive stresses on elements have possibility of tensile damages to avoid or close cracking.
Repointing	Improvement and reinforcement at the damaged mortar joints
Replacement	Replacement at the damaged section with similar materials
Seismic isolation	Arrangement devices between the foundation and the structure to absorb the seismic vibration.
Soil stabilization	In case of buildings with differential settlements, control piles, under excavation, jet-grouting, micro-piling are used to control differential settlements.
Structural substitution	Construction of a new structure substituting the old one to recover the functionality.

Table 2.3. Strengthening Methods in Masonry Structures.

Strengthening Methods in Masonry Structures	
Anchoring	Increasing the stability of the load bearing structures.
Buttressing	Improves the resistance to lateral forces.
Covering	Covering for increasing the strength and stiffness
Discrete confinement	Impeding the separation of supporting walls using punctual confinement.
Discrete confinement in piers	In case of piers suffering too high compressive force, steel rings are used to get punctual confinement.
Dismantling	Remove, substitute or repair some parts to restore the functionality of a structure.
Enlargement	Enlargement of the high stressed sections to distribute load to a larger section.
External reinforcement	Application of high performance materials to increase the ductility and resistance.

## 2.6. Physical Modeling

Shake-table tests are usually performed on reduced-scaled models. Physical modeling and scaling is an economical method utilizing a better understanding of the complex behavior of masonry structures due to the prohibitive cost of full scale testing of masonry systems. Moreover the physical modeling technique provides for the modeling and testing of three dimensional, complex structures under controlled conditions which are very important to determine the response of structures. In the physical model method the full-scale of a structure is called the “prototype” and the constructed replica of the full scale structure with a certain scale is called the “model”. This methodology is capable of reproducing model results which are equivalent to the prototype.

The capability of the physical model to predict the behavior of a real masonry structure is in close relation with the fulfillment of some scaling laws. In literature, two fundamental techniques are used to derive the appropriate scaling laws; dimensional analysis, and similitude theory (Sedov, 1959).

### 2.6.1. Dimensional Analysis

Dimensional analysis is a mathematical technique that uses an equation consisting of dimensionless products of powers of the physical quantities of structures. This equation is determined using the dimensionally homogeneous equation of structure with physical quantities, and identifies the same physical phenomena both in prototypes and models. Since the dimensionless products describe the same physical phenomena, it is well suited for designing model investigation and scaling relationships for models.

### 2.6.2. Similitude Theory

Similitude theory identifies the acting forces in the system and uses dimensional analysis to construct and equate dimensionless terms for the model and prototype (Sulaeman, 2010).

A model has similitude with the real structure if the two share geometric, kinematic, and dynamic similarities. These similarities are derived from a dimensional analysis of the physical phenomena and provide testing conditions capable of reproducing test results which are equal to the prototype.

### 2.6.3. Geometric Similarity

When the prototype structure and scaled model have similar geometry - such as all corresponding lengths are proportional and all corresponding angles are equal - it can be stated that they have geometric similarity. This similarity can be expressed as: (Langhaar, 1951).

$$\lambda = L_m/L_p \quad (2.5)$$

where;

L= any dimension in the prototype or model

m = model

p = prototype systems

#### 2.6.4. Kinematic Similarity

In case the prototype and model have similar velocity and acceleration time history, it can be considered that these systems have kinematic similarity.

#### 2.6.5. Dynamic Similarity

It can be considered that both prototype system and model have dynamic similarity on the condition that they have kinematic similarity and similar mass distributions (Baker *et al.*, 1973). There is a relationship between the physical quantifications of prototype systems and models. This ratio is considered as similitude coefficient  $S$ . In case of similar properties such as the yield and ultimate strengths of the materials and the stress-strain relationship between the model and prototype, it is possible to sustain the similitude of the model behavior from linear phase to nonlinear phase. Similitude parameters can be determined with respect to fundamental parameters or they have independent similitude coefficient.

A summary of scale factors for the masonry structures in civil engineering structural materials is given in Table 2.4 for the case of static loading.  $S_l$  represents the length of scaling factor and  $S_\sigma$  represents the weight or force scaling factor. For the static case, only two dimensions are involved - force and length. One therefore can select only two independent scale factors for true modeling (Schriever, 1980).

Similitude requirements for dynamically loaded structures must include an additional variable, time. Dynamic scaling coefficients are one of the most difficult and important similitude factors and can be properly defined using the Cauchy number and Froude number. The Cauchy number can be expressed as the ratio between the dynamic inertial forces and the elastic restoring forces, while the Froude number is defined as the ratio between the inertial and gravity forces. Both the Cauchy and Froude numbers have the same scale factor for the mass, which should be the inverse of the length scale factor and that the time scale factor that should be the square root of the length scale factor.

Table 2.5 summaries the Cauchy and Froude similitude relationships for some quantities more usually considered in structural engineering, where symbol M refers to the model and symbol P to the prototype (Bairrao and Vaz, 2000). According to the Cauchy similitude relationships the frequency is scaled by the square root of the scale factor based on the dynamic similitude laws requirements. In other words, the time-histories have to be compressed in time by this factor.

Similitude in the dynamic behavior as well as the failure mechanism of the prototype and model is considered to be an important factor in modeling. Distribution of masses and stiffness in the prototype and models need to be simulated. However, the failure mechanism requires similar working stress levels; that is - working stresses in load bearing walls and compressive strength of masonry of prototype and model. Although all the structural details are not precisely modeled, the global seismic behavior of a prototype building could be accurately simulated if the behavior of model wallets is similar to prototype (Tomzevic, 2000). The accuracy of prediction is in accordance with the capability of the physical model to simulate the dynamic response of the real structure. Experimental study methods for investigating masonry structure are given in Figure 2.3.

Table 2.4. Summary of scale factors for reinforced masonry structural materials (Schriever, 1980).

<b>Reinforced Masonry</b>			
		<b>Static Loading</b>	
<b>Quantity</b>	<b>Dimension</b>	<b>True Model</b>	<b>Practical True Model</b>
Masonry unit stress, $\sigma_m$	$FL^{-2}$	$S_\sigma$	1
Masonry unit strain, $\epsilon_m$	...	1	1
Modulus of masonry unit, $E_m$	$FL^{-2}$	$S_\sigma$	1
Masonry unit Poisson's ratio, $\nu_m$	...	1	1
Specific mass, $\rho_m$	$FL^{-3}$	$S_\sigma/S_1$	$S_\sigma/S_1$
Mortar stress, $\sigma'_m$	$FL^{-2}$	$S_\sigma$	1
Mortar strain, $\epsilon'_m$	...	1	1
Modulus of mortar, $E'_m$	$FL^{-2}$	$S_\sigma$	1
Mortar Poisson's ratio, $\nu'_m$	...	1	1
Reinforcement stress $\sigma_{rm}$	$FL^{-2}$	$S_\sigma$	1
Reinforcement strain, $\epsilon_{rm}$	...	1	1
Modulus of reinforcement, $E_{rm}$	$FL^{-2}$	$S_\sigma$	1

Table 2.5. Scale factors of the Cauchy and Froude similitude law.

<b>Parameter</b>	<b>Symbol</b>	<b>Cauchy similitude</b>	<b>Froude similitude</b>
Length	L	$L_p/L_m=\lambda$	$L_p/L_m=\lambda$
Elasticity modulus	E	$E_p/E_m=e=1$	$E_p/E_m=e=1$
Specific mass	$\rho$	$\rho_p/\rho_m=\rho=1$	$\rho_p/\rho_m=\rho=1$
Area	A	$A_p/A_m=\lambda^2$	$A_p/A_m=\lambda^2$
Volume	V	$V_p/V_m=\lambda^3$	$V_p/V_m=\lambda^3$
Mass	m	$m_p/m_m=\lambda^3$	$m_p/m_m=\lambda^3$
Velocity	v	$v_p/v_m=1$	$v_p/v_m=\lambda^{1/2}$
Acceleration	a	$a_p/a_m=\lambda^{-1}$	$a_p/a_m=1$
Force	F	$F_p/F_m=\lambda^2$	$F_p/F_m=\lambda^3$
Moment	M	$M_p/M_m=\lambda^3$	$M_p/M_m=\lambda^4$
Stress	$\sigma$	$\sigma_p/\sigma_m=1$	$\sigma_p/\sigma_m=\lambda$
Strain	$\epsilon$	$\epsilon_p/\epsilon_m=1$	$\epsilon_p/\epsilon_m=\lambda$
Time	t	$t_p/t_m=\lambda$	$t_p/t_m=\lambda^{1/2}$
Frequency	f	$f_p/f_m=\lambda^{-1}$	$f_p/f_m=\lambda^{-1/2}$

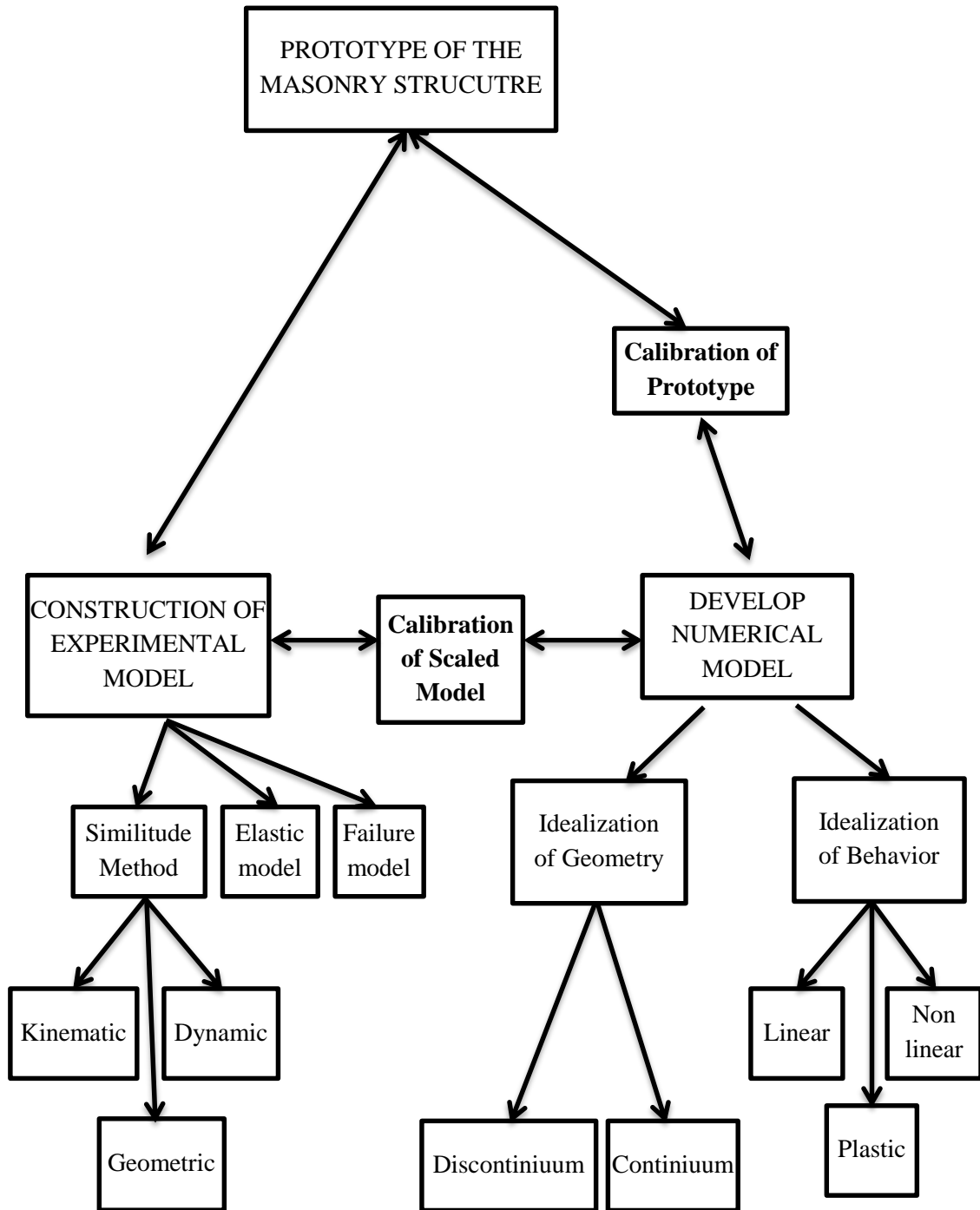


Figure 2.3. An experimental study method for investigating masonry structure.

## **2.7. Analytical (Numerical) Modeling**

### **2.7.1. Fundamentals of Analytical Modeling**

Seismic behavior analysis of a real structure is illustrated using analytical modeling in mathematical terms. The analytical modeling focuses on understanding the effects of loads, load capacity, material behavior and the load transfer mechanism within the structure. However it is a difficult subject, because of problems about representing the behavior of a real structure using non-linear material behavior.

Masonry structures have complexity of nature due to the heterogeneity of materials and some simplifications and assumptions are required for modeling. Different approaches adopted in the research field to the idealizations in modeling of masonry structures. Idealization of geometry, material behavior, boundary conditions, magnitude, direction and orientation of load are used while creating an analytical model. Material, geometry and structural behavior idealizations are fundamental simplifications and assumptions regarding the masonry structure modeling and briefly described below.

### **2.7.2. Idealization of the Geometry and Material**

The geometrical representation is difficult because there are some difficulties about understanding the response of masonry structures. Frame, shell or three dimensional solid elements are used for developing the model to perform the calculations and to analyze the results. From the point of view of material properties blocks are stiffer than mortar and stiffness of the vertical joints is smaller than the one of the horizontal joints. Using shell elements rather than solid elements is not a good choice for modeling a thick masonry wall for in-plane loading due to difficulties analyzing the results because of the variation of stresses along the thickness of the elements. The fundamental difficulties in the progress of accurate stress analysis for masonry structures are the definition and the use of appropriate material constitutive laws. Constituent materials are characterized through strength and deformation parameters, stress-strain relationships, and strength models. The physico-chemical and mechanical parameters in the interaction between the stone units and the mortar joints are due to the following factors (Ricamato, 2007):

**Effects of the stone elements:**

- Compression and tension strength with axial stresses
- Young modulus
- Poisson ratio
- Ductility and creep
- Water proof and superficial (roughness) characteristics
- Chemical agent resistance
- Volume variation for humidity
- Temperature and chemical reaction
- Weight
- Shape and holes dimensions

**Effects of the mortar:**

- Compression strength and behavior under pluri-axial stresses
- Elasticity module
- Poisson coefficient
- Ductility and creep
- Adhesive force
- Workmanship
- Plasticity
- Capacity of detaining water

**Effects of Construction formality:**

- Geometry and placing of the stone elements
- Filling of the joints at the head
- Ratio of the joint thickness and dimensions of the stone elements
- Placing hand crafty

Selection of the technically and economically correct element type to preparation of the model is based on the problem being analyzed. Taking into account the heterogeneity and anisotropy of the masonry structures, it is sometimes better to model structural parts rather than the whole structure to have less complicated results.

2.7.2.1. Idealization of the Geometry. Evaluation of the seismic responses of masonry structures depends on the desired level of accuracy, and simplicity requires assumptions about geometry. Detailed micro, simplified micro and macro modeling methods are common approaches for masonry structures. One modeling strategy cannot be preferred over the other because different application fields exist for each one, according to the complexity and detail requirements. Representations of computational strategies for masonry structures by Lourenço (1996) are given in Figure 2.4.

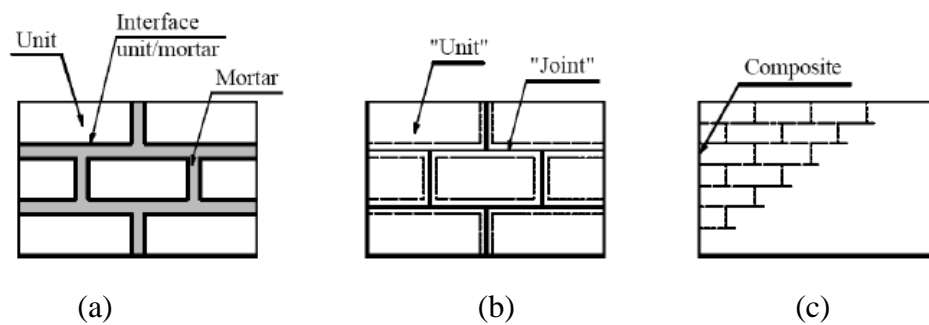


Figure 2.4. (a) Detailed micro modeling; (b) Simplified micro modeling; (c) Macro modeling (Lourenço, 1996).

Continuum models are the best methods to analyze the real behavior of large scale masonry structures in a simple manner, particularly concerning its local response. For large structural deformations, however, the anisotropy of the walls, caused by the discontinuous and blocky nature of the masonry, plays an important role and reduces the effectiveness of methods, which are based on continuum mechanics, to predict the failure mechanisms (Ricamato, 2007). These models consider constitutive equations of an equivalent homogeneous medium whose characteristics have to be obtained through homogenization procedures for mortar joints and bricks. Dis-continuum (Discrete) models consider the discretization of the brick masonry walls in terms of rigid bodies as bricks and straight interface elements as mortar joints, connecting two bricks. This methodology based on mortar joint interface as a discontinuity element that connects brick units. At each contact, the mechanical interaction between blocks is represented by a force (stress), resolved into a normal and a shear component as shown in Figure 2.5. Contact displacements are defined as the relative displacement between two blocks at the contact point.

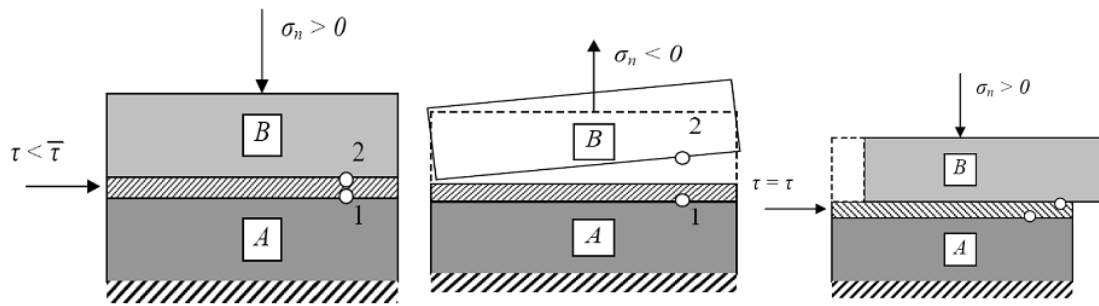


Figure 2.5. Coulomb slip model with residual strength (shear and normal behavior) (Al-Heib, 2012).

Generally structural analysis techniques concerning masonry structures do not perform advanced analysis to evaluate the dynamic behavior of the structure. These methodologies use elastic or inelastic finite element analyses, which can provide the stress distribution over the structure and the results. These results provide insight into the failure mechanisms. However the non-linear structural behavior of masonry structures depends on the mortar joints where the softening behavior can only occur. Discrete models require intensive computation and capability for treating the softening behavior of masonry structures under possible damages even after the initiation of cracking.

2.7.2.2. Detailed Micro Modeling. Detailed micro methodology considers inelastic and material properties of both units and the mortar joints separately. The block, mortar and interface are represented by different constitutive laws. Continuum models are used for units and mortar in the joints and dis-continuum models represent the unit mortar interface. Therefore this modeling allows one to characterize a possible crack or slip plane between unit mortar interfaces.

Structural response analyses are performed based on mechanical material properties such as young modulus, Poisson coefficient and the inelastic properties of the units and the mortar. These properties are estimated by conducting experimental tests such as compressive, tension, shear and bending tests. Detailed micro modeling technique requires more computational effort and time with respect to other approaches. However this method can be successfully used for reproducing laboratory tests (Lofti and Shing, 1994; Giambanco and Di Gati, 1997; Alfano and Sacco, 2006; DeJong and Vibert, 2012; Mele *et al.*, 2012).

2.7.2.3. Simplified Micro Modeling. Each joint on the simplified micro model consists of the mortar and the two unit-mortar interfaces and the behavior of mortar joints and unit mortar interface is lumped in dis-continuum elements such a whole of elastic blocks surrounded by fracture lines in the joints. The simplified micro models allow for deriving in a rational way the stress-strain relationship of the masonry, accounting in a suitable manner for the mechanical properties of each material component. Besides, this procedure can lead to effective models, with reduced computational effort for a structural analysis (Luciano and Sacco, 1997; Milani *et al.*, 2006; Mojsilovic' *et al.*, 2013). Sandoval *et al.* (2011) performed the numerical simulation of the buckling response by means of a simplified micro-model and conclude that the micro-modeling approach has shown its ability to assess the load-bearing capacity of masonry walls subjected to concentric or eccentric vertical loading.

2.7.2.4. Macro Modeling. The macro modeling technique is based on the representation of units, mortar and unit-mortar interface as a homogenous continuum which is spread in a continuum. This approach uses continuum finite elements or structural component models. The units and the mortar behavior are not distinguished, they are considered as a homogenous, anisotropic continuum. Macro modeling approach is a quite capable technique for modeling solid elements with large dimensions. With this type of modeling, less time and less material properties for mortar and unit-mortar interface are used. Experimental tests are used for defining the stress-strain relationships to use for the structural analysis. Dis-continuum models, component models and finite element models generally use macro modeling technique which has an easygoing mesh generation.

Micro modeling is the most suitable structural modeling strategy to determine the local behavior of masonry structures in detailed. This method is very effective from a computational point of view when structural analyses are performed. On the other hand, macro-modeling is more suitable when the structure is composed of walls of sufficient dimensions so that the stresses along the length of the element are uniform. So this strategy is more suitable when a compromise between accuracy and efficiency is required.

When compared to other strategies macro modeling takes less time and is less demanding in terms of modeling of geometry and mechanical properties since the duration of structural analysis depends significantly on the model dimensions.

Giordano *et al.* (2002) investigated the applicability of different numerical techniques for the analysis of masonry structures using finite element method, finite element method with discontinuous elements and discrete element modeling. They concluded that in spite of the specific limitations of each model, all three methods are able, to some extent, to correctly grasp the global behavior of the tested specimens, thus proving that they can be effectively used in the study of masonry structural elements.

Pena *et al.* (2010) created two models using finite element method. Both are three-dimensional models but one uses 3-D solid elements while the other one has 3-D composite beams. They also created 2D in-plane elements based on the rigid element method and these models were considered to evaluate the structural behavior of the minaret. This study concludes that the models present similar behavior under the same loads and types of analysis. However, the results obtained from the non-linear static and dynamic analyses indicate quite a different response of the structure to earthquakes.

Li and Atamtürktür (2013) investigated the three modeling techniques, detailed micro modeling, simplified micro modeling and macro modeling considering the accuracy and the robustness of the model predictions for a masonry dome. They concluded that the detailed micro-model proves to be the most accurate model for predicting the load carrying capacity and stiffness of the dome. The simplified micro model underestimates the stiffness of the dome with respect to the detailed model and the macro model is deemed least accurate in representing the experimental load-displacement relationship among the three models.

It is a complex topic in modeling of masonry structures to choose a suitable model representing the structure. Detailed micro modeling considers the behavior of mortar and masonry separately. Simplified micro-element represents the blocks as a continuum, however the mortar interface is assumed to be a lumped interface.

The macro models are used for plastic analysis and they represent the mechanical properties of masonry as a homogeneous material. Considering the analysis of masonry structures, it cannot be claimed that one analysis method is superior to another. The method for analytical modeling depends on the scale of the problem, the availability of the mechanical properties and the intended calculations.

### **2.7.3. Idealization of the Behavior**

The common idealizations for the analysis of the structural behavior of masonry buildings are elastic behavior, plastic behavior, and inelastic behavior.

2.7.3.1. Elastic (Linear) Behavior. The linear elastic model is the basic approach which considers that the material obeys Hooke's Law and gives general information about the behavior of the structure. According to linear behavior the materials of a masonry structure have an infinite linear elastic behavior, both in compression and tension which is not reliable under tensional loading. The common usage of an elastic model is for the verification of both ultimate limit states and serviceability limit states. With respect to the nonlinear and plastic model, idealization of an elastic behavior takes less time for input data and requirement for resources.

2.7.3.2. Plastic Behavior. Plastic analysis methods are commonly used for examining the capacity and load at failure for verification of ultimate limit states. However, the application of plastic analysis is usually valid for simple structures and not practical for the investigation of large and complex geometrical formed structures. According to the plastic analysis, masonry structures have zero tensile stress that exhibit a ductile response and infinite compressive strength result with no energy dissipation for the crack occurrence.

2.7.3.3. Inelastic (Non-linear) Behavior. Non-linear or inelastic analysis is capable for both ultimate limit states and serviceability limit states. This analysis observes the behavior of masonry structures from the elastic range through cracking and crushing up to the time of failure. Non-linear models allow for physical, geometrical, material and contact non-linearity behavior. The physical non-linearity concern that the material behaves inelastic in compression and tension.

Geometric non-linearity assumes that the point of applied loads changes with the increase of load and instability by large strains or displacements. Geometrical non-linearity has an impact on the behavior of structures that have lower tensile strength than compressive strength like masonry structures. With respect to the linear and plastic models, non-linear analysis require more time and material properties such as the compressive, shear, and tensile strength, the stress-strain relationship, Poisson's ratio and the modulus of elasticity and these material properties should be determined through experimental tests to get reasonable results.

## **2.8. Analysis**

### **2.8.1. Structural Analysis Methods**

The analyses of masonry structures have received great advances in the last decades, and it is one of the most important research fields in civil engineering, receiving great attention from the scientific and professional community. The analytical model is very important since it represents the structural behavior of the real structure in mathematical terms and it can overcome a lot of difficulties in experimental tests. In any case, it is important to know the capabilities and limitations of the analytical model to be used for predicting the seismic behavior of the real structure. Depending on the stress strain behavior and force displacement relations, structural analyses can be performed in linear or non-linear range, statically or dynamically.

2.8.1.1. Linear Analysis. In linear analysis, material obeys the elasticity law established by R. Hooke in 1676 that stress is directly proportional to strain. The theory requires the elastic properties of the material and the maximum allowable stresses and gets deformed shapes and stress distribution in the structure. This method is extensively used when the material still shows an elastic behavior. However, it has limitations and deficiencies in performing the collapse limits. In case of linear analysis, only one solution of structural equilibrium exists according to the Kirchhoff's principle of uniqueness.

Linear model is particular effective in the identification of the global behavior tendency of the building and the identification of the points where the structure is subjected to tension stresses able to break the continuity of masonry elements (Romano, 2005). Commonly, linear static and modal dynamic analyses are performed for evaluation of seismic behavior of structures. Linear static analysis based on an idealization of a linear relationship between loads and induced responses. The reliability of linear static analysis, when applied to masonry structures, is still an open research issue. This approach fails to give an idea of the structural behavior near collapse and it is recommendable to use different analysis methods for the same structure and critically compare the results.

Modal analysis is commonly used for assessing the stresses in the masonry structures based on the superimposition of independent vibration modes and linear material behavior. In spite of the fact that calculus of the frequencies and modal shapes allow one to validate the models in the elastic field, this approach provides unsatisfied information on the global behavior of the masonry structures.

2.8.1.2. Nonlinear Analysis. Masonry material presents a strongly non-linear behavior, so that linear elastic analyses generally cannot be considered as accurate tool for seismic assessment. In the last decades, the continuous increase of computational capacity has permitted the use of mathematical models which explicitly account for the non-linear static analysis and the non-linear dynamic analysis which is also called non-linear time history analysis. Dynamic response of non-linear systems can be modeled using step by step time history analysis procedures with acceptable accuracy. This method provides the model incorporates a good approximation of the system's dynamic properties, including the mass, damping and nonlinear load displacement behavior. Non-linear static analysis which is also called pushover analysis consists of the application on the structure of the vertical loads and considers self-weight and dead loads, besides horizontal forces with the system unvaryingly increasing until the reaching of the limit conditions. The accuracy of this approach is based on a proper determination of the force pattern or of the incremental control criterion of the analysis. The problems of non-linear pushover methods counterbalance to some extent the limits of linear analysis.

2.8.1.3. Limit Analysis. The limit analysis which has been developed mainly by Heyman (1966) is used in the assessment of the collapse loads of curved masonry structures. This approach based on constituent blocks possesses infinite compressive strength and zero tensile strength joints, and sliding between masonry units cannot occur. This methodology is not practical for explaining the cause and the extension of the cracks and strains not developed by collapse generation since generally failure occurs with some sliding or crushing of the material. Non-linear dynamic analysis is used for seismic assessment and design retrofitting strategies for existing materials or for the use of new materials for designing new structures. This methodology requires the elastic and inelastic properties and the strength of the material. Non-linear dynamic analysis allows assessing the complete loading process, from the initial stress-free state, through the weakly non-linear behavior under service loading, up to the strongly non-linear behavior leading to collapse. The strain behavior, the stress distribution and the collapse mechanism of the structure are obtained which proved to be efficient in preventing destructive consequences from earthquakes.

There are a numbers of works in the literature which address the characterization of the behavior of masonry subjected to monotonic compression or shear-compression loading (Sinha, 1978; Calvi, 1996; Magenes and Calvi, 1997; Syrmankezis and Asteris, 2001). Naraine and Sinha (1989) investigated the deformation characteristics of brick masonry with low levels of compressive strength under cyclic loading. This research was later extended to the deformation characteristics of brick masonry with higher levels of compressive strength subjected to uniaxial cyclic and biaxial cyclic loading in (AlShebani and Sinha, 1999; 2000). Generally papers and researches propose two or more analysis types, identifying the advantages and disadvantages, comparing and contrasting the results and the reliability for predicting the structural response of masonry structures particularly in the field of finite and discrete element analyses (Milani *et al.*, 2006; Casolo and Peña, 2007; Brasile *et al.*, 2007; Calderini and Lagomarsino, 2008; Calìò *et al.*, 2008; Belmouden and Lestuzzi, 2009). Button and Mayes (1992) created an analytical model to predict the out-of-plane seismic behavior of reinforced masonry walls and the model was calibrated using full-scale dynamic tests results by Blondet *et al.* (1990). Lagomarsino *et al.* (1998) introduces the approach of macro elements combined to collapse mechanisms applied on churches.

Zhuge *et al.* (1998) presented an analytical model for studying the response of unreinforced masonry under in-plane dynamic loads and calibration of this model with various experimental tests. Pegon *et al.* (2001) investigate the approach of 2D and 3D modeling to design a representative model of a built cultural heritage structure to test at the laboratory and to characterize its behavior. Details on the models, starting from mesh generation and material description up to their non-linear results are given. Performance-based concepts are discussed and applied in seismic assessment, rehabilitation and design of unreinforced masonry buildings in (Abrams, 2001). Comparing the computed results of physical non-linear analysis and limit analysis on a masonry arch, Lourenco (2002) yield the same failure mechanisms and safety factors, if a zero tensile strength is assumed. Giordano and De Luca (2002) investigate the applicability of different modeling techniques by comparing models of ABAQUS, CASTEM 2000, UDEC with experimental test data obtained on a full scale model. Salonikios (2003) presented the results of comparative pushover analyses of masonry plane frames performed on SAP2000 Nonlinear and CAST3M software. Griffith *et al.* (2004) investigated the dynamic analysis of unreinforced masonry walls subjected to out-of plane loading and ground acceleration using single degree of freedom system. Wu *et al.* (2005) use the finite element method for dynamic analysis of masonry walls. They conclude that the damage assessment methods such as ductility or the inter-story drift that is commonly adopted in earthquake engineering are not applicable for assessing the structure response to blast excitations and the out-of-plane damage of the masonry walls is a lot more severe than the in-plane damage. Hamed and Rabinovitch (2008) proposed an analytical model for the non-linear dynamic behavior of unreinforced masonry walls subjected to out of plane loading. This model accounts for the rocking effects, geometric non-linearity and the non-linear constitutive behavior of the materials. They compare the results with test results available in literature and the theoretical model can describe the decrease in the natural frequency with the increase of amplitude of vibration. Penna *et al.* (2013) presented a procedure for the identification of limit states describing the global building performance, i.e. taking into account not only the peak concentrated damage in a single element, but also the diffusion of damage through the different structural elements and the evolution of the global collapse mechanism. Theodossopoulos and Sinha (2013) reviewed the current analytical trends with regards to their ability to improve practice in the design of modern structures or the repair of historic fabric.

### 3. MODELING MUSTAFA PAŞA MOSQUE IN SKOPJE

#### 3.1. Introduction

The Mustafa Paşa Mosque is located in Skopje, Macedonia. It is a masonry building constructed in 1492 during the Ottoman era (Figure 3.1). The structural framework of the monument is typical of mosques in the provinces of the Ottoman Empire. The mosque has a square plan and is topped by a monumental dome supported by a polygonal tambour and four pendentives. The dimensions of the main square area are 20 m × 20 m. The diameter of the dome spanning over the main part is about 16 m. The main structure is about 22 m high. The massive walls and the tambour of the dome are composed of two exterior layers of natural stone, brick and mortar combination with an inner core of stone and brick rubble set in lime mortar, in accordance with the typical construction technique of Byzantine churches in Macedonia (Portioli *et al.*, 2011). The dome is of brick masonry. The minaret of the Mustafa Paşa Mosque is 42 m high. It is constructed of cut-stone.



Figure 3.1. Image of Mustafa Paşa Mosque in Skopje, Macedonia (Tashkov *et al.*, 2012).

The bilateral project “Harmonization of the testing procedure of large scale and medium scale models on seismic shake table” was carried out by the Department of Earthquake Engineering of Boğaziçi University, Kandilli Observatory and Earthquake Research Institute (KOERI), Istanbul, Turkey and the Institute of Earthquake Engineering and Engineering Seismology (IZIIS), Skopje, Macedonia.

Within the scope of the project a reduced-scale model of the Mustafa Paşa Mosque was constructed in Istanbul and was subject to shake table testing in the shake table laboratory of the Department of Earthquake Engineering. The aim of the project was to compare the performance of models of different scales. In this particular case the two models were the 1:6 scale model of the Mustafa Paşa Mosque built and tested in Skopje; and the 1:10 scale model of the same mosque built and tested in Istanbul.

The 1:10 scale model constructed in Istanbul and the data obtained from the sensors on it during its testing on the shake table are the starting point of this chapter. The original bilateral project program involved only testing of the model until damage is invoked. We have extended the experimental program so that it included testing of the base-isolated model and that of the strengthened model. The results of this three-stage program are used in the calibration/validation of the numerical model created on the basis of the 1:10 scale model built for shake table testing. Our aim is to develop a 3D distinct element model that represents the linear and nonlinear behavior of the shake table model as closely as possible during three stages of testing: base-isolated model, the model as it is and strengthened model.

This chapter starts with sections that describe the development of the 1:10 scale model of the Mustafa Paşa Mosque. The construction process is outlined and several material tests conducted are presented. These sections are followed by those which explain the shake table testing program, instrumentation of the model, and ground motion selection and preparation. Details of the numerical model that is developed using distinct element approach are provided. Finally, comparisons of results of numerical analyses with those from the three-stage experimental program are given and discussed in three consequent sections.

### 3.2. Development of Test Structure

The experimental study was carried out in the shake-table facility of the Department of Earthquake Engineering of Boğaziçi University, in 2012. The preparation of the physical model involved the study of several aspects related to the reproduction of the main geometrical, physical and behavioral characteristics of the original mosque. Therefore, in the first place, because of the shaking table size and load capacity, the model was geometrically reduced to adopt a geometrical scale factor of 1:10. Due to the limited size of the shake table, the overall dimensions of the model became 2.01 m × 2.01 m in plan and 2.20 m in height. The minaret has a height of 4.00 m. The model was constructed based on the gravity forces neglected approach. As a consequence of the reduction factor, all phenomena involved in the dynamic tests that were being set are scaled according to a similitude law (Tashkov *et al.*, 2012). For satisfying the similitude requirements the forces in the model are also reduced by 1:10 to produce the same elastic stress and strain level in test structure.

#### 3.2.1. Construction of the Shake Table Model

The test structure was constructed off the shake table by professional masons. A steel plate with plan dimensions similar to shake table was prepared. It had two beams that stiffened the plate, assisted the placement of the foundation of the model and at the same time bore the hooks to be used during the transfer of the model on to the shake table. First the foundation of the model, which is basically a square, is constructed. Then the walls, the pendentives, the drum and the dome were completed. Finally the minaret of the mosque was constructed up until 1.75 m elevation. The walls of the body of the mosque were built in three layers through their thickness. The two exterior layers, 6 cm thick each, are made of stone, brick and lime mortar. The 6 cm thick interior layer is, an infill of mortar, brick and stone fragments. The total thickness of the walls is 18 cm. The pendentives are made of masonry in brick and lime mortar. The drum is made of stone, brick and lime mortar and has 0.23 m height. The outer diameter of the drum is 188 cm and the inner diameter is 162 cm. The thickness of the brick masonry dome is 12 cm. The outer diameter of the dome is 174 cm. The inner diameter is 150 cm. The minaret is constructed in two stages.

The lower part of the minaret, built in the first stage, is embedded in the wall of the mosque. This part rises until 1.75 m elevation that is basically the dome base level. The outer diameter of the minaret is 30 cm. The inner diameter is 18 cm (Figure 3.2).

For transporting the model, strong wide ropes were attached through hinges to the foundation plate (Figure 3.3). A rectangular steel frame placed between the crane and the model prevented the contact between the model walls and the ropes. The test structure was then lifted with the help of a crane. Once the test structure was secured to the shake table, professional masons constructed the minaret up to 4 m height. Upon completion of the construction of the mosque, a month of curing time was allowed before the start of the experiments (Figure 3.3).



(a)



(b)



(c)



(d)

Figure 3.2. Images of 1:10 scale model of the Mustafa Paşa Mosque during its construction (a,b,c,d).



(e)

(f)

Figure 3.2. Images of 1:10 scale model of the Mustafa Paşa Mosque during its construction (e,f).



Figure 3.3. Images of 1:10 scale model of the Mustafa Paşa Mosque during its transfer on to the shake table.

### 3.2.2. Material Testing

Evaluation of material properties of any existing masonry structure has a significant difficulty during the structural assessment due to large variations in material properties, that can be attributed to composite nature of masonry, to variations in workmanship during construction (i.e. mason qualities), to weathering, to reconstructions, additions, and repair. An inadequate material characterization may lead to unrealistic structural assessment results. A reliable analysis requires the material properties to be determined through experimental testing.

For the case of Mustafa Paşa Mosque model mortar, compression and shear tests performed are on masonry prisms and masonry panels in the Materials Laboratory of the Department of Civil Engineering of, Boğaziçi University. (<http://ce.boun.edu.tr/en/construction-materials-laboratory>). Mortar mixes were prepared before the start of wall construction, as the aim was the determination of the most realistic mixture for the masonry. Once the mix is decided on, samples were prepared and tested for their tensile strength. The samples for compression and shear testing were prepared during the construction of the model wall. The dimensions of the specimens used for mortar tests are 40 mm x 40 mm x 160 mm. The dimensions of the specimens used for compression and shear tests are 400 mm x 400 mm x 200 mm. The results of these compression and shear tests were used in calibrating and validating the analytical model of the test structure and to document the state of the test structure at the beginning of the shake-table experiments as a point of reference when discussing the results of these experiments.

In the following subsections mortar, compression and shear testing procedures are explained, tests carried out on samples of the model are described and their results are presented.

3.2.2.1. Mortar Test. European Standard for masonry mortar EN 1015-11:1999 defines for hardened mortar performances related to flexural and compressive strength. This European Standard indicates no difference between testing historic or new construction mortar (ES 1999). For determination of flexural strength it specifies a specimen with dimensions of 40 mm x 40 mm x 160 mm to be tested under three-point bending. A total of 10 mortar mixture combinations were prepared in accordance with EN 1015-11:1999. Mortar mixture combinations used for the specimens are given in Table 3.1. Compression and shear tests were performed on 40 mm x 40 mm x 160 mm mortar samples. The shear test setup is such that the middle third of the span of the specimen is subjected to bending moment as shown in Figure 3.4. The results of three samples of combination 1, 2, 3 and one sample of combination 5 and 7 are given in Table 3.2. The model tested at IZIIS has a scale factor of 1:6. Since the strength characteristics of the mortar should be directly proportional to the geometrical scale, the ratio between the 1:6 and 1:10 which is 1.7 was used to determine the strength values of the 1:10 model mortar. Mortar characteristics of the 1:10 model were defined by dividing the shear and compression strengths of 1/6 model by 1.7 (For the 1:6 scale model the mortar characteristics were:  $\sigma_c = 0,5$  MPa ;  $\sigma_t = 0.4$  MPa.) (Tashkov, 2012). The closest values to these were yielded by mixture 1, which had  $\sigma_c = 0.4$  MPa (compression strength), and  $\sigma_s = 0.2$  MPa (shear strength) (Table 3.2) and as such was chosen for the construction of the 1/10 model.

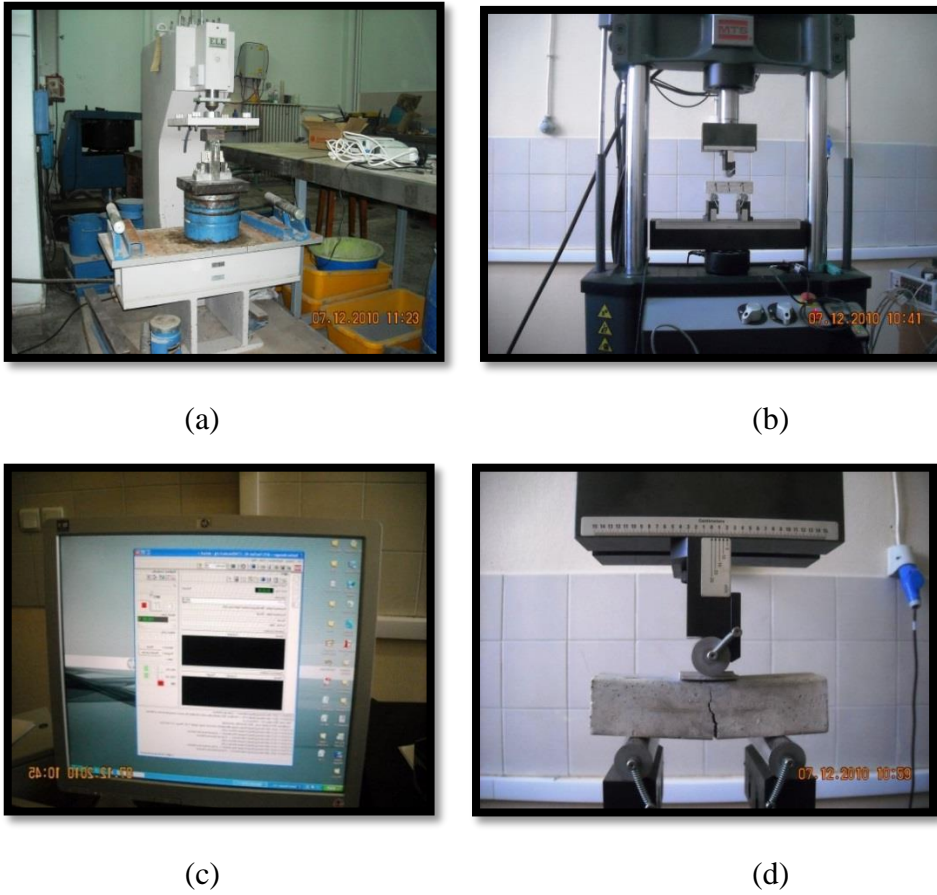


Figure 3.4. Test set up for mortar testing (a, b), the control software (c) and the mortar specimen in failure (d) at the Materials Laboratory of Department of Civil Engineering, Boğaziçi University.

Table 3.1. Mortar Mixture Combinations.

No of mix	BASF	Lime	Sand	Water
1	1		3	1
2	1		4	1
3	1		5	1
4	1		6	1
5		1	3	1
6		1	4	1
7		1	5	1
8		1	6	1
9		1	5	2
10		1	6	2

Table 3.2. Compression and tension strength results for mortar samples.

No of sample	Shear force (N)	Shear strength (MPa)	Comp. force (N)	Comp. Strength (MPa)
1-1	66		600	
1-2	76		690	
1-3	76		600	
<b>average</b>	<b>72,7</b>	<b>0.17</b>	<b>630</b>	<b>0.39</b>
2-1	73		500	
2-2	61		530	
2-3	/		440	
<b>average</b>	<b>68,5</b>	<b>0.16</b>	<b>490</b>	<b>0.31</b>
3-1	23		470	
3-2	46		360	
3-3	39		400	
<b>average</b>	<b>36</b>	<b>0.08</b>	<b>410</b>	<b>0.26</b>
5-1	12	0.03	260	0.16
7-1	11	0.025	290	

3.2.2.2. Compression Tests. Three masonry prisms were prepared at the time of the construction of the wall of the mosque model. The prisms were capped and secured to two steel plates on top and bottom. Their dimensions were 400 mm x 400 mm x 200 mm. They were tested under uniaxial compression 28 days after their preparation in accordance with ASTM C 1314. Axial load and the axial displacement between the two steel plates of the masonry prisms were recorded. Figure 3.4 shows the configuration of the masonry prism tests. Expected failure force of compression tests is determined using the equation of;

$$P = a \times d \times \sigma_c \quad (3.1)$$

$$P = 400 \times 200 \times 0.4 = 32 \text{ kN}$$

Although expected failure force determined as 32 kN, four specimens did not failed under axial compression of 210 kN. Due to limit of the testing machine, the masonry compressive strength,  $f'_m$ , could not calculated by testing masonry prisms.

3.2.2.3. Diagonal Tension (Shear) Tests. In order to determine the shear strength of masonry, diagonal tension (shear) tests were performed on three specimens with dimensions of 400 mm x 400 mm x 200 mm. The specimens were loaded in compression along their diagonal, and the applied load and its corresponding vertical according to the requirements of the ASTM E 519-02. Horizontal deformations were recorded. The loading cause diagonal cracking along an axis parallel to the direction of loading. The load was applied until the collapse of the specimens. Compression and shear test set up and a failure mode specimen under diagonal tension test is shown in Figure 3.5. Following the ASTM E 519-02 standard, shear stress for specimens is calculated from the experimental test. Expected failure force for diagonal shear tests is determined by;

$$P = a \times d \times \sigma_s \times \cos 45 \quad (3.2)$$

$$P = 400 \times 200 \times 0.2 \times 0.707 = 11.3 \text{ kN}$$

The shear stress,  $\tau$  calculated using the equation;

$$\tau = \frac{\cos 45 \times P}{A_n} \quad (3.3)$$

where,  $P$  is the applied load and  $A_n$  is the net area of the specimen calculated as follow:

$$\tau = \left( \frac{w+h}{2} \right) t \times n \quad (3.4)$$

where,  $w$  is the width of specimen,  $h$  is the height of specimen;  $t$  is the total thickness and  $n$  is the percent of the gross area of the unit that is solid. In this study  $n = 1$  was adopted.

The applied peak compressive force and shear stress for the three specimens obtained by diagonal shear tests is given in Table 3.3.

Table 3.3. Diagonal shear test results for masonry specimens.

Masonry Specimen	$P_{max}$ (N)	$\tau$ (MPa)
1	68000	0.6
2	81900	0.7
3	82000	0.7



(a)



(b)



(c)



(d)

Figure 3.5. Compression (a, b) and shear test setup (c), and failure mode of a specimen during shear test (d). Images taken during testing at the Materials Laboratory of Department of Civil Engineering of Boğaziçi University.

### 3.3. Shake Table Testing

#### 3.3.1. Description of the DEE-KOERI Shake Table

The shake table facility at the Department of Earthquake Engineering of Kandilli Observatory and Earthquake Research Institute of Boğaziçi University houses a 3 m x 3 m shake table, its actuator, sensors of several types utilized to measure motion during testing, the control system to command the table and to send data to and receive data from the sensors for instrumentation, a crane with 15 t capacity and peripheral equipment to assist at several stages of testing. The following description of the shake-table, is get from the link [http://www.koeri.boun.edu.tr/Research/ShakIng%20Table%20Laboratory\\_13\\_140.depmuh](http://www.koeri.boun.edu.tr/Research/ShakIng%20Table%20Laboratory_13_140.depmuh)

The shake table has a size 3 m × 3 m. ANCO R-148 type uniaxial shake table driven by a servo-hydraulic actuator. It is used to reproduce earthquake motion within the capacities of force, velocity, displacement, and frequency of the system for dynamic testing and research (Figure 3.6). Table is capable of shaking test objects up to 10 tons with 2 g acceleration over a frequency range of 0-50 Hz. The tabletop is of welded steel construction and has tapped holes for attaching test items to the table. The table has precision ground rails, which engage eleven roller linear bearings on the base to allow for the desired linear horizontal motion. The foundation is designed to minimize vibration transmitted to the soil and structures surrounding the table. The system is provided with a dual 60 HP motor 30 GPM hydraulic pump to supply a total of 60 GPM at 3,000 PSI continuous. Table motion and data acquisition are carried out by a Data Physics 550 WIN digital data control and acquisition system. The maximum displacement of the shake table in the horizontal directions is limited to + - 12 cm. The maximum velocity of the table is limited by its hydraulic system and it is +-1.2 m/s. In There exist smaller size shake tables in the shake table facility. The information on them can be found at link: [http://www.koeri.boun.edu.tr/Research/ShakIng%20Table%20Laboratory\\_13\\_140.depmuh](http://www.koeri.boun.edu.tr/Research/ShakIng%20Table%20Laboratory_13_140.depmuh)

### 3.3.2. Instrumentation of the Model

The model was instrumented with the help of accelerometers, and displacement transducers. The instrumental setup can be seen in Figures 3.7 to 3.9. Altogether ten uniaxial accelerometers, seven triaxial accelerometers, one LVDT and three laser displacement transducers were employed. Eight uniaxial accelerometers were utilized in the instrumentation of the minaret. Four of them were installed parallel to the excitation direction of the shake table at 1.75 m, 2.45 m, 3.25 m and 3.90 m heights of the minaret. Remaining four accelerometers were placed at the same heights but in the perpendicular direction to the first group. Two uniaxial accelerometers were installed directly onto the shake table in orthogonal directions (Figure 3.8). Seven tri-axial accelerometers were utilized during the shake table experiments. Four of them were installed on the four top corners of the walls, one was placed on top of the dome, one on the drum, and finally one tri-axial accelerometer was fixed to the shake tabletop (Figure 3.8).

Four displacement transducers were employed during the tests. Three laser transducers were installed parallel to the excitation direction of the shake table at three different levels: on the top of the dome, at dome base (i.e. top of the wall) and at the shake tabletop (Figure 3.9). One LVDT was attached on one of the model walls (Figure 3.8, Figure 3.9).



Figure 3.6. Image of shake table at the Department of Earthquake Engineering of Kandilli Observatory and Earthquake Research Institute of Boğaziçi University.

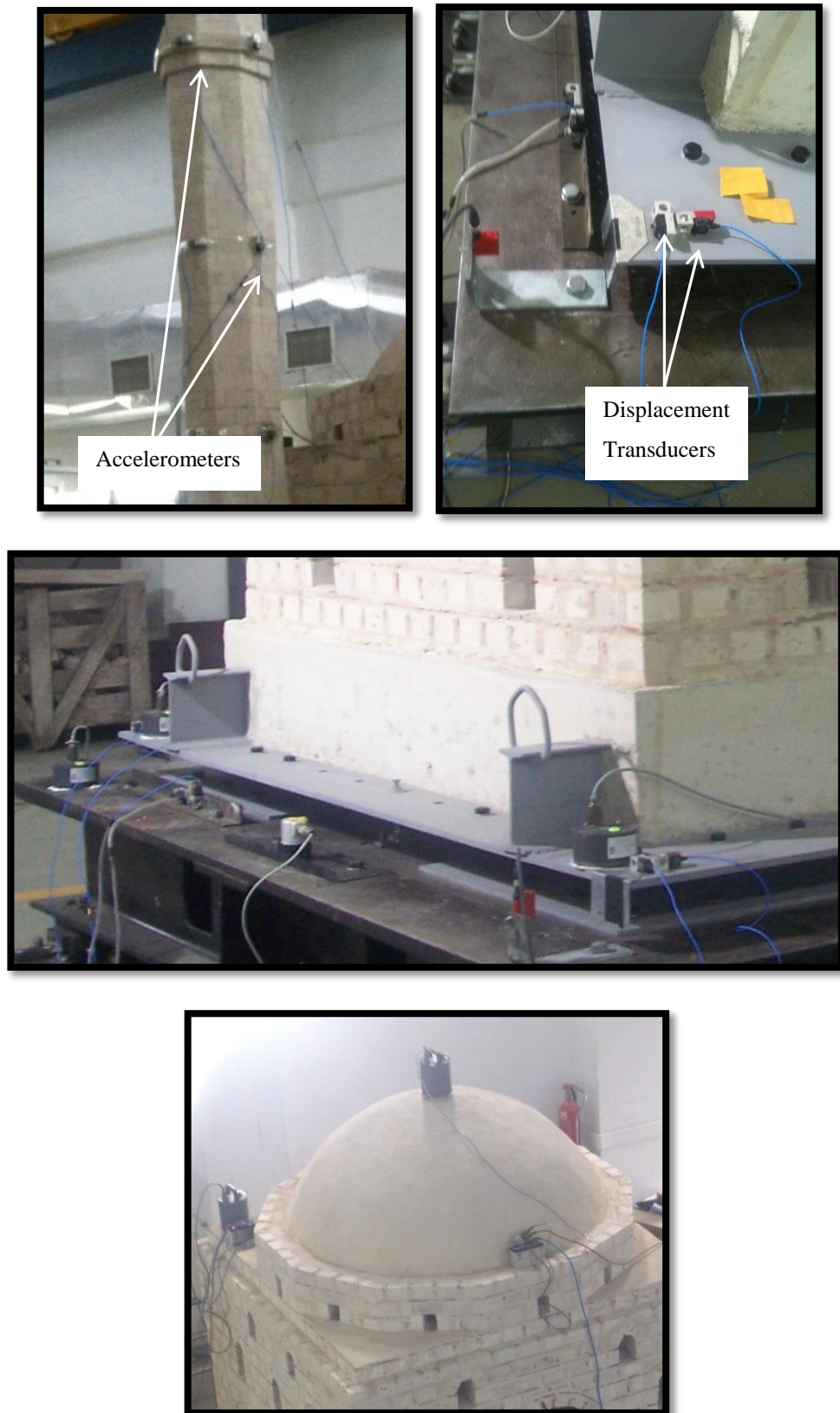


Figure 3.7. Accelerometer installation and displacement transducer set up (1).

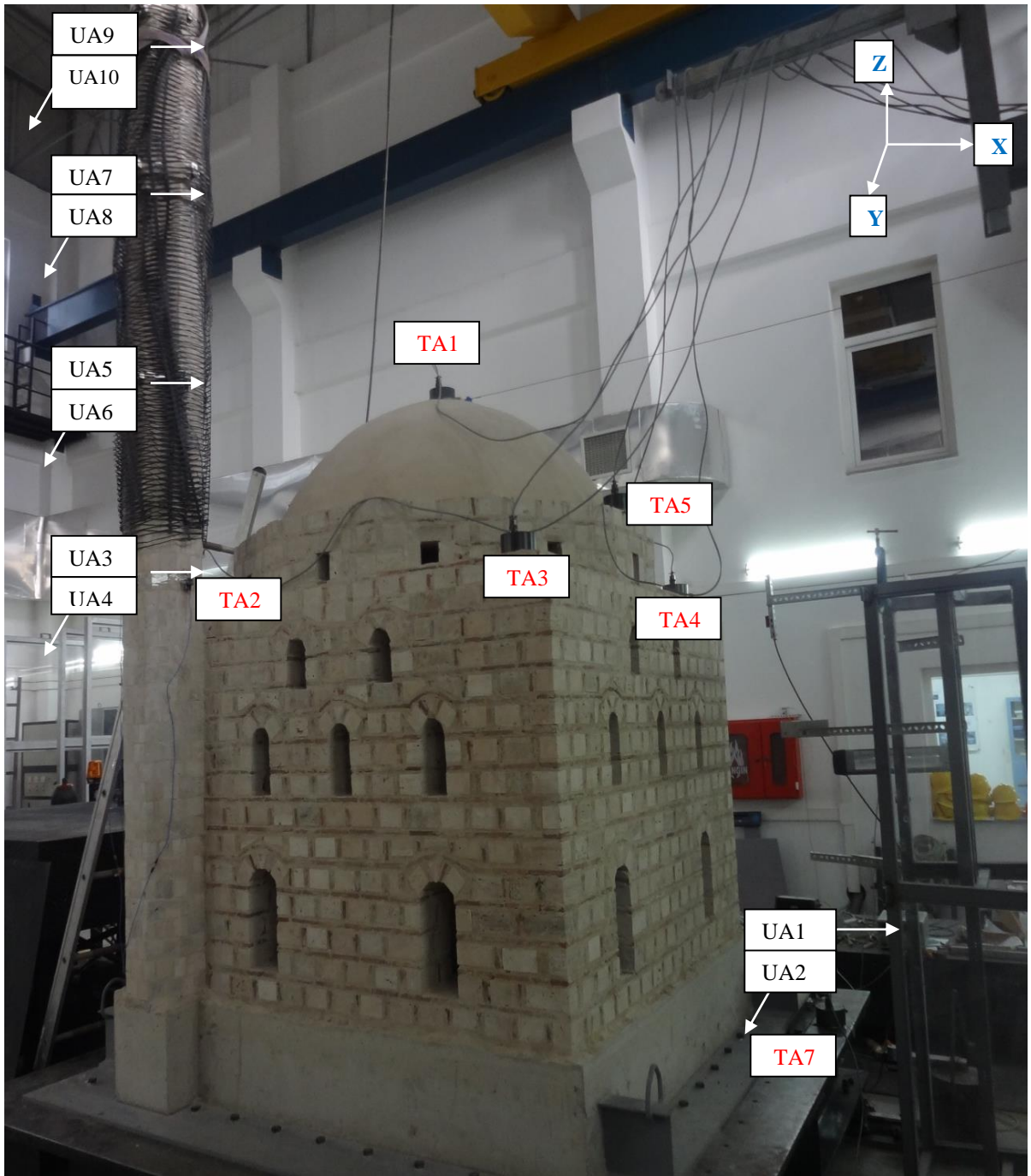


Figure 3.8. Accelerometer installation and displacement transducer set up (2).

UA1 -UA10: Uniaxial Accelerometers (g)

TA1 –TA7: Tri-axial Accelerometers (g) (TA6 placed at the opposite corner of TA3)

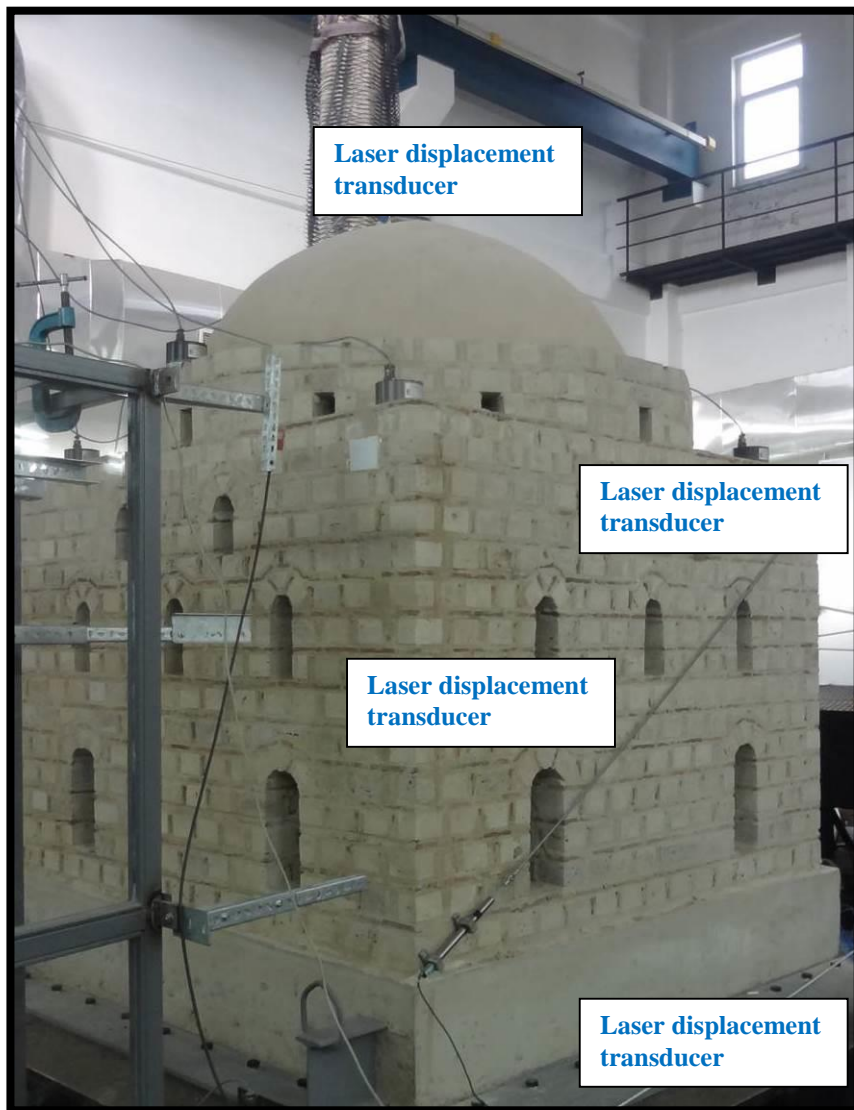
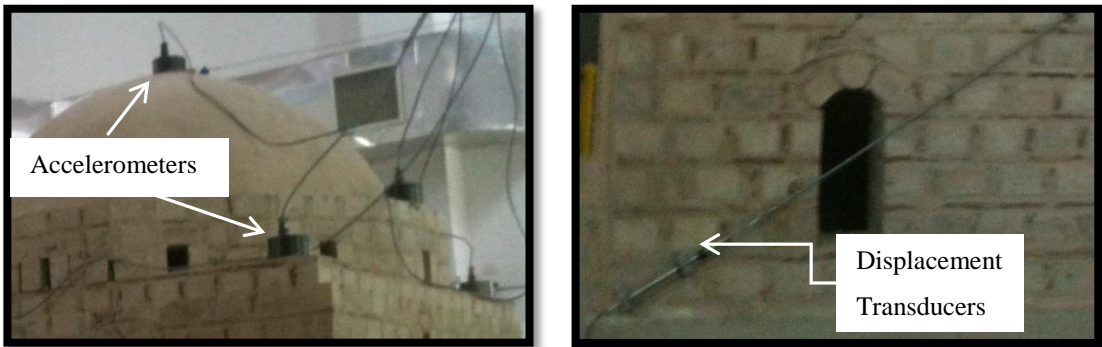


Figure 3.9. Accelerometer installation and displacement transducer set up (3).

### 3.3.3. Preparation of Input Motion

North-south component of the Montenegro (1979) and that of the Sakarya record of the Kocaeli Earthquake (1999) were intended to be applied as unidirectional horizontal motions to the model. The ground motion records were compressed in time to satisfy the similitude requirements and to account for the reduced scale of the model (Sabnis *et al.*, 1983). The model parameters and scaling factors for the model is defined based on the gravity forces neglected approach. The model parameters and scaling ratios are given in Table 3.4 (Tashkov *et al.*, 2012). The selected input data were filtered using a trapezoidal band-pass filter. By this way the high-frequency and the low-frequency content that exceeds the range and displacement limits of the shake table is removed. The earthquake excitation was applied to the model until crack initiation and further damage in a sequence that involved motions of increasing amplitudes.

Table 3.4. Similitude laws for the model (Tashkov *et al.*, 2012).

Scaling Parameters	Scaling Factor	Units	Prototype values	Adopted values Model 1/10
Length	$I_r$	m	20/20	2.0/2.0
Time history	$I_r$	sec	60	6
Natural frequency	$I_r^{-1}$	Hz	3.0	30
Gravity acceleration	neglected			
Input acceleration	$I_r^{-1}$	g	0.1-0.2g	1.0-2.0g
Mass density	$I$	kN/m <sup>3</sup>	19	19
Strain	$I$	μstr	1	1
Modulus of elasticity	$I$	MPa	6800	6800
Compressive strength	$I$	MPa	27	27
Shear strength	$I$	MPa		
stone	$I$	MPa	0.15	0.15
brick	$I$	MPa	4.7	4.7
mortar	$I$	MPa	0.1	0.1
Displacement	$I_r$	mm	1	1/10
Force	$I_r^2$	kN	1	1/100

### 3.3.4. Testing Program and Results

A three-stage experimental program was followed: (1) testing of the base-isolated model, (2) testing of the model as it is and (3) testing of the strengthened model.

During the first-stage of testing the model was installed by four rubber isolators. Isolators had a shear modulus of 0.551 MPa and their dimensions were 15 cm x 15 cm x 8.5 cm. They were fixed to the tabletop with the help of steel plates. The steel plates were fixed first to the table top (Figure 3.10). Then the four bearings were placed on them (Figure 3.10). The model was transferred to the shake table and placed directly on the bearings with the bearings coinciding with the four corners of the model foundation (Figure 3.10). The base isolated model was tested under one directional and properly scaled Montenegro (1979) Earthquake. Ten input motion were used to perform the tests and repeated under sequentially increased input motion with amplitudes scaled between 10 % and 100 %. In these tests four uniaxial and eleven triaxial accelerometers were used to measure the acceleration in the direction parallel to the shake table excitation. Three of uniaxial accelerometers were installed on the corners of the foundation. One uniaxial accelerometer was placed on the table level. Locations of instruments used in the base isolated shake-table experiments given in Figure 3.8. Sample acceleration recordings observed during part one is given in Figure 3.11. The aim of this part is to evaluate the efficiency of the isolators. No damage is intended to be induced.



(a) Fixing steel plates to the table top



(b) Placing bearings



(c) Transporting model to shaketable



(d) Isolated model

Figure 3.10. Supporting the test structure with four isolators.

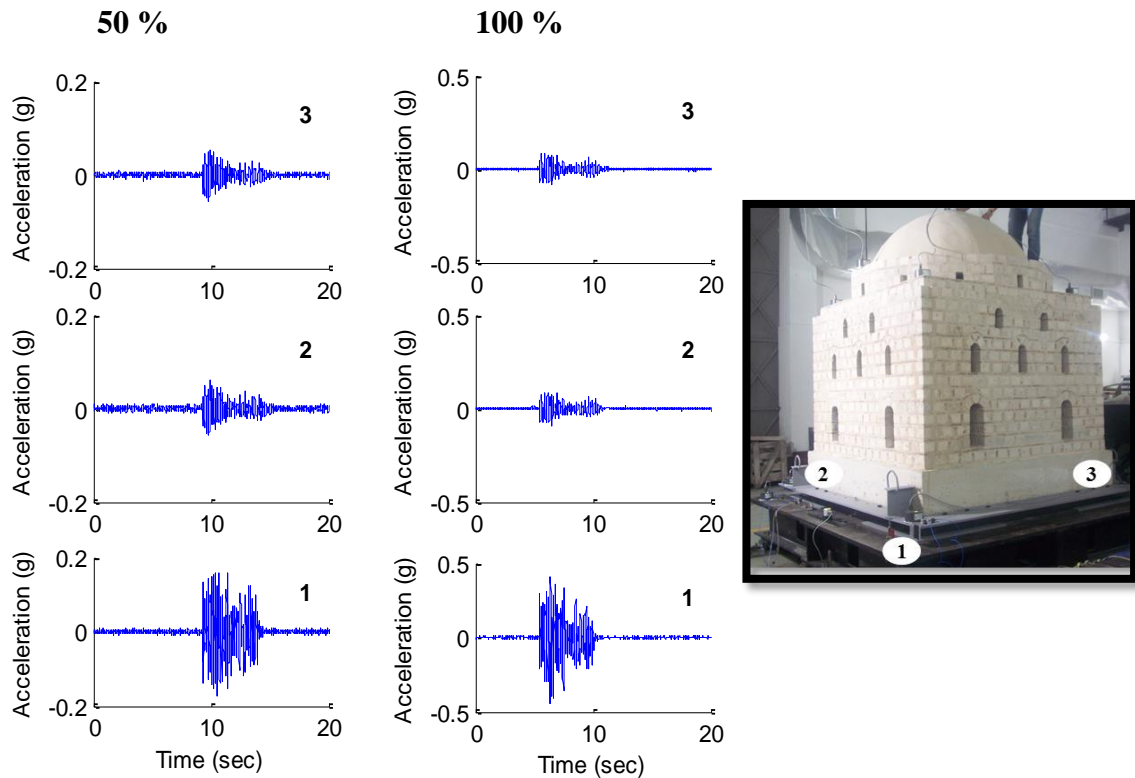


Figure 3.11. Time domain shake table output observed during stage one (base-isolated model). Left: 50 % Montenegro Earthquake. Right: 100 % Montenegro Earthquake.

For stage two, base isolators were removed. Following that, the model, which received no damage in the previous stage, was bolted directly to the shake tabletop. The construction of the minaret was completed. A total of 26 tests were performed using the Montenegro Earthquake record that was sequentially increased from 5 % to 250 % taking peak acceleration of the original record as reference. A total of 3 tests have been performed with the Sakarya Earthquake data that was scaled for 30 %, 70 % and 80 % of peak acceleration. The tests were recorded on video. Example records can be seen in Figure 3.12. The first crack was observed in the minaret right after 155 % Montenegro input. It developed slightly above the accelerometer at 1.75 m height as shown in Figure 3.13. The minaret is adjacent to the body of the model up until the base of the drum that supports the dome. The crack initiated just above this level, above which the minaret rises as a free-standing structural element. Before this level of input ground motion, the minaret behaved as a monolithic body as can be seen from the displacements, which are all in phase, particularly during the free vibration part of recorded motion after the termination of input (Figure 3.14).

At higher amplitude input motions the part of the minaret above the crack started to rock. The rocking could be seen with naked eye. Additionally, it is evidenced from the displacement plots presented in Figure 3.14, where we see rocking at the tail of the input associated with three instruments installed above the crack. Displacements from the instruments at the minaret base and at 1.75 m elevation right below the crack are completely different than those above them. At input amplitudes larger than 155 % Montenegro, cracks started to develop in the body of the model. Preliminarily they were observed at the corners of the openings in the drum and in the walls (Figure 3.15). The cracks in the drum preceded those in the walls. They slowly started to propagate down through the walls and up to the dome. In the walls they jumped from opening to opening following a diagonal path (Figure 3.15). Stones were displaced, some of them fell. In the dome both horizontal and vertical cracks developed. The vertical cracks were mostly continuation of the cracks that started in the drum (Figure 3.16). A horizontal crack at the base of dome where it sits on the drum was also observed (Figure 3.16).

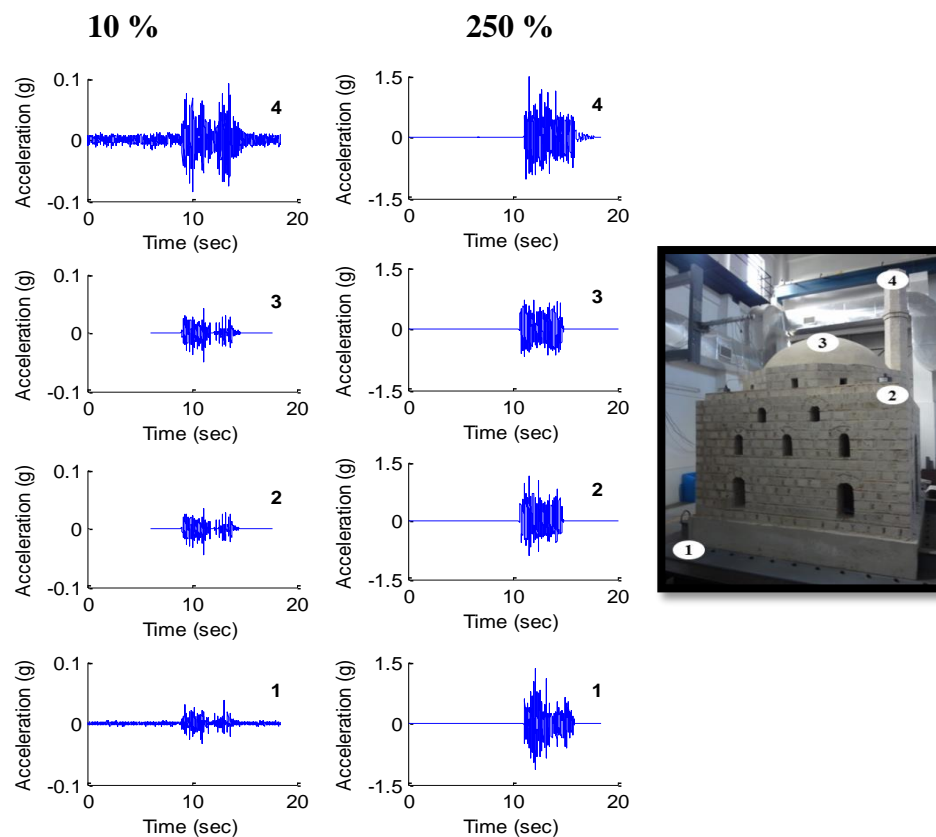


Figure 3.12. Time domain shake table output observed during stage two (model as it is).

Left: 10 % Montenegro Earthquake. Right: 250 % Montenegro Earthquake.

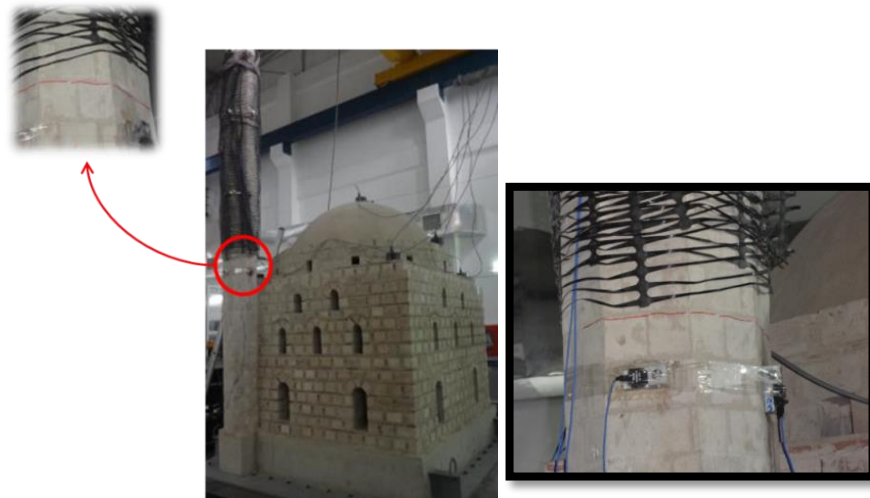


Figure 3.13. Image of the first crack in the minaret right after 155 % Montenegro input.

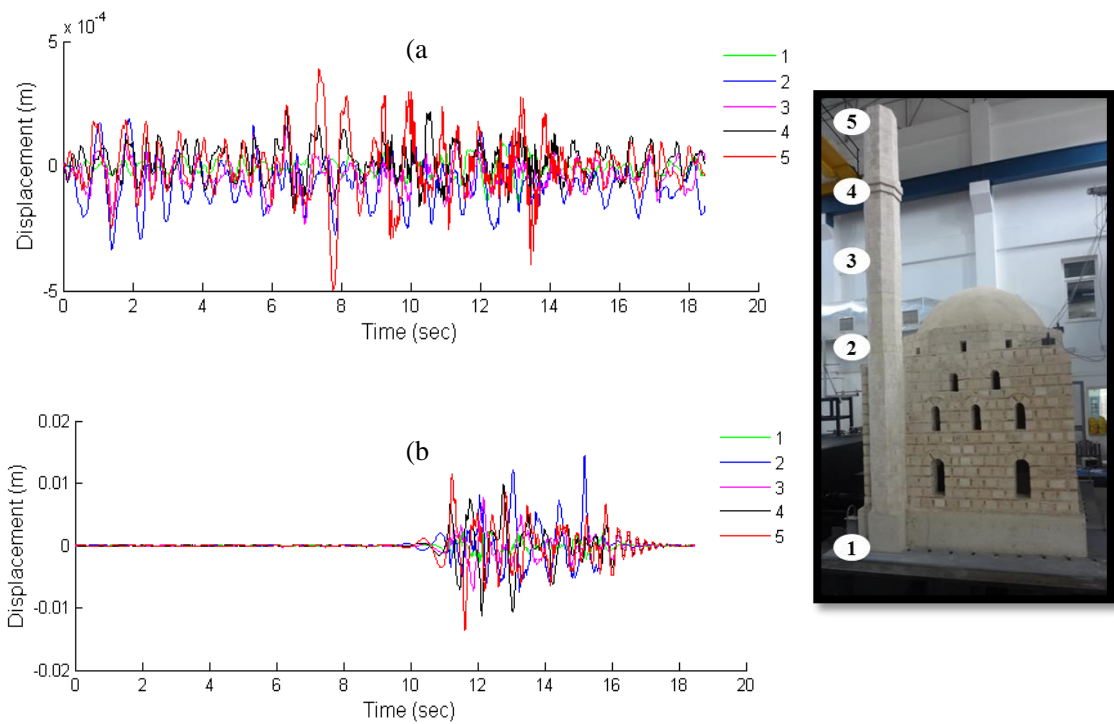


Figure 3.14. Displacement time histories observed during stage two (model as it is). Top: 10 % Montenegro Earthquake. Bottom: 250 % Montenegro Earthquake.



Figure 3.15. Damage to the drum, walls and dome.



Figure 3.16. Damage to the experimental model, details from the windows and the dome base.

As part of the final stage of the testing program, the model that was damaged in the previous stage was strengthened by crack injection and with the help of Fiber Reinforced Polymers (FRPs). Strengthening was performed using the same approach and same type of materials that were employed in the strengthening of the 1:6 scale model built and tested in Skopje (Tashkov *et al.*, 2012). Strengthening of 1:10 scaled test structure (Mustafa Paşa Mosque) by FRPs consists of few steps. The installation procedure was fast, easy and less dangerous for the operator, when compared with traditional strengthening techniques. Firstly the surfaces that FRPs will be applied on main wall of mosque, dome and minaret were cleaned. Following to cleaning a very thin layer of primer was applied to the surfaces by brushes. Secondly; a layer of tack coat composed of high-viscosity epoxy, about 1mm thick was applied to the surfaces. Then; saturated fabric bonded and pressed on to the tack coat few hours after the application of the tack coat component to ensure complete bond and removal of any air bubbles. The structure strengthened with FRPs dried in ambient temperature within a few hours and it cured in a week.

Images of the strengthened model are given in Figure 3.17. Strengthened model was subjected to the same ground motion as in stage one and two with amplitudes scaled between 20 % and 400 %. Example records can be seen in Figure 3.18. The goal of this part was to investigate the performance of FRP strengthening through comparisons with the results of stage two. Twenty four input motion having different amplitudes were applied to the model and acceleration data were recorded. The orientations of accelerometers are same as part two. The first cracks on the minaret were observed at 250 % Montenegro input while on the mosque model the initial cracks appeared in the drum at 275 % input data. During the excitation levels following 275 % Montenegro, the cracks continued to develop in the drum. The damage was quite very concentrated in the drum. With increasing excitation levels the stones beneath the FRP layer confining the dome base started to displace. At 400 % Montenegro input, the dome was sliding independently along the full horizontal crack developed in the drum. Images of described damage can be found in Figure 3.19.



Figure 3.17. Images from FRP application (upper two images) and the strengthened model.

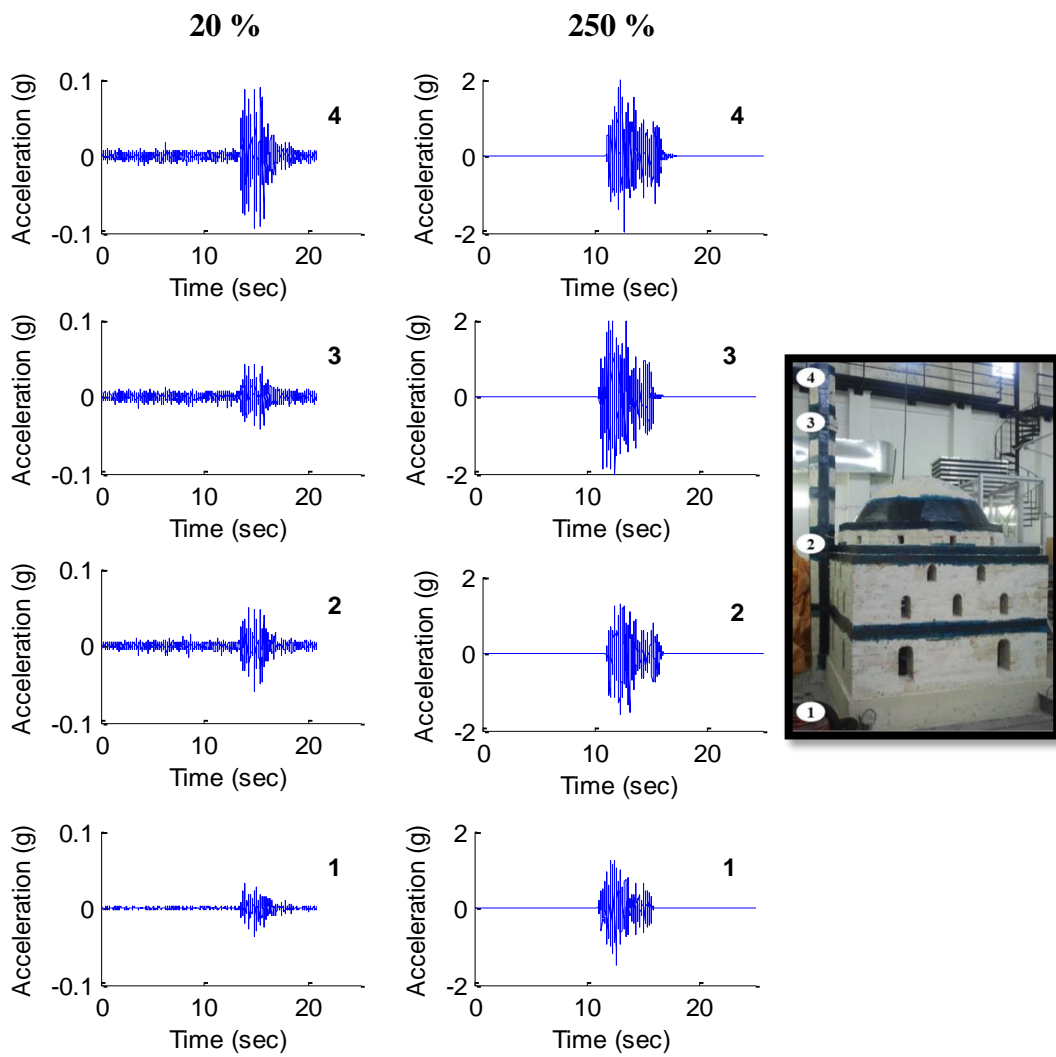


Figure 3.18. Time domain shake table output observed during stage three (strengthened model.) left: 20 % Montenegro Earthquake, right: 250 % Montenegro Earthquake.



Figure 3.19. Damage to the strengthened model, details from the windows and the dome base.

### 3.4. Development of the Distinct Element Model

Development of a reliable analytical model is very important since it aims to represent the structural behavior of a real structure in mathematical terms. The purpose for preparing an analytical model is to create the model that satisfactorily represents the effects of static and dynamic loads on a structure. Particularly for historical masonry constructions, it is difficult to select the best, technically suitable method to create the analytical model because construction materials have a complex nature.

In order to fully understand the behavior of the 1:10 scale shake table model, a numerical model was developed. The three dimensional numerical model was created in 3DEC environment. The model is shown in Figure 3.20. 3DEC is a three-dimensional numerical program based on the distinct element method for dis-continuum modeling and applicable to simulate progressive failure associated with crack propagation.

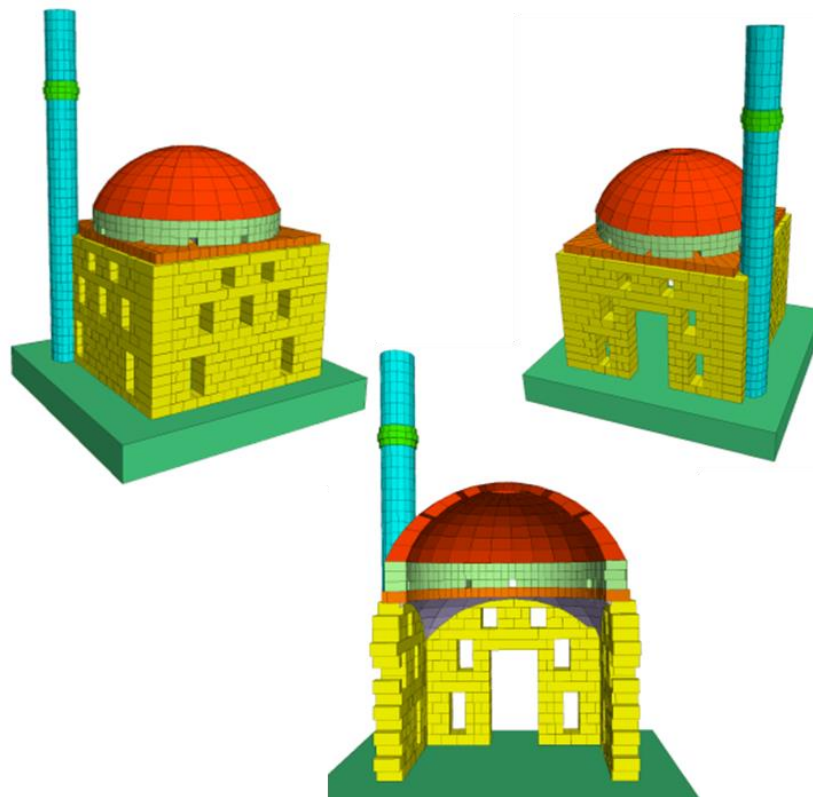


Figure 3. 20. Numerical model developed using 3DEC.

### 3.4.1. Modeling Assumptions and Contacts

The solutions of 3DEC based on the numerical integration in time of the equations of motion of the system by means of an explicit finite difference method. The explicit solution procedure uses small time-stepping for numerical stability and this methodology allows a general analysis to assess the joint separation and sliding. In this study, rigid blocks are employed at the numerical model because rigid blocks significantly reduce computation time and have advantages in time stepping algorithms. In rigid block models, all the system deformation is lumped at the joints. This assumption provides a good approximation to the behavior of masonry structures built in stiff, strong materials, since most of the deformation of the system, as well as the failure mechanisms, originate at the joints. All material models for rigid blocks in 3DEC assume an isotropic material behavior in the elastic range described by two elastic constants (bulk modulus,  $K$ , and shear modulus,  $G$ ). The elastic constants,  $K$  and  $G$ , are used in 3DEC instead of Young's modulus,  $E$ , and Poisson's ratio,  $\nu$ , because it is believed that bulk and shear moduli correspond to more fundamental aspects of material behavior than do Young's modulus and Poisson's ratio (Lemos, 2007).

The equations to convert from  $(E, \nu)$  to  $(K, G)$  are:

$$K = E/3(1 - 2\nu) \quad (3.5)$$

$$G = E/2(1 + \nu) \quad (3.6)$$

The equations of translational and rotational motion for rigid blocks are expressed by the following equations and a central finite difference procedure is used to integrate the equations of motion (Itasca, 2013).

- **Translational motion**

Translational motion for a single block is expressed as (Itasca, 2013);

$$\ddot{x}_i + \alpha \dot{x}_i = \frac{F_i}{m} + g_i \quad (3.7)$$

where

$\ddot{x}_i$  = the acceleration of the block centroid;

$\dot{x}_i$  = the velocity of the block centroid;

$\alpha$  = the viscous (mass-proportional) damping constant;

$m$  = the block mass;

$g_i$  = the gravity acceleration vector.

The translational velocities at time  $t$  described are calculated by;

$$\dot{x}_i(t) = \frac{1}{2} \left[ \dot{x}_{i1} \left[ t - \frac{\Delta t}{2} \right] + \dot{x}_{i1} \left[ t + \frac{\Delta t}{2} \right] \right] \quad (3.8)$$

$$\ddot{x}_i(t) = \frac{1}{\Delta t} \left[ \dot{x}_i \left[ t + \frac{\Delta t}{2} \right] - \dot{x}_i \left[ t - \frac{\Delta t}{2} \right] \right] \quad (3.9)$$

And for the velocities at time  $[t + (\Delta t/2)]$ ;

$$\dot{x}_i \left( t + \frac{\Delta t}{2} \right) = \left[ D_1 \dot{x}_i \left[ t - \frac{\Delta t}{2} \right] + \left[ \frac{F_i(t)}{m} + g_i \right] \Delta t \right] D_2 \quad (3.10)$$

$$D_1 = 1 - \left( \alpha \frac{\Delta t}{2} \right), \quad D_2 = \frac{1}{1 + \left( \alpha \frac{\Delta t}{2} \right)} \quad (3.11)$$

The increments of translation velocity are expressed as;

$$\Delta x_i = \dot{x}_i \left[ t + \frac{\Delta t}{2} \right] \Delta t \quad (3.12)$$

- **Rotational motion**

The rotational motion of an undamped rigid body is expressed as (Itasca, 2013);

$$I_1 \dot{\omega}_1 + (I_3 - I_2) \omega_3 \omega_2 = M_1 \quad (3.13)$$

$$I_2 \dot{\omega}_2 + (I_1 - I_3) \omega_1 \omega_3 = M_2 \quad (3.14)$$

$$I_3 \dot{\omega}_3 + (I_2 - I_1) \omega_2 \omega_1 = M_3 \quad (3.15)$$

where

$I_1, I_2, I_3$  = principal moments of inertia of the block;

$\dot{\omega}_1, \dot{\omega}_2, \dot{\omega}_3$  = angular accelerations about the principal axes;

$\omega_1, \omega_2, \omega_3$  = angular velocities about the principal axes;

$M_1, M_2, M_3$  = components of torque applied to the block referred to the principal axis.

The rotational velocities at time  $t$  in terms of the values at mid-intervals are determined by:

$$\omega_i(t) = \frac{1}{2} \left[ \omega_i \left[ t - \frac{\Delta t}{2} \right] + \omega_i \left[ t + \frac{\Delta t}{2} \right] \right] \quad (3.16)$$

Accelerations are calculated by;

$$\dot{\omega}_i(t) = \frac{1}{\Delta t} \left[ \omega_i \left[ t + \frac{\Delta t}{2} \right] - \omega_i \left[ t - \frac{\Delta t}{2} \right] \right] \quad (3.17)$$

For the velocities at time  $[t + (\Delta t/2)]$  ;

$$\omega_i \left( t + \frac{\Delta t}{2} \right) = \left[ D_1 \omega_i \left[ t - \frac{\Delta t}{2} \right] + \left[ \frac{M_i(t)}{m} \Delta t \right] \right] D_2 \quad (3.18)$$

$$\text{and } D_1 = 1 - \left( \alpha \frac{\Delta t}{2} \right), \quad D_2 = \frac{1}{1 + \left( \alpha \frac{\Delta t}{2} \right)} \quad (3.19)$$

The increments of rotation are expressed as;

$$\Delta \theta_i = \omega_i \left[ t + \frac{\Delta t}{2} \right] \Delta t \quad (3.20)$$

For a single block, the positions of the block centroid are updated by;

$$x_i(t + \Delta t) = x_i(t) + \Delta x_i \quad (3.21)$$

For group of joined blocks, firstly the motion is calculated for the master block, whose mass, moment of inertia and centroid position are modified to represent the group of blocks, and then the new position of the centroid and vertices of the other blocks are determined using the equation of ;

$$x_i^{\vartheta}(t + \Delta t) = x_i^{\vartheta}(t) + \Delta x_i + e_{ijk} \Delta \theta_i [x_k^{\vartheta}(t) - x_k(t)] \quad (3.22)$$

Tensile, shear strength and cohesion and friction parameters control the nonlinear behavior of masonry structures since the flexural and diagonal cracks and failures occur between the unit-mortar interfaces. The characteristic failure surface for the Mohr–Coulomb type failure criteria is widely used in numerical modeling of masonry structures. (Lourenco, 1996; Giambanco and Gati, 1997; Lourenço and Rots, 1997; Giambanco *et al.*, 2001; Chaimoon and Attard, 2007; Chaimoon and Attard, 2009; Spada *et al.*, 2009; Augenti and Parisi, 2011). In this study a Mohr–Coulomb type failure criterion is used to represent the mortar interfaces, where the nonlinear behavior is assumed to be concentrated for the numerical modeling of mosque. A Mohr–Coulomb type failure criterion that requires the failure condition to be satisfied on a potential failure plane corresponding to a maximum of the failure function was adapted for shear and compression parameters. The unit – mortar interface model and the evolution of joint behavior under normal and shear loads shown in Figure 3.21 and Figure 3.22.

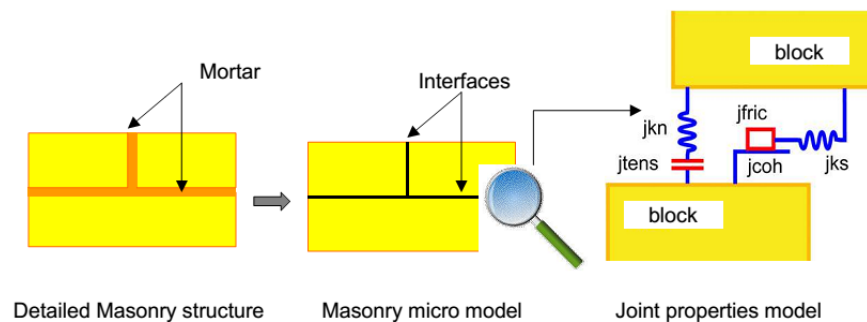


Figure 3.21. Interface model (Idris *et al.*, 2009).

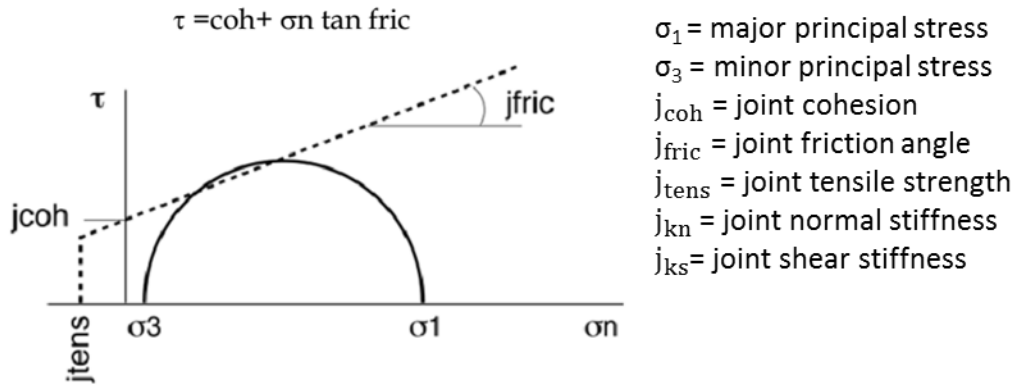


Figure 3.22. Elasto-plastic Mohr-Coulomb joint model (Itasca, 2000).

Assume a plane that bisects the space between the blocks, referred as *common plane*, and if a block face is in contact with the common plan, then it is discretized in to sub-contacts. Maximum joint tensile strength,  $T_{max}$ , is calculated using area of the sub-contact,  $A_c$ . In case of a joint that do not have previous slip or separation, there is a following relationship between the tensile normal force,  $F^n$ , and the shear force,  $F^S$  (Itasca, 2013),

$$T_{max} = -TA_c \quad (3.23)$$

$$F_{max}^S = cA_c + F^n \tan \emptyset \quad (3.24)$$

where

$c$  = the joint cohesion stress;

$\emptyset$  = the friction angle.

In the event of tensile or shear failure at the sub-contact,  $A_c$ , then the tensile strength and cohesion are considered as zero. This sudden decrease of strength approaches the “*displacement-weakening*” behavior of a joint. The new contact forces are updated base on the below described procedure and the shear force displacement magnitude,  $F^S$ , expressed by the equation of (Itasca, 2013);

$$F^S = (F_i^S F_i^S)^{1/2} \quad (3.25)$$

In case of tensile failure:

$$\text{If } F^n < T_{max}, \text{ then } F^n = 0 \text{ and } F_i^S = 0 \quad (3.26)$$

In case of shear failure:

$$\text{If } F^S > F_{max}^S, \text{ then } F_i^S := F_i^S \frac{F_{max}^S}{F^S} \quad (3.27)$$

The objective of the static analysis is to absorb the vibrational energy as rapidly as possible. In that condition, viscous damping is defined for the blocks; this causes energy to be absorbed in proportion to the rate of change of kinetic energy. For dynamic analysis, a certain fraction of critical damping over a given frequency range to energy loss is required. Two types of damping, mass proportional and stiffness proportional, are available in 3DEC. Mass proportional damping applies a force that is proportional to absolute velocity and mass while the force applied by stiffness proportional damping is proportional to incremental stiffness matrix multiplied by relative velocities to contacts. The equation of Rayleigh damping,  $C$ , is typically expressed in a matrix form;

$$C = \alpha M + \beta K \quad (3.28)$$

where

$\alpha$  = the mass proportional damping constant;

$\beta$  = the stiffness proportional damping constant.

In case of multi degree of systems, the critical damping ratio,  $\xi_i$ , at any angular frequency of the system,  $\omega_i$ , is calculated from (Bathe and Wilson, 1976),

$$\alpha + \beta \omega_i^2 = 2\omega_i \xi_i \quad (3.29)$$

Rayleigh damping is frequency dependent but has a “flat” region that spans about a 3:1 frequency range, as shown in Figure 3.23 that shows the variation of the normalized critical damping ratio with angular frequency,  $\omega_i$ . As shown in figure mass-proportional damping is dominant at lower angular frequency ranges, while stiffness proportional damping dominates at higher angular frequencies (Itasca, 2013). The required input parameters for Rayleigh damping in 3DEC are fundamental frequency,  $f_{min}$  and  $\xi_{min}$  where

$$\xi_{min} = (\alpha \beta)^{\frac{1}{2}} \quad (3.30)$$

$$\omega_{min} = (\alpha/\beta)^{\frac{1}{2}} \quad (3.31)$$

$$f_{min} = \omega_{min}/2\pi \quad (3.32)$$

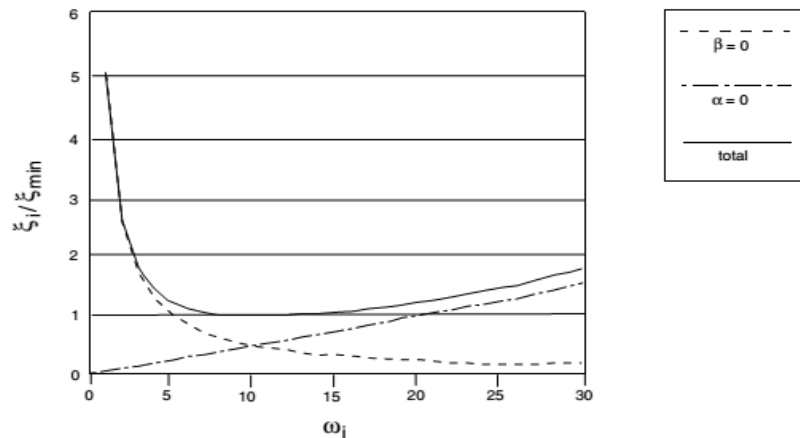


Figure 3. 23. Variation of normalized critical damping ratio with angular frequency (Itasca, 2013).

For dynamic analyses of masonry models, instead of stiffness proportional damping, mass proportional damping is used to damp the natural oscillation modes of the models and this provides to limit high-frequency vibrations which can cause erroneous computational results. Because the introduction of stiffness proportional damping highly increased the integration steps which made the dynamic analysis practically impossible.

3DEC requires the mass density for every non-void material in a model. This property has units of mass divided by volume, and does not include the gravitational acceleration. Unit weight was given with units of force divided by volume, then this value was divided by the gravitational acceleration before entering it as 3DEC input for density.

Firstly model parameters in 3DEC were defined according to the material test results. However the numerical model could not match the natural frequency of the experimental model, in the initial runs as would be expected. The new material properties were estimated by trial and error to yield frequencies similar to those obtained experimentally. During first trials the minaret behaved in accordance with experimental results while the model body and the dome still did not yield results similar to those recorded during shake table tests. Thus it was decided to specify joint normal and shear stiffness of the main walls and the dome larger than the minaret to minimize joint deformations with respect to the minaret. Since the frictional behavior plays a leading role in shear, the cohesion and tension properties of the minaret were defined comparably lower than those assigned to the main body and dome.

The friction angle of the minaret was specified smaller than 50 so that it allowed sliding cracks in minaret and comparable results with the experiments. Different levels of damping were set for the model main body and minaret. The model body and the dome were assigned 6 % damping while the minaret was assigned 2 % damping in order to match the amplitudes of time history responses from the shaking table tests. The natural frequency of the minaret of the experimental model is 12.11 Hz which is very similar to the value obtained numerically (12.43 Hz). Table 3.5 represents the material properties used in the dynamic nonlinear analyses.  $j_{kn}$  is the joint normal stiffness and  $j_{ks}$  is the joint normal stiffness.

Table 3.5. Nonlinear material properties.

		<b>Joints</b>				
		<b>Minaret</b>	<b>Minaret balcony</b>	<b>Mosque body</b>	<b>Dome</b>	<b>Pendantives</b>
<b>Horizontal joints</b>	<b><math>j_{kn}</math> (kN/m)</b>	5.67E+6	1.13E+6	4.54E+7	3.49E+7	4.54E+7
	<b><math>j_{ks}</math> (kN/m)</b>	2.27E+6	4.54E+5	1.82E+7	1.40E+7	1.82E+7
	<b>Cohesion (kPa)</b>	80	200	800	800	1.00E+20
	<b>Tension (kPa)</b>	40	100	400	400	1.00E+20
<b>Vertical joints</b>	<b><math>j_{kn}</math> (kN/m)</b>	5.67E+6	1.13E+6	3.03E+07	2.52E+7	3.03E+7
	<b><math>j_{ks}</math> (kN/m)</b>	2.27E+6	4.54E+5	1.21E+07	1.01E+7	1.21E+7
	<b>Cohesion (kPa)</b>	80	400	800	800	1.00E+20
	<b>Tension (kPa)</b>	40	200	400	400	1.00E+20
<b>Friction Angle (°)</b>		35	35	35	35	35
<b>Density (<math>10^3\text{kg/m}^3</math>)</b>		1.886	1.886	1.886	1.886	1.886

### 3.5. Numerical Investigation of the Distinct Element Model with Base Isolation and Comparison with Experimental Data

For the representation of the base isolation system installed beneath the shake table model, additional elements needed to be defined in 3DEC. For that we have used rigid blocks to represent the base isolation system that act as viscous dampers in the shear direction.

The joint normal,  $j_{kn}$  and joint stiffness,  $j_{ks}$  properties between base and foundation blocks were defined as elastic to avoid separation or slip between the two blocks. These properties were calculated based on Mohr Coulomb joint model using the shear modulus of base isolators used at the experimental tests. Damping is defined by trial and error to reach amplitudes similar to between experimental results. Mechanical properties of base isolators are the same as those used in the experimental model given in Table 3.6.

Table 3.6. Mechanical properties of base isolators (Erdik, 2012).

<b>Dimension (m)</b>	0.15 x 0.15 x 0.085
<b>Shear modulus (MPa)</b>	0.551
<b><math>j_{kn}</math> (kN/m)</b>	3.47E+07
<b><math>j_{ks}</math> (kN/m)</b>	6.49E+04
<b>Damping (%)</b>	0.06

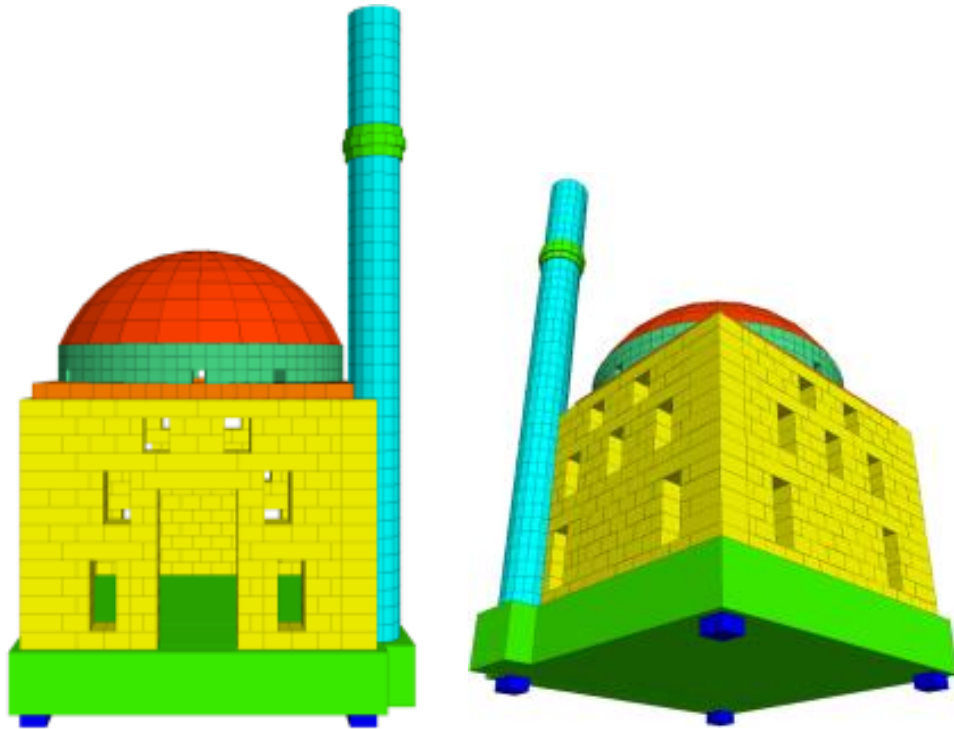


Figure 3.24. Numerical model with elements representing isolators.

The numerical model developed for the representation of base isolation consists of 1784 rigid blocks (Figure 3.24). The maximum unbalanced force is determined at time step 8.892E-06. 3DEC took a longer time in small time stepping since the solution time increases as more contacts are created. For this reason only the strong motion part of input motion was applied to the numerical model.

Comparison of numerical model results and experimental results of base isolated test structure under 50 %, 70 % and 100 % of Montenegro Earthquake in terms of velocity time history and FAS (Fourier amplitude spectrum) are given from Figure 3.25 to Figure 3.30. The primary point of interest for the assessment of base isolation modeling is the foundation level, which is located right above the isolators. The comparison of recorded and estimated motion in time and frequency domains at this location will provide the best information on the efficiency of our modeling.

They are provided at four points: at three corners of the foundation and the base level. The input motion to the numerical model is applied below the four isolators, as is the case during the shake table testing. Under larger amplitude input motions (> 70 % Montenegro) the results show a very reasonable agreement between experimental and analytical results with amplitudes and frequencies exhibiting deviations in an acceptable range (Figure 3.28 and Figure 3.30). Analytical and experimental results become more similar to each other under 100 % Montenegro input (Figure 3.29 and Figure 3.30). The dominant frequency of the mosque model is estimated to be in the range of 20-25 Hz. From the FAS in Figures 3.25 to 3.30 we observe that the energy is concentrated in the 0-5 Hz range. This shows the performance of the isolators, at the same time it shows the numerical model response with isolators is good enough. The peak at about 4 Hz, which exists in both experimental and numerical data (Figure 3.30) is not related to the modal response of the shake table model, as we expect it to be effective at higher frequencies. It is excited during the experiments and replicated well during the analyses. In Figure 3.31 the variation of peak experimental and analytical velocities are plotted. The variation of frequencies corresponding to peak FAS, with respect to the change in the amplitude of input motion are plotted (Figure 3.32). As shown, peak experimental and analytical velocities and FAS stabilize starting with 70 % Montenegro Earthquake loading.

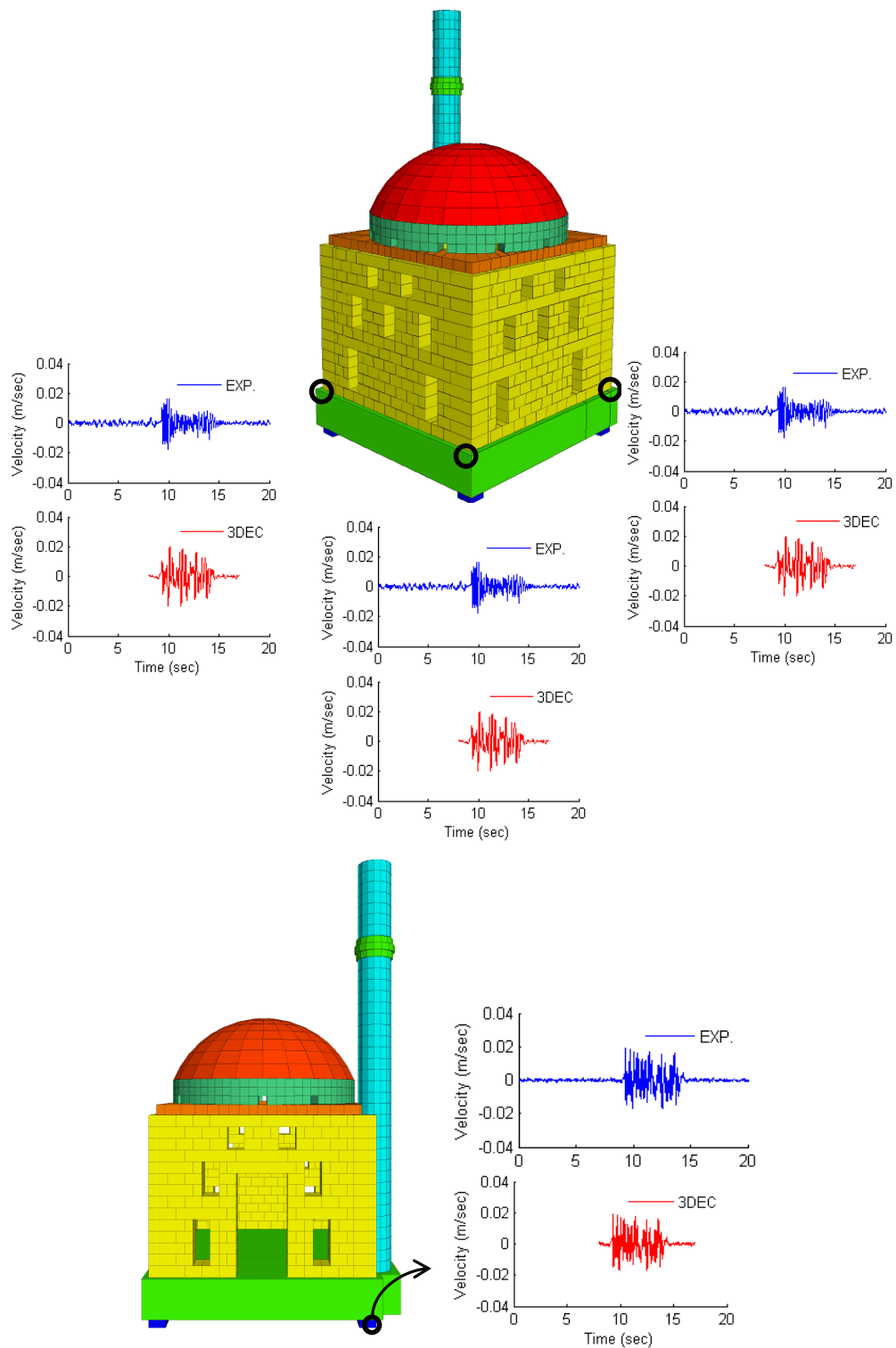


Figure 3.25. Velocity time history comparisons between isolated experimental and numerical model under 50 % Montenegro Earthquake. The input to the numerical model is applied under the four isolators. Comparisons are provided at four locations: at the isolation level and at the three corners of the foundation.

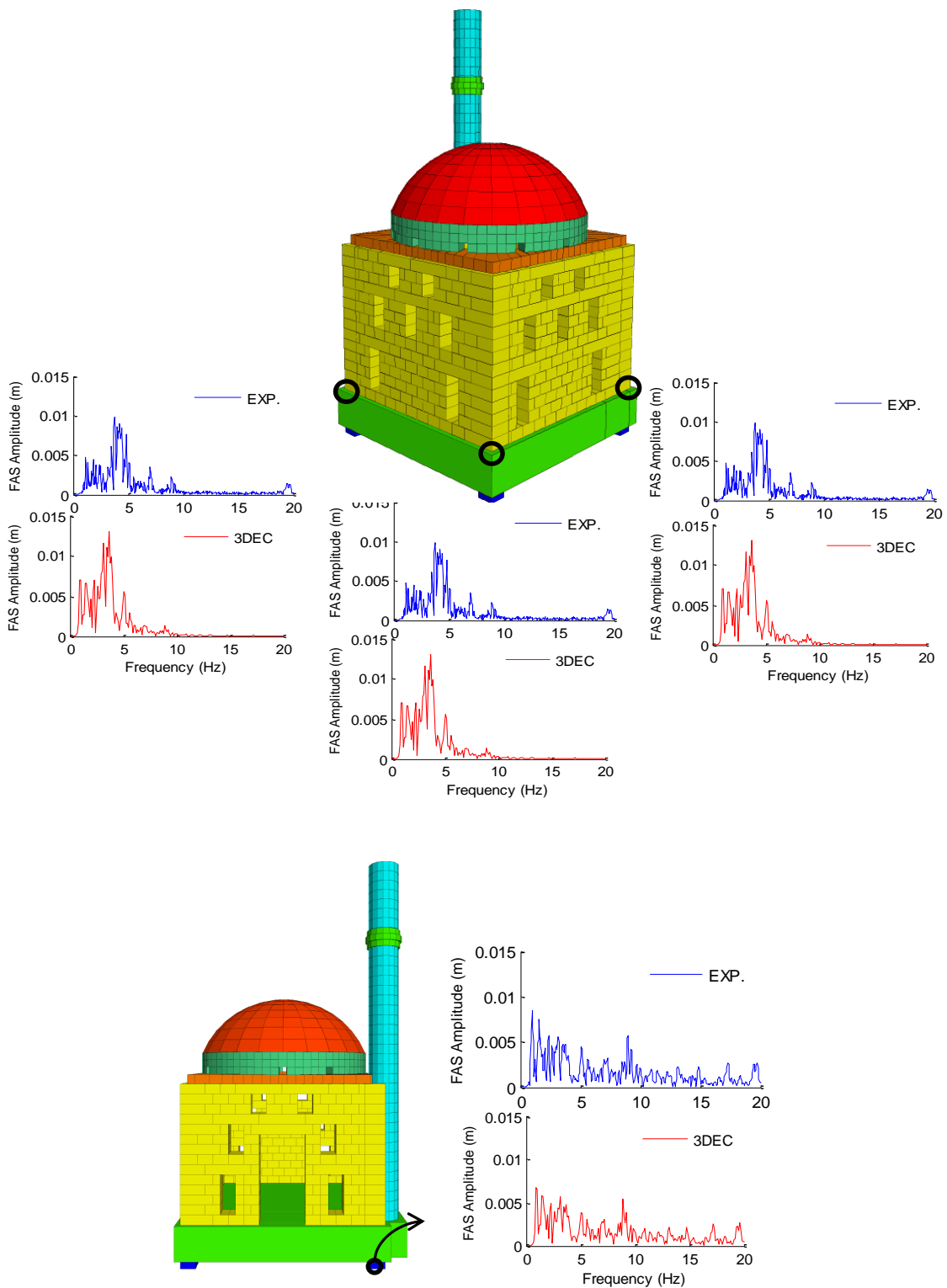


Figure 3.26. FAS comparisons between isolated experimental and numerical model under 50 % Montenegro Earthquake. The input to the numerical model is applied under the four isolators. Comparisons are provided at four locations: at the isolation level and at the three corners of the foundation.

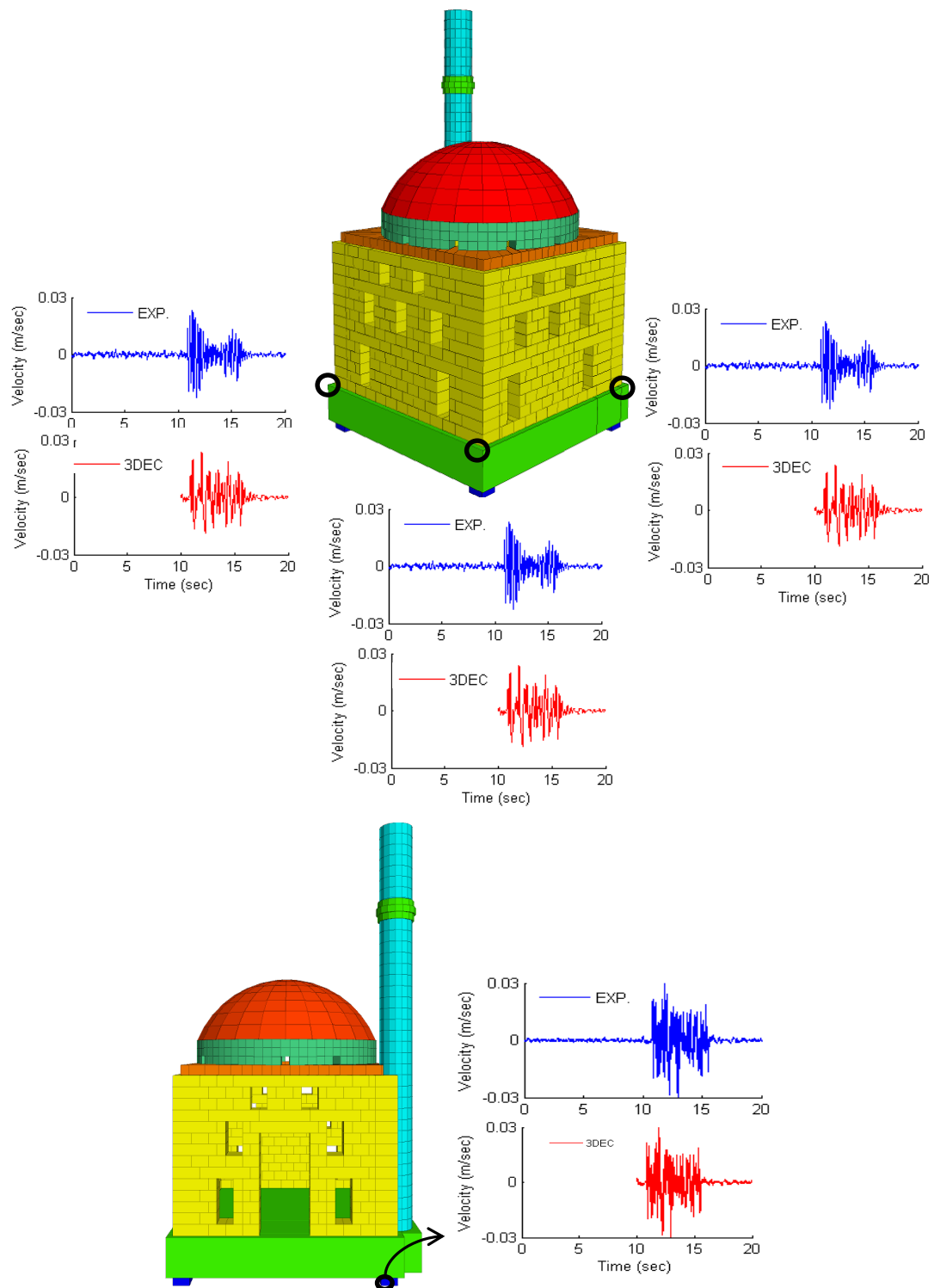


Figure 3.27. Velocity time history comparisons between isolated experimental and numerical model under 70 % Montenegro Earthquake. The input to the numerical model is applied under the four isolators. Comparisons are provided at four locations: at the isolation level and at the three corners of the foundation.

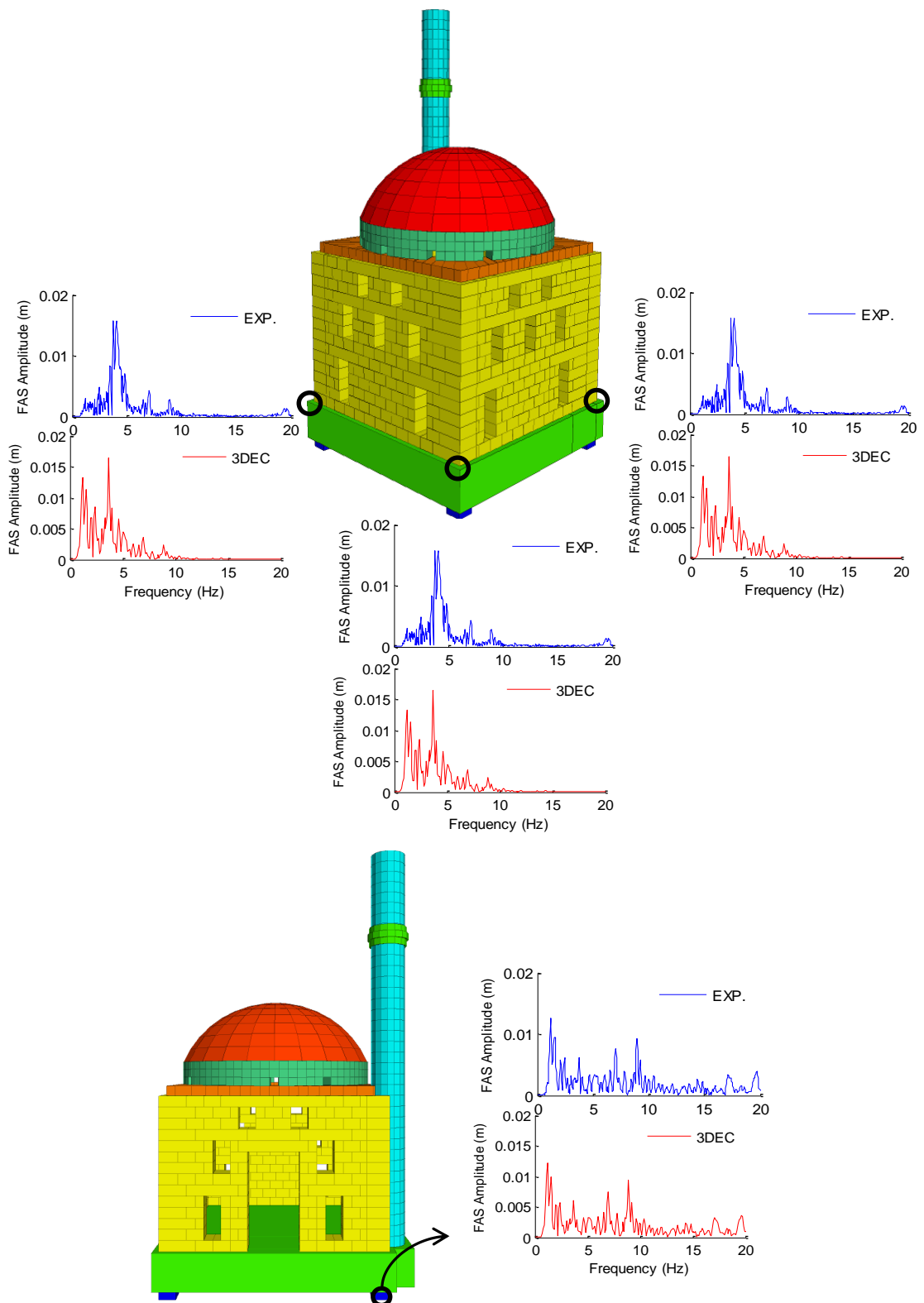


Figure 3.28. FAS comparisons between isolated experimental and numerical model under 70 % Montenegro Earthquake. The input to the numerical model is applied under the four isolators. Comparisons are provided at four locations: at the isolation level and at the three corners of the foundation.

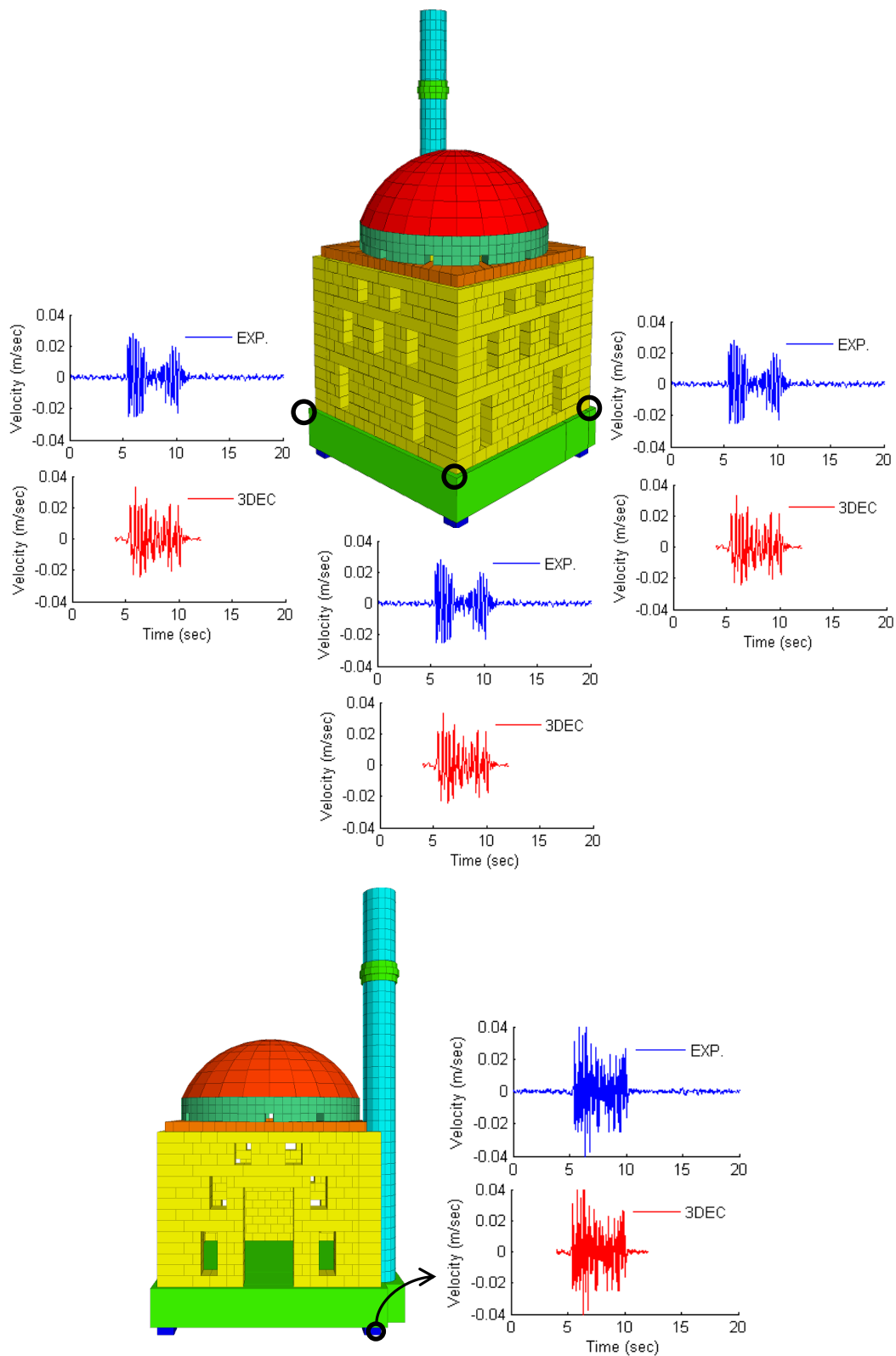


Figure 3.29. Velocity time history comparisons between isolated experimental and numerical model under 100 % Montenegro Earthquake. The input to the numerical model is applied under the four isolators. Comparisons are provided at four locations: at the isolation level and at the three corners of the foundation.

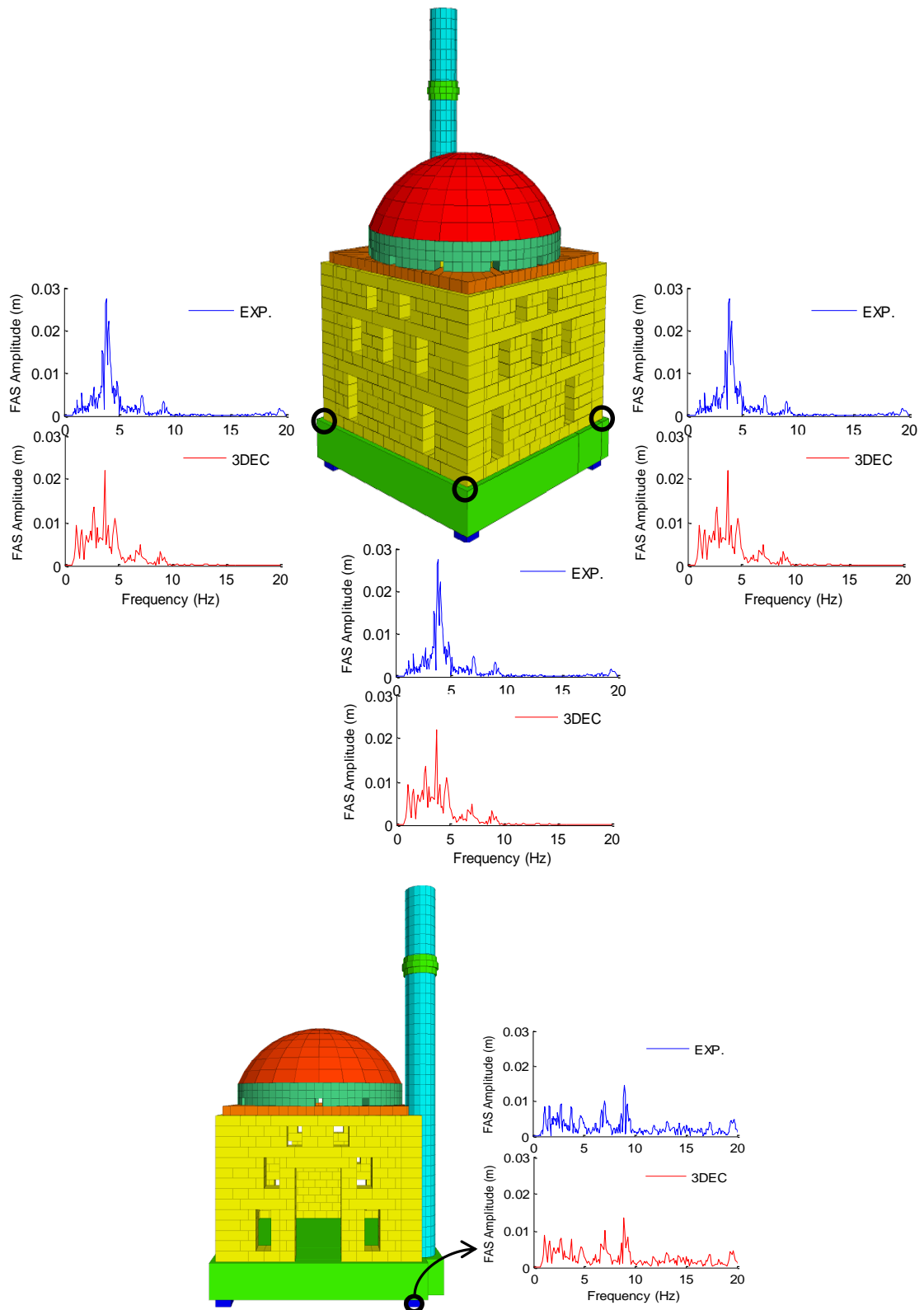


Figure 3.30. FAS comparisons between isolated experimental and numerical model under 100 % Montenegro Earthquake. The input to the numerical model is applied under the four isolators. Comparisons are provided at four locations: at the isolation level and at the three corners of the foundation.

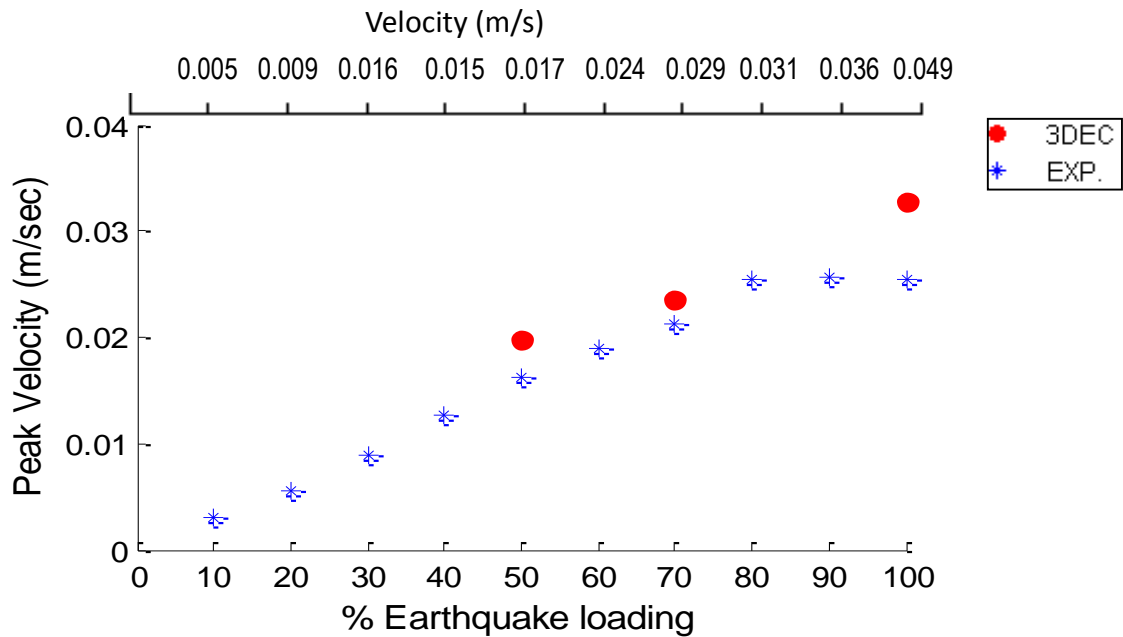


Figure 3.31. The variation of peak experimental and analytical velocities at the instrument 1. Refer to Figure 3.34 for the instrumentation on the foundation of the shake table model and corresponding point on the numerical model. Top x axis of the figure displays the peak velocities equaled to % earthquake loading.

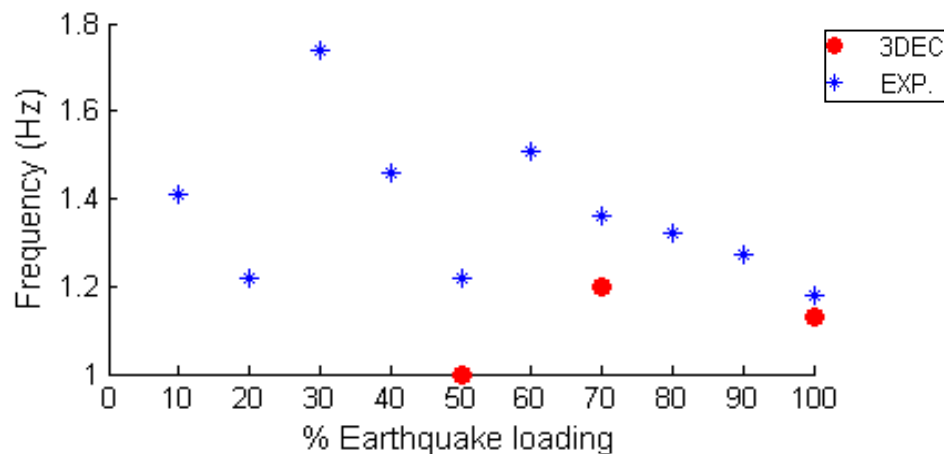


Figure 3.32. The variation of peak experimental and analytical FAS with respect to the change in the amplitude of input motion.

### **3.6. Numerical Investigation of the Distinct Element Model and Comparison with Experimental Data**

Normally discrete elements are used in cases where modeling with relatively small number of elements is possible, because of long run times. The solution time for a 3DEC run is a function of both the number of rigid blocks, and the number of contacts in a model. In 3DEC forces are accumulated at the centroid of each rigid block. At equilibrium, the algebraic sum of these forces is almost zero. During time stepping, the maximum unbalanced force is determined for the whole model. The unbalanced force is important in assessing the state of the model for the first static analysis. By this way the solution time increased as more contacts were created in the model because 3DEC took a longer time in small time stepping. The maximum unbalanced force is determined in time step 3.339E-06.

The numerical model consists of 1784 rigid blocks. As far as boundary conditions are concerned, the base of the mosque model is considered as completely constrained. Static analysis, considered as the preliminary study provides valuable information both on global behavior and on interaction among the structural parts. Indeed, the analysis of the structure under gravity loading provides significant data, such as stress distribution, weak elements of potential failure and displacements. Dynamic analysis followed the self-weight static analysis with elastic and nonlinear properties. This nonlinear model allows for predicting the nonlinear seismic response of mosque model provided that it is calibrated. In the nonlinear dynamic analysis; 1:10 scaled numerical model was subjected to the same dynamic loading sequence as the test structure during the shake-table experiments until damage to the dome, drum, walls and minaret became visible. Since the solution time increases as more contacts are created only the strong motion of earthquake were used for the dynamic nonlinear analyses. Velocity input data were applied to the centroids of rigid blocks of the foundation. Following each analysis, the model that already received damaged was used in the next step to ensure accumulation of effects over the range of applied input motion. The values for velocity, displacement, normal stress, shear stress, normal displacement, shear displacement, peak normal and shear stresses at given locations were stored during each model run.

### 3.6.1. Analytical Model Predictions and Comparison with Experimental Results

There are two criteria for affirming the representativeness of the numerical model developed on the basis of the 1:10 scale shake table model of the Mustafa Paşa Mosque: (1) numerical model needs to replicate the experimental data recorded at various locations of the shake table model as closely as possible; (2) the numerical model needs to develop crack, deformation and collapse patterns similar to those observed during the tests on the shake table model. In the comparison of analytical and experimental results, velocity time histories, Fourier amplitude spectra and transfer functions are used. The analyses are carried out for 10 %, 30 %, 50 %, 70 %, 100 %, 150 %, 160 %, 170 %, 220 % and 250 % Montenegro input. In Figure 3.33 measurement locations on the minaret of the shake table model and corresponding points on the numerical model are shown. In Figure 3.34 measurement locations on the body of the shake table model and corresponding points on the numerical model are indicated. The comparisons of experimental and analytical velocities and their Fourier amplitude spectra can be found as a complete set (for minaret and body; for all input motion levels) in the attached CD as Appendix A. In the present section the comparisons for 10 %, 100 % and 250 % Montenegro input are included (Figure 3.35 – Figure 3.46). Under 10 % Montenegro a good match of experimental and analytical velocities (Figure 3.35) and their FAS (Figure 3.36) is observed. While the minaret behaves as a monolithic, element, with a regular increase of recorded and calculated velocities and FAS over its height (Figure 3.36, Figure 3.37), the body exhibits a rigid body behavior. The differences between the recordings on the walls of the mosque body and on the dome top are almost identical (Figure 3.41 - Figure 3.46). During the increase of input levels from 10 % to 100 % Montenegro, the experimental data suggest a decrease of the fundamental frequency of the minaret from about 12 Hz (Figure 3.36) to 6 Hz (Figure 3.38). A similar decrease is evident from the analytical results. The analytical fundamental frequency of the minaret is found as 12.4 Hz under 10 % Montenegro (Figure 3.36). It drops to 6.8 Hz when the input is increased to 100 % Montenegro. The first visible crack during the experiments was observed after 150 % Montenegro. The decrease in the fundamental frequency that apparently starts soon after 10 % Montenegro continues through all levels of input motions and is well replicated by numerical analyses, suggests the existence and validation of nonlinear action.

250 % input was the final level of ground motion used in the experimental stage, where significant cracks took place in the body and the minaret was rocking. The damages observed on the shake table model and on the numerical model are presented in Figure 3.47 and Figure 3.48.

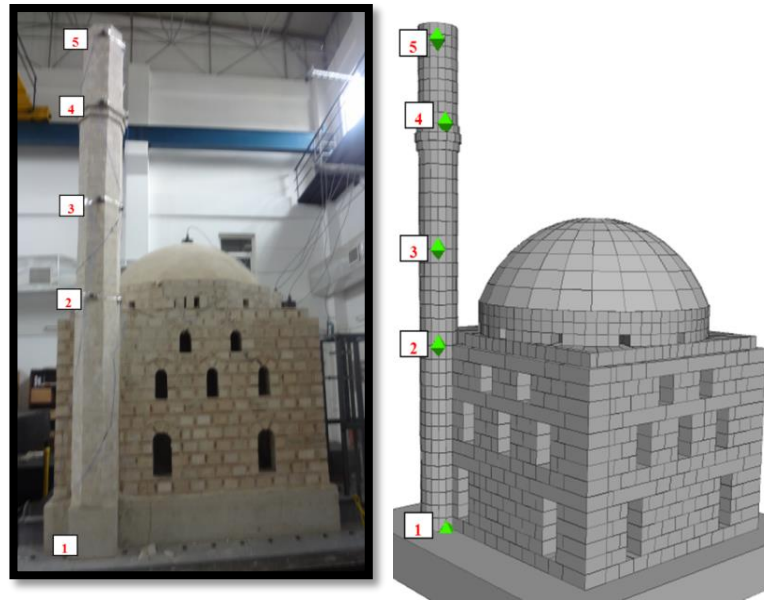


Figure 3.33. Measurement locations on the minaret of the shake table model and corresponding points on the numerical model.

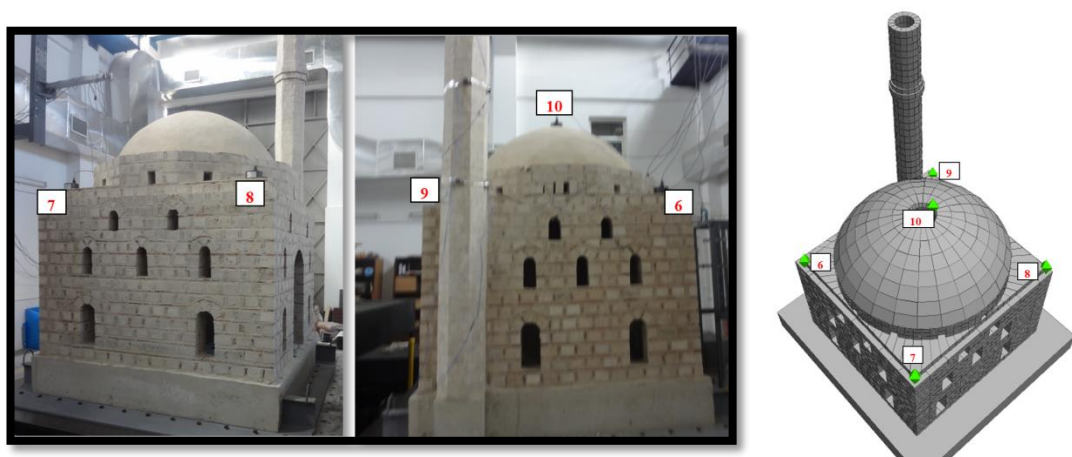


Figure 3.34. Measurement locations on the body of the shake table model and corresponding points on the numerical model.

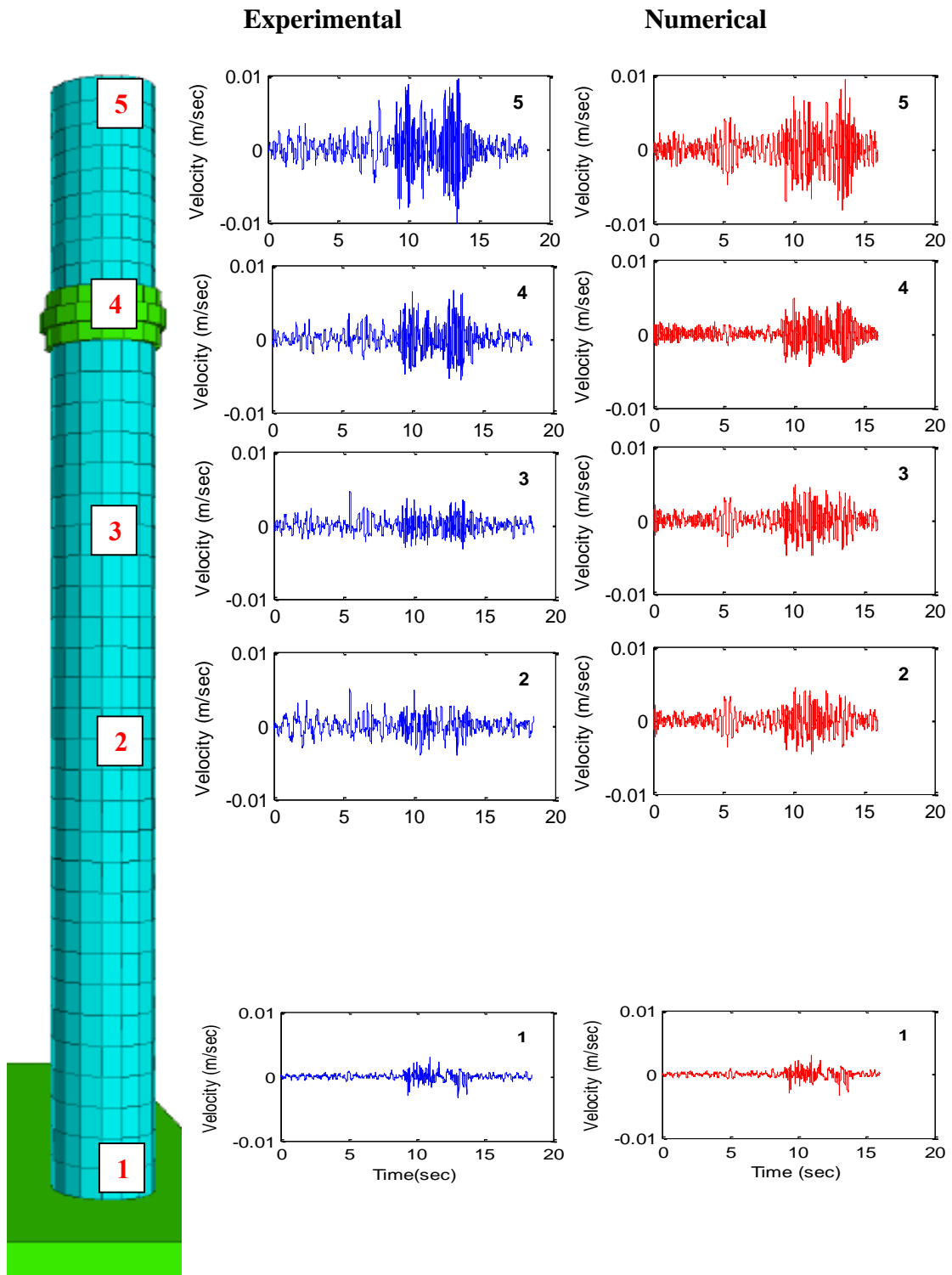


Figure 3.35. Comparisons of experimental and analytical velocities along the minaret under 10 % Montenegro Earthquake loading. 1, 2, 3, 4, 5 indicate the measurement locations. Refer to Figure 3.33 for the measurement locations on the minaret and corresponding points on the numerical model.

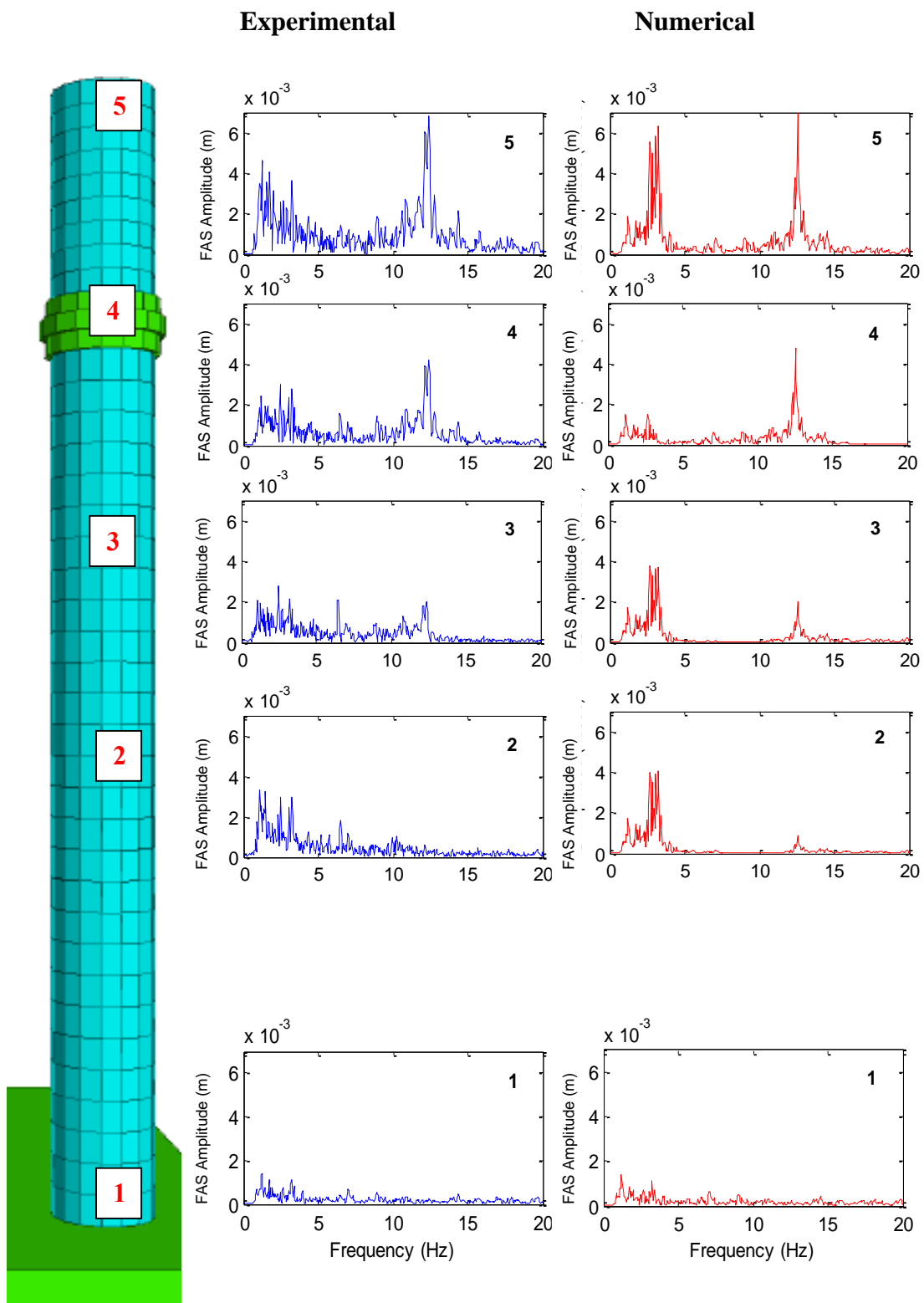


Figure 3.36. Comparisons of experimental and numerical FAS amplitude along the minaret under 10 % Montenegro Earthquake loading. 1, 2, 3, 4, 5 indicate the measurement locations. Refer to Figure 3.33 for the measurement locations on the minaret and corresponding points on the numerical model.

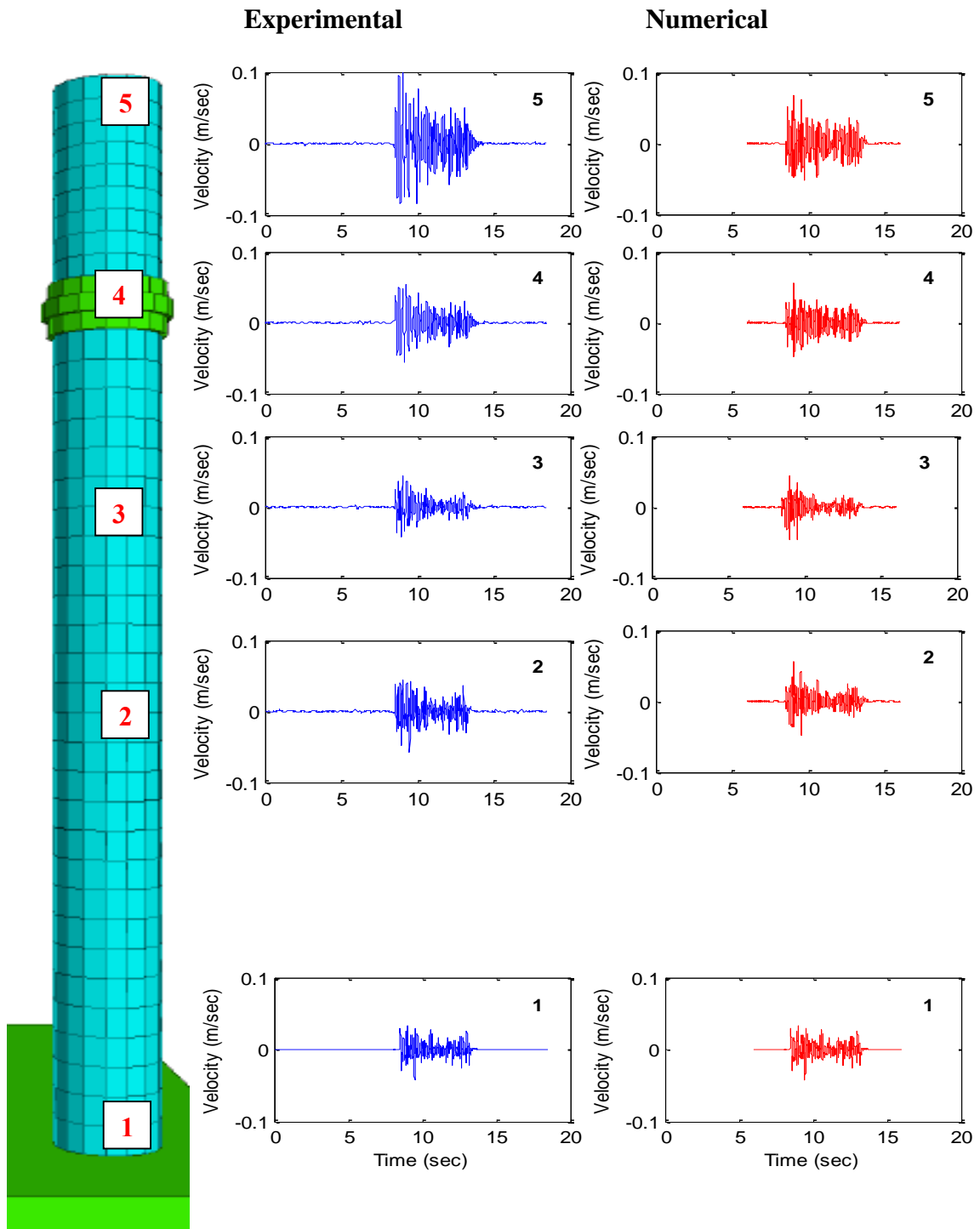


Figure 3.37. Comparisons of experimental and analytical velocities along the minaret under 100 % Montenegro Earthquake loading. 1, 2, 3, 4, 5 indicate the measurement locations. Refer to Figure 3.33 for the measurement locations on the minaret and corresponding points on the numerical model.

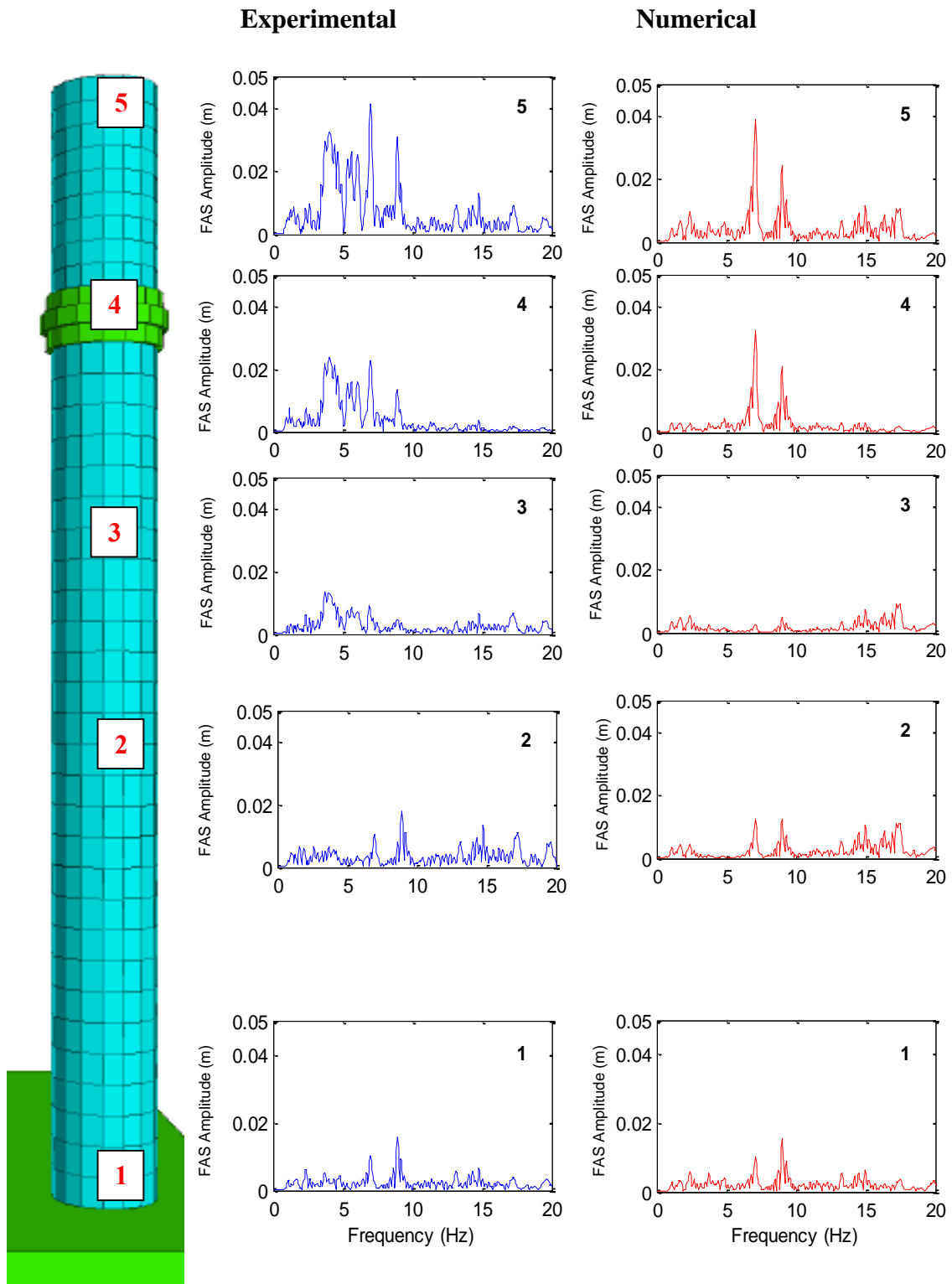


Figure 3.38. Comparisons of experimental and numerical FAS amplitude along the minaret under 100 % Montenegro Earthquake loading. 1, 2, 3, 4, 5 indicate the measurement locations. Refer to Figure 3.33 for the measurement locations on the minaret and corresponding points on the numerical model.

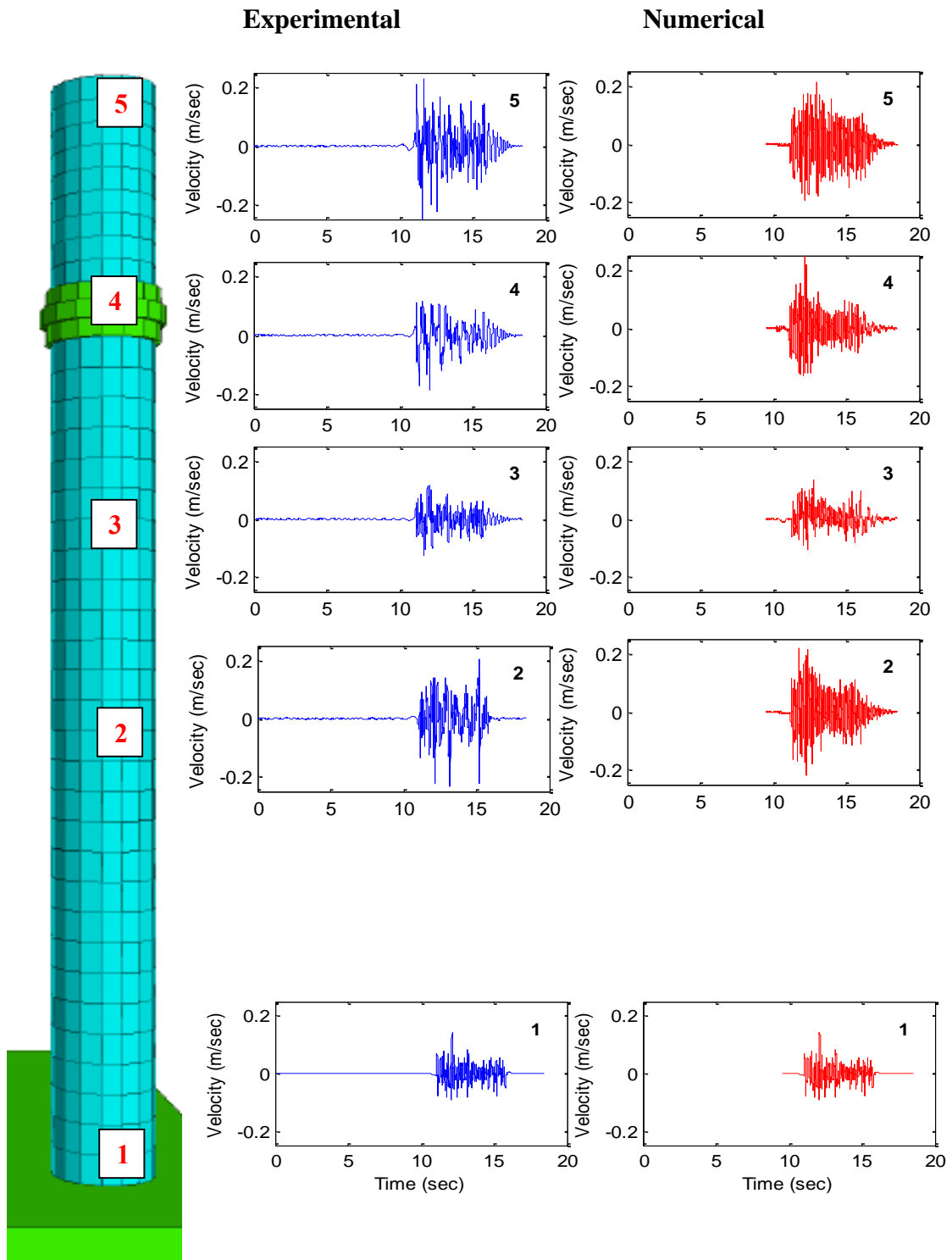


Figure 3.39. Comparisons of experimental and analytical velocities along the minaret under 250 % Montenegro Earthquake loading. 1, 2, 3, 4, 5 indicate the measurement locations. Refer to Figure 3.33 for the measurement locations on the minaret and corresponding points on the numerical model.

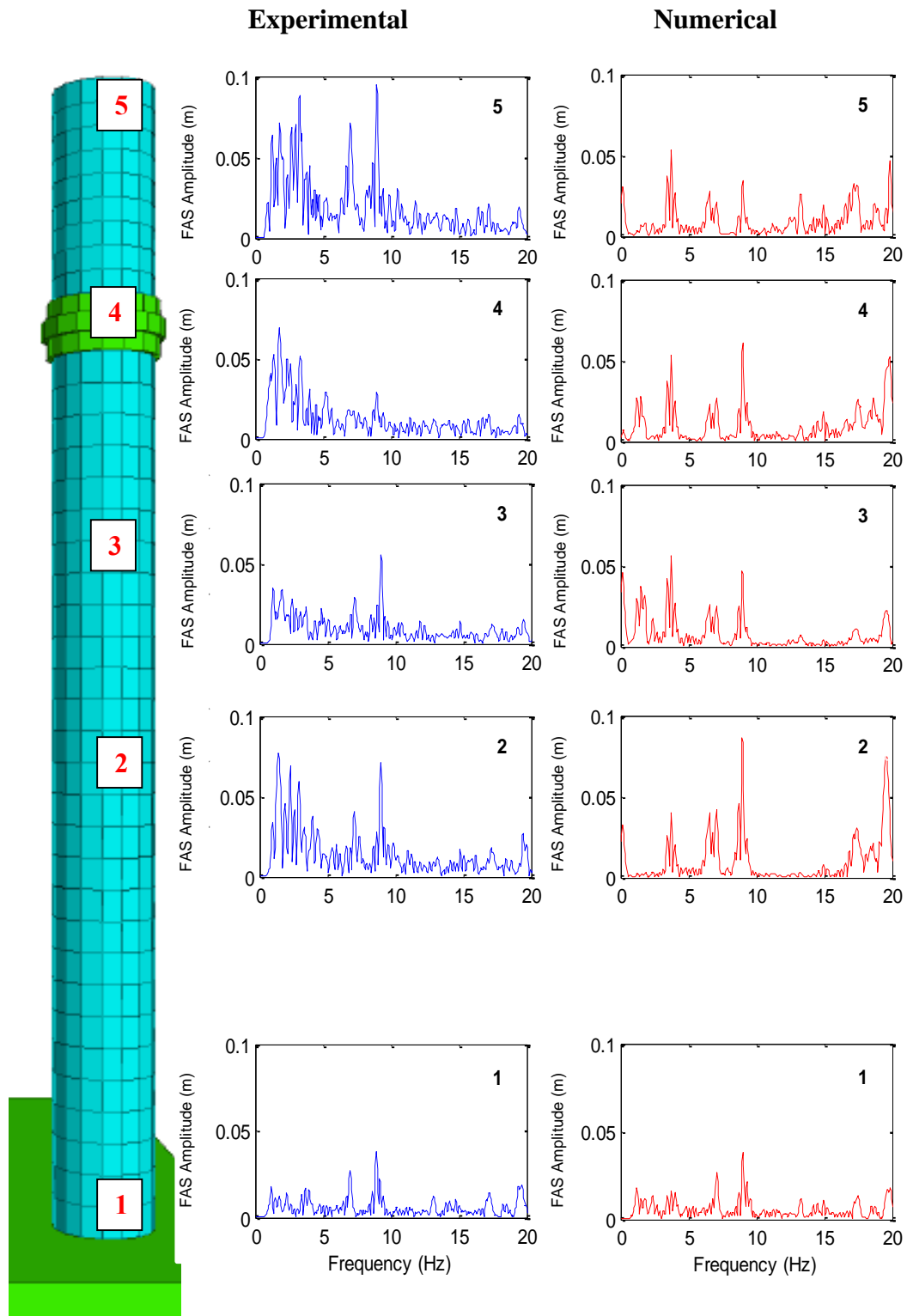


Figure 3.40. Comparisons of experimental and numerical FAS amplitude along the minaret under 250 % Montenegro Earthquake loading. 1, 2, 3, 4, 5 indicate the measurement locations. Refer to Figure 3.33 for the measurement locations on the minaret and corresponding points on the numerical model.

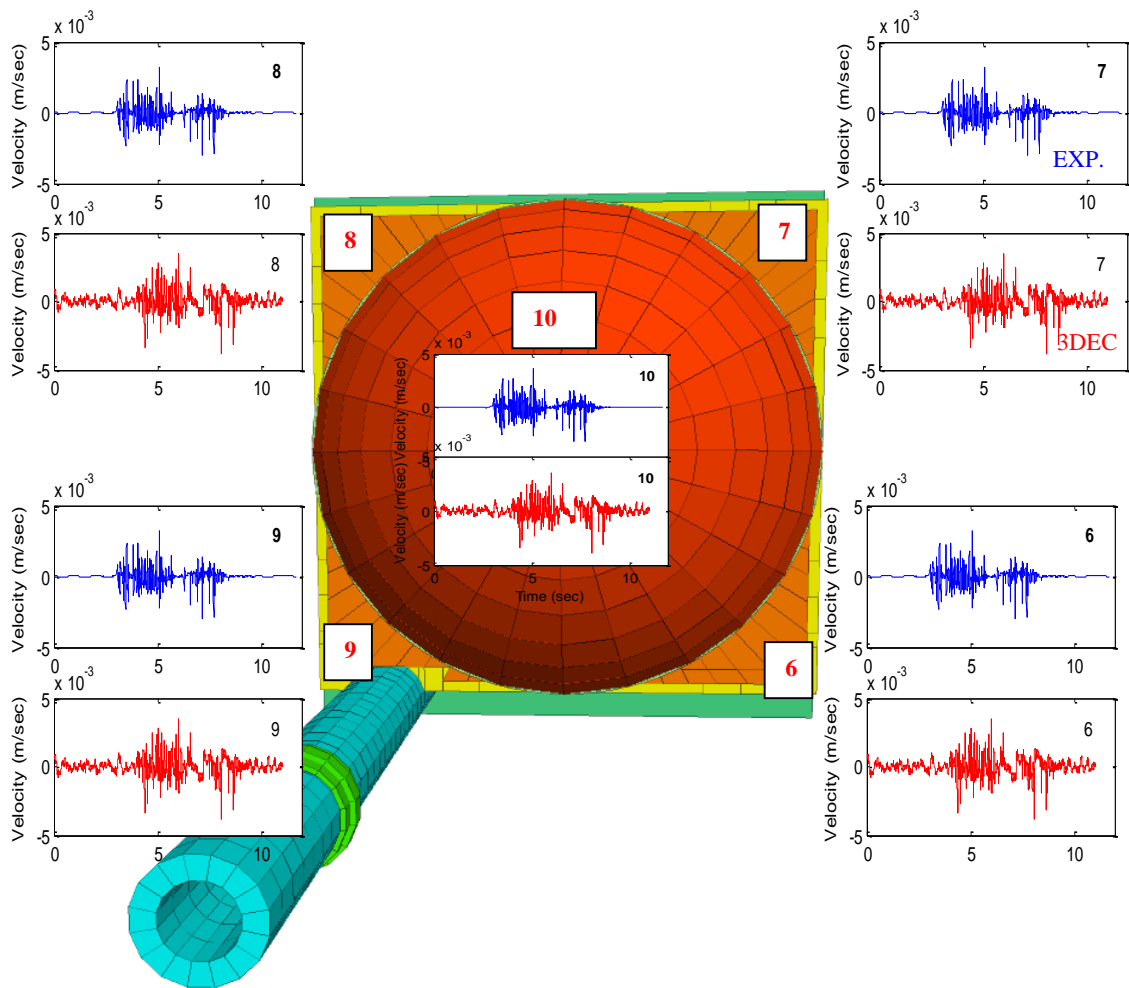


Figure 3.41. Comparisons of experimental and analytical velocities on the body of mosque model under 10 % Montenegro Earthquake loading. 10, 9, 8, 7 and 6 indicate the locations of accelerometers on the top of the dome and 4 at the four top corners of the body respectively. Refer to Figure 3.34 for the on the body of the shake table model and corresponding points on the numerical model.

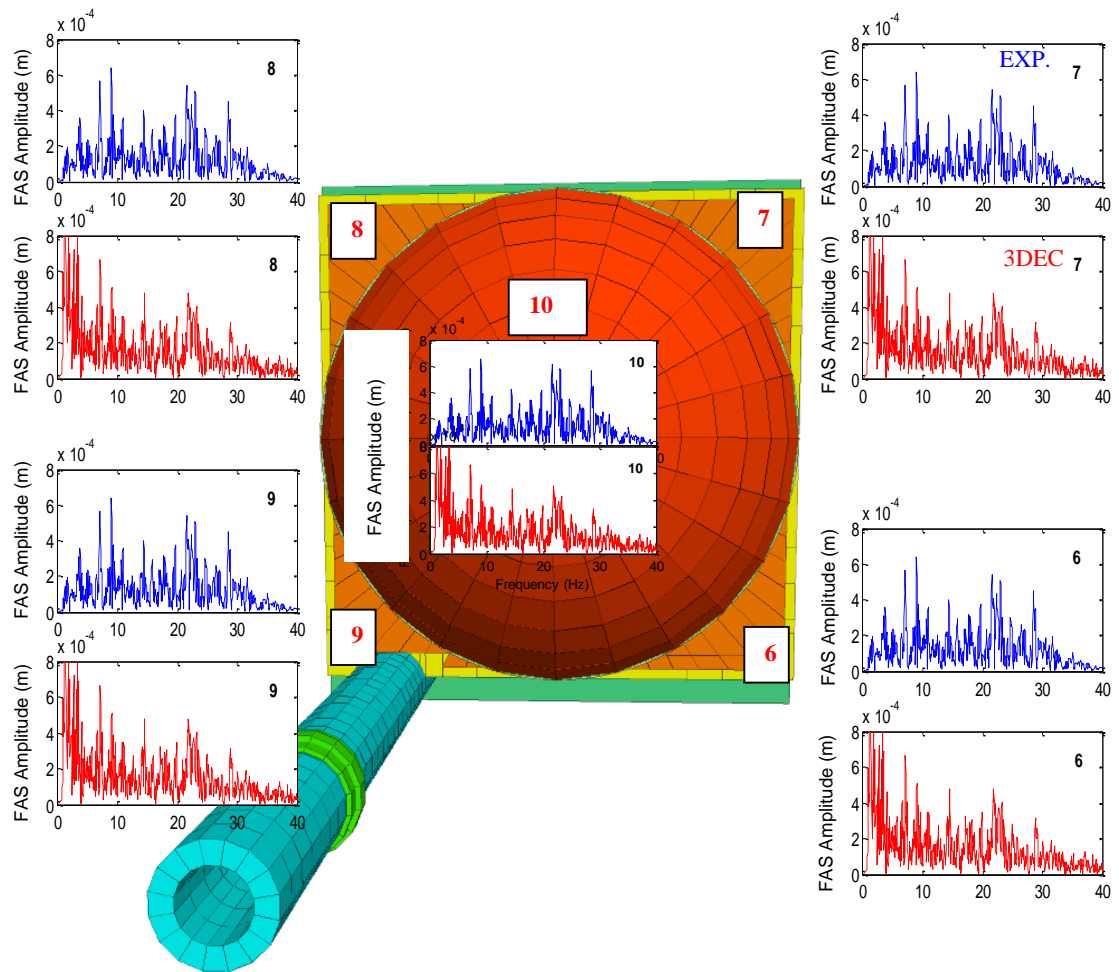


Figure 3.42. Comparisons of experimental and numerical FAS amplitude on the body of mosque under 10 % Montenegro Earthquake loading. 10, 9, 8, 7 and 6 indicate the locations of accelerometers on the top of the dome and 4 at the four top corners of the body respectively. Refer to Figure 3.34 for the on the body of the shake table model and corresponding points on the numerical model.

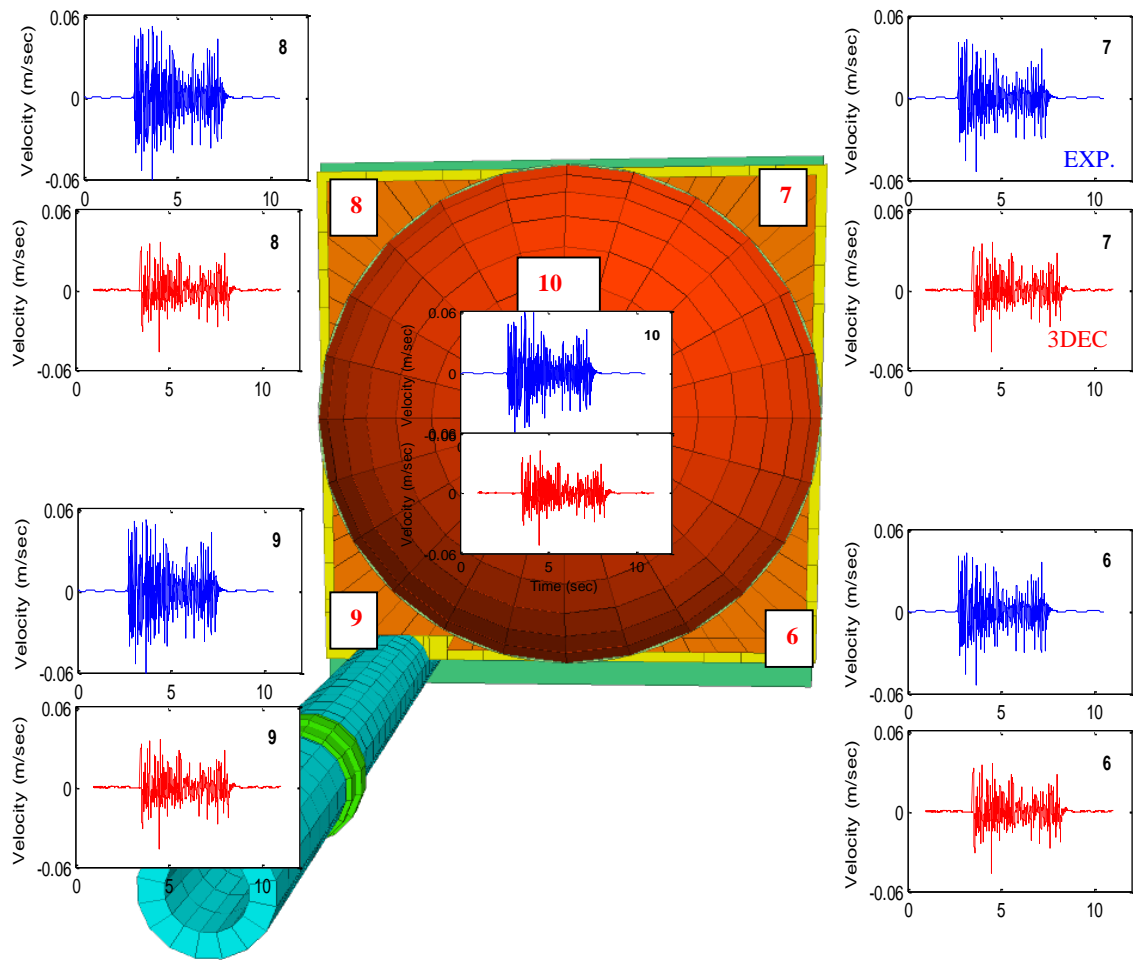


Figure 3.43. Comparisons of experimental and analytical velocities on the body of mosque model under 100 % Montenegro Earthquake loading. 10, 9, 8, 7 and 6 indicate the locations of accelerometers on the top of the dome and 4 at the four top corners of the body respectively. Refer to Figure 3.34 for the on the body of the shake table model and corresponding points on the numerical model.

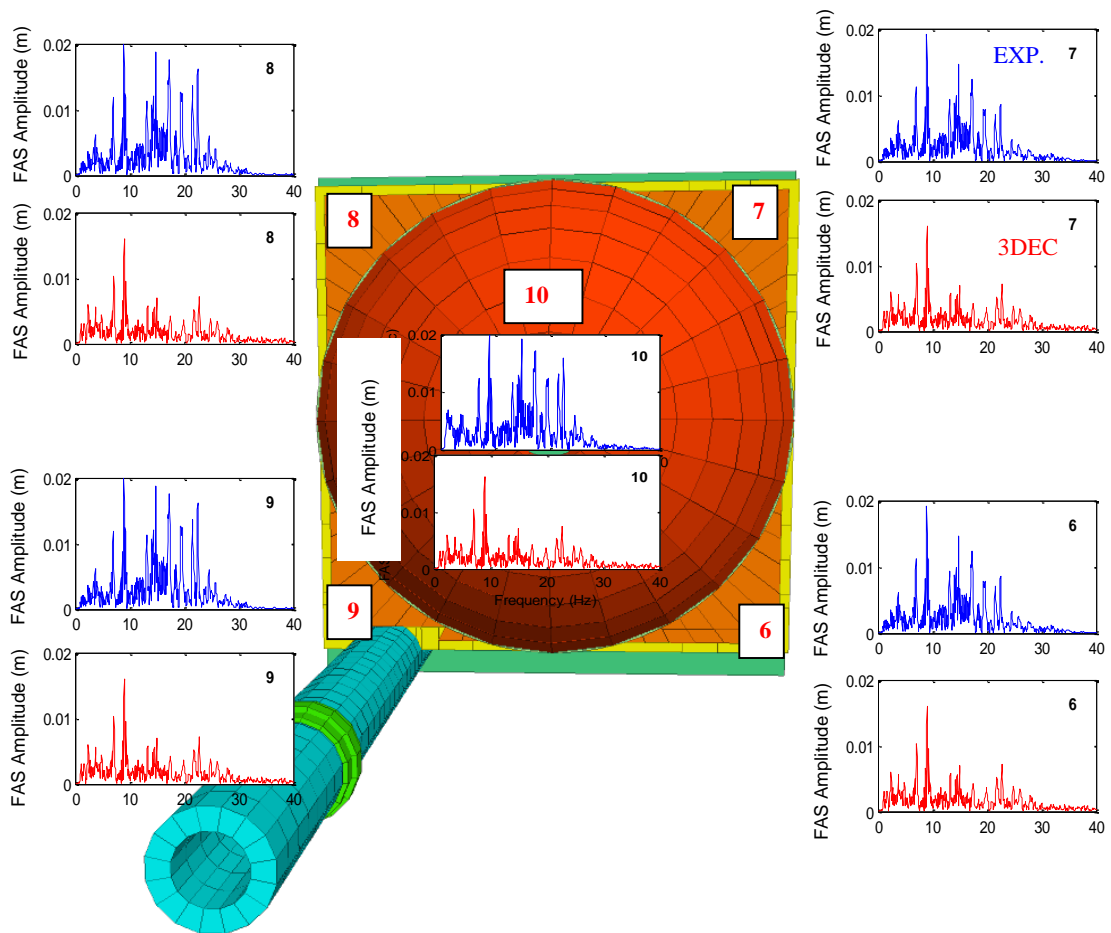


Figure 3. 44. Comparisons of experimental and numerical FAS amplitude on the body of mosque under 100 % Montenegro Earthquake loading. 10, 9, 8, 7 and 6 indicate the locations of accelerometers on the top of the dome and 4 at the four top corners of the body respectively. Refer to Figure 3.34 for the on the body of the shake table model and corresponding points on the numerical model.

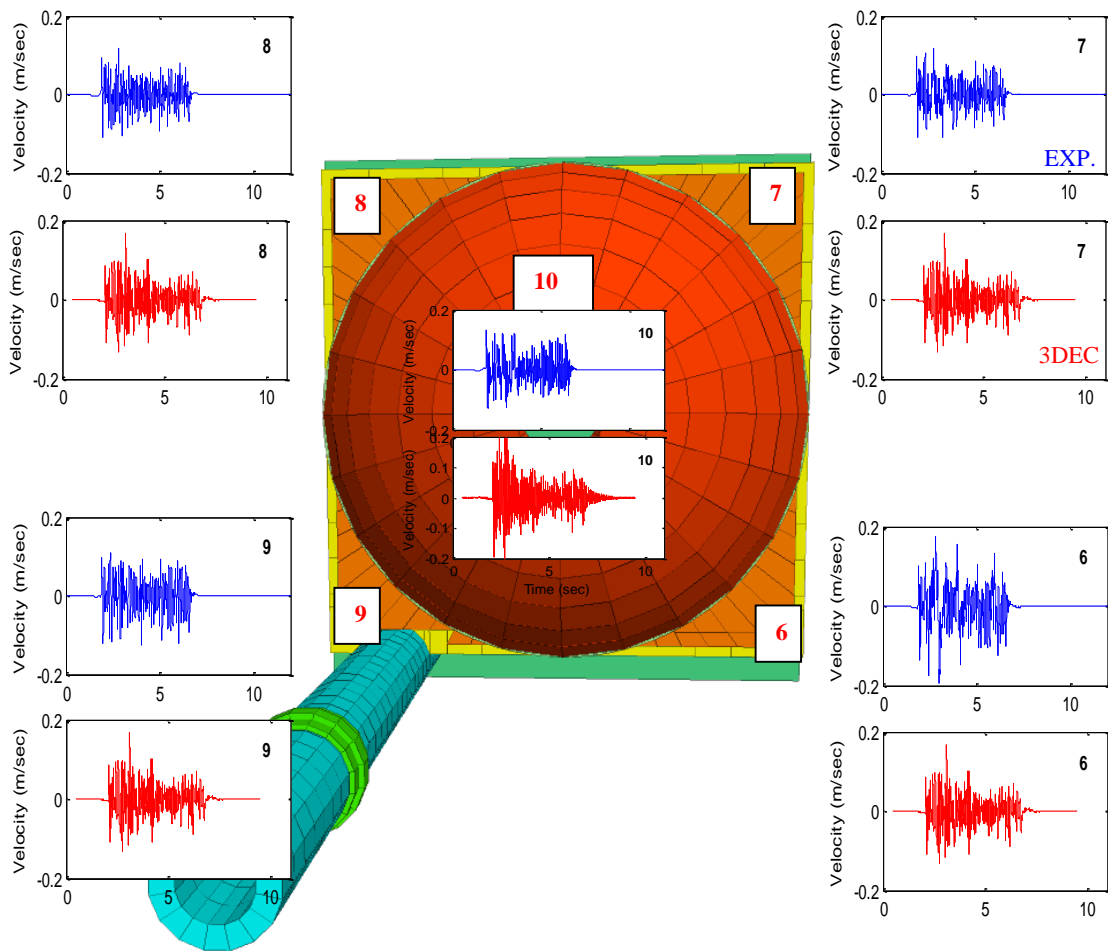


Figure 3.45. Comparisons of experimental and analytical velocities on the body of mosque model under 250 % Montenegro Earthquake loading. 10, 9, 8, 7 and 6 indicate the locations of accelerometers on the top of the dome and 4 at the four top corners of the body respectively. Refer to Figure 3.34 for the on the body of the shake table model and corresponding points on the numerical model.

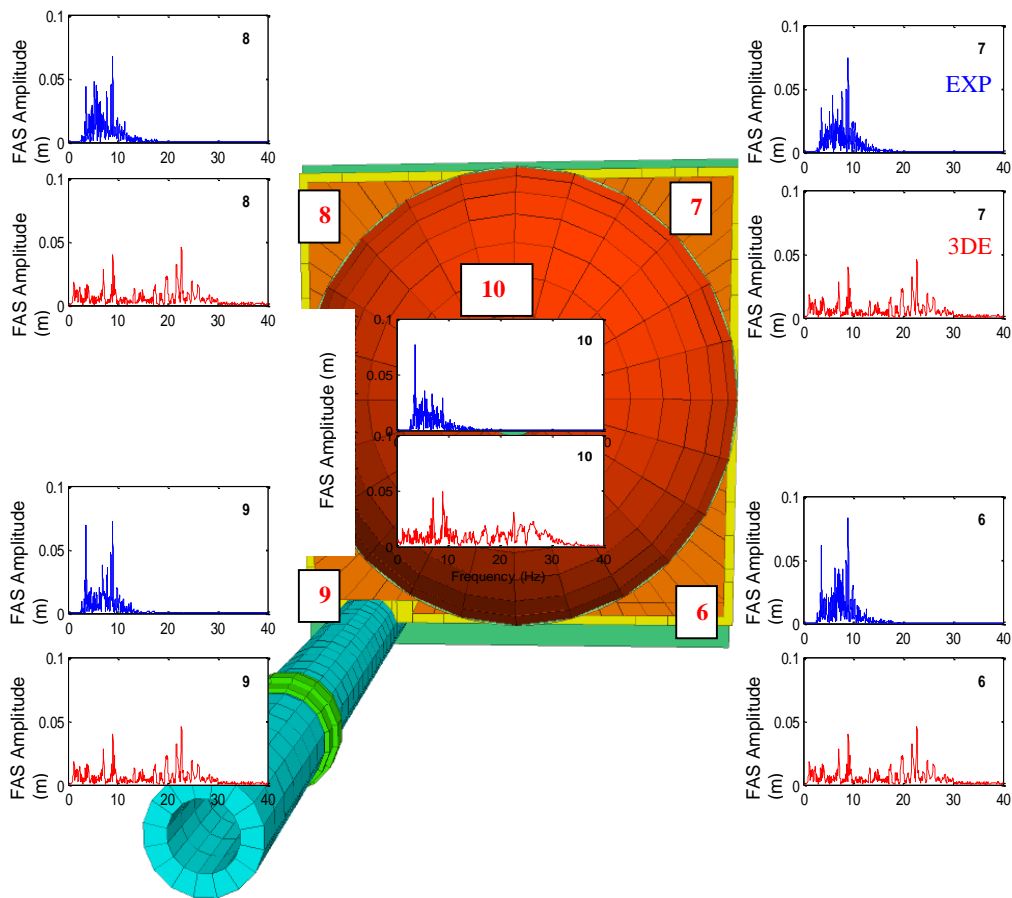


Figure 3.46. Comparisons of experimental and numerical FAS amplitude on the body of mosque under 250 % Montenegro Earthquake loading. 10, 9, 8, 7 and 6 indicate the locations of accelerometers on the top of the dome and 4 at the four top corners of the body respectively. Refer to Figure 3.34 for the on the body of the shake table model and corresponding points on the numerical model.

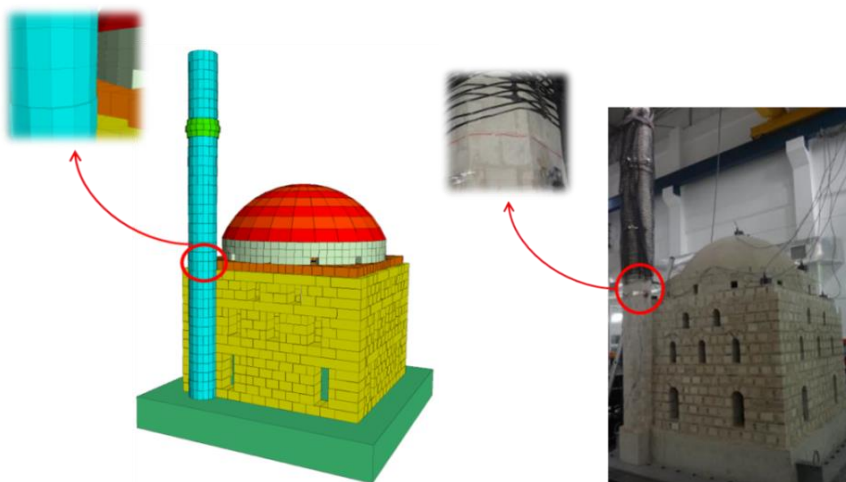


Figure 3.47. Comparison of numerical model and experimental results of test structure under 160 % Montenegro Earthquake.

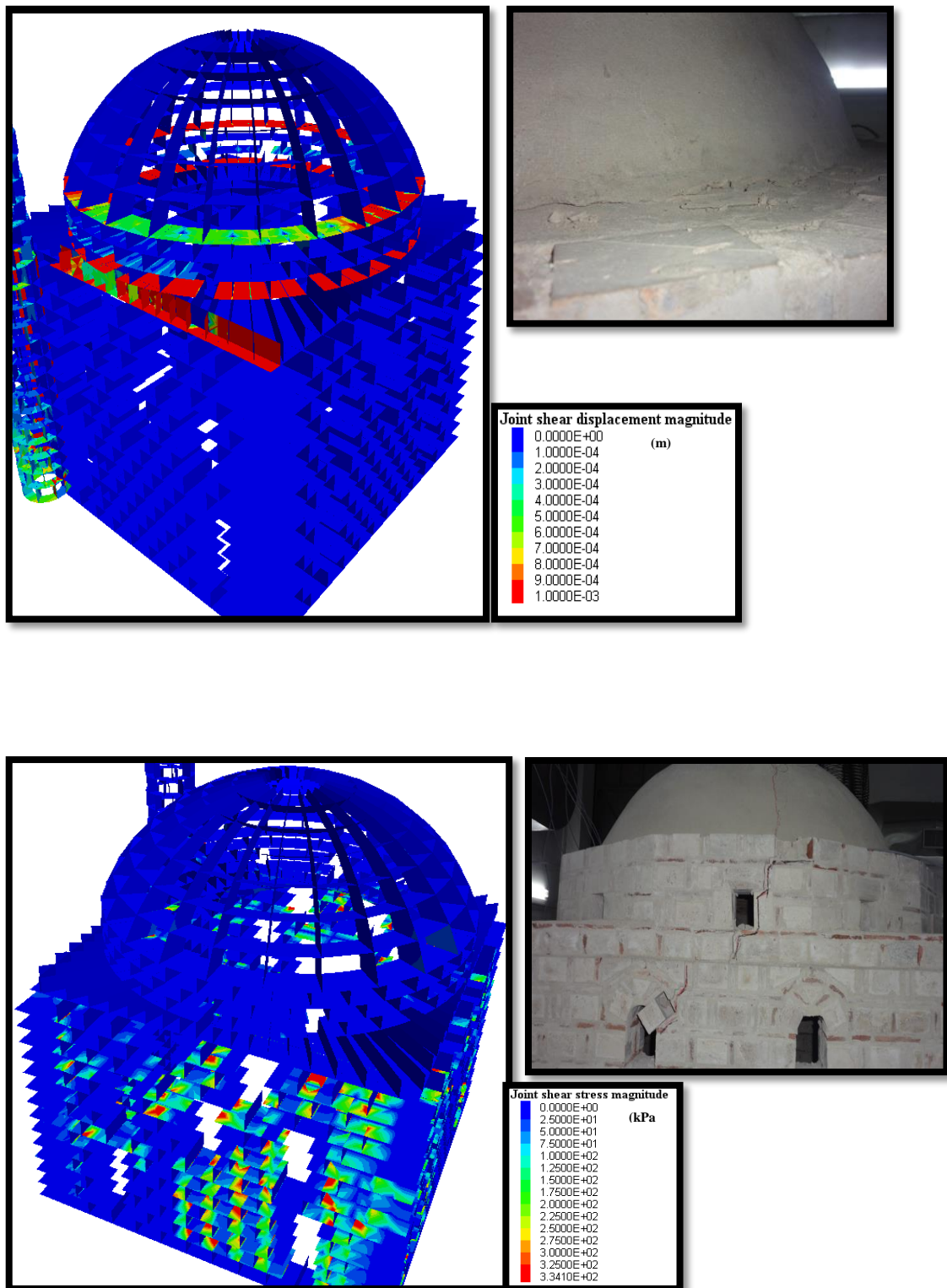


Figure 3.48. Comparison of numerical shear displacement and shear stresses at the joints under 250 % Montenegro Earthquake with damages that took place on the experimental model under the same level input motion.

Starting with 150 % Montenegro (Figure A15 is included in CD) and continuing up until 250 % (Figure A21 is included in CD) there is a decrease in recorded and calculated velocities between observation points 2 and 3 on the minaret. This is explained as the result of detachment of the upper part of the minaret from its lower portion that is adjacent to the body. The recorded and calculated velocities at level 2 increases with input motion, which is also a consequence of progressive failure in the body. The minaret detached from the remaining model, continues to respond as an almost independent body as can be seen from velocities and FAS at points 3, 4 and 5.

In addition to velocities and FAS, experimental and analytical transfer functions of the minaret are also compared. They are smoothed by a triangular running window of length 11 in the numerical model and a 21 point window in the experimental model. They are given in Figures 3.49-3.52 for all levels of Montenegro input. The transfer functions are calculated with respect to instrument 1. The decrease in the fundamental frequency of the minarets that starts soon after the 10 % Montenegro is well observed in the experimental transfer functions. The numerical model responds with the same frequencies, is however less responsive than the experimental model as is evident from the transfer function amplitudes. It should be noted that different smoothing windows are applied to experimental and analytical transfer functions, as they have different sampling rates. The smoothing window sizes are determined following Kaya and Şafak (2013). Transfer functions suggest two stages of minaret response. The first stage is between 10 % and 100 % Montenegro input. Under these input levels, the minaret responds in systematic way during the experiments. The transfer function between instrument 1 and 2 is almost 1 throughout the studied frequency range and input range. The transfer function amplitudes at instruments 3, 4 and 5 maintain the same order of increase. After 100 % Montenegro, i.e. stage two, the response of instrument at level 2 is almost identical with that of level 3, and larger than level 3 starting at 160 % Montenegro. It should be noted that the crack on the minaret was first noticed 150 % Montenegro. The numerical model appears to be significantly less responsive as judged from transfer function amplitudes, although the frequency match is satisfactory. In the first stage (10 %-100 % Montenegro) a decreasing fundamental frequency is evident (Figure A4 and Figure A12 are included in CD). In the second stage the (130 % - 250 % Montenegro) no clear dominant frequencies exist in the transfer functions, which can be related to experimental transfer functions.

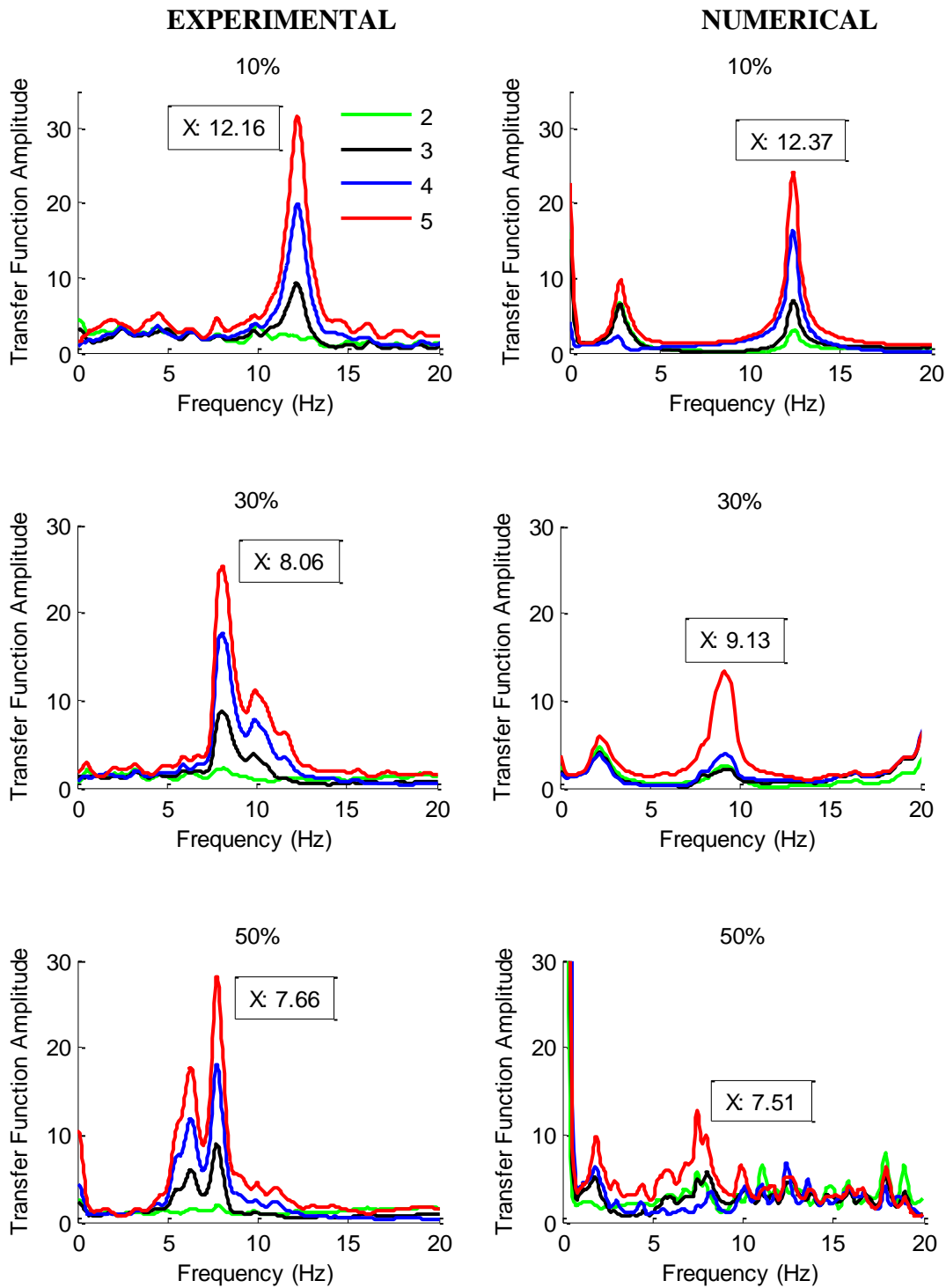


Figure 3.49. Experimental and numerical transfer function amplitude for levels of 2, 3, 4 and 5 respectively at 1.75 m, 2.45 m, 3.25 m and 3.90 m of minaret under 10 %, 30 % and 50 % earthquake loading.

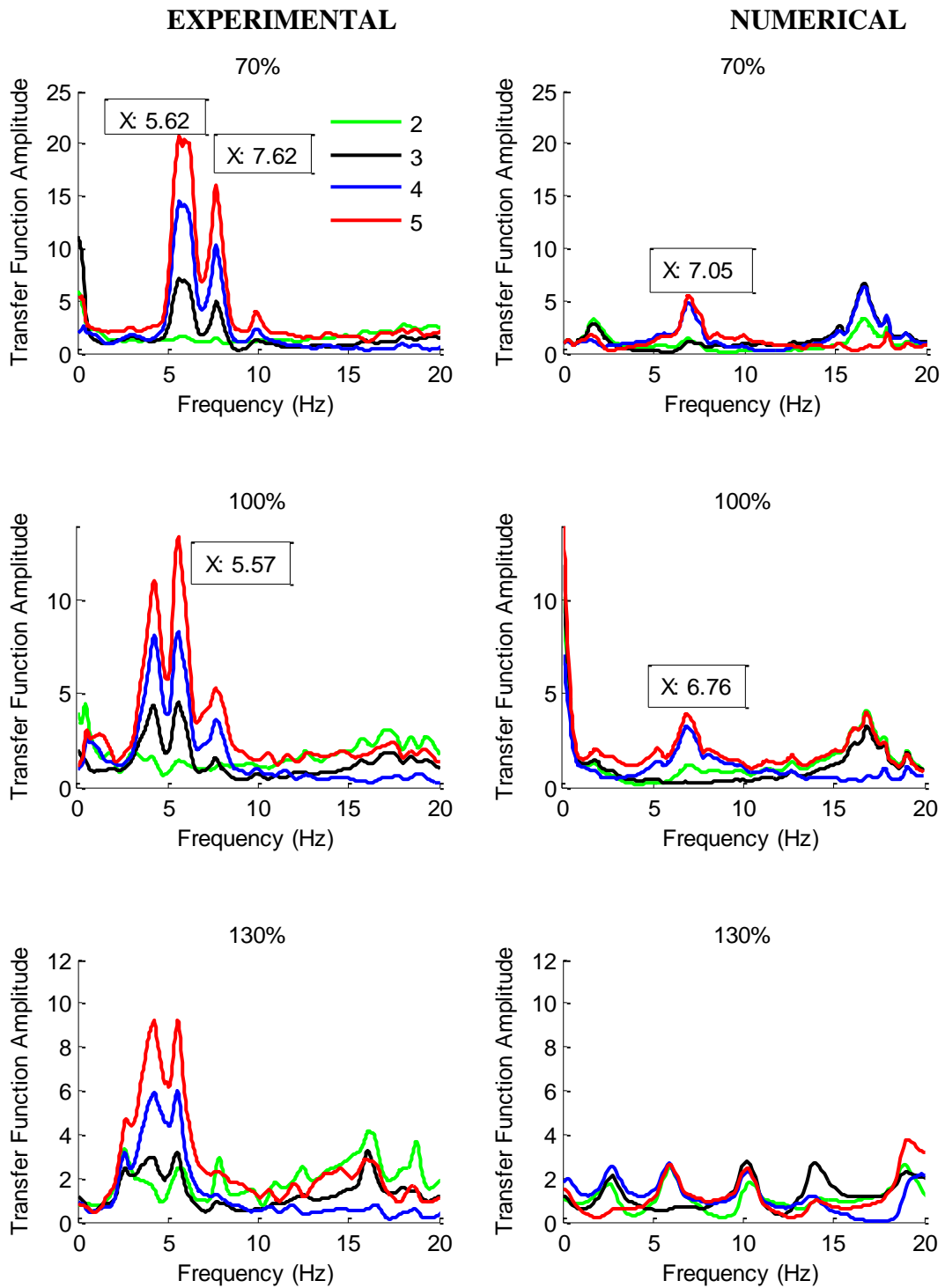


Figure 3.50. Experimental and numerical transfer function amplitude for levels of 2, 3, 4 and 5 respectively at 1.75 m, 2.45 m, 3.25 m and 3.90 m of minaret under 70 %, 100 % and 130 % earthquake loading.

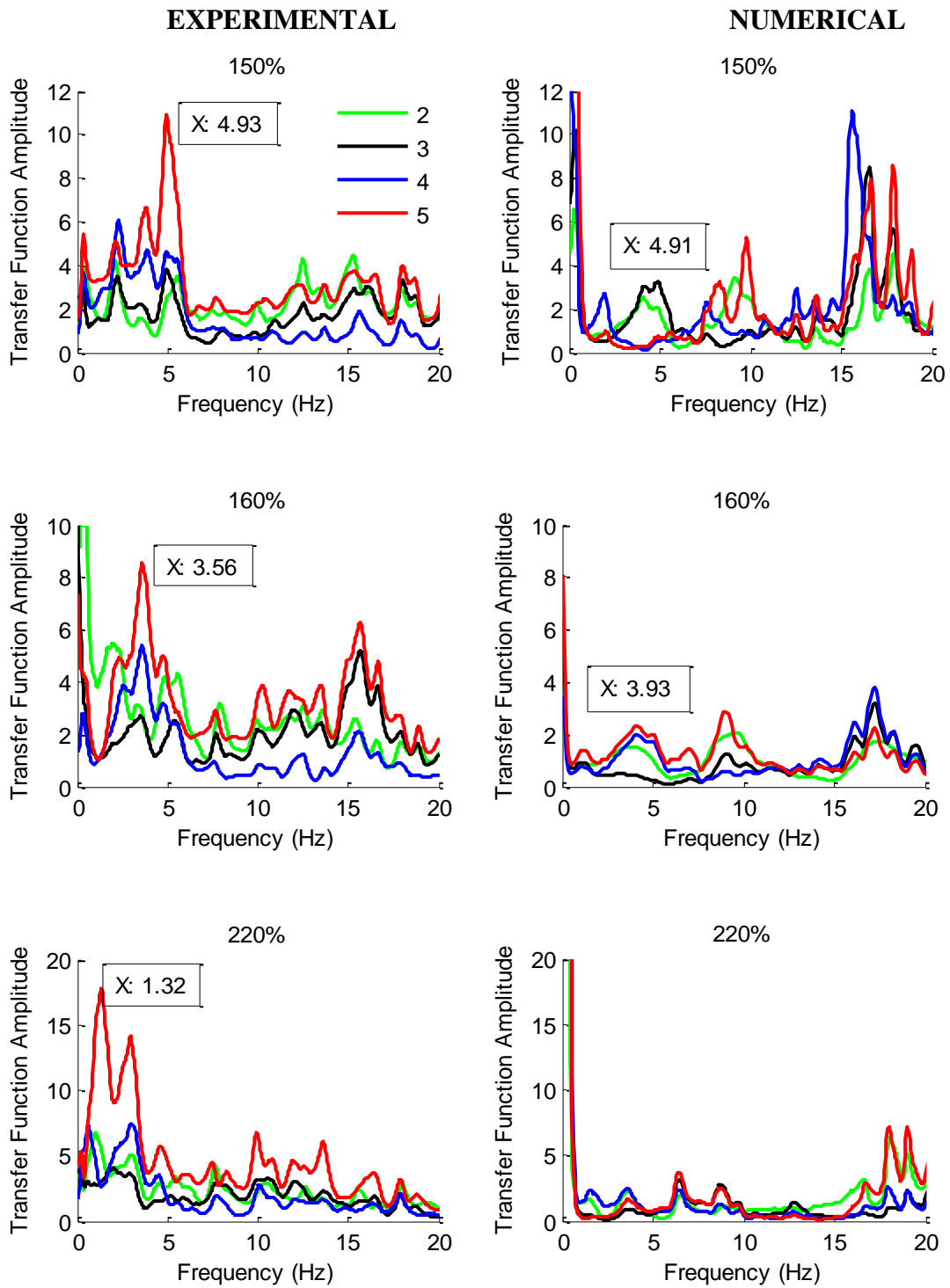


Figure 3.51. Experimental and numerical transfer function amplitude for levels of 2, 3, 4 and 5 respectively at 1.75 m, 2.45 m, 3.25 m and 3.90 m of minaret under 150 %, 160 % and 220 % earthquake loading.

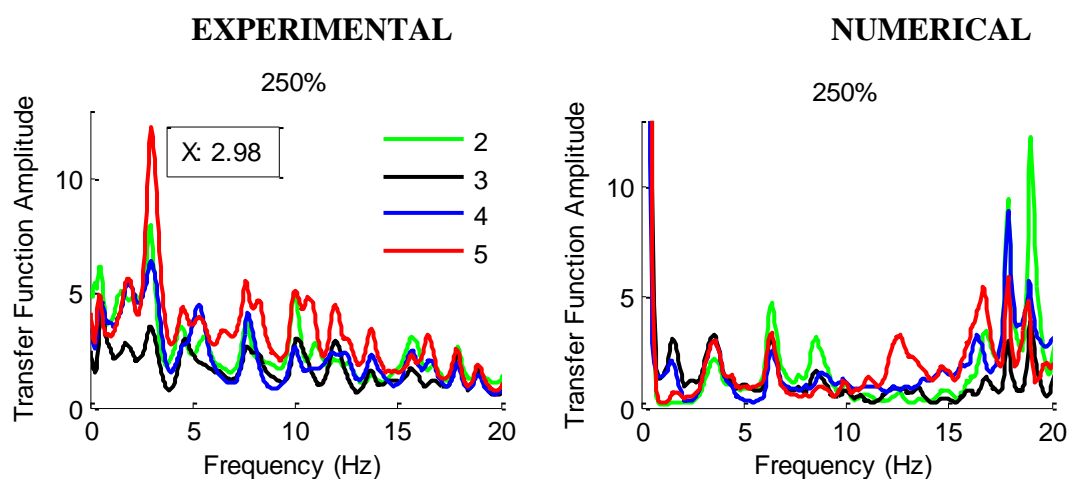


Figure 3.52. Experimental and numerical transfer function amplitude for levels of 2, 3, 4 and 5 respectively at 1.75 m, 2.45 m, 3.25 m and 3.90 m of minaret under 250 % earthquake loading.

Comparing recorded and analytical displacements is probably asking too much from the numerical model. Yet, in the results obtained from the dynamic nonlinear analyses in terms of horizontal displacements at the 5th instrument on the minaret (3.90 m) under the 30 %, 50 %, 70 %, 100 %, 150 %, 160 %, 170 %, 220 % and 250 % Montenegro Earthquake are shown. It can be said that a good correlation between numerical predictions and experimental results observed. The fit between the experimental and analytical displacements is better in the 10 % - 100 % Montenegro range. After 100 % the fit becomes poor in terms of both amplitude and phase. The numerical model predicts displacements with smaller amplitude than observed during the experiments. After 100 % Montenegro, particularly starting with 150 % the minaret was clearly damaged. Yet in general it can be said, that the maximum displacements obtained from 3DEC are very close to those obtained from the experimental tests. Under 220 % and 250 % input, permanent displacements occur at the end of the numerical dynamic analysis (Figure 3.54). Displacement vectors magnified by 2 are given in Figure 3.55. It should be noted that the experimental displacements co-shown with analytical ones are high-pass filtered at 0.1 Hz. They are thus do not show the experimental permanent displacements.

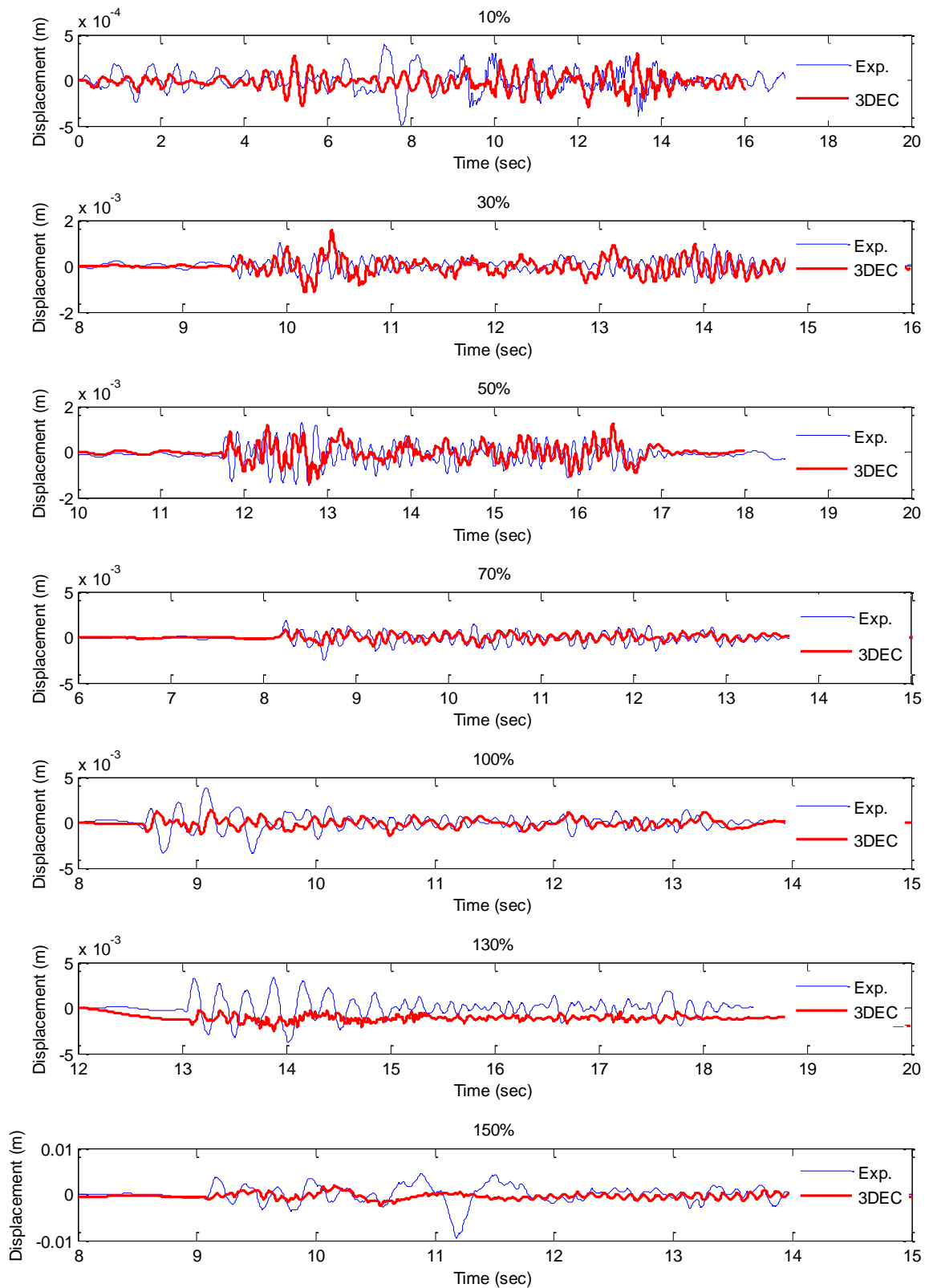


Figure 3.53. Time domain comparisons of experimental and numerical displacement under 10 %, 30 %, 50 %, 70 %, 100 %, 130 % and 150 % earthquake loading.

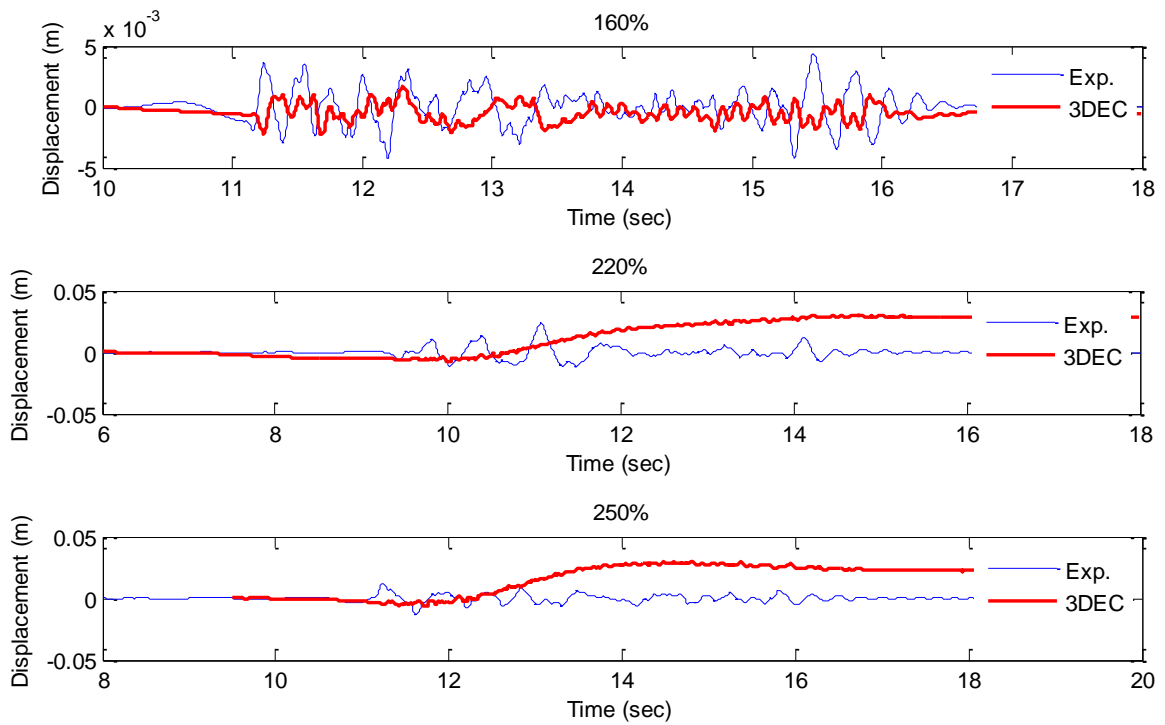


Figure 3.54. Time domain comparisons of experimental and numerical displacement under 160 %, 220 % and 250 % earthquake loading.

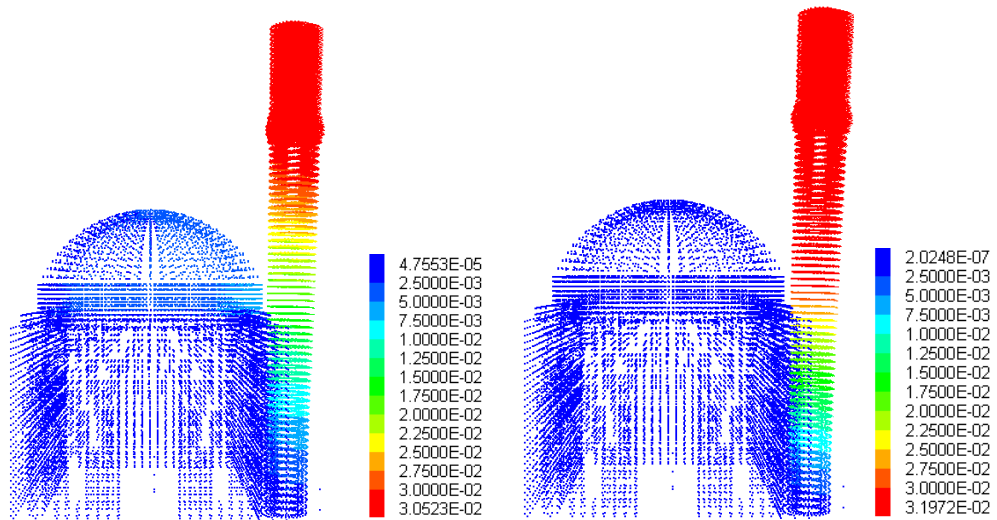


Figure 3.55. Displacement vectors under 220 % (left), and 250 % (right) Montenegro Earthquake.

### 3.7. Numerical Investigation of the Distinct Element Model with FRP Strengthening and Comparison with Experimental Data

The numerical FRP model was developed and calibrated by experimental data so that it satisfactorily represents measured model behavior. FRP application was represented in the numerical model by axial reinforcements. The experimental and analytical model is shown in Figure 3.56. Same mechanical characteristics as those used in the FRP application in the experimental model are used to define the geometry and properties for axial reinforcing elements. In 3DEC axial reinforcement with local normal restraint across discontinuities is provided. The axial element material properties were assigned using axial stiffness (force/displacement), shear stiffness (force/displacement) and ultimate axial and shear capacities which were determined by multiplying tensile strength and cross section area. Shear and axial rupture strains were assumed as 0.1. The mechanical properties of FRP are given in Table 3.7. After the development of the numerical model, self-weight static analysis was performed to verify the correct geometrical description of the structure and the properties of the materials. Following the static analysis FRP strengthened model developed with 3DEC was subjected to the same dynamic loading sequence in the nonlinear field as the test structure during the shake-table experiments.

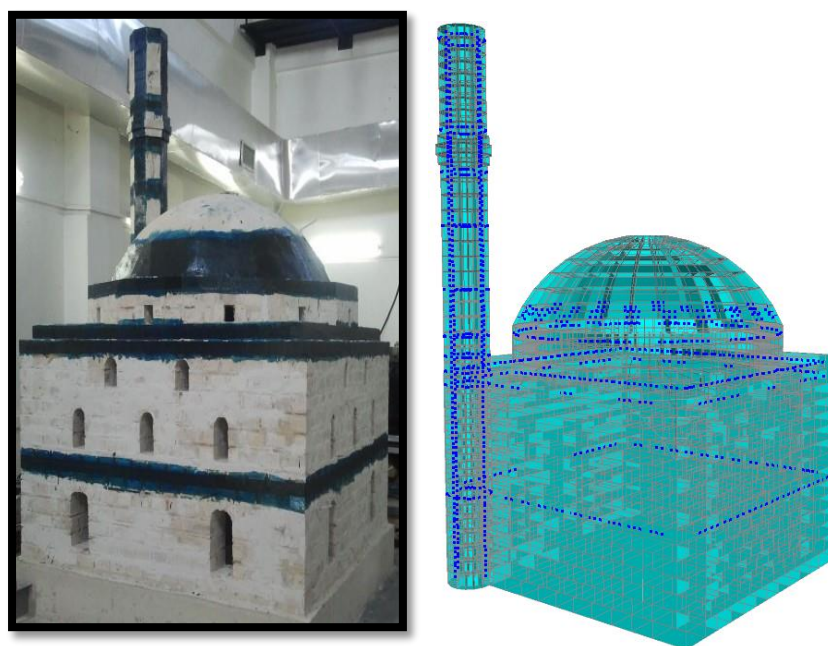


Figure 3.56. Images of experimental and analytical strengthened models.

Table 3.7. FRP properties used in the numerical and experimental analysis.

<b>MBRACE FIBRE CF230/4900 - 200 g/m<sup>2</sup></b>	
Material Type	Carbon
Elasticity Modulus (N/mm <sup>2</sup> )	230.000
Tensile Strength (N/mm <sup>2</sup> )	4900
Design Cross section thickness (mm)	0.111
Fiber weight ((g/m <sup>2</sup> )	210
Elongation at break (%)	2.10
Width (mm)	500

### 3.7.1. Analytical Model Predictions and Comparison with Experimental Results

The numerical simulations were compared with experimental results and the effectiveness of FRP subjected to different seismic actions was investigated. In the comparisons of analytical and experimental results, velocity time histories, Fourier amplitude spectra and transfer functions are used. The analyses are carried out for 60 %, 160 %, 190 %, 210 %, 230%, 250 % and 375 % Montenegro input. In Figure 3.33 measurement locations on the minaret of the shake table model and corresponding points on the numerical model are shown. The comparisons of experimental and analytical velocities and their Fourier amplitude spectra can be found as a complete set (for the minaret; for all input motion levels) in the attached CD as Appendix B. In addition to velocities and FAS, experimental and analytical transfer functions of the minaret are also compared. They are smoothed by a triangular running window of length 11 in the numerical model and a 21 point window in the experimental model. They are given in Figures 3.57-3.59 for all levels of Montenegro input. The transfer functions are calculated with respect to instrument 1. (see Figure 3.33 for its location). The same smoothing windows are applied to the data as described in Section 3.8.1. At lower levels of input there is almost a perfect match between the numerical and experimental model (Figure 3.57, top). Experimental results suggest that the frequency that was about 11.06 Hz under 60 % Montenegro, drops all the way down to 6.64 Hz under 230 % Montenegro (Figure 3.57, Figure 3.58). Under 250 % and 325 % Montenegro, although vague, the dominant frequency is still traceable (Figure 3.59). The numerical model however appears to be relatively less efficient in estimating the experimental response than it was in modeling of the base isolated and the un-strengthened model under higher levels of input.

Starting with 160 % Montenegro input (Figure 3.57) we start to see a frequency response that involves a frequency band rather than a peak. Analytical model is generally less responsive than the experimental model looking at the transfer function amplitudes (Figures 3.57-3.59). However velocity time history and FAS comparisons provided in Appendix B, have a better fit. It is clearly seen from Figure 3.60 under 160 % Montenegro Earthquake loading natural frequency of strengthened model obtained from 3DEC is 9.03 Hz which is very close to that obtained from the test (9.48 Hz). In Figure 3.61 the variation of frequencies corresponding to peak FAS, with respect to the change in the amplitude of input motion are plotted. Natural frequencies of non-strengthened analytical and experimental model die out under larger earthquakes. The contribution of this strengthening approach to the structural response in terms of natural frequency is considerable (Figure 3.60).

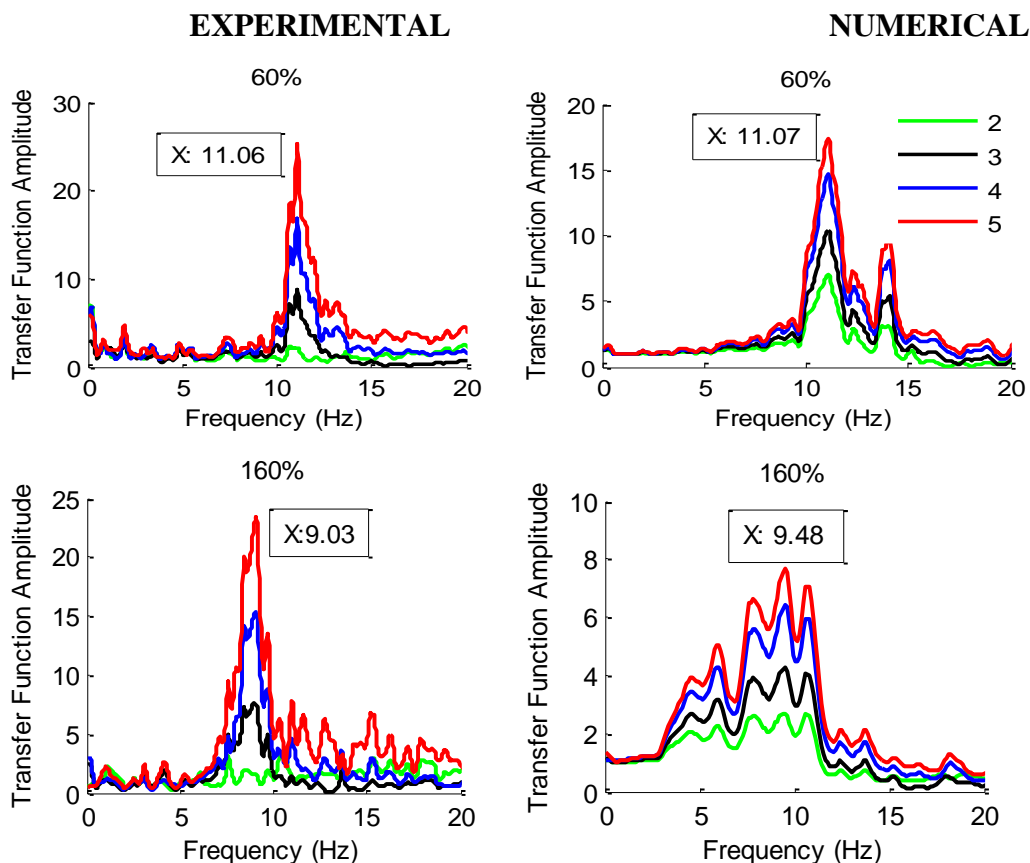


Figure 3.57. FRP-strengthened experimental and numerical transfer function amplitude for levels of 2, 3, 4 and 5 respectively at 1.75 m, 2.45 m, 3.25 m and 3.90 m of minaret under 60 % and 160 % earthquake loading.

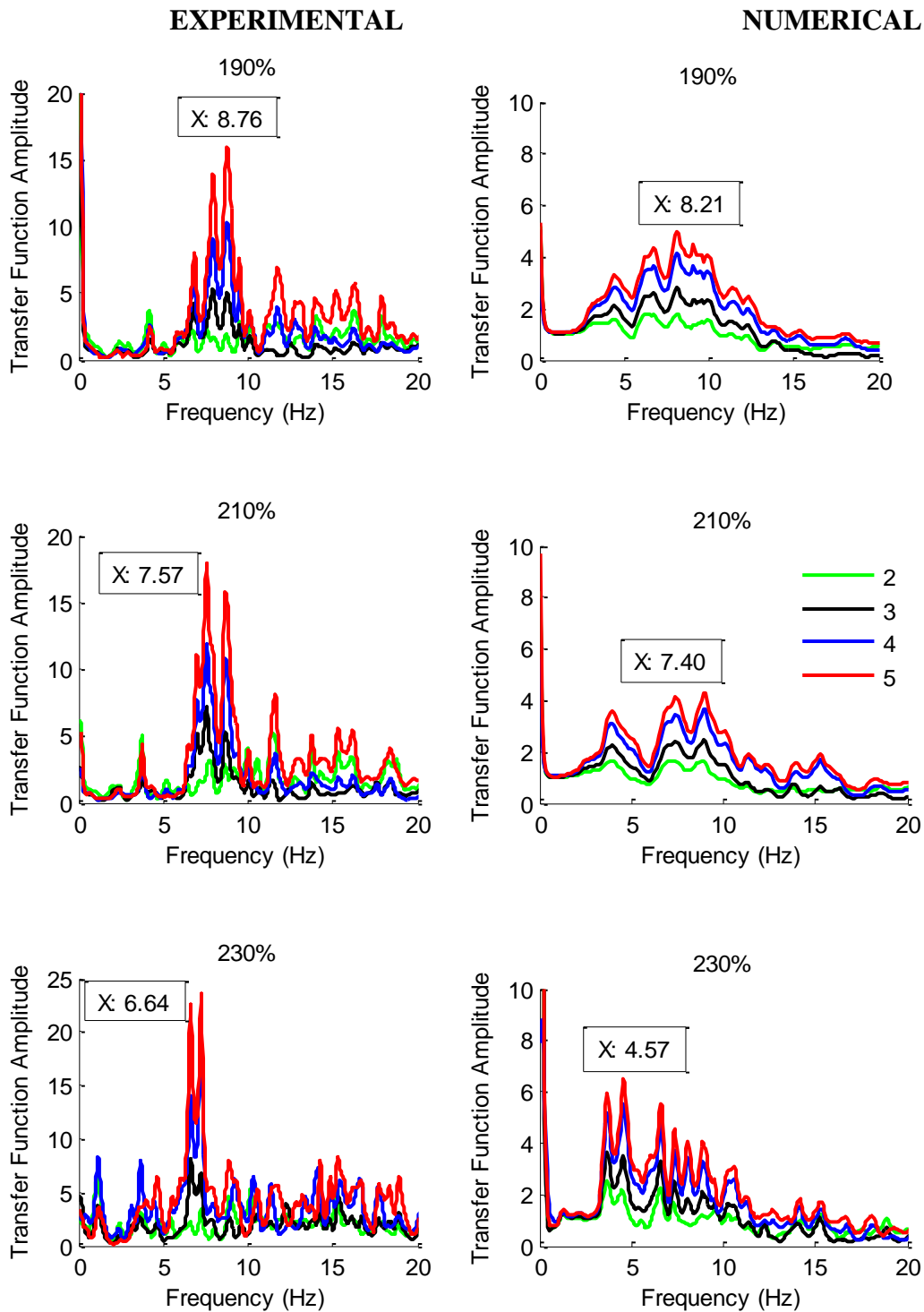


Figure 3.58. FRP-strengthened experimental and numerical transfer function amplitude for levels of 2, 3, 4 and 5 respectively at 1.75 m, 2.45 m, 3.25 m and 3.90 m of minaret under 190 % 210 % and 230 % earthquake loading.

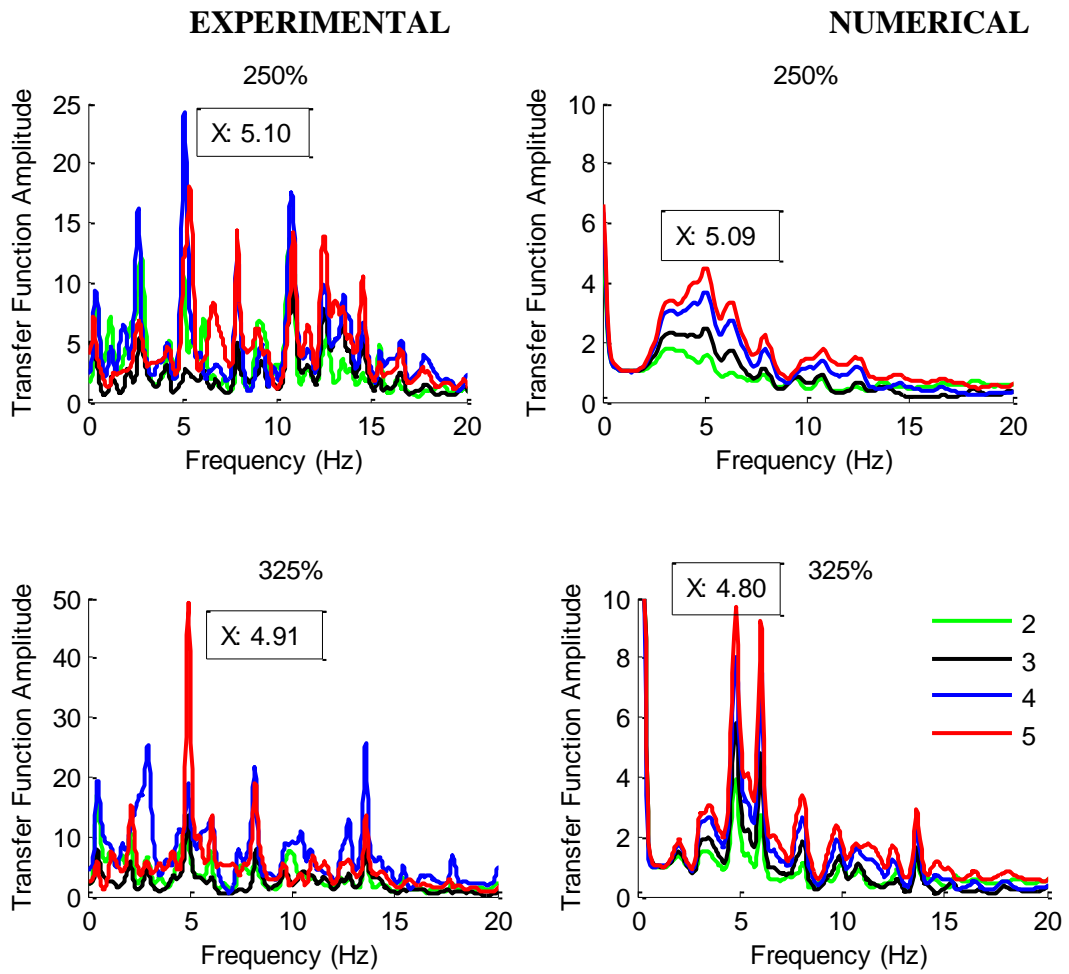


Figure 3.59. FRP-strengthened experimental and numerical transfer function amplitude for levels of 2, 3, 4 and 5 respectively at 1.75 m, 2.45 m, 3.25 m and 3.90 m of minaret under 250 % and 325 % earthquake loading.

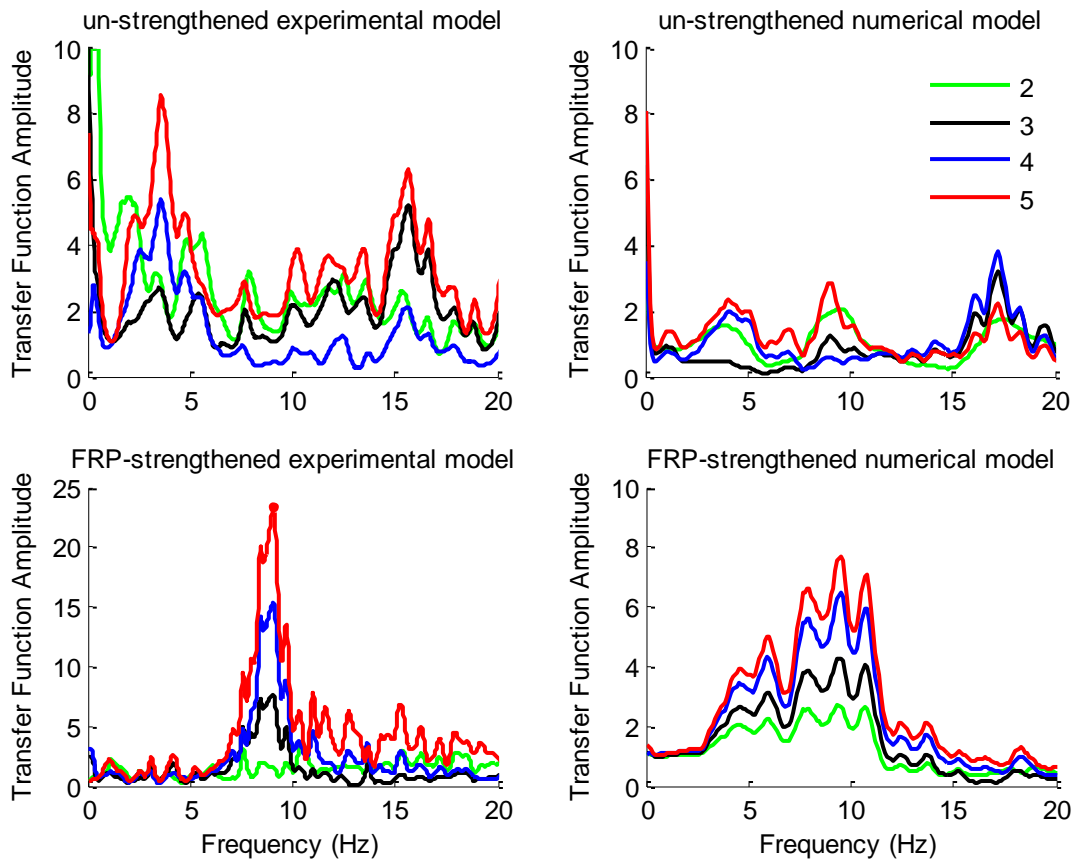


Figure 3.60. Transfer function amplitude of FRP-strengthened and un-strengthened models for levels of 2, 3, 4 and 5 respectively at 1.75 m, 2.45 m, 3.25 m and 3.90 m of minaret under 160 % earthquake loading.

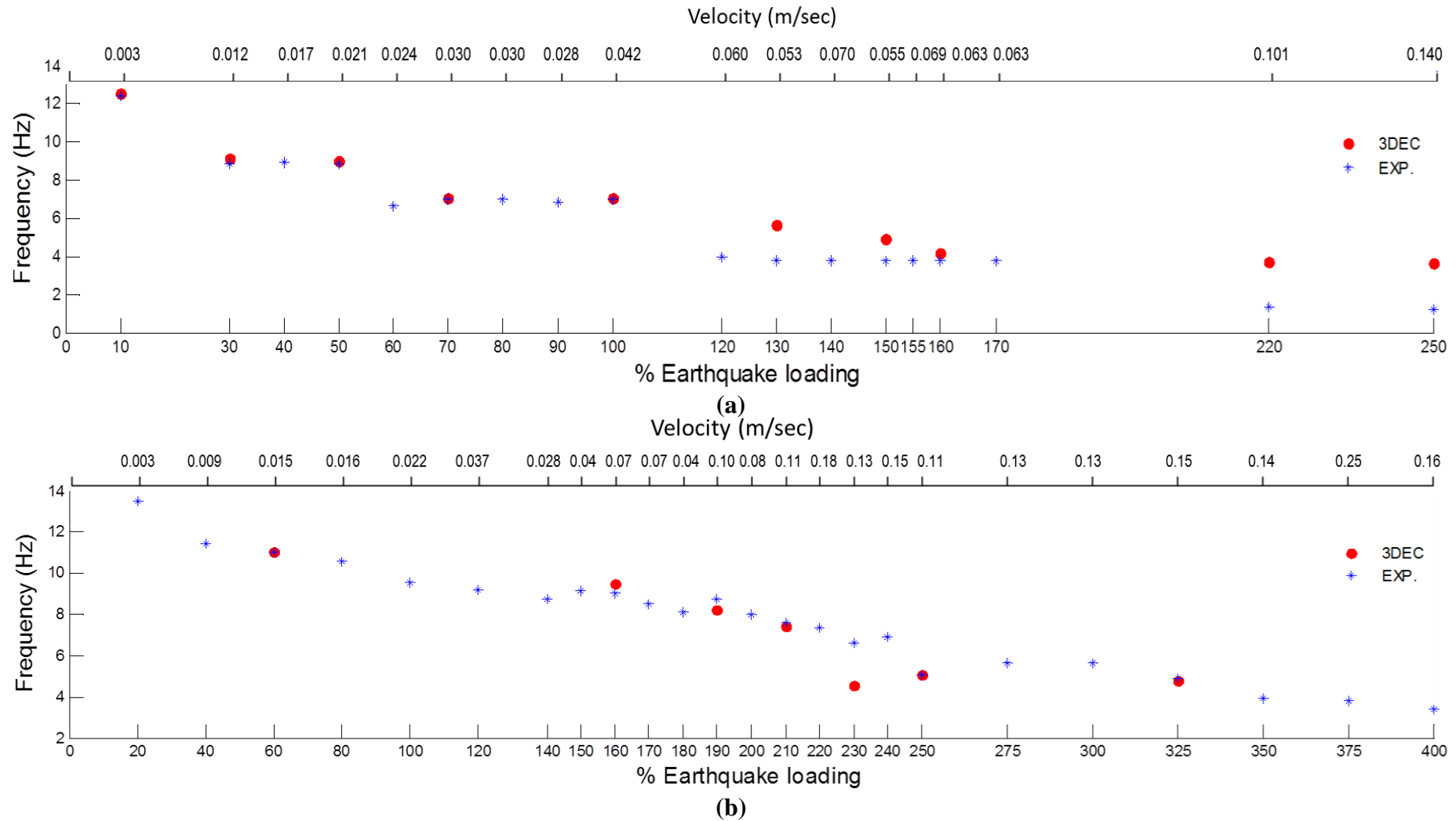


Figure 3.61. Comparisons of experimental and numerical fundamental frequencies of un-strengthened (a) and FRP- strengthened (b) models under sequential loadings. Top x axes of the figures display the peak velocities corresponding % earthquake loading.

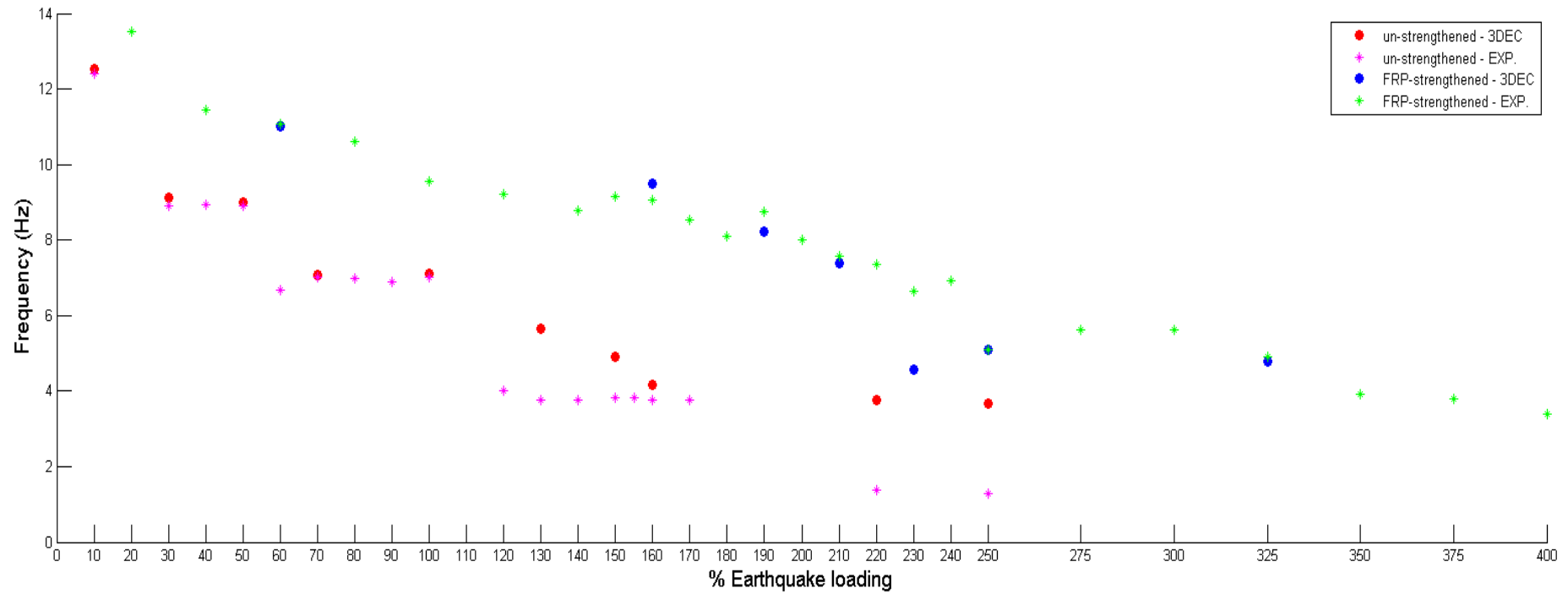


Figure 3.62. Variation of experimental and numerical fundamental frequencies of un-strengthened and FRP- strengthened models under sequential loadings.

### 3.8. Discussion and Conclusions

The motivation behind the effort presented in this chapter was to answer the question whether we can use the distinct elements method, in the earthquake performance analysis of masonry structures, and in the investigation of two commonly applied methods for their earthquake rehabilitation; base isolation and FRP application.

Analytical model provided to get accurate predictions of the actual response of the experimental model. Nonlinear behavior of mortar joints played a crucial role in the response of the minaret subjected to lateral loading. Generated stresses led to tensile failure and shear sliding along the mortar joints that are controlled by their bond characteristics. It is concluded that the accuracy between experimental and numerical models is very reasonable in terms of measured and calculated response and in terms of actual damage that took place on the shake table model, and analytical damage on the 3DEC model.

Rigid blocks are used to represent the base isolation system for the analytical model that act as viscous dampers in the shear direction. The results show a very reasonable agreement between experimental and analytical results, with amplitudes and frequencies exhibiting deviations in an acceptable range. The comparisons of recorded and estimated motion in time and frequency domain at the foundation level provide the best information on the efficiency of our modeling.

Although satisfactory, the numerical FRP model appears to be relatively less efficient in estimating the experimental response than it was in modeling of the base isolated and the un-strengthened model under higher levels of input. The contribution of this strengthening approach to the structural response is considerable (Figure 3.62). This has been observed during the experimental stage and was successfully replicated by distinct element modeling. Development and successful calibration of the model in the nonlinear range suggest that the distinct element method can reliably be employed in the investigation of dynamic behavior of minarets.

## 4. BEHAVIOR ANALYSIS OF MASONRY MINARETS

### 4.1. Introduction

Minarets, which symbolize the spiritual elevation of man towards God, are important elements of mosques that constitute the essence of Islamic art. Seismic behavior of minarets is different than other common structures. Old ones are mostly made of cut-stone-block masonry and occasionally of brick masonry, while the new ones are generally of reinforced concrete. Minarets have a strong presence in Turkey. They have suffered significant damage during past earthquakes underlining the need for their maintenance, preservation and protection. As they will continue to get affected by the earthquakes, it is worthwhile to understand their damage and collapse mechanisms.

Istanbul, the largest city of Turkey, is home to many historical and modern minarets. Within the scope of this chapter three minarets in Istanbul are studied to investigate how their seismic response is influenced by their geometry. Three selected minarets are adjacent to the main mosque at their pulpit and stand free starting with their transition segment. Discrete elements method is employed in the analysis. Main elements a minaret can be seen in Figure 4.1.

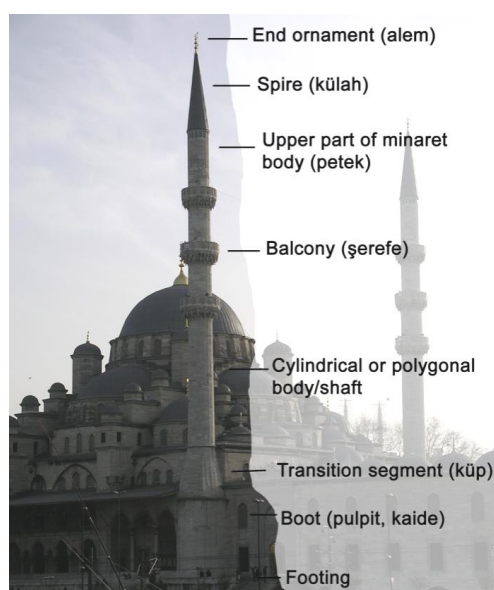


Figure 4.1. Elements of a typical Ottoman minaret (Oliveira *et al.*, 2012).

#### 4.1.1. Previous Studies

Elwan (1996) studied the mechanical behavior of masonry minarets through seismic analysis of the minaret of Al-Ghuri Mosque (46 m height), ancient Cairo, Egypt using Drain-2DX code and proposed a method for the evaluation of the safety level of masonry minarets. Oğuzmert (2002) studied the Minaret of Dolmabahçe Mosque in Istanbul by creating its numerical model using finite element method and estimated its mechanical properties through modal analysis. Sezen *et al.* (2003) evaluated the fundamental vulnerabilities and damages to 64 masonry and reinforced concrete minarets after the 1999 Kocaeli and Düzce Earthquakes. Acar *et al.* (2007) studied the response of a reinforced concrete minarets located on the four different subsoil classes defined in the Turkish Earthquake Code and concluded that the dynamic response of the minarets changes significantly depending on the soil condition. Sezen *et al.* (2008) investigated the cause of extensive damage to reinforced concrete minarets by studying observed failure modes and their seismic performance during the 1999 Kocaeli and Düzce Earthquakes. Representative reinforced and unreinforced minarets with 20, 25, and 30 m height were modeled and analyzed using two recorded ground motions. The modal analyses of minaret models showed that the structural periods and the overall structural response were influenced by minaret height and spectral characteristics of the input motion respectively (Doğangün *et al.*, 2008). Türk and Coşgun (2010) presented a strengthening method by using FRP wrapping on the minaret of Dolmabahçe Mosque. Hacıfendi and Fahri (2011) presented a stochastic seismic response analysis of masonry minarets subjected to random underground blast and earthquake-induced ground motion and performed a parametric study to estimate the effects of the blast-induced ground motion on the stochastic response of the minaret. Study results showed that the stochastic dynamic response values increase with the increase of the blast charge weight, but decrease with the increase in the distance between the structure and blast center. Altunışık (2011) investigated dynamic response of masonry minarets before/after FRP composite strengthening through analyzing the numerical model under seismic. Sezen *et al.* (2012) studied the seismic performance of the mosques and minarets during the 1999 earthquakes through dynamic analyses of a masonry minaret example. In Doğangün *et al.* (2012) five historical masonry mosques were surveyed and the factors contributing to their deterioration were presented.

Dynamic behavior of typical historical minarets in Istanbul made of natural block stone were investigated by using ambient vibration approach and finite element method (Oliveira *et al.*, 2012). Tabeshpour (2012) investigate the seismic response of chimney-like towers through nonlinear dynamic analysis and concluded that the simplified model provided sufficient accuracy based on a nonlinear discrete model. In Mortezaei *et al.* (2012) the issue of modelling and seismic analysis of the minaret, dome and the semi-dome shaped masonry mosque was investigated based on dynamic analysis of 3D numerical models. In order to assess the structural behavior and evaluate the seismic vulnerability of the Jam'e mosque of Semnan, it was subjected to seismic analysis through application of horizontal forces perpendicular to one another not acting simultaneously. Also the effects of the current techniques of repair and strengthening were investigated in order to evaluate the effectiveness of these techniques in retrofitting historical buildings. Effectiveness of the vertical post-tensioning technique to reinforce the unreinforced masonry minarets was investigated by Pekgökgöz *et al.* (2013) and it was concluded that the vertical post-tensioning application is an efficient method to reduce axial tensile stresses and lateral displacements, and to assure the overturning safety of masonry minarets against earthquakes. Abdel-Motaal (2014) studied a 60.0 m height minaret to investigate the effect of pile length, diameter, and soil stiffness on its dynamic response of the minaret.

## **4.2. General Description of Minarets Selected for Analysis**

### **4.2.1. The Minaret of the Mihrimah Sultan Mosque**

Mihrimah was the daughter of Suleiman I and Hürrem Sultan. She was born in 1522 in Istanbul and died in 1578 in the same city. She was a politically influential and wealthy person. There are two mosque complexes in Istanbul founded by Mihrimah Sultan. The subject of this section is the Mihrimah Sultan Mosque in Edirnekapı located near the land walls of the old city of Istanbul (Figure 4.2). The mosque was a complex of structures composed of a mosque, madrassa, double bath, sepulcher, market and primary school. Unfortunately many of them do not exist today. Earthquakes repeatedly caused harm to the mosque, to its minaret and to the adjacent units. The earthquakes of 1719, 1766 and 1894 led to partial collapses (Müller-Wiener, 1977).

An image of the minaret taken sometime after the 1894 earthquake and before its repair in 1907 is shown in Figure 4.3. The whole complex, including the minaret, underwent a comprehensive restoration scheme after the damages sustained during the Mw 7.4, 1999 Kocaeli Earthquake. The minaret of the Mihrimah Sultan Mosque built of cut-stone masonry and rises to 39.86 m from the ground level including its spire. The body diameter is 2.30 m.



Figure 4.2. Images of the Mihrimah Sultan Mosque (left), its minaret before its disassemblage (center), cross-section of the minaret (right).



Figure 4.3. Image of the Mihrimah Sultan Mosque with the minaret that collapsed in the 1894 earthquake. Image taken sometime between 1894 and 1907 (Gurlitt, 1999).

#### 4.2.2. The Minaret of the Hagia Sophia Museum

The Hagia Sophia is one of the most magnificent historical structures in Turkey. It is built as a Byzantine Church in 532-537 during the reign of Justinian. It is located on the first hill of Istanbul surrounded by the Sea of Marmara, the Bosphorus and the Golden Horn on three sides. Its cultural, religious and architectural influence is unprecedented. The main load bearing elements of the Hagia Sophia are its enormous dome, the four main arches, the four main piers, the two semi domes, and the four secondary piers.

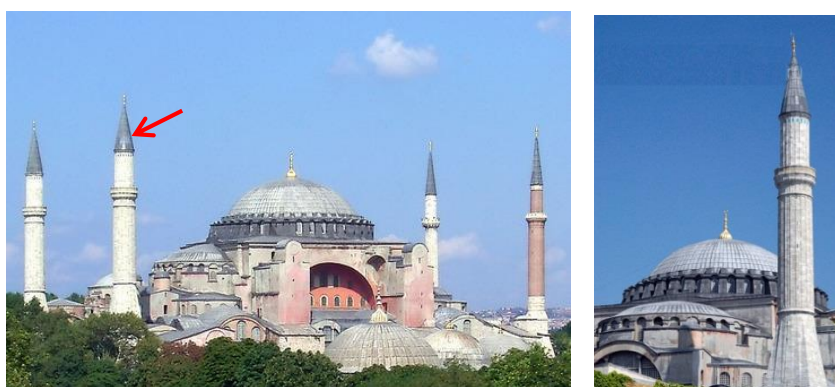


Figure 4.4. The Hagia Sophia Mosque (left), study case minaret (right).

The Hagia Sophia has four minarets constructed in different times using different materials. The earliest minaret, built in red brick (Figure 4.4) was added soon after the conquest that took place in 1453 during the reign of Mehmed II. The second minaret, located to the north of the first one, was constructed during the reign of Beyazıd II. The two remaining minarets were added during the reign of Murad III (1574-1595) by Sinan (Müller-Wiener, 1977). For the current study, the southern one of the two final additions is selected (Figure 4.4). The minaret rises to 72.86 m starting from the ground level including the 11.57 m spire. Its body diameter is 4.86 m.

#### 4.2.3. The Minaret of the Süleymaniye Mosque

The Süleymaniye Mosque was designed by the Ottoman architect Sinan and constructed between 1550 and 1557. The shape of the Süleymaniye Mosque floor plan is basically a square on which the major praying hall, with a central main dome rises.

The main dome is supported by four main arches, two semi domes, four main piers and the secondary piers and arches surrounding and thus supporting the central structural elements (Figure 4.5). Main dome has a diameter of 26.5 m. It rises to 47.50 m height from the ground. (Durukal *et al.*, 2003; Yükçü *et al.*, 2007; Eilouti, 2012). The mosque has four minarets. The two of them are adjacent to the main building. The other two, shorter in height than the first pair, are located across the courtyard (Figure 4.5). The minarets are of cut-stone, that are infixed with iron tie elements forming a belt across the perimeter.

The minaret selected for the current study is indicated in Figure 4.5. It rises to 74.16 m starting from the ground level including the 10.76 m spire. Its body diameter between transition and second balcony is 3.86 m. The diameter of the body between the second balcony and the top of the minaret is 3.12 m.

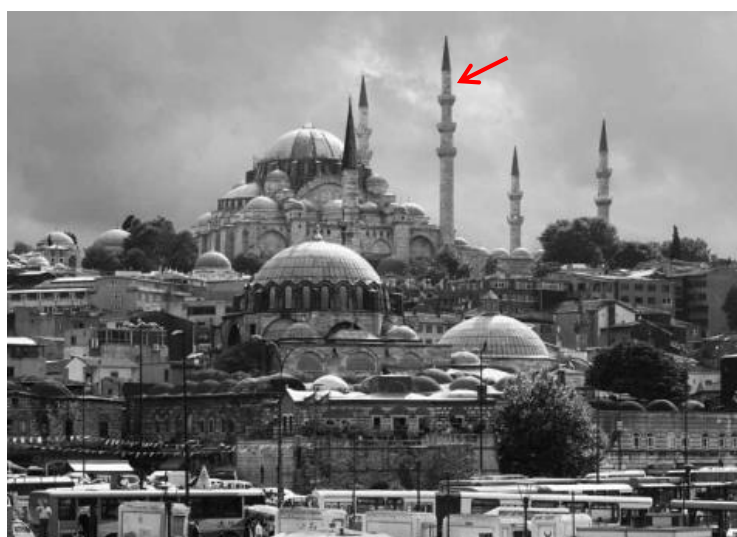


Figure 4.5. View of the Süleymaniye Complex (Ediz and Ostwald, 2012).

### 4.3. Ultrasonic Testing of the Mihrimah Minaret

The ultrasonic testing is a useful technique for investigating the presence of subsurface discontinuities such as cracks and internal masonry damages. The sonic waves are generated and transmitted through the masonry structure and the time that takes to reach the receiver is measured since the stress wave velocity is depend on the density in masonry. Signal travel times can be directly related to the reflector distance and this time is evaluated for determining the asperities or void locations.

A beam of ultrasonic energy is launched inside the material by exciting, with a high-voltage pulse, a piezo-electric crystal contained in a transducer, which is called transmitter probe, in contact with the material (Meola, *et al.*, 2005). Ultrasonic pulse velocity measurement can be performed in three different ways, which are direct, semi-direct and indirect methods. As shown in Figure 4.6, in direct method, transmitter and receiver are placed on opposite surfaces of tested object to measure the transit time. The two transducers are arranged at a 90° angle in semi-direct transmission mode. Transducers are placed on the same surface of the specimen tested in indirect measurement method and the points of receiver arranged are changed along a specific line.

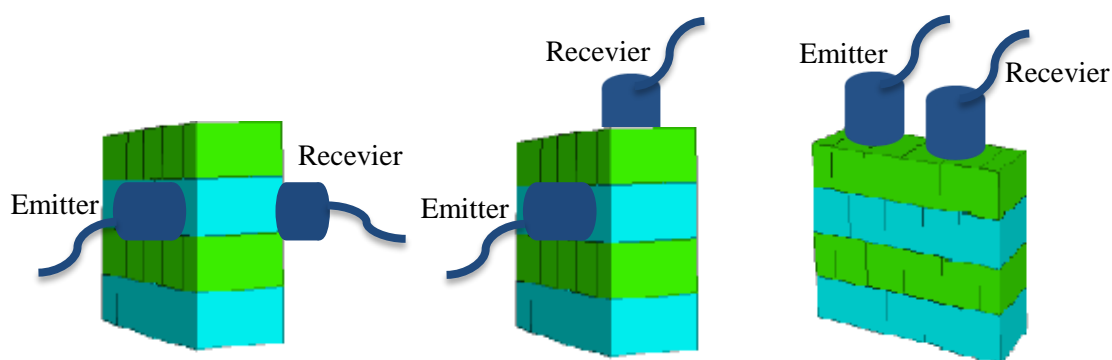


Figure 4.6. Schematic views direct (right), semi-direct (center) and indirect (left) methods of ultrasonic measurements.

Lemoni and Christaras (1999) proposed that the direct transmission method is more effective and has more sensitive and reliable results than other methods, because the direction of waves is normally parallel to the transducers and the ultrasonic waves prefer the shortest way to reach the receiver.

In the scope of this study Pundit Lab + ultrasonic testing instrument with 54 kHz UPV and 250 kHz shear wave transducers were used. The tests were carried out in three different sections of the minaret: in the pulpit, in the transition segment and in the body. In order to get correct data the surfaces of the probe and of the tested material need to be in full contact with each other. A coupling gel was used on probe surfaces to ensure. 37 direct ultrasonic pulse velocity (UPV) measurements were taken in the pulpit, 20 in the transition segment and 58 in the body. The numbers of readings were 97, 32 and 113 for the pulpit, the transition segment and the body respectively.

The results suggest that the properties of stone used in the pulpit, in the transition segment and in the body are different from each other. The variation in readings with respect to different regions is justified; as the  $V_p$  measurements carried out by two different sensor types (54 kHz and 250 kHz) confirm each other. It should be noted that the pulpit and the transition segment are original, while the body is newly built. There is no evidence that the pulpit and the transition segment date from the same period. The stone used in the transition segment is probably similar to the stones used in the construction of the body. On the other hand, the properties of stone used in the pulpit and the body are clearly different from each other (Çaktı *et al.*, 2013). Summary of results of ultrasonic testing in the Mihrimah minaret is given in Figure 4.7. Region 1, 2 and 3 represent the pulpit, transition segment and the body of the minaret respectively.

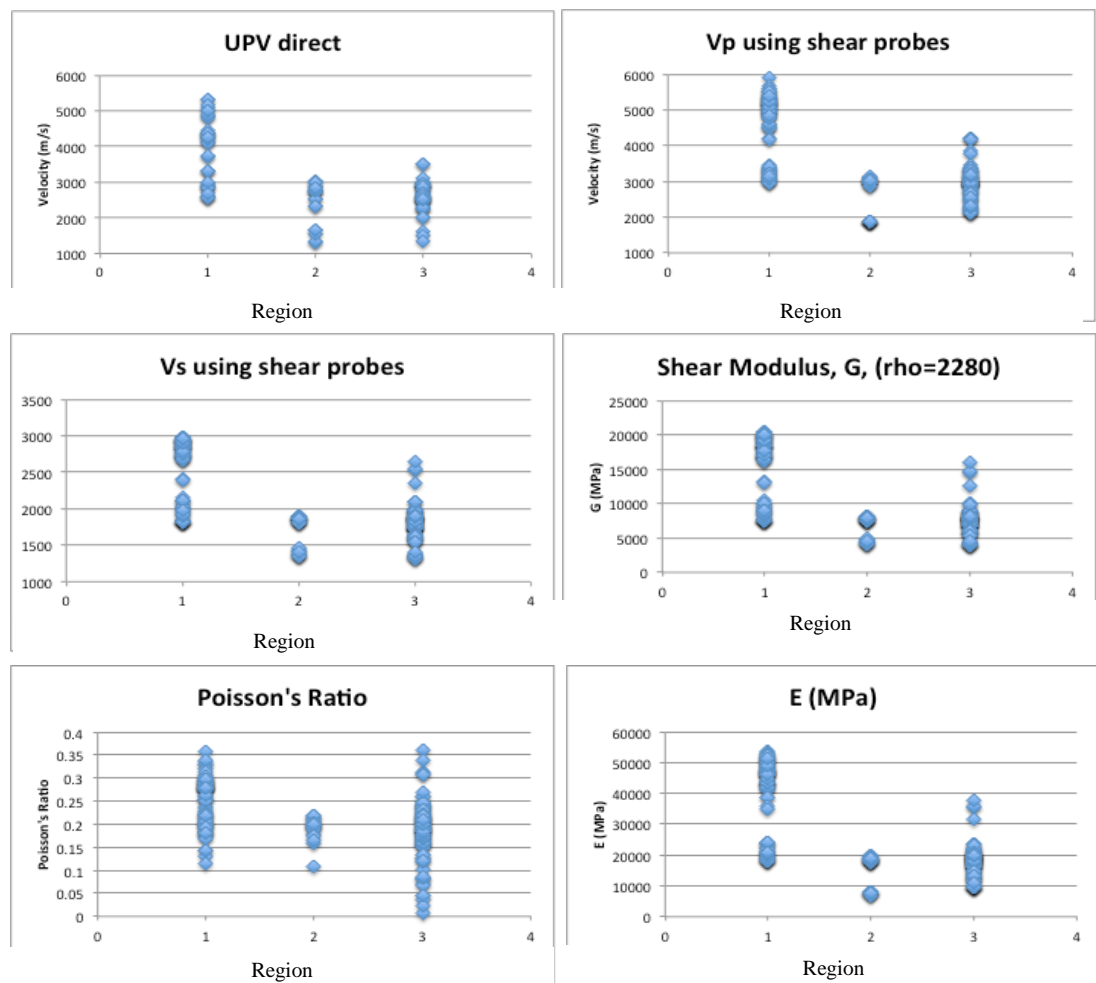


Figure 4.7. Summary of results of ultrasonic testing in the Mihrimah minaret. In the upper row velocity readings are shown. Lower row includes shear modulus  $G$ , Poisson's ratio and modulus of elasticity  $E$  estimated from the velocities (Çaktı *et al.*, 2014).

#### 4.4. Analytical Modeling and Assumptions

Three dimensional models are developed to study the response of the three minarets to seismic loading. 3D analytical models created in 3DEC are shown in Figure 4.8. 3DEC can simulate progressive failure associated with crack propagation and provides insight into the development of local crack patterns, local failures or evaluation of block mortar interface deformations and allows a general analysis to assess joint separation and sliding.

In this study, rigid blocks are employed in the analytical models because rigid blocks significantly reduce computation time and have advantages in time stepping algorithms. In rigid block models, all the system deformation is lumped at the joints. This assumption provides a good approximation to the behavior of masonry structures built in stiff, strong materials, since most of the deformation of the system, as well as the failure mechanisms, originate at the joints. The iron bars connecting the stone blocks were also represented in the numerical models using axial element. For each minaret models, elasticity modulus of axial elements is assumed as 230 GPa to define the properties of axial stiffness and shear stiffness. Tensile strength is assumed as 100 MPa to define ultimate axial and shear capacities which were determined by multiplying tensile strength and cross section area.

For dynamic analyses of masonry minarets, instead of stiffness proportional damping, mass proportional damping is used to damp the natural oscillation modes of the models since stiffness proportional damping increases the integration steps which make the dynamic analysis practically impossible. Mass proportional damping provides to limit high-frequency vibrations which can cause erroneous computational results. The model parameters used in the 3DEC models and geometrical properties of minarets are given in Table 4.1 - 4.6.

Joint normal stiffness ( $k_N$ ), and shear stiffness ( $k_S$ ), cohesion, tension and friction angle are major parameters of the , numerical models. The geometry of the minarets is based on the models developed for finite element analysis in Oliveira *et al.* (2011). Each minaret is remodeled in 3DEC environment.

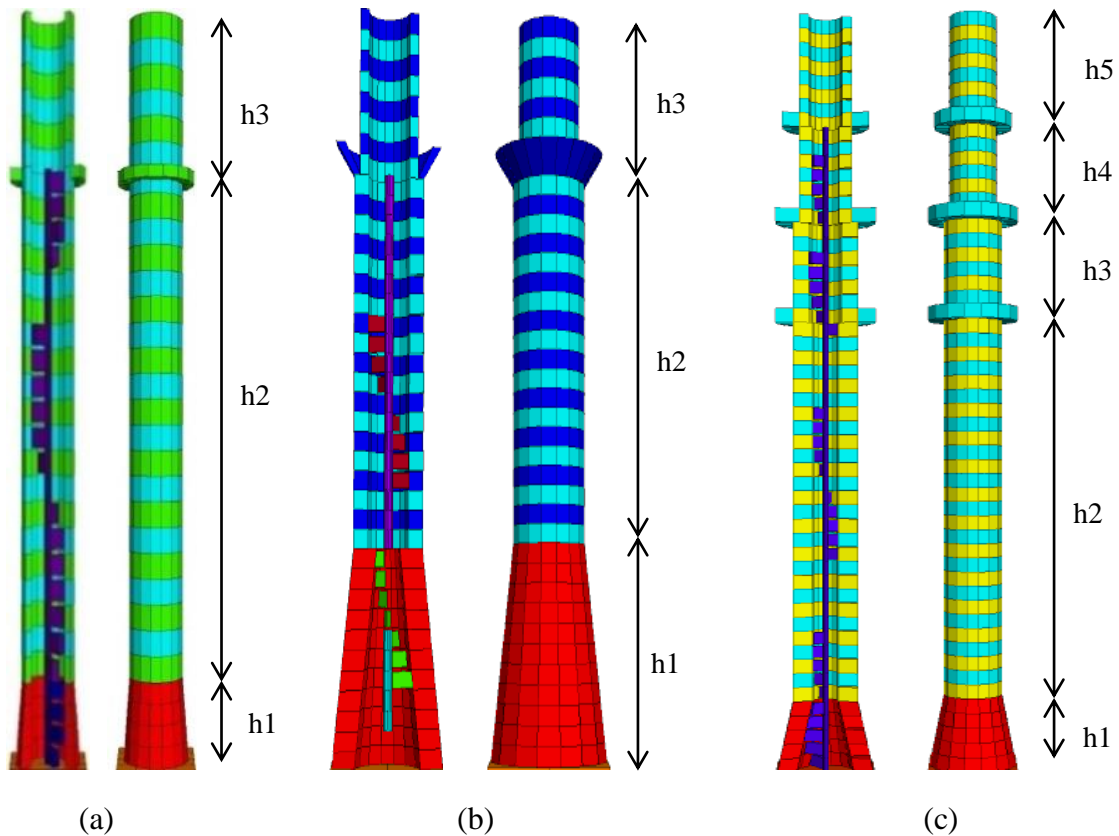


Figure 4.8. Model of the Mihrimah (a), Hagia Sophia (b) and Süleymaniye minarets (c), general view and cross-section.

Table 4.1. Geometrical properties of the Mihrimah minaret model.

Location	Height (m)	Wall thickness (m)	Exterior radius (m)
Transition segment (h1)	3.44	0.30	1.41
Body (h2)	21.00	0.30	1.15
Top (h3)	6.30	0.30	1.15

Table 4.2. Geometrical properties of the Hagia Sophia minaret model.

Location	Height (m)	Wall thickness (m)	Exterior radius (m)
Transition segment (h1)	11.96	1.60	3.97
Body (h2)	19.77	1.00	2.43
Top (h3)	8.67	0.60	2.43

Table 4.3. Geometrical properties of the Süleymaniye minaret model.

Location	Height (m)	Wall thickness (m)	Exterior radius (m)
Transition segment (h1)	5.10	1.15	2.87
Body (h2)	27.30	1.15	1.93
Body (h3)	7.20	0.95	1.93
Body (h4)	6.90	0.75	1.56
Top (h5)	8.10	0.75	1.56

Table 4.4. Modeling parameters for the Mihrimah minaret.

Location		$k_N$ (MPa/m)	$k_s$ (MPa/m)	Cohesion (MPa)	Tension (MPa)	Friction angle (°)
Wall (body)	Horiz. joints	8100	3200	0.5	0.25	35
	Vertical joints	10800	4300	0.5	0.25	35
Wall (trans. segment)	Horiz. joints	9900	3900	0.5	0.25	35
	Vertical joints	10200	4100	0.5	0.25	35
Core (trans. segment)	Horiz. joints	9900	3900	0.5	0.25	35
Core (body)	Horiz. joints	8100	3200	0.5	0.25	35
Core-stair (trans. segment)	Vertical joints	14800	5900	1.0E+20	1.0E+20	35
Core - stair (body)	Vertical joints	14800	5900	1.0E+20	1.0E+20	35

Table 4.5. Modeling parameters for the Hagia Sophia minaret.

Location		$k_N$ (MPa/m)	$k_s$ (MPa/m)	Cohesion (MPa)	Tension (MPa)	Friction angle (°)
Wall (body)	Horiz. joints	9500	3800	0.5	0.25	35
	Vertical joints	9500	3800	0.5	0.25	35
Wall (trans. segment)	Horiz. joints	9500	3800	0.5	0.25	35
	Vertical joints	9500	3800	0.5	0.25	35
Core (trans. segment)	Horiz. joints	9500	3800	0.5	0.25	35
Core (body)	Horiz. joints	9500	3800	0.5	0.25	35
Core-stair (trans. segment)	Vertical joints	18200	7270	1.0E+20	1.0E+20	35
Core - stair (body)	Vertical joints	18200	7270	1.0E+20	1.0E+20	35

Table 4.6. Modeling parameters for the Süleymaniye minaret.

Location		$k_N$ (MPa/m)	$k_S$ (MPa/m)	Cohesion (MPa)	Tension (MPa)	Friction angle (°)
Wall (body)	Horiz. joints	38000	15200	20	10	35
	Vertical joints	38000	15200	20	10	35
Wall (trans. segment)	Horiz. joints	38000	15200	20	10	35
	Vertical joints	38000	15200	20	10	35
Core (trans. segment)	Horiz. joints	38000	15200	20	10	35
Core (body)	Horiz. joints	38000	15200	20	10	35
Core-stair (trans. segment)	Vertical joints	38000	15200	1.0E+20	1.0E+20	35
Core - stair (body)	Vertical joints	38000	15200	1.0E+20	1.0E+20	35

#### 4.5. Comparative Analyses Using Sine Waves

3D minaret models including interior spiral stairs are firstly analyzed using linear material properties with the aim of defining valuable information both on global behavior and on interaction among the structural parts. Self-weight analysis using linear and nonlinear material properties gives useful information about the sections undergoing high compression levels. However static analysis is unable to give precise information on the failure mechanisms and the areas which undergo damages. Consequently nonlinear dynamic analysis of the 3D models with elastic and nonlinear properties are performed under horizontal actions. The values of a set of variables such as velocity, displacement, normal stress, shear stress, normal displacement, shear displacement, are stored during a model run. Besides histories at given locations, the distribution of peak values of joint displacements and stresses throughout the structure are covered in detail to analyze the damage processes.

Solution time increases as more contacts are created in the model because 3DEC takes longer time in small time stepping. The analytical model of the Mihrimah minaret consists of 577 rigid blocks and 17618 sub-contacts, the Hagia Sophia minaret consists of 697 rigid blocks and 20572 sub-contacts and the Süleymaniye minaret consist of 1005 rigid blocks and 29250 sub-contacts.

The maximum unbalanced force is determined in time step 4.215E-05 in the case of Mihrimah minaret, 2.072E-05 in the Hagia Sophia minaret and 3.009E-0.5 in the minaret of Süleymaniye.

Preliminarily, the analysis of the minaret models under gravity loads only was performed. The maximum vertical stress in this loading condition is 6.58E-01 MPa in the Mihrimah minaret, 9.21E-01 MPa in the Hagia Sophia minaret and 1.43E+00 MPa in the Süleymaniye minaret. Full dynamic nonlinear analysis followed the static analyses. Analytical simulations of minarets are carried out by subjecting them a series of sine-wave excitations by gradually changing the frequency and amplitude of input velocity. The frequency ranges covered in this study and the first natural frequencies of vibration of the minarets as obtained by ambient vibration testing by Olivera *et al.* (2011) are given in Table 4.7 and 4.8 respectively.

The sine waves to be used as input are varied between 10%, and 100% with 10% increments. 100% corresponds to 100 cm/s and 10% corresponds to 10 cm/s. It should be pointed out that combinations of high velocity-high frequency are not plausible as they are unlikely to occur. Yet for the sake of uniformity of analysis it was decided to keep them. Finally all sine waves produced in this manner are subjected to a Tukey (tapered cosine) type window, which is a rectangular window with the first and last  $r/2$  percent of the samples equal to parts of a cosine. The window was applied in the following manner (Bloomfield, 2000);

$$\omega(x) = \frac{1}{2} \left\{ 1 + \cos \left( \frac{2\pi}{r} [x - r/2] \right) \right\} \quad 0 \leq x < \frac{r}{2} \quad (4.1)$$

$$\omega(x) = 1 \quad \frac{r}{2} \leq x < 1 - \frac{r}{2} \quad (4.2)$$

$$\omega(x) = \frac{1}{2} \left\{ 1 + \cos \left( \frac{2\pi}{r} [x - 1 + r/2] \right) \right\} \quad 1 - \frac{r}{2} \leq x < 1 \quad (4.3)$$

where  $x$  is a  $L$ -point linearly spaced vector and  $r = 1.0$ .  $1/2$  of the entire window length consists of segments of a phase-shifted cosine with period  $r = 1$ . In Figure 4.9 an example family of sine waves used in the analysis of the Hagia Sophia minaret can be seen.

Table 4.7. Covered frequency ranges for three minarets.

Frequency range (Hz)		
Mihrimah	Hagia Sophia	Süleymaniye
0.10	1.02	0.70
0.30	1.07	0.75
0.50	1.11	0.80
0.70	1.16	0.85
0.73	1.20	0.90
0.76	1.25	0.95
0.79	1.29	1.00
0.82	1.34	2.00
0.85	1.38	3.00
0.88	2.00	4.00
0.91	3.00	5.00
0.94	4.00	6.00
2.00	5.00	7.00
3.00	6.00	8.00
4.00	7.00	9.00
5.00	8.00	10.00
6.00	9.00	-
7.00	10.00	-
8.00	11.00	-
9.00	12.00	-
10.00	13.00	-

Table 4.8. Experimental and analytical frequencies of vibration.

Minaret	Exp. first mode of vibration (Hz)	Exp. second mode of vibration (Hz)	Exp. torsional mode of vibration (Hz)	Analytical first mode of vibration (Hz)
Mihrimah	0.80-0.84	4.24-4.52	-	0.82
Hagia Sophia	1.17-1.27	3.37-4.05	9.67-10.64	1.20
Süleymaniye	0.82-0.85	3.68-3.84	-	0.73

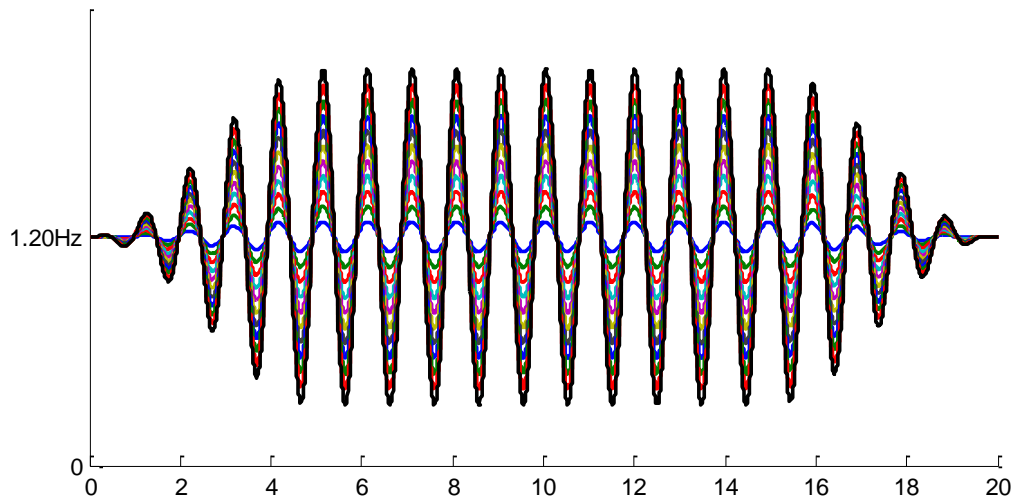


Figure 4.9. The example of plot of the 1.20Hz sine-waves for the dynamic analysis of the Hagia Sophia.

Within the scope of this study, two engineering demand parameters were used: the maximum relative dislocation of adjacent drums normalized by the drum diameter at their interface, and the maximum displacement at the top of the minaret normalized by the drum diameter. The first parameter, the relative dislocation of adjacent drums normalized by the drum diameter at their interface,  $u_d$ , is defined as;

$$u_d = \frac{\max(resu_i)}{D_i} \quad (4.4)$$

where  $resu_i$  is the relative drum dislocations at the end of the seismic loading and  $D_i$  is drum diameter.

The second parameter is calculated using the equation of;

$$u_{top} = \frac{u_{max}}{D_{drum}} \quad (4.5)$$

where  $u_{top}$  is the maximum top displacement at the end of the seismic loading normalized by the diameter of the top drum of minaret,  $D_{drum}$ .

#### 4.5.1. Patterns of Deformation and Collapse

Sample images of damage and collapse are presented in Figure 4.10, 4.11 and 4.12 for the Mihrimah, Hagia Sophia and Süleymaniye minarets respectively. These images represent the state of the minarets at the end of sine wave input. They are useful to roughly evaluate whether the structure reaches state of collapse and to have insight into failure typology if it is local or global. In the case of the Mihrimah minaret, notable deformations observed particularly at runs with frequencies larger than 0.91Hz and sine wave amplitudes larger than 70 cm/s and with frequencies lower than 0.73 Hz and sine wave amplitudes larger than 80 cm/s. Collapse took place in 25 out of 210 runs. Relative drum displacements exceeded 15cm in 44 runs. The minaret top has seen displacements exceeding 150 cm without collapse under frequencies less than 0.8 Hz and velocities larger than 90 cm/s. Typical examples of damage and collapse of the Mihrimah minaret can be seen in Figure 4.10. Collapse takes place either following the development of a full horizontal crack in the body of the minaret below the balcony and rocking of the upper part of the minaret under low frequency-high velocity sine waves as in #9 and #10 situations in Figure 4.10; or it occurs as a result of progressive disintegration of blocks in the transition segment, in the body or a-near the balcony at frequencies at frequencies larger than 2 and velocities larger than 60 cm/s (between #4 and #8 situations in Figure 4.10);. In case of damages that involve large displacements without collapse, (between #1 and #3 situations in Figure 4.10), displacements of the minaret top vary between 58 cm and 147 cm, while the deformations associated with the blocks for the cases shown in the figures vary between 7 cm and 20 cm. Stone displacements concentrate in the transition zone, and disturb the alignment of the minaret resulting in significant relative displacements of the minaret top. No collapse took place in the Hagia Sophia minaret during 210 runs, while damage was evident particularly after 2 Hz and sine wave amplitude of 60 cm/s. Typical deformation patterns can be seen in Figure 4.11. It is evident that the along the transition part there are large deformations. Also relative displacements in the part of the minaret above the balcony are significant. In general, relative drum displacements along the minaret reached 37 cm in the runs. At the end of the runs, the general geometry of the minaret more or less maintained its continuity except in a few cases (as in #6, #8 and #10 situations in Figure 4.11). The minaret top however has seen displacements reaching 180 cm.

In a narrow frequency band centered around 3 Hz, the Hagia Sophia minaret experienced displacements of its top larger than 1 m, as early as 40 cm/s, which increased regularly with the increase in the sine wave amplitude. In the case of the Süleymaniye minaret significant deformations and collapse took place notably at runs with frequencies 0.95 Hz and sine wave amplitudes larger than 60 cm/s. Collapse occurred in 16 of 160 runs. Relative drum displacements were greater than 40 cm in 17 of 160 runs. The minaret top has seen displacements of about 150 cm only once (2 Hz & 80 cm/s). The frequency range of 5-7 Hz appears to be important for the Süleymaniye, as in these frequencies top displacements of 80 cm developed as early as 20 cm/s. Typical examples of damage and collapse pattern of the Süleymaniye minaret can be seen in Figure 4.12. They took place around the second balcony where there is change in the cross-section, in the transition segment or in the part of the body between the transition segment and the first balcony. The damage patterns are associated with excessive local deformations of stone blocks, which develop to collapse when the input amplitude increases.

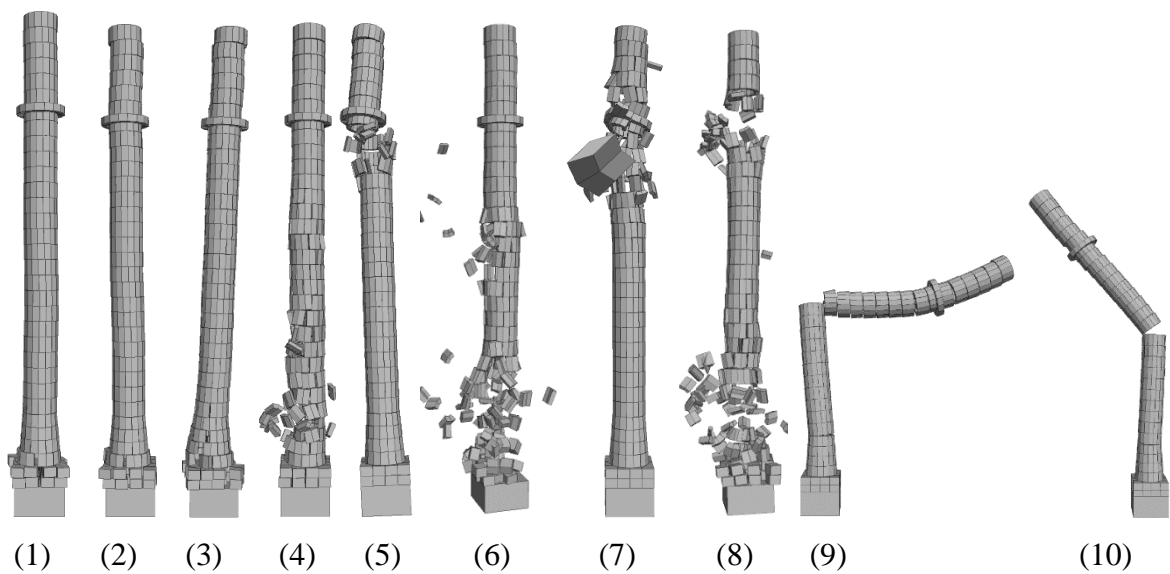


Figure 4.10. Heavy damage patterns for the Mihrimah minaret during the combination of  $f=7$  Hz & 60 cm/s (1),  $f=6$  Hz & 70 cm/s (2),  $f=4$  Hz & 90 cm/s (3) and collapse patterns during the combination of  $f=9$  Hz & 60 cm/s (4),  $f=4$  Hz & 70 cm/s (5),  $f=5$  Hz & 80 cm/s (6),  $f=0.9$  Hz & 90 cm/s (7),  $f=9$  Hz & 90 cm/s (8),  $f=0.5$  Hz & 100 cm/s (9) and  $f=0.7$  Hz & 100 cm/s (10).

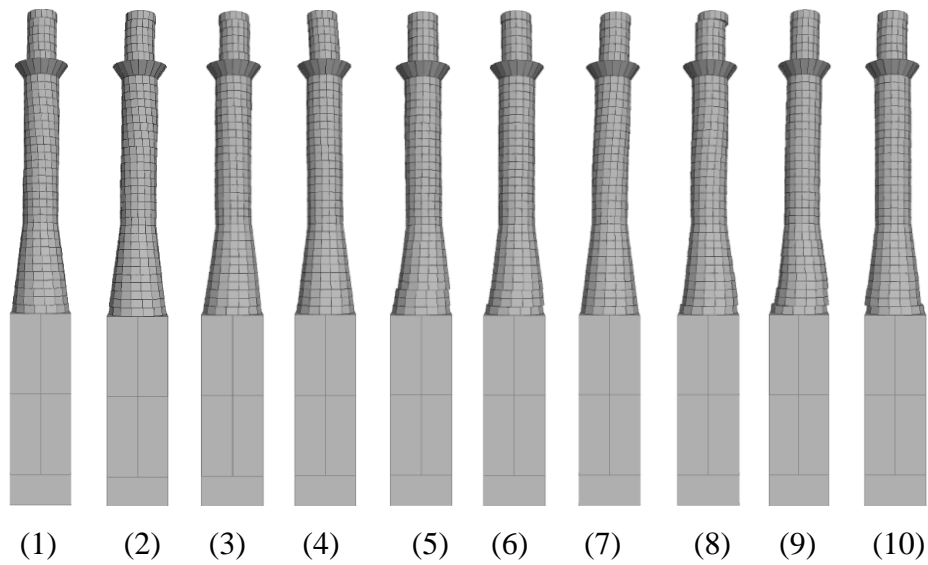


Figure 4.11. Damage patterns for the Hagia Sophia minaret during the combination of  $f=3$  Hz & 60 cm/s (1),  $f=3$  Hz & 70 cm/s (2),  $f=3$  Hz & 80 cm/s (3),  $f=3$  Hz & 90 cm/s (4),  $f=8$  Hz & 90 cm/s (5),  $f=13$  Hz & 90 cm/s (6),  $f=2$  Hz & 100 cm/s (7),  $f=4$  Hz & 100 cm/s (8),  $f=6$  Hz & 100 cm/s (9) and  $f=11$  Hz & 100 cm/s (10).

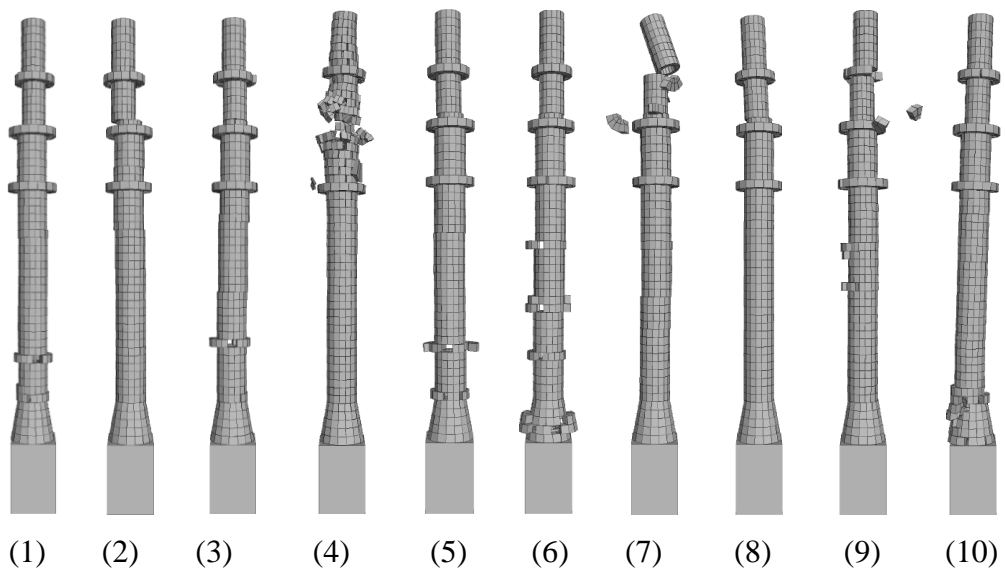


Figure 4.12. Heavy damage patterns for the Süleymaniye minaret during the combination of  $f=8$  Hz & 70 cm/s (1),  $f=2$  Hz & 80 cm/s (2),  $f=6$  Hz & 80 cm/s (3) and collapse patterns during the combination of  $f=6$  Hz & 60 cm/s (4),  $f=7$  Hz & 90 cm/s (5),  $f=8$  Hz & 90 cm/s (6),  $f=2$  Hz & 100 cm/s (7),  $f=8$  Hz & 100 cm/s (8),  $f=4$  Hz & 100 cm/s (9) and  $f=0.95$  Hz & 100 cm/s (10).

#### 4.5.2. Assessment of Absolute Top and Relative Drum Deformations

Figure 4.13 plot maximum normalized relative displacement,  $u_d$ , versus maximum normalized top displacement,  $u_{top}$  in terms of velocity amplitude for the Mihrimah, Hagia Sophia and Süleymaniye minarets. It is clear from the figures that the same group of input velocities produced largest normalized top displacements in the Mihrimah and largest relative displacements in the Süleymaniye. In the Hagia Sophia the responses are about half of those observed in the Mihrimah and Süleymaniye. In the Mihrimah minaret there are normalized top displacements larger than 0.5 with relative drum displacements less than 0.1.

For the Hagia Sophia minaret there is an almost linear relation between  $u_{top}$  and  $u_d$ . For velocities between 10 and 30 cm/s the scatter has a narrow band, which widens up at larger velocities, it should be remembered no collapse took place in the Hagia Sophia minaret during these runs. Largest normalized drum displacements took place in the Süleymaniye minaret (0.34). This is more than three times larger than those that took place in the Hagia Sophia and Mihrimah for the same normalized top displacement. It should be noted in figures between Figure 4.13 and Figure 4.18 for the minaret of Mihrimah at the collapse cases assumed as  $u_{top} = 1$  and  $u_d = 0.24$  and for the minaret of Süleymaniye at the collapse cases assumed as  $u_{top} = 0.6$  and  $u_d = 0.35$ . Figure 4.14 plot maximum normalized relative displacement,  $u_d$ , versus maximum normalized top displacement,  $u_{top}$  in terms of input frequency for the Mihrimah, Hagia Sophia and Süleymaniye minarets. Different frequency band are used in the analyses of the minarets (0.1-10.0 Hz for the Mihrimah, 1.02-13.0 Hz for the Hagia Sophia, 0.70 – 10.0 Hz for the Süleymaniye). The low frequencies employed in the Mihrimah are chosen to take a look at the minaret response under long period ground motions. From Figure 4.14 (a) it can be observed that such frequencies (<1Hz) produce large normalized top displacements, without necessarily exciting large relative drum displacements. In the case of Mihrimah and also to a certain extent for the Süleymaniye, high frequencies affect more the drum displacements. When the low frequencies are removed from Figure 4.14 (a) (not shown in here), it is observed that both in the Mihrimah and Hagia Sophia a linear relationship between drum and top displacements exists, although their levels are different from each other.

Large deformations and collapse cases mostly occurred during high frequencies. In the case of Süleymaniye minaret large maximum top displacements were observed at lower frequencies ( $< 1$  Hz), while the maximum normalized relative displacements occurred at frequencies higher than 2 Hz. Large drum displacements do not necessarily mean large top displacements particularly for the Süleymaniye. For the Hagia Sophia for where the structural stability is maintained, more analyses including lower and higher frequencies should be performed.

In Figure 4.15 and Figure 4.16 variation of maximum normalized relative displacement with sine wave amplitude and frequency in Figure 4.17 and Figure 4.18 variation of maximum normalized top displacement with sine wave amplitude and frequency are shown. These figures in fact support the findings of the previous paragraph by providing a more detailed perspective.  $u_d$  generally increase with the frequency of the sine wave. This is particularly evident at the Mihrimah and Süleymaniye minarets. Starting with sine wave amplitude of 10 cm/s the minaret of Mihrimah has larger normalized relative displacements than the Hagia Sophia at frequencies larger than 0.85 Hz. For the Mihrimah and Süleymaniye minarets it is clear that the minarets have larger drum dislocations at high frequencies that the nonlinearity completely dominates the behavior. However it is not obvious for the minaret of Hagia Sophia. It is concluded that large normalized top displacement do not necessarily mean collapse while there is a relation between normalized relative displacement and damage pattern.

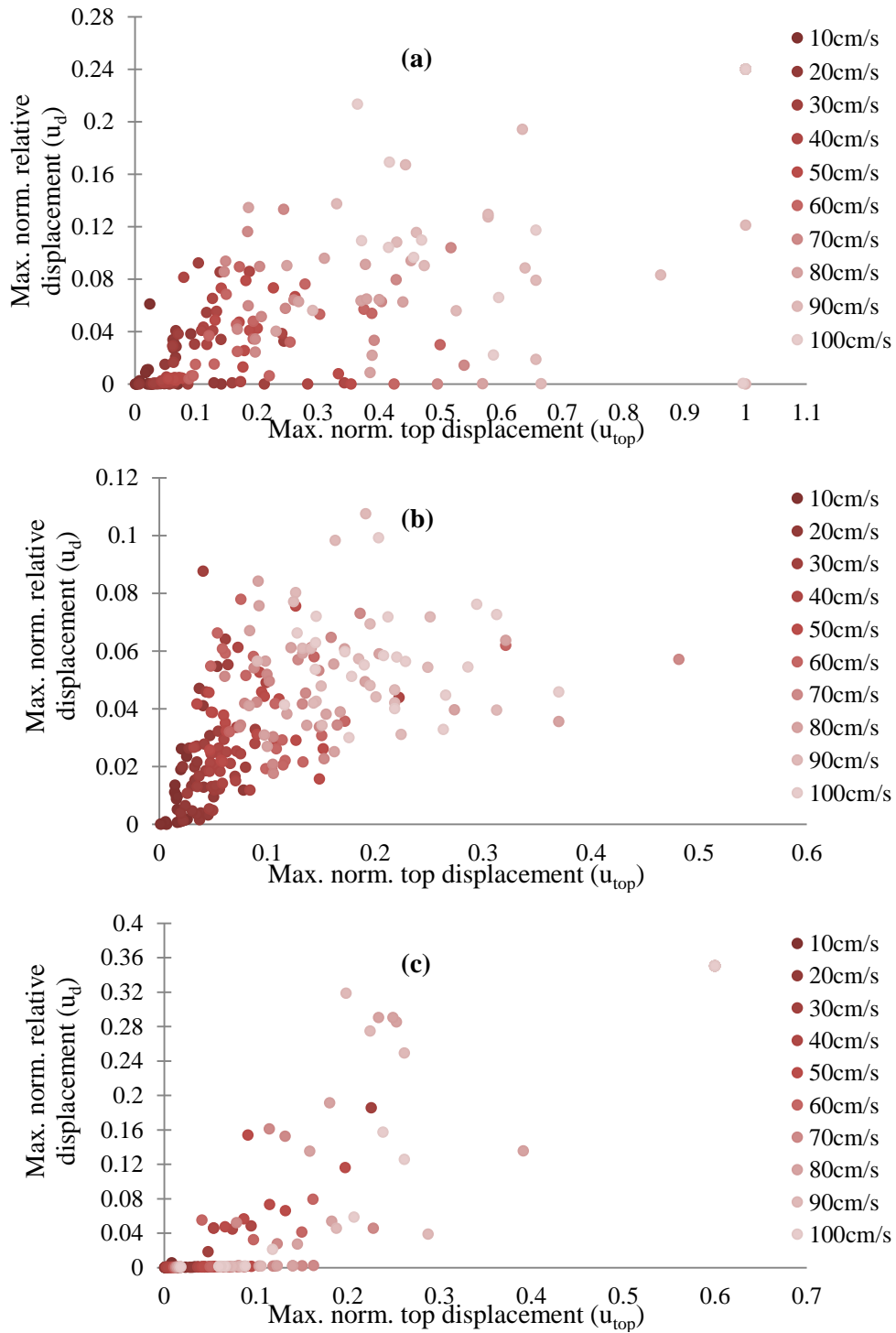


Figure 4.13. Scatter plot of maximum normalized relative displacement versus normalized maximum top displacement in terms of amplitude for minaret of the Mihrimah (a), Hagia Sophia (b) and Süleymaniye (c). Note that for the minaret of Mihrimah at the collapse cases assumed as  $u_{top}=1$  and  $u_d=0.24$  and for the minaret of Süleymaniye at the collapse cases assumed as  $u_{top}=0.6$  and  $u_d=0.35$ .

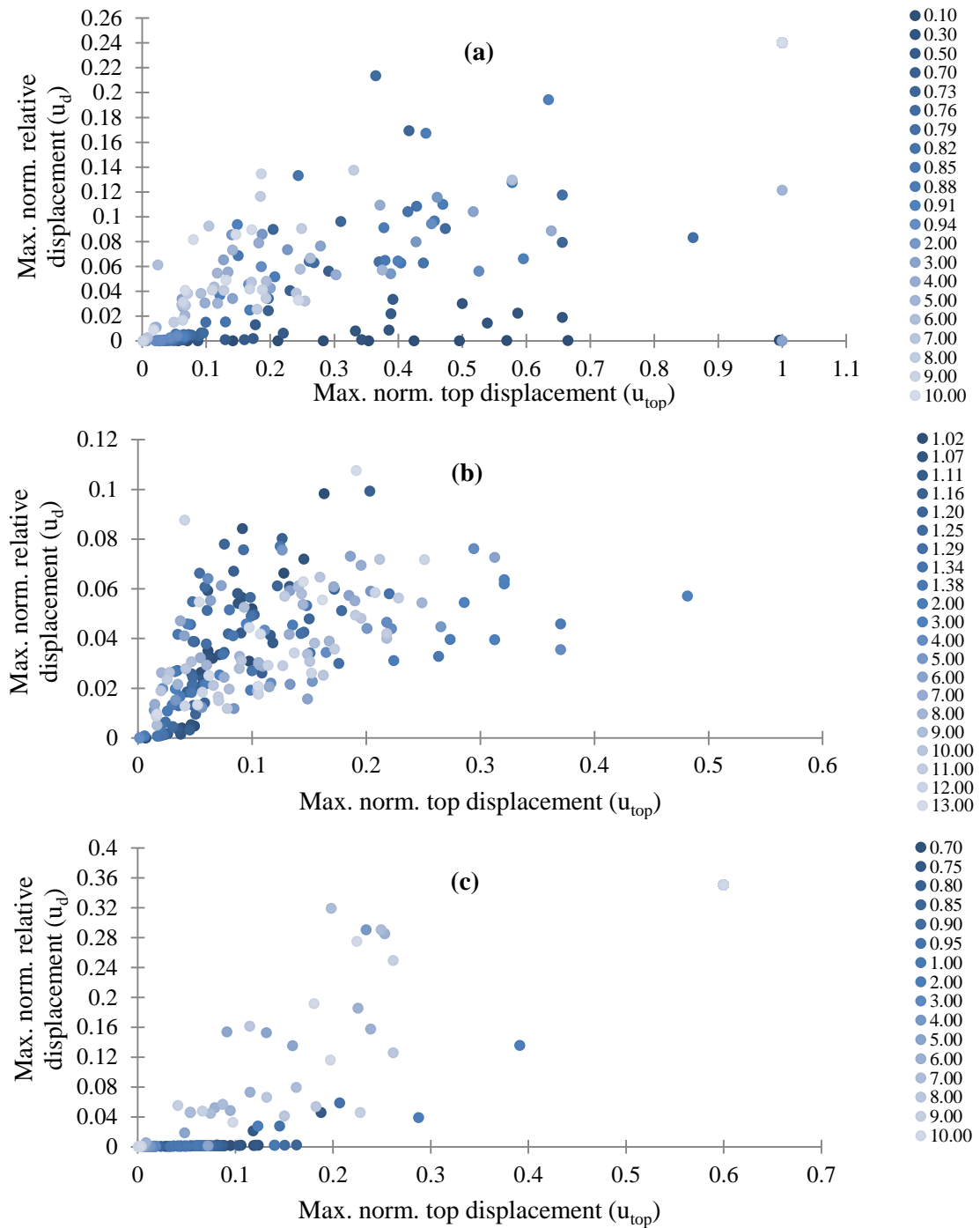


Figure 4.14. Scatter plot of maximum normalized relative displacement versus normalized top displacement in terms of frequency for minaret of the Mihrimah (a), Hagia Sophia (b) and Süleymaniye (c). Refer to the Table 4.7 for the first dominant frequency of the minarets. Note that for the minaret of Mihrimah at the collapse cases assumed as  $u_{top} = 1$  and  $u_d = 0.24$  and for the minaret of Süleymaniye at the collapse cases assumed as  $u_{top} = 0.6$  and  $u_d = 0.35$ .

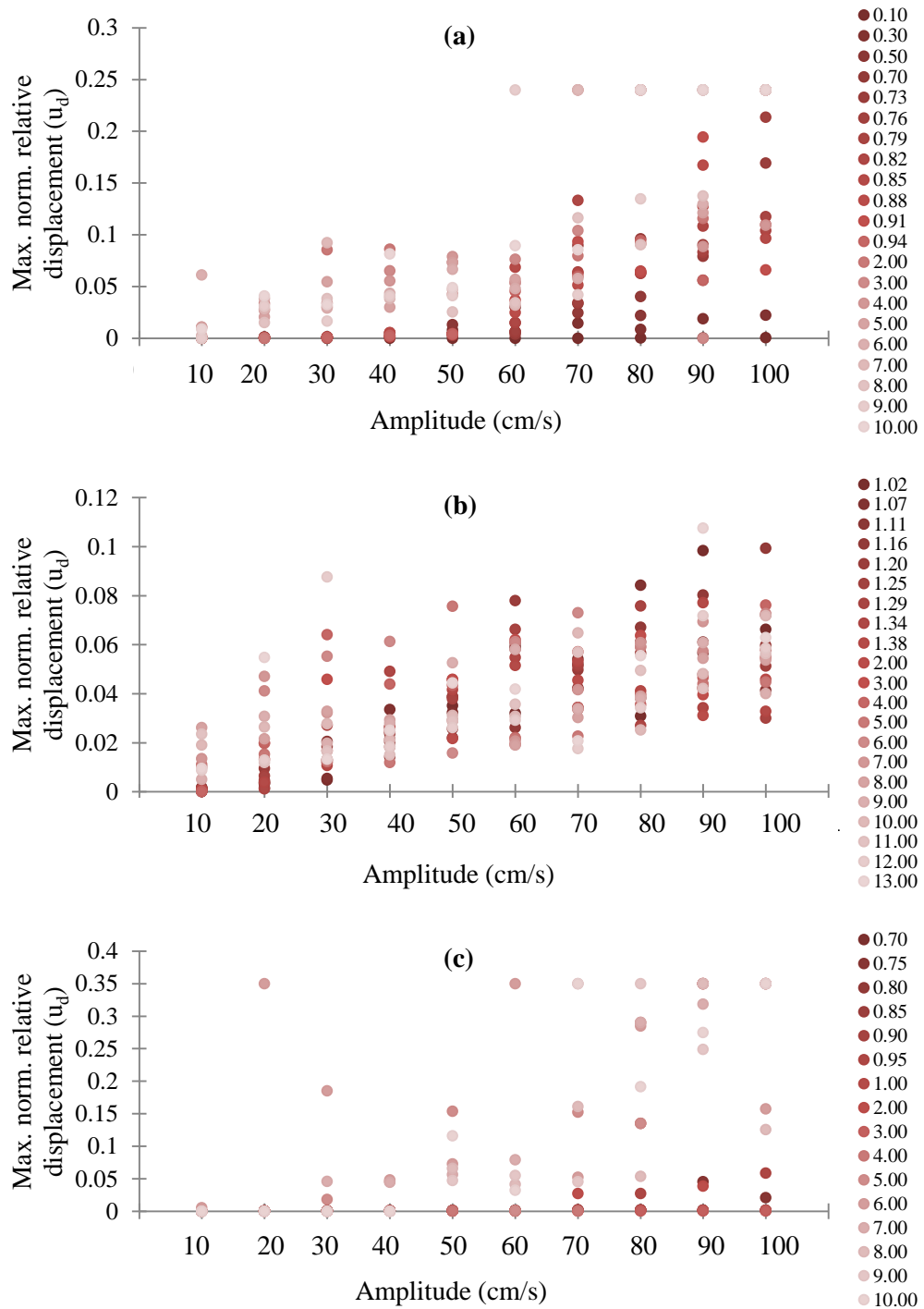


Figure 4.15. Variation of maximum normalized relative displacement with sine wave amplitude for the case of Mihrimah (a), Hagia Sophia (b) and Süleymaniye (c). Refer to the Table 4.7 for the first dominant frequency of the minarets. Note that for the minaret of Mihrimah at the collapse cases assumed as  $u_{top}=1$  and  $u_d=0.24$  and for the minaret of Süleymaniye at the collapse cases assumed as  $u_{top}=0.6$  and  $u_d=0.35$ .

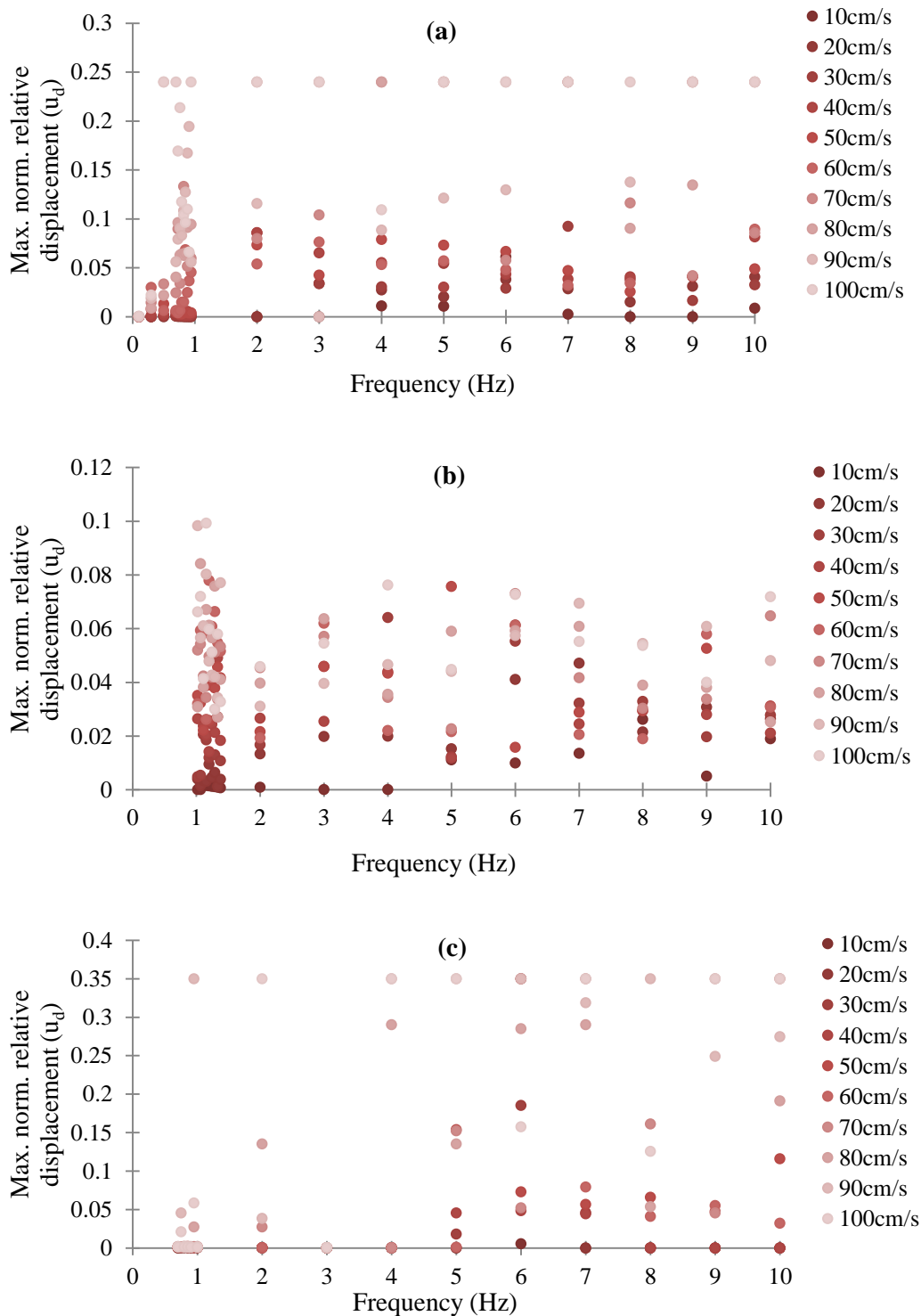


Figure 4.16. Variation of maximum normalized relative displacement with frequency for the case of Mihrimah (a), Hagia Sophia (b) and Süleymaniye (c) minaret. Refer to the Table 4.7 for the first dominant frequency of the minarets. Note that for the minaret of Mihrimah at the collapse cases assumed as  $u_{top}=1$  and  $u_d=0.24$  and for the minaret of Süleymaniye at the collapse cases assumed as  $u_{top}=0.6$  and  $u_d=0.35$ .

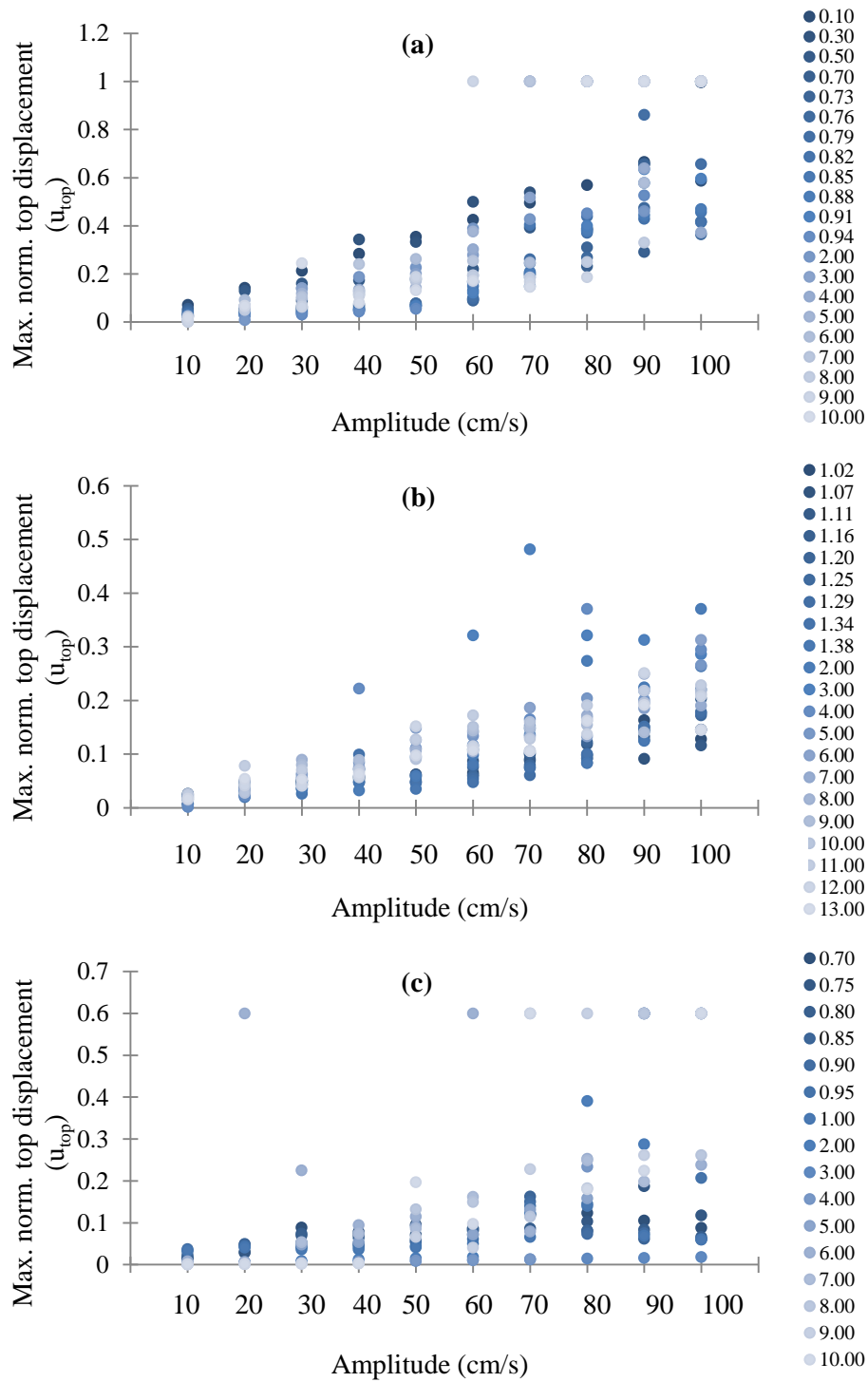


Figure 4.17. Variation of maximum normalized top displacement with sine wave amplitude for the case of Mihrimah (a), Hagia Sophia (b) and Süleymaniye (c) minaret. Refer to the Table 4.7 for the first dominant frequency of the minarets. Note that for the minaret of Mihrimah at the collapse cases assumed as  $u_{top}=1$  and  $u_d=0.24$  and for the minaret of Süleymaniye at the collapse cases assumed as  $u_{top}=0.6$  and  $u_d=0.35$ .

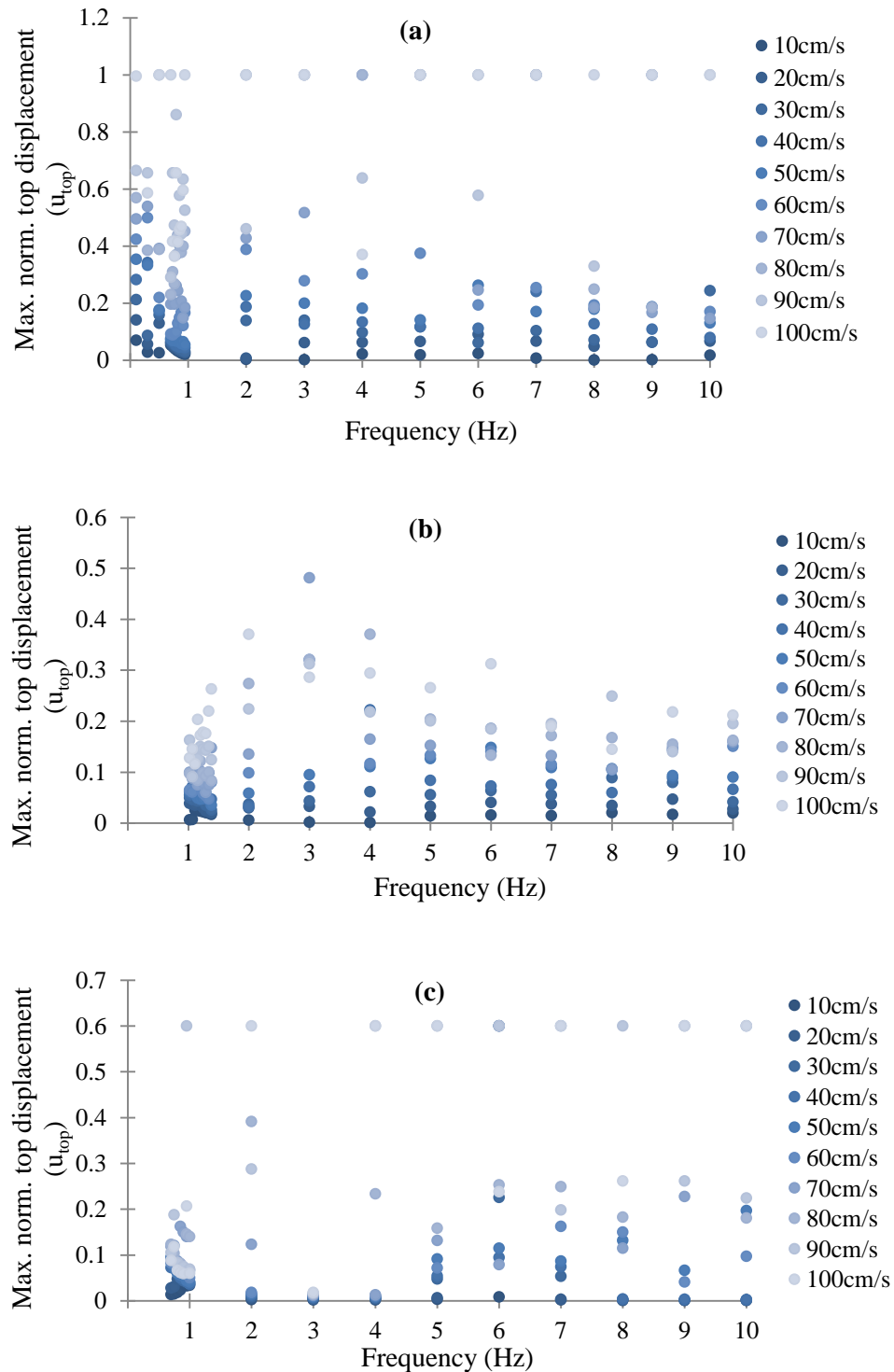


Figure 4.18. Variation of maximum normalized top displacement with frequency for the case of Mihrimah (a), Hagia Sophia (b) and Süleymaniye (c) minaret. Refer to the Table 4.7 for the first dominant frequency of the minarets. Note that for the minaret of Mihrimah at the collapse cases assumed as  $u_{top}=1$  and  $u_d=0.24$  and for the minaret of Süleymaniye at the collapse cases assumed as  $u_{top}=0.6$  and  $u_d=0.35$ .

### 4.5.3. Energy Parameters

Some insight into the structural behavior can be gained by considering energy balance in system. Total of global energy stored and dissipated in minarets have been computed and evaluated. The objective of these computational analysis efforts is to find out the correlation between the global energy dissipation of the minarets and damage. Resulting from the solutions of 3DEC based on the numerical integration in time of the equations of motion of the system, the incremental change in energy components is also determined at each time step as the system approaches to equilibrium.

The total energy balance can be expressed in terms of the released energy ( $W_r$ ), which is the difference between the work done at the boundary of the model and the total stored and dissipated strain energies. The change of kinetic energy and the work by external forces is calculated by the following methodology in a three dimensional manner which the equations are extended to the third dimension components. (Itasca, 2000);

$$W_r = E_k + W_\xi + W_v + E_m \quad (4.6)$$

where

$W_r$ = difference between the work done at the boundary of the model;

$E_k$  = current value of kinetic energy in the system;

$W_\xi$ = total mass damping work;

$W_v$  = total viscous (non-reflecting) boundaries work;

$E_m$ = total stored strain energy in excavated material.

The kinetic energy is calculated for each block at each time step, and is summed for all blocks at that time step. A running total of the kinetic energy is not kept; so, as the system approaches equilibrium, the kinetic energy will approach zero. The kinetic energy is expressed as

$$E_k = \sum_{i=1}^{nblock} \frac{1}{2} m_i (\dot{u}_i)^2 \quad (4.7)$$

where

$E_k$ = kinetic energy of all blocks in a given time step;

$m_i$ = mass of block  $i$ ;

$\dot{u}_i$ = velocity at block  $i$ .

The mass-damping work is the summation of all energy absorbed by damping and for dynamic analyses it controls the calculated value of the total released energy. The damped energy can most easily be seen by examining a simplified version of the equation of motion,

$$\frac{\partial \dot{u}}{\partial t} = \frac{\sum F}{m} - \alpha \dot{u} \quad \text{and} \quad \alpha = 2\pi f \gamma \quad (4.8)$$

where

$\dot{u}$ = velocity of a block of mass,  $m$ ;

$\sum F$ = the force sum at the block;

$\alpha$ = damping coefficient;

$f$ = natural frequency of the system;

$\gamma$ = fraction of critical damping.

The damping force,  $F_d$ , and the rate of damped energy change at a block,  $\dot{W}_d$ , expressed as;

$$F_d = m \alpha \dot{u} \quad \text{and} \quad \dot{W}_d = F_d \dot{u} = m \alpha \dot{u}^2 \quad (4.9)$$

The strain energy stored in the joints is determined based on the Coulomb slip model where the joint normal and shear stiffness are linear. Total energy stored in compression,  $E_{jc}$ , tension,  $E_{jt}$ , and shear,  $E_{js}$ , calculated by the following approach,

$$\text{If } f_n \geq 0 \quad E_{jc} = -\frac{1}{2}(f_n + f'_n)u_n \quad (4.10)$$

$$\text{If } f_n < 0 \quad E_{jt} = -\frac{1}{2}(f_n + f'_n)u_n \quad (4.11)$$

$$\text{If } f_s < f_{smax} \quad E_{js} = -\frac{1}{2}(f_s + f'_s)u_s \quad (4.12)$$

where

$f_n$ =current normal force at a contact, compression positive;

$f_s$ =current shear force at a contact, compression positive;

$f'_n$ = previous normal force at a contact;

$f'_s$ = previous shear force at a contact;

$u_n$ = incremental normal displacements at the contact over the current time step;

$u_s$ = incremental shear displacements at the contact over the current time step;

$f_{smax}$ = shear stress at which the Coulomb slip condition is met ( $f_{smax} < f_n \tan \phi + C$ ).

The total input energy,  $E_i(t)$ , at time t, can be expressed as sum of the total kinetic energy, damping energy, hysteretic and strain energy.

$$E_i(t) = E_k(t) + E_\xi(t) + E_H(t) + E_S(t) \quad (4.13)$$

At the end of the dynamic loading ( $t=T$ , T is duration of ground shaking), kinetic and strain energy get zero and the total input energy become;

$$E_i(T) = E_\xi(T) + E_H(T) \quad (4.14)$$

In Figures from 4.19 to 4.24 total for the global energy stored and dissipated in the Mihrimah, Hagia Sophia and Süleymaniye minarets under sine wave amplitude of 0.6m/s can be seen. It has been found that the comparison among energies dissipated and absorbed by the minarets during seismic loading is meaningful. In these figures for the Mihrimah minaret the case with collapse which is combination of  $f=9$  Hz & 60 cm/s and for the Süleymaniye minaret the case with collapse which is combination of  $f=6$  Hz & 60 cm/s are not included. The figures contain only data of cases where structural stability is maintained. It is clearly seen from figures that the amount of energy stored in tension and shear is strongly correlated with drum dislocations and change of the damage patterns of the minarets during seismic loading. As the frequency of the sine wave amplitude increases, the minarets lose their potential energy and the minarets absorb inelastic energy which is directly related to level of damage. The failure of blocks along the minaret produced loss of resistance capacity while the frequency of sine wave is increased gradually and result in energy release (Figure 4.20, 4.22 and 4.24).

The results obtained show the strong dependence of the minaret's seismic behavior on the frequency content of data and energy dissipation. Total released energy cause to loss of stiffness in minarets and this loss alter the model frequencies and modal damping values. Minarets show quite relevant elastic behavior close to the vibration frequencies and then the brittle nature of the masonry does not allow increasing its elasticity without damaging it and point to inelastic deformations and in case of high frequency loading result in clear damages. In Figures 4.25 and 4.26 the amounts of total released energy in terms of frequencies are given. As shown in the figures total released energy increases monotonically with the frequency and amplitude of sine wave. It has been found that, the total released energy has a physical meaning concerning the cracks. In the case of Mihrimah minaret it is clearly seen from Figures 4.25 and 4.26 that for the 100 cm/s amplitude sine wave the rate of energy release is smaller for the frequencies lower than 4 Hz where the minaret has heavy damage or notable cracking layers. It is evident for the Süleymaniye minaret as at the end of the combination of  $f=6$  Hz & 100 cm/s and  $f=8$  Hz & 100 cm/s minaret released lower energy with respect to the cases without any damage. From the above results it should be concluded that the total released energy in a cracking layer or drum dislocation is proper variable reflecting the damage or collapse. Based on the numerical results concerning energy balance a quite regular trend can be observed. Damage and cracking layer will increase only if the available amount of released energy equals or less than the amount of released energy that would be dissipated during a damage process.

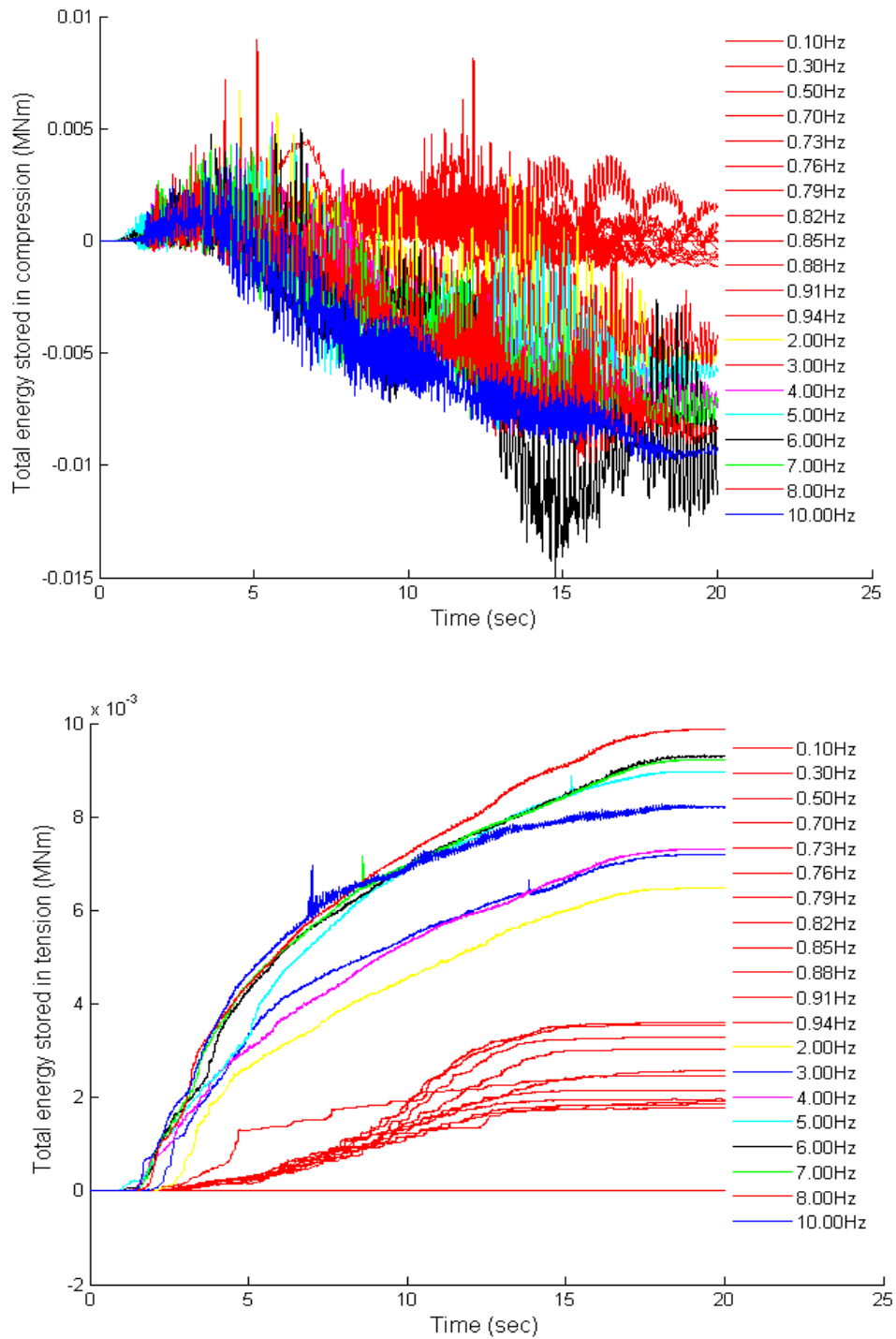


Figure 4.19. Total energy stored in compression and tension for the Mihrimah minaret under sine wave amplitude of 0.6 m/s. Note that the case with collapse, frequency of 9 Hz, is not included.

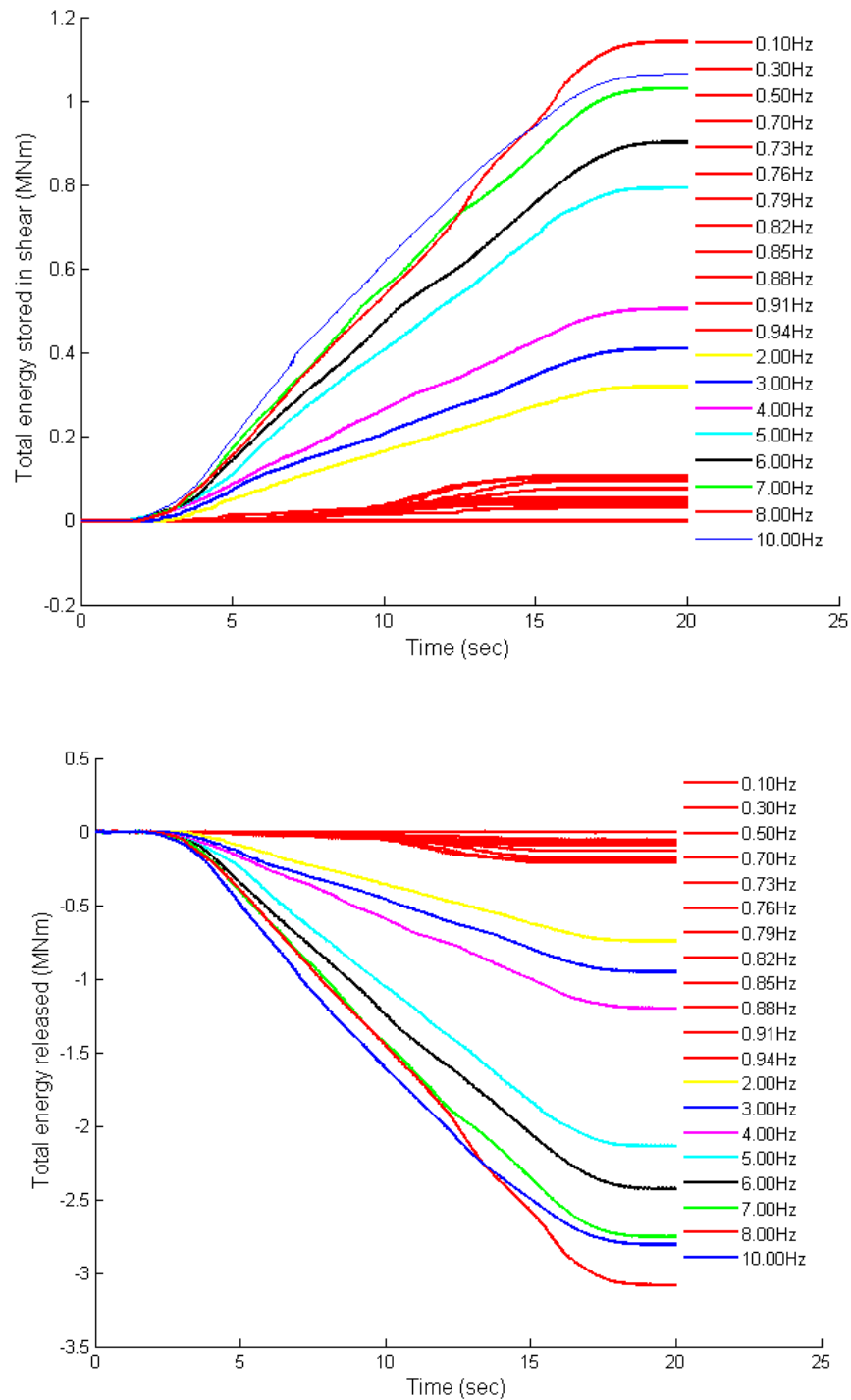


Figure 4.20. Total energy stored in shear and total released energy for the Mihrimah minaret under sine wave amplitude of 0.6 m/s. Note that the case with collapse, frequency of 9 Hz, is not included.

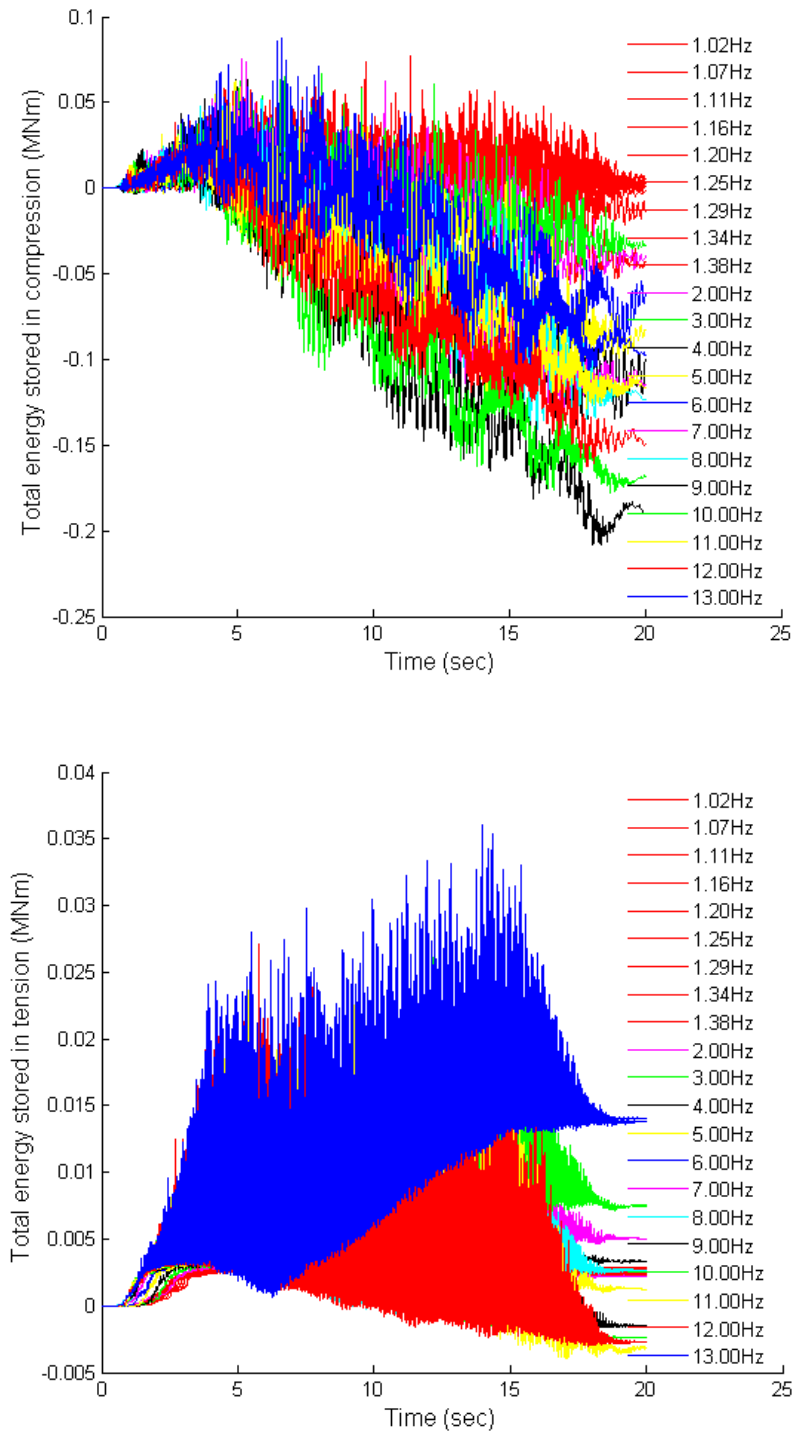


Figure 4.21. Total energy stored in compression and tension for the Hagia Sophia minaret under sine wave amplitude of 0.6 m/s.

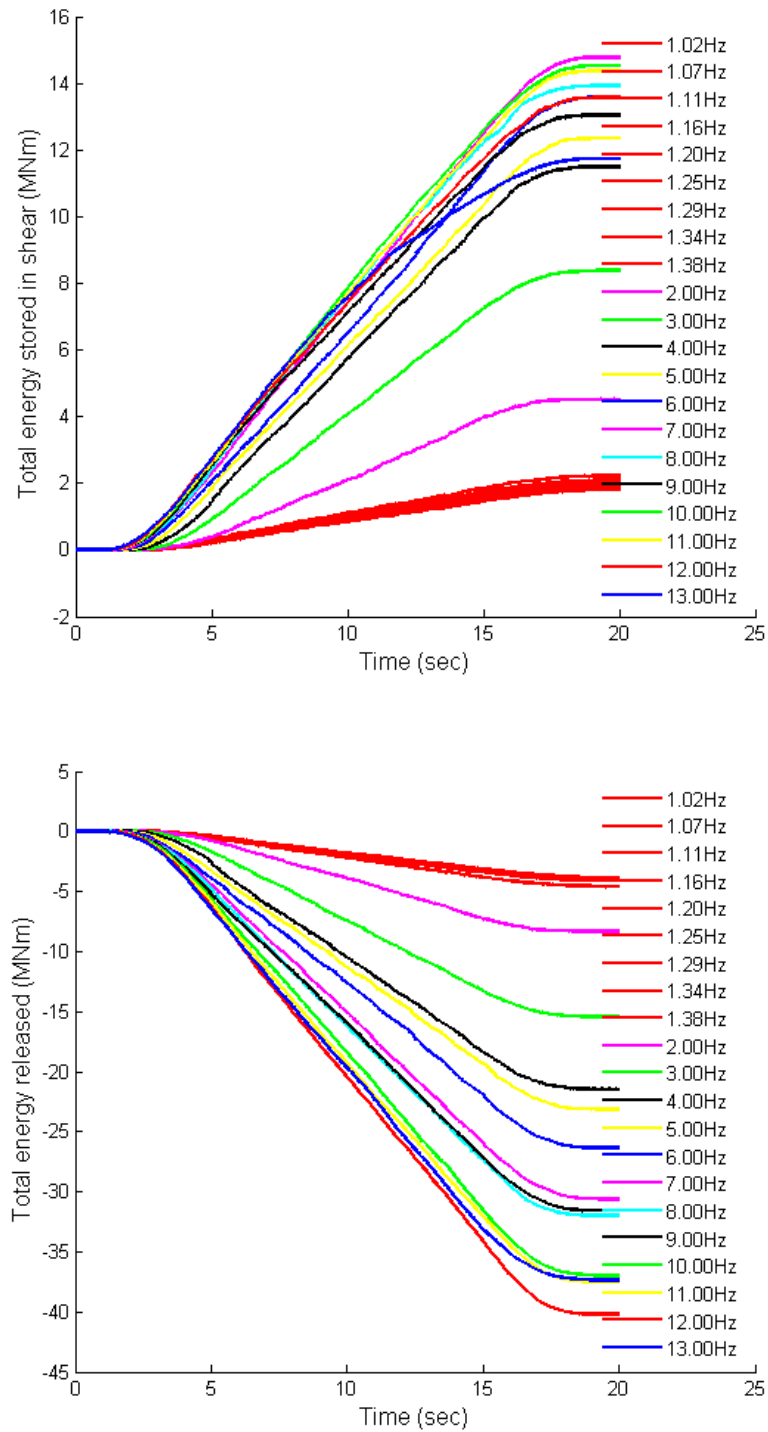


Figure 4.22. Total energy stored in shear and total released energy for the Hagia Sophia minaret under sine wave amplitude of 0.6 m/s.

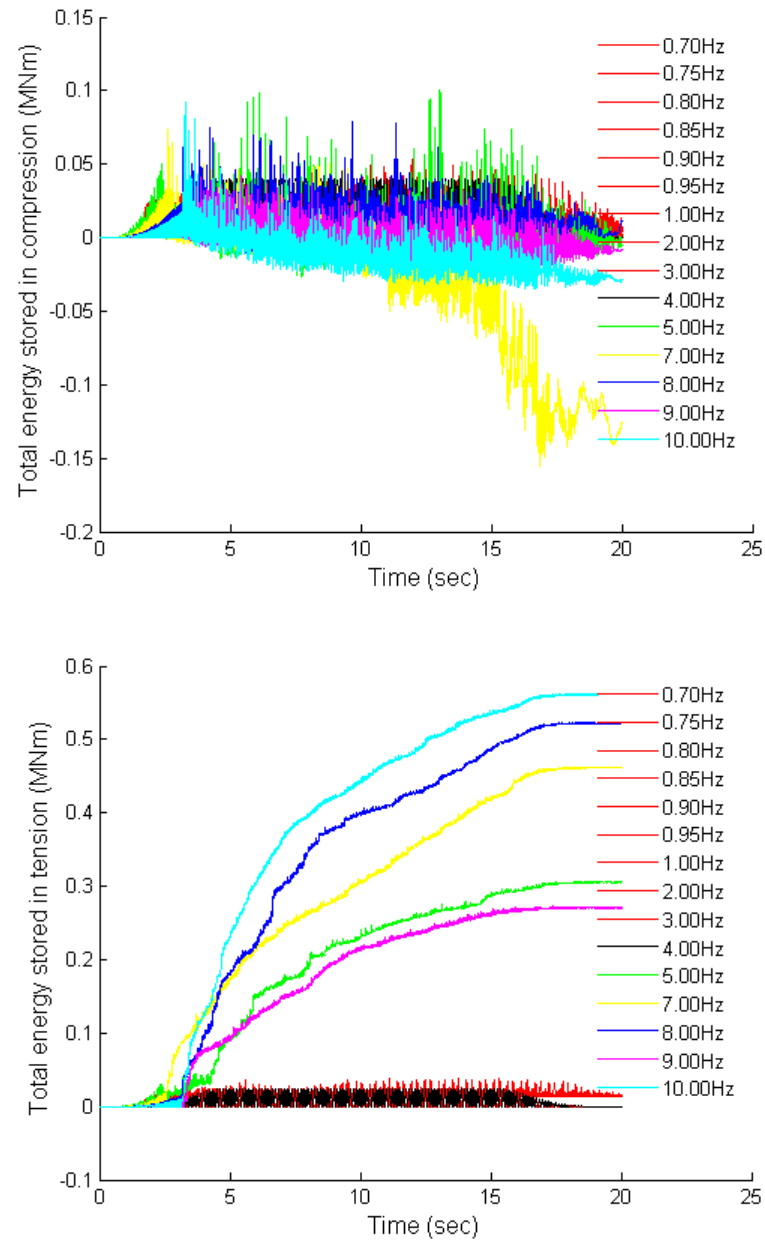


Figure 4.23. Total energy stored in compression and tension for the Süleymaniye minaret under sine wave amplitude of 0.6 m/s. Note that the case with collapse, frequency of 6 Hz, is not included.

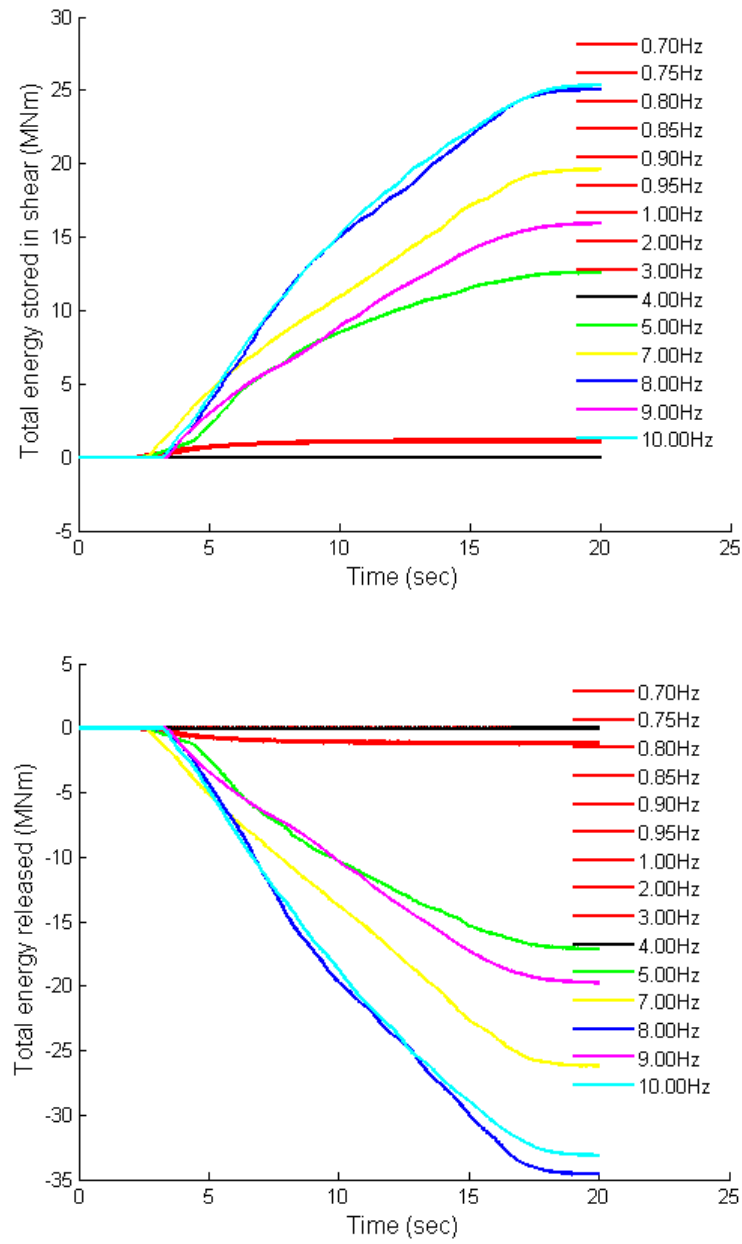


Figure 4.24. Total energy stored in shear and total released energy for the Süleymaniye minaret under sine wave amplitude of 0.6 m/s. Note that the case with collapse, frequency of 6 Hz, is not included.

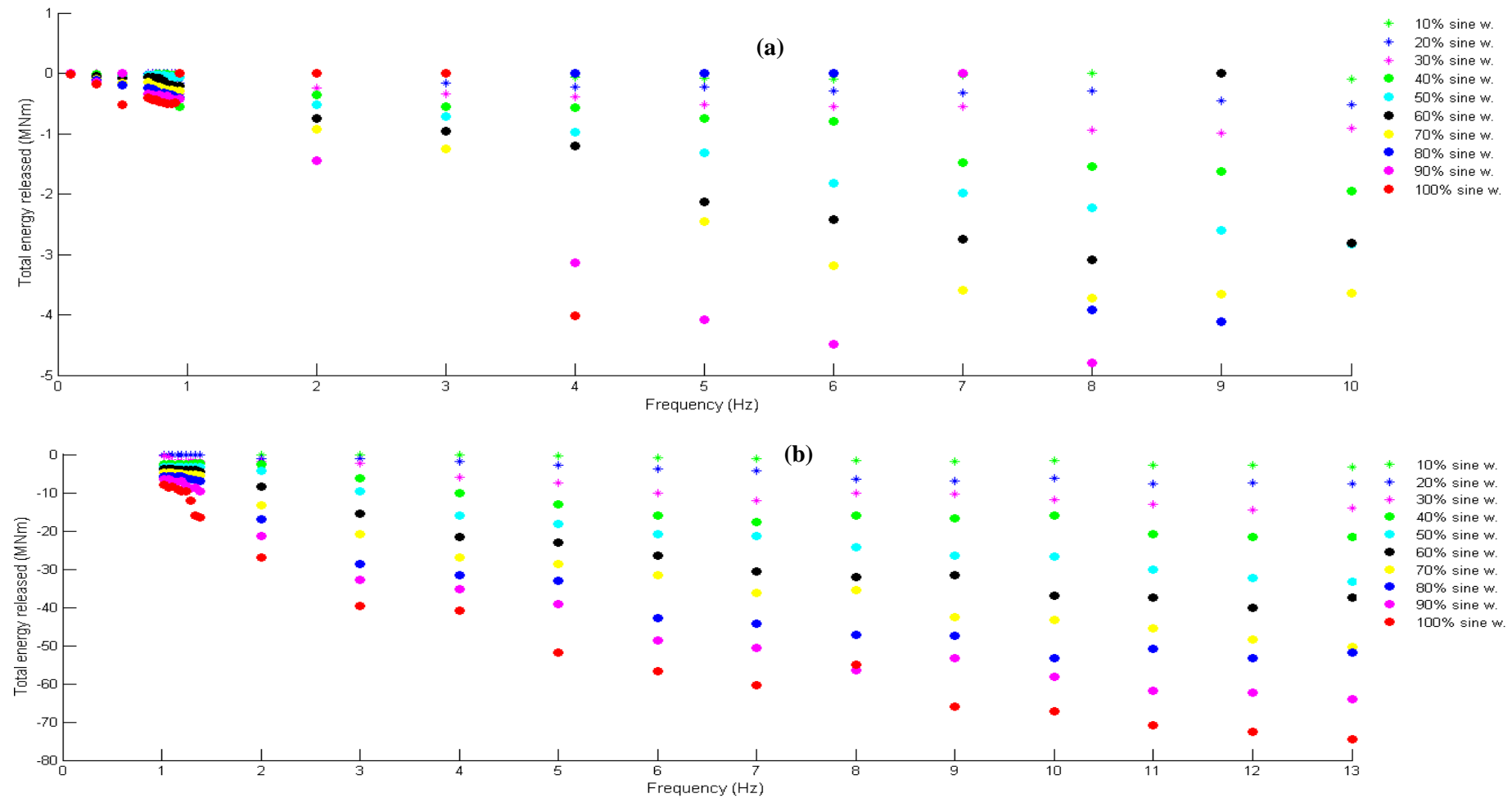


Figure 4.25. Total released energy of the (a) Mihrimah and (b) Hagia Sophia minarets. Note that for the Mihrimah minaret the cases with collapse are not included.

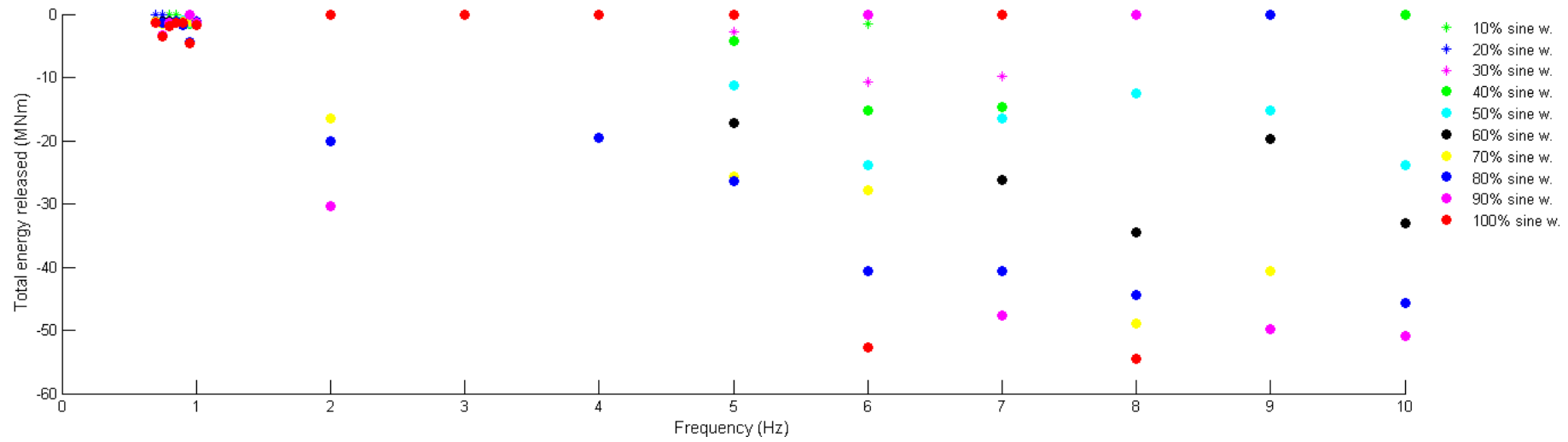


Figure 4.26. Total released energy of the Süleymaniye minaret. Note that the cases with collapse are not included.

#### 4.6. Employment of Real Earthquakes and Broadband Simulations in the Assessment of Minaret Models

In this section earthquake behavior of the Mihrimah, Hagia Sophia and Süleymaniye minarets is investigated. 10 different ground motion time histories are used as input in the non-linear dynamic analyses. They are all consistent with the earthquake hazard levels and conditions that would be occurrence of a large earthquake near Istanbul. Two time-history analyses are made with ground motions from the 1999 Kocaeli Earthquake: Yarımcı record with a PGA of 0.35 g; and Fatih record, with a PGA of 0.19 g (Çaktı *et al.*, 2013). Additionally five simulated ground motion time histories are used as input. They are broadband hybrid simulations due to five rupture scenarios to take place on the central Marmara (CMF1, CMF2, CMF3) and northern boundary segments (NB1, NB2) of the North Anatolian Fault in the Marmara Sea. The largest simulated PGA is 0.39 g. Finally three ground motion time histories simulated using the stochastic approach by code EXSIM (EXSIM-SC1, -SC2, -SC3) to represent three ruptures on the central Marmara segment (Çaktı *et al.*, 2013) are used. The response spectra of all records employed in the analyses are shown in Figure 4.27. Their PGAs and PGVs are shown in Table 4.9.

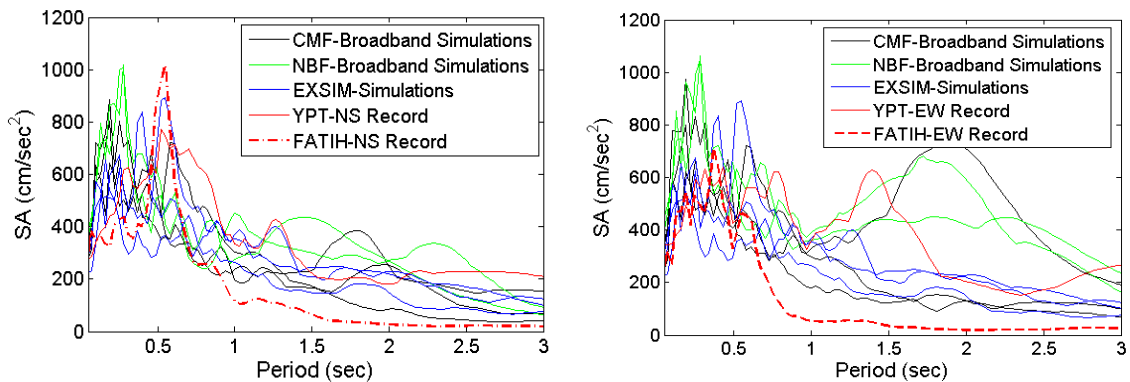


Figure 4.27. Response spectra of simulated and recorded ground motions used in non-linear dynamic analyses (left: NS components, right: EW components). Note that EXSIM simulates the random component. Therefore three stochastic simulations are shown in both plots (Çaktı *et al.*, 2013).

Table 4.9. PGAs and PGVs of all records employed in the analyses.

	Duration (s)	PGA (g)			PGV (m/s)		
		EW	NS	UD	EW	NS	UD
NBF1	18	0.31	0.22	0.16	0.59	0.22	0.22
NBF2	18	0.39	0.32	0.31	0.63	0.48	0.21
NBF3	20	0.32	0.29	0.32	0.7	0.36	0.7
CMF1	40	0.27	0.28	0.19	0.36	0.25	0.2
CMF3	40	0.22	0.24	0.15	0.22	0.34	0.17
SCENARIO1	80	0.21	-	-	0.26	-	-
SCENARIO2	80	0.20	-	-	0.22	-	-
SCENARIO3	110	0.15	-	-	0.22	-	-
YARIMCA	36	0.24	0.35	0.27	0.31	0.62	0.66
FATIH	155	0.19	0.16	0.13	0.19	0.14	0.08

The investigation is carried out in two parts. In the first part dynamic nonlinear analysis of the minaret models were performed under 10 earthquake time histories. Their response is assessed in terms of peak displacement amplitudes, peak stress amplitudes and their locations. In the second part PGVs of input motion were scaled in order to carry on the models to failure. This enabled a window to understand the collapse mechanisms associated with the Mihrimah Sultan, Hagia Sophia and Süleymaniye minarets.

#### 4.6.1. Assessment of Earthquake Behavior

Earthquake behavior of the three minaret models are studied in terms of relative block displacements, peak joint shear displacements, peak joint normal displacements, peak joint normal stresses and joint normal displacement vectors. In Table 4.10 the results of all analyses are summarized, where the peak values associated with each parameter mentioned in the previous sentence is given for all earthquake inputs. From Table 4.10 it is evident that Yarımca record leads to highest response values in the Mihrimah and Süleymaniye minarets. The record causes large displacements and stresses in the Hagia Sophia minaret as well, although NBF1 and NBF2 also lead to significant displacements. The response of the minarets to Yarımca record is shown in Figure 4.28, Figure 4.29 and Figure 4.30 for the Mihrimah, Hagia Sophia and Süleymaniye minarets respectively.

In the case of Mihrimah minaret, peak normal joint displacements reached 6.5 cm at about 13 m from the ground level. Shear displacements of 3.4 cm took place above the balcony (Figure 4.28). For the Hagia Sophia minaret, peak normal joint displacements reached 4.35 cm at about 32 m from the ground level close to the transition part of the minaret. Shear displacements of 5 cm took place above the balcony (Figure 4.29). For the Süleymaniye minaret, peak normal joint displacements reached 17.1 cm at about 14 m from the ground level. Shear displacements of 9.6 cm took place at the transition part of the minaret (Figure 4.30). Distribution of relative block displacements are shown in Figures 4.31 to 4.35 indicates how differently the same ground motion may affect the three minarets. No local collapse takes place in any of them. The Mihrimah minaret has blocks displaced for about 10 cm in the upper half of its body, whereas the blocks in the body of the Hagia Sophia minaret gets displaced for about 30 cm and for about 5 cm in the Süleymaniye just above the transition segment. It should be noted that these deformations are quite large and are most likely to be considered under heavy damage classification. The Yarımcı record minimally affects the foundations of all three cases. In the transition segments of the Mihrimah and Hagia Sophia tensile stresses do develop without leading to significant deformations.

The results suggest that failure takes place due to excessive normal deformations and rocking at the base of the minaret body and due to shear deformations at upper levels. Tensile failure on the horizontal joints was widespread, as indicated by the joint normal displacements (separation). The disintegration of blocks for the Mihrimah minaret and damages for the Süleymaniye and Hagia Sophia minarets as a result their differential displacements are evident from displacement magnitudes and joint shear displacements.

Looking at Table 4.10, it can be seen that stochastically simulated earthquakes lead to minimum response values in all minarets and suggest the employment of real or properly simulated earthquakes for such assessment.

Table 4.10. Residual block displacements, peak shear displacements, peak normal stresses and peak normal displacements during seismic loading.

	Peak shear displacement (cm)			Peak normal displacement (cm)		
	Mihrimah	Süleymaniye	Hagia Sophia	Mihrimah	Süleymaniye	Hagia Sophia
Self-Weight	-	-	-	-	-	-
NBF1	1.20	2.50	7.21	1.38	3.60	7.32
NBF2	1.60	3.30	4.94	2.27	6.16	7.13
NBF3	1.58	3.80	7.20	2.96	6.04	6.02
CMF1	1.65	0.38	3.78	1.28	1.78	5.56
CMF3	1.52	2.08	2.00	1.73	5.35	0.41
SC1	0.40	0.27	0.58	1.14	0.58	0.76
SC2	0.19	0.18	0.46	0.95	0.50	0.52
SC3	0.11	0.07	0.17	0.30	0.03	0.44
FATİH	0.33	0.00	0.80	0.28	0.03	0.46
YARIMCA	2.10	9.60	6.40	7.03	17.10	4.35

	Peak normal stresses (MPa)			Displacement magnitude (cm)		
	Mihrimah	Süleymaniye	Hagia Sophia	Mihrimah	Süleymaniye	Hagia Sophia
Self-Weight	-	-	-	0.12	0.07	0.12
NBF1	15.31	42.48	24.89	38.60	39.60	55.20
NBF2	12.82	57.51	37.79	21.10	16.80	32.50
NBF3	17.08	52.92	34.81	20.47	15.70	48.90
CMF1	25.95	37.27	40.56	23.30	24.20	25.30
CMF3	12.54	43.23	97.26	19.83	18.90	39.50
SC1	9.17	34.99	17.75	0.64	0.20	2.18
SC2	9.33	26.07	7.48	0.15	0.22	0.48
SC3	13.96	18.26	7.05	1.01	1.04	1.08
FATİH	4.33	10.73	25.44	0.36	0.01	2.46
YARIMCA	52.78	108.03	30.02	14.29	4.39	41.40

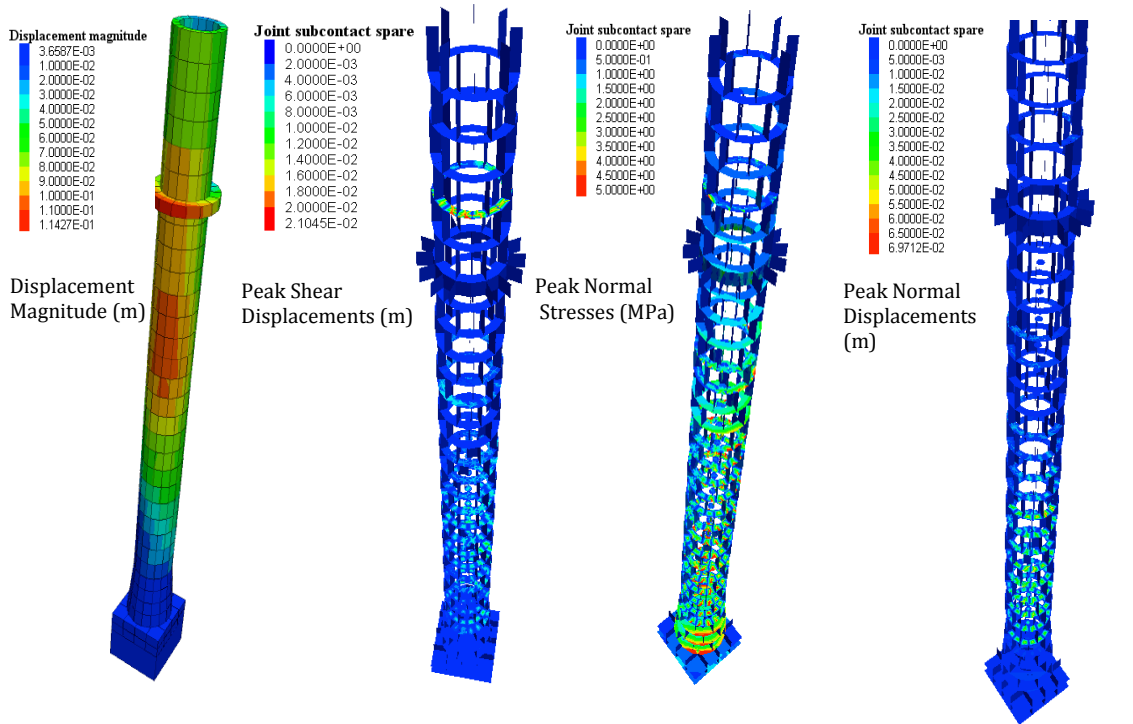


Figure 4.28. Response of the Mihrimah minaret under Yarımca record from the Kocaeli Earthquake, from left to right: residual block displacements, maximum joint shear displacements, maximum joint normal stresses and maximum joint normal displacements.

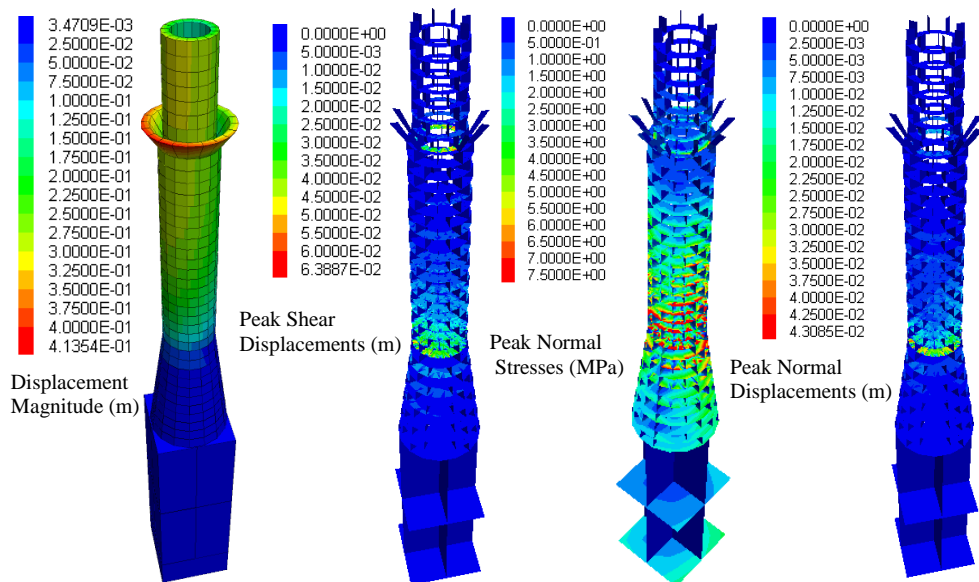


Figure 4.29. Response of the Hagia Sophia minaret under Yarımca record from the Kocaeli Earthquake, from left to right: residual block displacements, maximum joint shear displacements, maximum joint normal stresses and maximum joint normal displacements.

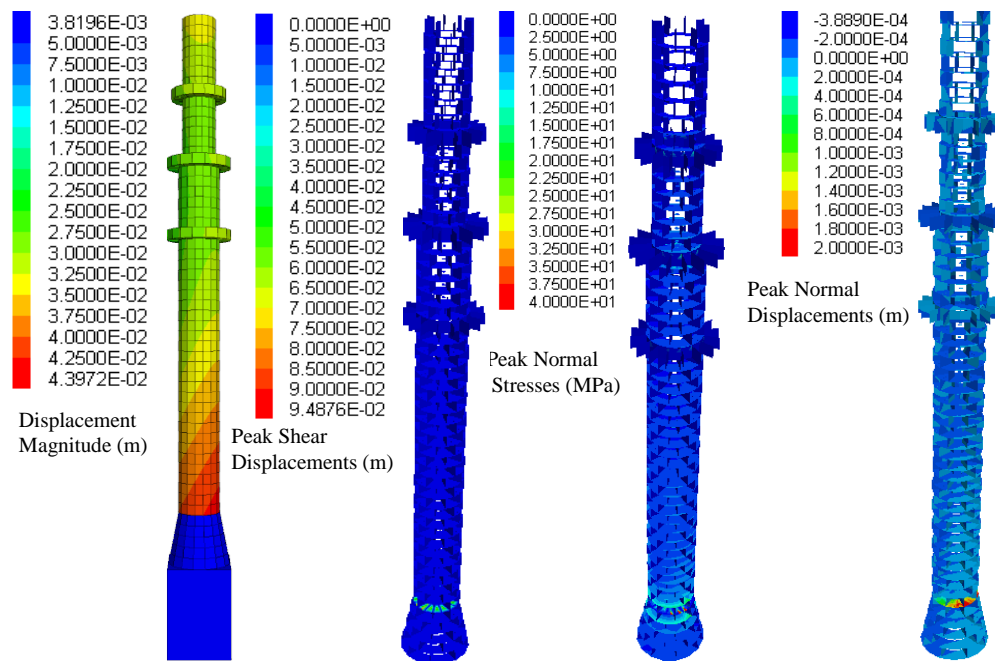


Figure 4.30. Response of the Süleymaniye minaret under Yarımca record from the Kocaeli Earthquake, from left to right: residual block displacements, maximum joint shear displacements, maximum joint normal stresses and maximum joint normal displacements.

Magnitude of displacements and joint normal displacement vectors at the end of the record provided precise information on the deformation of the minarets under seismic loading. In Figures 4.31, 4.33 and 4.35 the residual model deformations under 10 earthquake inputs are shown for three minaret cases along with the results of the self-weight analysis. The scale of each subplot is different from each other as scaling them together causes loss of details. The maximum deformation for each case however is given in Table 4.10. Abrupt color changes in these figures (such as Figure 4.2-g,h or i) suggest sudden changes in deformation and indicates displaced blocks. All deformation values are with respect to original geometry. To establish if the failure mechanism is local or global the deformed shapes and vertical stress distributions at the end of the seismic excitation were helpful. They allowed quantitative data about failure pattern, which may be result of sliding, bending, cracking under direct tension or partial collapse of the block of the minaret. In the case of Mihrimah minaret, peak values of shear and normal displacements were observed under Yarımca record. Peak normal stress of the Mihrimah minaret was 52.78 MPa and observed during Yarımca record. Peak displacement magnitude was 38.60 cm and occurred under NBF1 case. For the Hagia Sophia minaret, peak values of shear and normal displacements were observed under NBF1 record.

The Hagia Sophia minaret reached peak normal stress under CMF3 record. Peak displacement magnitude was observed under CMF1 record. For the Süleymaniye minaret, observed peak values appear similar to the results of the Mihrimah minaret. Peak shear and normal displacements were observed under Yarımca record. Peak normal stress of the Süleymaniye minaret was 108.03 MPa and observed during Yarımca record. Peak displacement magnitude was 39.60 cm and occurred under NBF1 record.

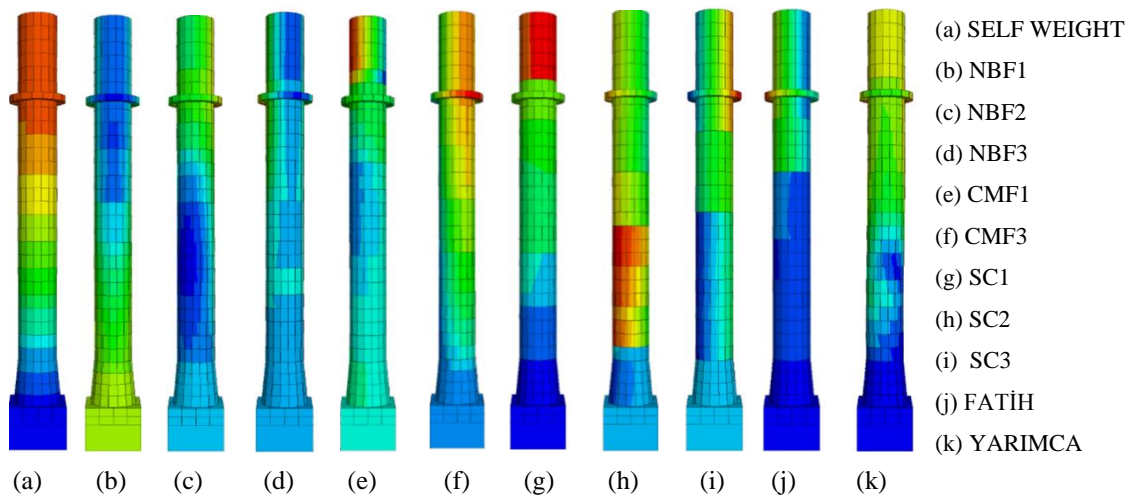


Figure 4.31. Magnitude of displacement of the Mihrimah minaret at end of the record. (a): self-weight static analysis under gravitational loads, (b)-(f) Broadband simulations, (g)-(i) EXSIM simulations, (j): Fatih record, (k): Yarımca record.

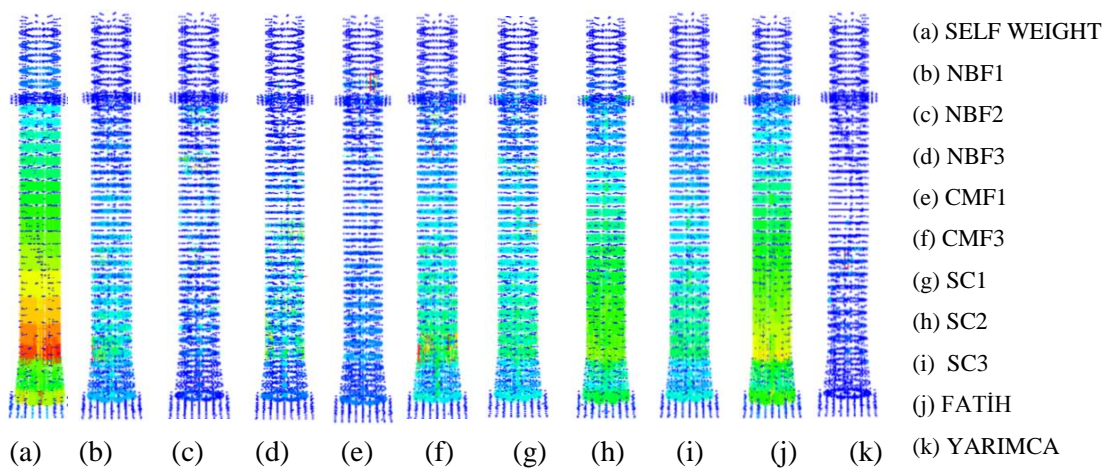


Figure 4.32. Joint normal displacement vectors of the Mihrimah minaret at end of the record for the minaret of Mihrimah. (a): self-weight static analysis under gravitational loads, (b)-(f) Broadband simulations, (g)-(i) EXSIM simulations, (j): Fatih record, (k): Yarımca record.

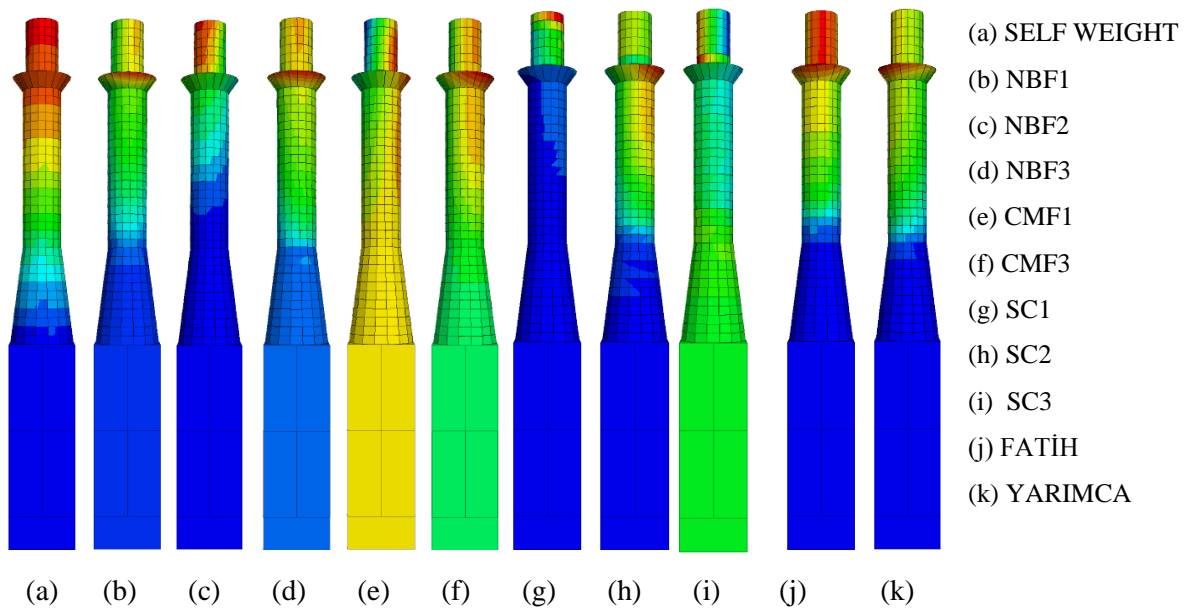


Figure 4.33. Magnitude of displacement of the Hagia Sophia minaret at end of the record. (a): self-weight static analysis under gravitational loads, (b)-(f) Broadband simulations, (g)-(i)EXSIM simulations, (j):Fatih record, (k):Yarımca record.

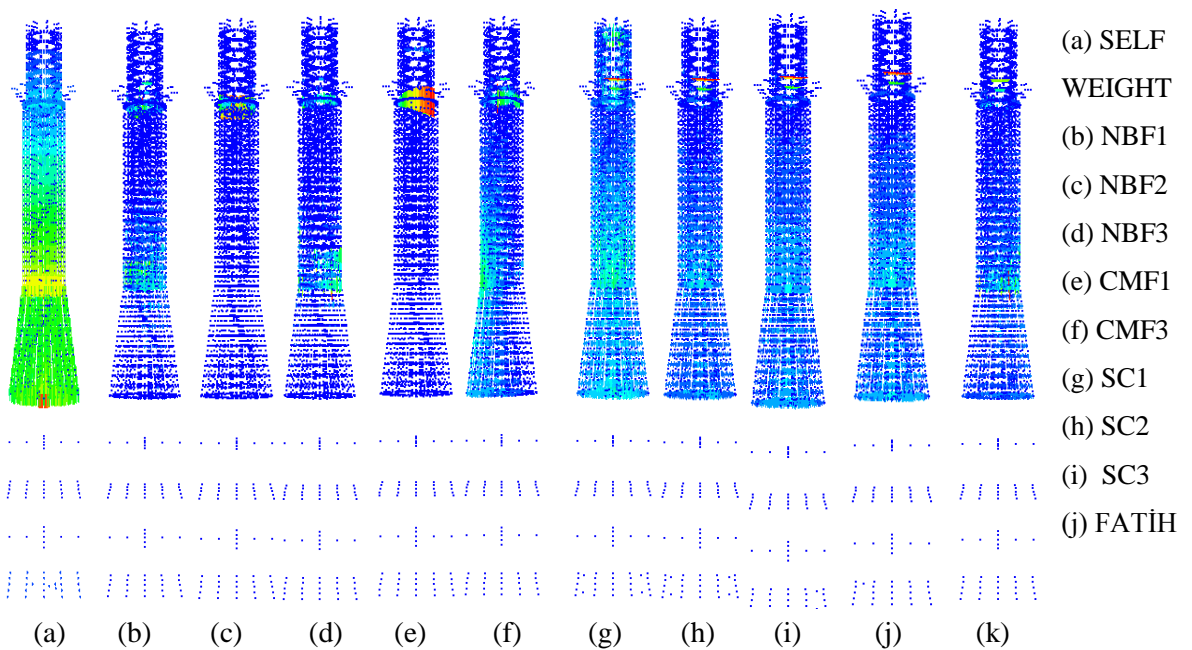


Figure 4.34. Joint normal displacement vectors of the Hagia Sophia minaret at end of the record. (a): self-weight static analysis under gravitational loads, (b)-(f) Broadband simulations, (g)-(i)EXSIM simulations, (j):Fatih record, (k):Yarımca record.

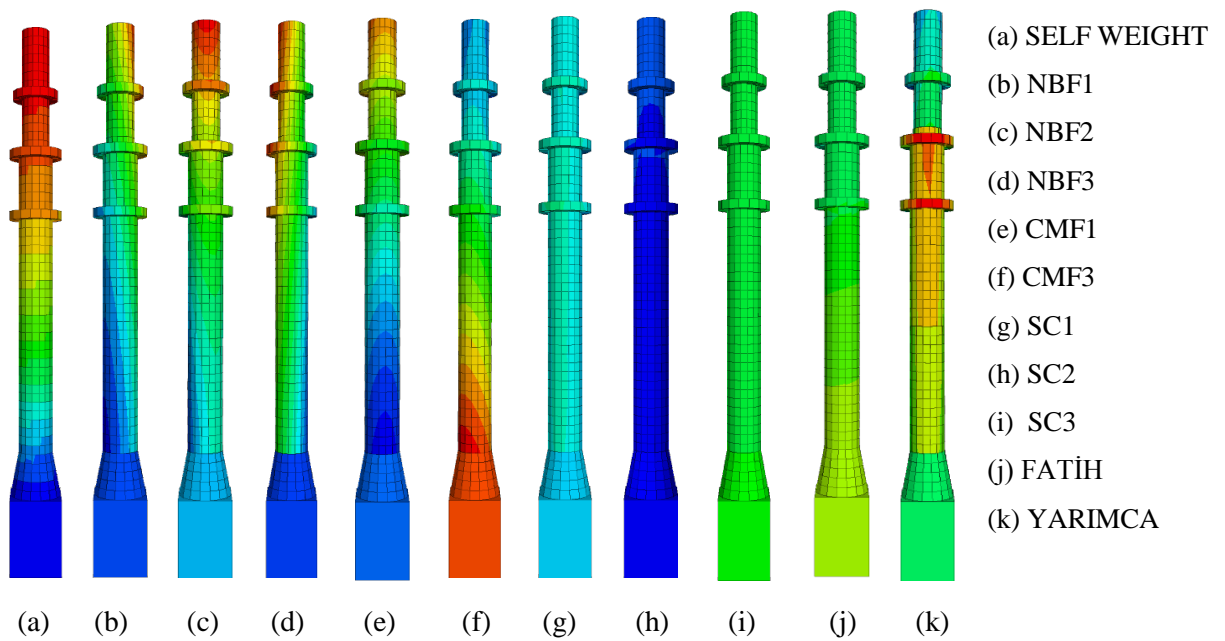


Figure 4.35. Magnitude of displacement of the Süleymaniye minaret at end of the record.

(a): self-weight static analysis under gravitational loads, (b)-(f) Broadband simulations, (g)-(i)EXSIM simulations, (j):Fatih record, (k):Yarımca record.

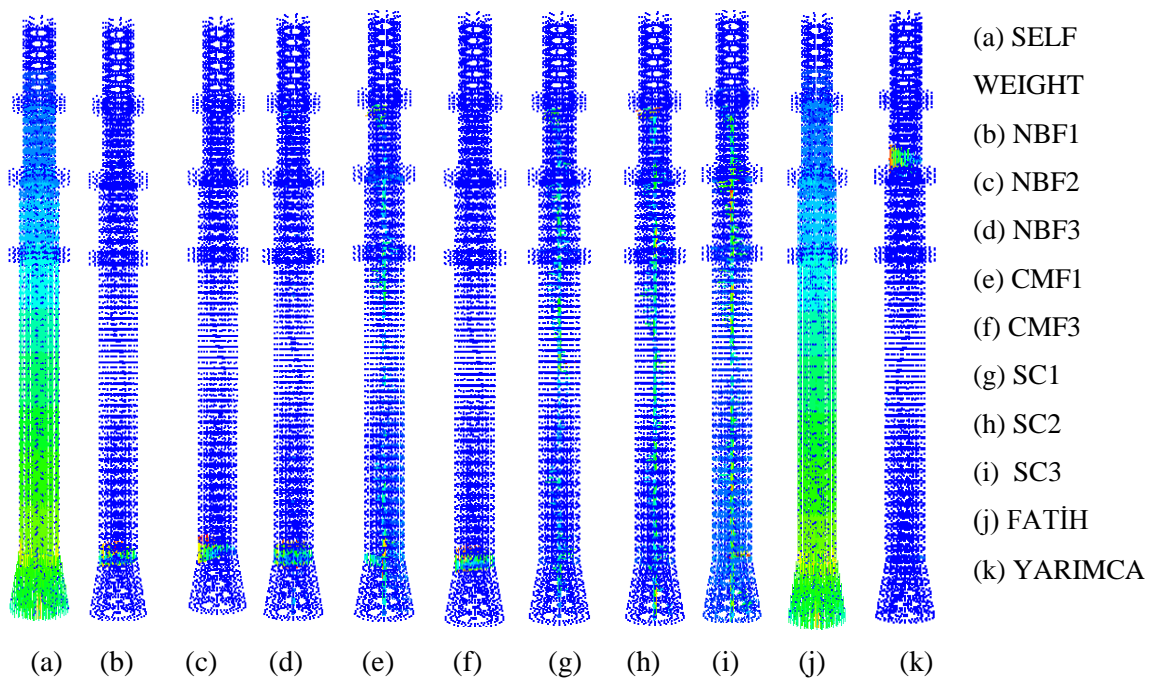


Figure 4.36. Joint normal displacement vectors of the Süleymaniye minaret at end of the record.

(a): self-weight static analysis under gravitational loads, (b)-(f) Broadband simulations, (g)-(i)EXSIM simulations, (j):Fatih record, (k):Yarımca record.

#### 4.6.2. Assessment of Collapse Mechanisms

No collapse or failure took place in any of the three cases discussed in the previous section. To force each model to collapse, the input velocities were scaled up progressively and analysis was repeated until instability in the model is reached.

Figures 4.37 to 4.39 illustrate minarets in the state of collapse under earthquake loadings for the cases of Mihrimah, Hagia Sophia and Süleymaniye minarets respectively. Following observations can be made on the basis of the figures:

Collapse starts with a PGV of about 100 cm/s in the case of Mihrimah minaret, at about 190 cm/s for the Hagia Sophia minaret and at about 110 cm/s for the Süleymaniye minaret. These are very large ground velocities. Particularly levels that force the Hagia Sophia minaret model to collapse are unrealistically high. This suggests that collapse of the twin minarets of the Hagia Sophia is an unlikely expectation. The Mihrimah and Süleymaniye minaret models tend to collapse at around 100 cm/s PGV. It appears that they are relatively more susceptible to collapse. The Mihrimah minaret collapsed in the past. No collapse took place in the Süleymaniye minaret. The agreement between the image of the minaret after its collapse in the 1894 earthquake (Figure 4.2) and the image of the numerical model during collapse (Figure 4.37) is remarkable.

- In the Mihrimah minaret, collapse takes place following the development of a complete separation of the minaret into two parts somewhere between the transition part and the balcony, and the fall of the upper part as a result of ongoing ground motion cycles. The same pattern is observed under all inputs and suggests it is independent of time and frequency domain characteristics of input ground motion.
- In the Hagia Sophia minarets there are two collapse patterns. In the first pattern the part of the minarets right above the balcony gets separated and collapses. In the second pattern a major separation occurs between the transition segment and the whole body above the transition segment falls down, probably following rocking.

- The Süleymaniye minaret has a reduced wall thickness starting at its second balcony (Figure 4.39). All collapses are associated with this part of the Süleymaniye minaret.
- In none of the models does the core with the staircase extend until the very top of the minaret (Figure 4.8). Therefore its nonexistence above the highest balcony of a minaret does not explain on its own the vulnerability of this part to collapse. The wall thickness appears to have more influence, as the Mihrimah minaret has the same wall thickness along its full height and no collapse involving this part is observed. On the other hand in both the Hagia Sophia and Süleymaniye, the wall thickness above their balconies are reduced and these sections are involved with collapse.
- Slenderness (i.e the relation between the body height and the body diameter) appears to have an important role when it comes to collapse. In this context body height is used as the height of a minaret above the transition segment (i.e 27.3 m for the Mihrimah, 28.44 m for the Hagia Sophia and 49.5 m for the Süleymaniye minarets - Table 4.1-Table 4.3). Using the diameter information in Tables 4.1, 4.2 and 4.3, it becomes evident that the Mihrimah and the Süleymaniye minarets have similar slenderness ratios, while the slenderness ratio of the Hagia Sophia minaret is about half. This can explain the higher levels of collapse velocity associated with the Hagia Sophia minaret.
- All results and discussions above suggests that although some very valuable case specific conclusions can be drawn, more case studies are needed, to be able to parameterize and/or systemize the collapse behavior of minarets.

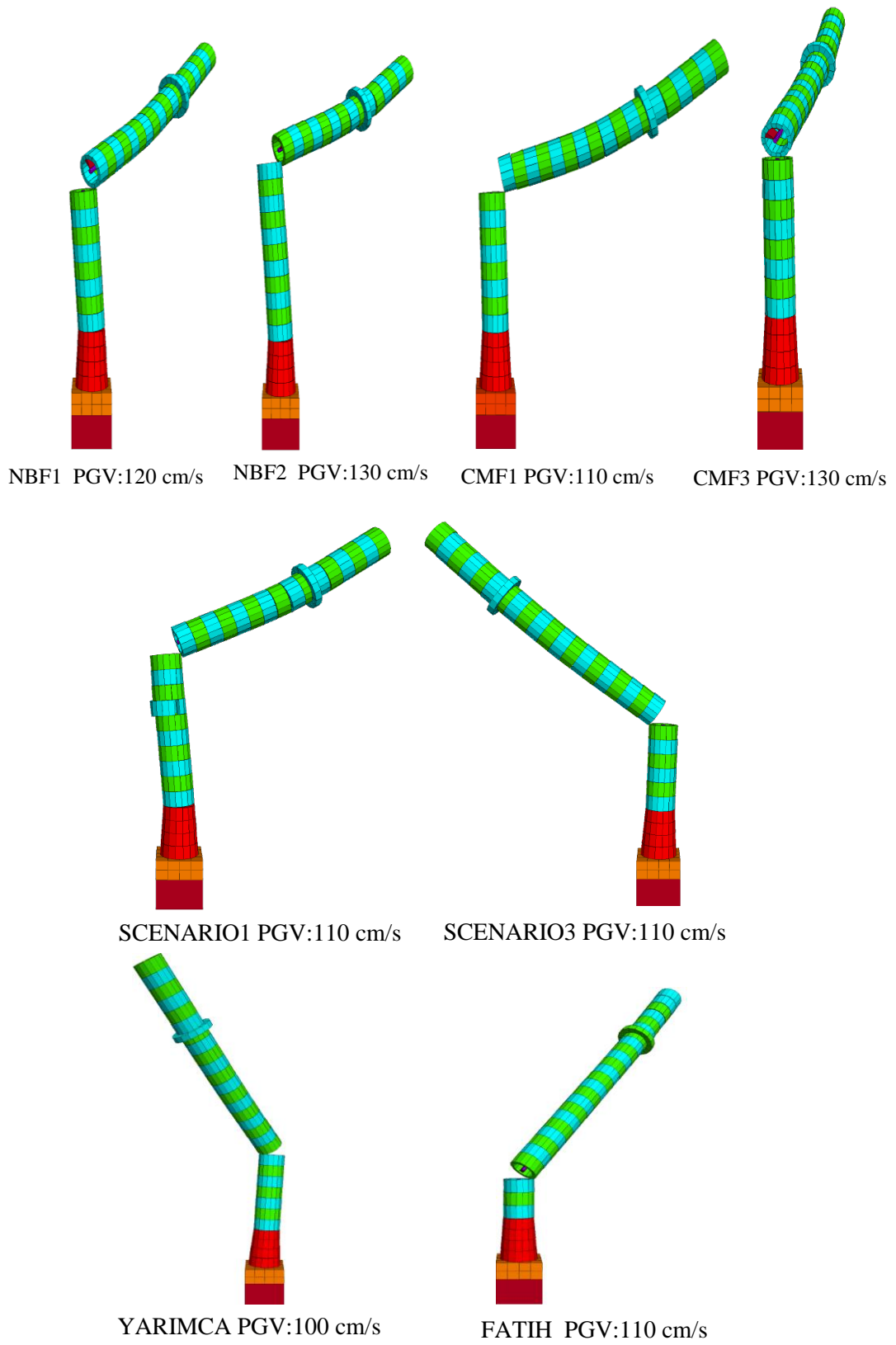


Figure 4.37. Collapse mechanisms of the Mihrimah minaret under eight scaled earthquake inputs.

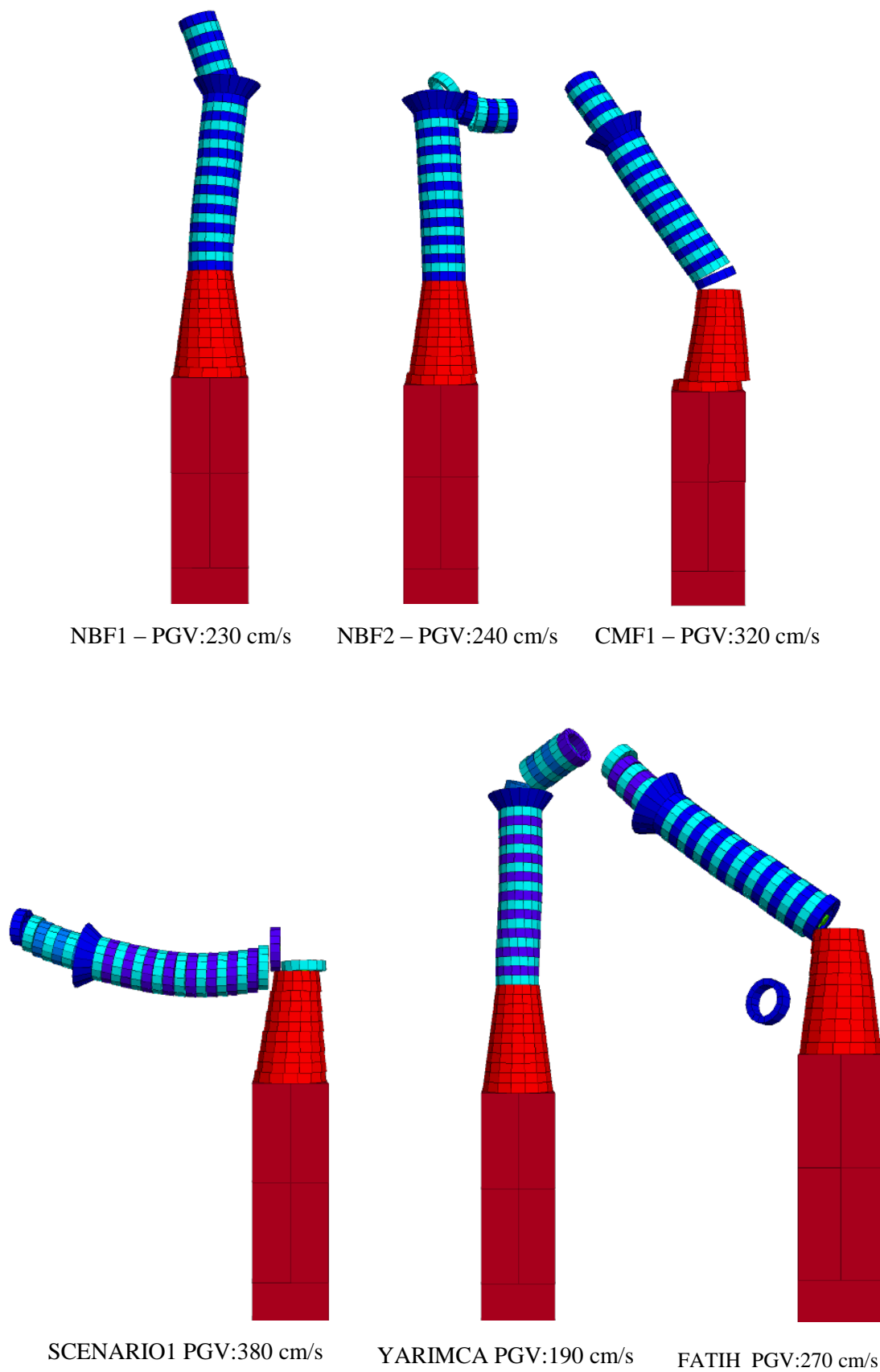
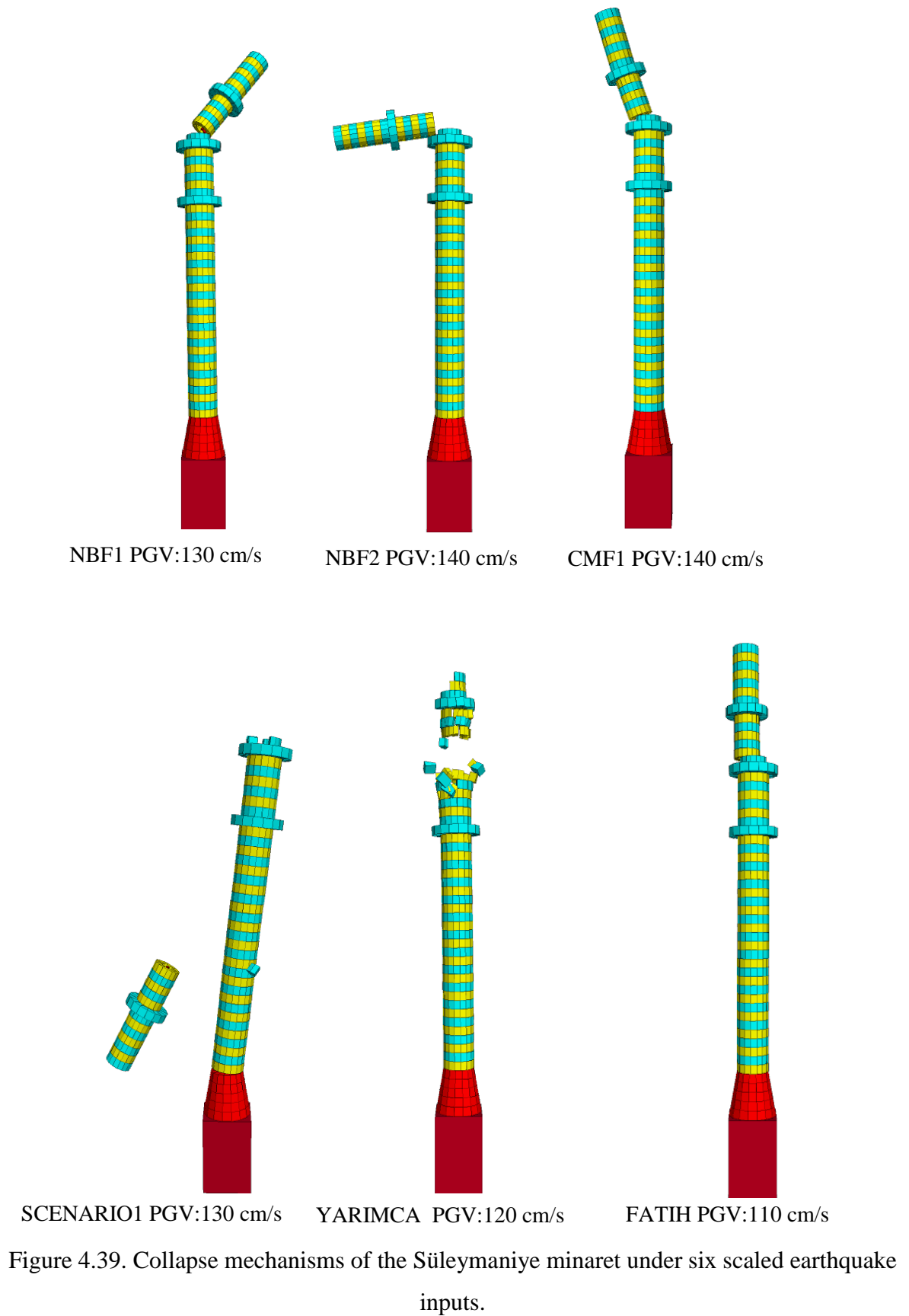


Figure 4.38. Collapse mechanisms of the Hagia Sophia minaret under six scaled earthquake inputs.



#### 4.7. Conclusion and Discussions

A profound parametric study aiming to understand the damage and collapse behavior of the minarets is presented. Three minarets of different heights and body diameter are modeled and analyzed using distinct element method.

Preliminarily the analyses are carried out using sine waves as input. The frequencies varied in a general band of 0.1 Hz and 13.00 Hz. There were some case specific variation in the applied frequency band. The velocity amplitudes varied between 10 and 100 cm/s. Altogether 210 runs for the Mihrimah, 210 for the Hagia Sophia and 160 for the Süleymaniye minaret were carried out. In the case of the Mihrimah minaret, collapse under the given sine wave and modeling assumptions occurred 1 time under 60 cm/s amplitude sine wave, 1 time under 70 cm/s amplitude sine wave, 7 times under 80 cm/s amplitude sine wave, 5 times under 90 cm/s amplitude sine wave and 11 times under 100 cm/s amplitude sine wave. No collapse took place in the Hagia Sophia minaret. Heavy damages of the Hagia Sophia minaret started at 80cm/s. Although the Hagia Sophia minaret is taller than that of the Mihrimah Sultan Mosque, its natural frequency of vibration is larger than the Mihrimah. This is probably due to the fact that, although the two minarets have elements of comparable total heights above the transition segment, the wall thickness in the Hagia Sophia minaret is larger and explains why the Mihrimah minaret experiences larger top displacements than the Hagia Sophia. In the case of the Süleymaniye minaret, collapse under the given ground motion and modeling assumptions occurred 1 time under 20 cm/s amplitude sine wave, 1 time under 60 cm/s amplitude sine wave, 2 times under 70 cm/s amplitude sine wave, 1 time under 80 cm/s amplitude sine wave, 5 times under 90 cm/s amplitude sine wave and 6 times under 100 cm/s amplitude sine wave.

Total of global energy stored and dissipated in minarets have been computed and evaluated. The objective of these computational analysis efforts is to find out the correlation between the global energy dissipation of the minarets and damage. The results obtained show the strong dependence of the minaret's seismic behavior on the frequency content of data and energy dissipation. Total released energy cause to loss of stiffness in minarets and this loss alter the model frequencies and modal damping values.

Dynamic analyses followed the preliminary analyses by performing a series of 10 different loading configurations as real and simulated earthquake time histories. Their response is assessed in terms of peak displacement amplitudes, peak stress amplitudes and their locations. The results suggest that failure takes place due to excessive normal deformations and rocking at the base of the minaret body and due to shear deformations at upper levels. To establish if the failure mechanism is local or global the deformed shapes and vertical stress distributions at the end of the seismic excitation were helpful. They allowed quantitative data about failure pattern, which may be result of sliding, bending, cracking under direct tension or partial collapse of the block of the minaret. No collapse or failure took place in minarets under real earthquakes and broadband simulations. To force each model to collapse, the input velocities were scaled up progressively and analysis was repeated until instability in the model is reached. These more refined analyses have the goal to establish possible relationships between the basic geometric properties of the minarets and their structural response to seismic excitations. General behavior of the minarets under controlled input motion, in terms development of stress concentrations and joint displacements, was not found to be strikingly different than that obtained by Çaktı *et al.* (2012) where the analysis had been carried out under real and simulated earthquakes. Stress concentrations were observed close to the transition part, near the middle of the minarets' body and above the balcony. Damage to the blocks took place due to shear deformations at heights above mid-body. Blocks get separated from each other when inertial forces in the out-of-plane directions exceed the shear strength of the mortar. This lateral thrust initiates the collapse of the minaret above the transition part as a result of additional inertial forces. All results suggest that although some very valuable case specific conclusions can be drawn, more case studies are needed, to be able to parameterize and/or systemize the collapse behavior of minarets.

## 5. CONCLUSIONS

The fundamental aim of this thesis was to extend numerical modeling and nonlinear structural analysis capabilities of historical masonry structures.

Distinct element method is tested and verified for modeling (1) the earthquake behavior of masonry buildings under earthquake loading; (2) the FRP application on masonry buildings; and (3) base isolation. This is achieved by comparing the results of analytical modeling with shake table experiments. Development and calibration of model to accurately predict the actual response of experimental model within the nonlinear range is used to understand the seismic behavior and capacity of the masonry mosque and then to be employed to investigate minaret behavior. Specific findings concerning the distinct element modeling of the Mustafa Paşa Mosque model are:

- Non-linear structural behavior of masonry structures depends on the mortar joints where the softening behavior can only occur. Distinct element method helps to understand the discretization of the masonry mosque in terms of rigid bodies as bricks and straight interface elements as mortar joints, connecting two bricks. This method allows evaluating a possible crack or slipping plane between unit mortar interfaces.
- Rigid blocks are used to represent the base isolation system for the analytical model that act as viscous dampers in the shear direction. The overall responses of the model structure with isolators were reduced significantly. The results show more than satisfactory agreement between experimental and analytical results with amplitudes and frequencies exhibiting deviations in an acceptable range.
- The numerical FRP model appears to be relatively less efficient in estimating the experimental response than it was in modeling of the base isolated and the un-strengthened model under higher levels of input.

- The numerical model replicated the damage patterns on the shake table model satisfactorily well. This suggests that such models can be used for the analysis collapse conditions, which may be very difficult, if not impossible, in laboratory conditions.

Dynamic behavior of three minarets in Istanbul, namely the minarets of the Mihirimah Sultan Mosque, Hagia Sophia Museum, and Süleymaniye Mosque, is studied under sine waves (velocity amplitude range: 10 cm/s – 100 cm/s; frequency range: 0.1 Hz – 13 Hz) and under ten real and simulated earthquakes. The use of sine waves provided a systematic look at the normalized top displacements; maximum normalized relative drum displacements; and energy parameters, although it can be argued that certain combinations, particularly those with high velocities and frequencies are unrealistic. The sine wave inputs were monochromatic, i.e. one frequency at one time and had a constant duration. The real and simulated earthquakes had naturally wider frequency bands and varying strong motion durations.

For the characterization of damage two parameters are defined: normalized top displacement and maximum normalized relative drum displacement. Normal top displacement is associated with the global behavior of a minaret. The maximum normalized relative drum displacement primarily gives an idea about local damages, is however also associated with the global minaret behavior when it becomes large. It should be noted that the normalization of this parameter is done with respect to body diameter. Minarets are simply cylinder type structures with a certain wall thickness. Therefore the local instabilities are in fact controlled by the wall thickness or better expressed by stone dimensions. Yet in the definition of this parameter the body diameter is preferred to be able to characterize this action in a more general manner. With the distinct element methodology it was possible to push minaret models to collapse which is very difficult, if not impossible, in laboratory conditions. Specific findings associated with the analyses of the minarets are as follows:

- The total of global energy stored and dissipated in minarets under sine waves show the strong dependence of the minaret's seismic behavior on the frequency content of data and energy dissipation.

- Under 10 different loading configurations as real and simulated earthquake time histories failure takes place due to excessive normal deformations and rocking at or near the base of the minaret body and due to shear deformations at upper levels.
- In the Mihrimah minaret, collapse takes place following the development of a complete separation of the minaret into two parts somewhere between the transition part and the balcony, and the fall of the upper part as a result of ongoing ground motion cycles. The same pattern is observed under all inputs and suggests it is independent of time and frequency domain characteristics of input ground motion.
- In the Hagia Sophia minarets there are two collapse patterns. In the first pattern the part of the minaret right above the balcony gets separated and collapses. In the second pattern a major separation occurs between the transition segment and the whole body above the transition segment falls down, following rocking.
- Süleymaniye minaret has a reduced wall thickness starting at its second balcony All collapses are associated with this part of the Süleymaniye minaret.
- Slenderness (i.e the relation between the body height and the body diameter) appears to have an important role when it comes to collapse. In this context body height is used as the height of a minaret above the transition segment. Mihrimah and the Süleymaniye minarets have similar slenderness ratios, while the slenderness ratio of the Hagia Sophia minaret is about half. This can explain the higher levels of collapse velocity associated with the Hagia Sophia minaret.

Further research on the minarets will focus on the development of new parameters for damage characterization and normalization of energy parameters.

There are many examples of earthquake damage to the minarets. Some of them are reported in the literature. Some of them are in the damage reports such as the cases of 2011 Van and 2014 Northern Aegean earthquakes. Additionally, studies exist in the literature that provide for analytical or descriptive information on the earthquake behavior of minarets. As such, when combined with the large analytical effort presented in this thesis, it can be said that we are getting ready for obtaining of fragility curves for minarets.

Given our current insight into the damage and collapse patterns of minarets, the natural step forward is the development and testing of strengthening proposals for the minarets.

## REFERENCES

- Abbaneo, S., M. Berra, L. Binda and A. Faticcioni, 1995, “Nondestructive Evaluation of Brick-Masonry Structures: Calibration of Sonic Wave Propagation Procedures”, *Proceedings of International Symposium Non-Destructive Testing in Civil Engineering*, 1995, Vol. 1, pp. 253-260, Berlin.
- Abdel-Motaal, M.A., 2014, “Effect of Piles on the Seismic Response of Mosques Minarets”, *Ain Shams Engineering Journal*, Vol. 5, No. 1, pp. 29-40.
- Abrams D.P., 2001, “Performance-Based Engineering Concepts for URM Structures”, *Progress in Structural Engineering and Materials*, Vol. 3 No.1 pp. 48-56, John Wiley & Sons.
- Acar, R., R. Livaoğlu, A. Doğangün and H. Sezen, 2007, “The Effect of Subsoil on the Seismic Response of Reinforced Concrete Cylindrical Minarets”, *Proceedings of Fifth International Conference on Seismology and Earthquake Engineering, International Institute of Earthquake Engineering and Seismology (IIEES)*, Tehran, 14-16 May, Iran.
- Alfano, G. and E. Sacco, 2006, “Combining Interface Damage and Friction in a Cohesive-Zone Model”, *International Journal for Numerical Methods in Engineering*, Vol. 68, No.5, pp. 542-582.
- Al-Heib, M., 2012, *Distinct Element Method Applied on Old Masonry Structures*, Numerical Modelling, Chapter 14, In Tech.
- Almeida, C., J. Paulo Guedes, A. Arêde, C. Q. Costa and A. Costa, 2012, “Physical Characterization and Compression Tests of One Leaf Stone Masonry Walls”, *Construction and Building Materials*, Vol. 30, pp. 188-197.

- Altunışık, A. C, 2011, “Dynamic Response of Masonry Minarets Strengthened with Fiber Reinforced Polymer (FRP) Composites”, *Natural Hazards and Earth System Sciences*, Vol. 11, No. 7, pp. 2011-2019.
- AlShwbani M.M. and S. N. Sinha, 1999, “Stress-Strain Characteristics of Brick under Uniaxial Cyclic Loading”, *Journal of Structural Engineering ASCE*, Vol. 125, No. 6, pp. 600-604.
- AlShwbani M.M. and S. N. Sinha, 2000, “Stress-Strain Characteristics of Brick under Biaxial Cyclic Loading”, *Journal of Structural Engineering ASCE*, Vol. 126, No. 9, pp. 1004-1007.
- An, D., T. J. Qu, and J. W. Liang, 2012, “Full-Scale Test on Seismic Performance of Masonry Structure”, *Applied Mechanics and Materials*, Vol. 204-208, pp. 2610-2617.
- An, D., T. J. Qu, and J. W. Liang, 2013, “Pseudo-Dynamic Test of Brick Masonry under Different Earthquake Motion”, *Applied Mechanics and Materials*, Vol. 256-259, pp. 2111-2116.
- Anthoine, A., 1992, *In-plane Behavior of Masonry: B Literature Review*, EUR-Report No.13840 EN, JRCIspra, pp. 64.
- Asteris, P.G. and I. P. Giannopoulos, 2012, “Vulnerability and Restoration Assessment of Masonry Structural Systems”, *Electronic Journal of Structural Engineering*, Vol. 12, No. 1, pp. 82-93.
- Asteris, P.G., F. P. Gazepidis and E. K. Polychroniou, 2012, “Structural Modeling and Seismic Protection of Masonry Structural Systems”, *Proceedings of EACS 2012 – Fifth European Conference on Structural Control*, Genoa, 18-20 June 2012, Italy.

ASTM, 2002, "Standard Test Method for Diagonal Tension (Shear) in Masonry Assemblages." ASTM Standard E 519-02, American Society for Testing and Materials, West Conshohocken, PA.

ASTM, 2003, "Standard Test Method for Compressive Strength of Masonry Prisms." ASTM Standard C1314, American Society for Testing and Materials, West Conshohocken, PA.

Atamtürktür, S. and B. Sevim, 2012, "Seismic Performance Assessment of Masonry Tile Domes through Nonlinear Finite-Element Analysis" *Journal of Performance of Constructed Facilities (ASCE)*, Vol. 26, No. 4, pp. 410-423.

Atkinson, R. H. and J. L. Noland, 1983. "A Proposed Failure Theory for Brick Masonry in Compression", *Proceedings of the third Canada, Masonry Symposium*, pp. 5-1-5-17, Canada.

Augenti N. and F. Parisi, 2011, "A Constitutive Modelling of tuff Masonry in Direct Shear", *Construction and Building Materials*, Vol. 25, No. 4, pp. 1612–20.

Avdelidis, N.P. and A. Moropoulou, 2004, "Applications of Infrared Thermography for the Investigation of Historic Structures", *Journal of Cultural Heritage*, Vol. 5, No. 1, pp. 119-127.

Bairrao, R. and C. T. Vaz, 2000, "Shaking Table Testing of Civil Engineering Structures – The LNEC 3D Simulator Experience", *Proceedings of the Twelfth World Conference on Earthquake Engineering*, Auckland, New Zealand, 2129.

Baker, W. E., P. S. Westine and F.T. Dodge, 1973, *Similarity Methods in Engineering Dynamics: Theory and Practice of Scale Modeling*, Rochelle Park, NJ: Hayden Books.

- Baronio, G. and L. Binda, 1995, “Experimental Approach to a Procedure for the Investigation of Historic Mortars”, *Proceedings of the Joint Int. Workshop Proposed by RILEM TC 127-MS and CIB W23: Evaluation and Strengthening of Existing Masonry Structures*, University of Padua, pp. 107-115, Italy.
- Baronio, G., L. Binda, C. Tedeschi and C. Tiraboschi, 2003, “Characterization of the Materials used in the Construction of the Noto Cathedral”, *Construction and Building Materials*, Vol. 17, No. 3, pp. 557-571.
- Bartoli, G., M. Betti, L. Facchini and M. Orlando, 2012, “Non-Destructive Characterization of Stone Columns by Dynamic Test: Application to the Lower Colonnade of the Dome of the Siena Cathedral”, *Engineering Structures*, Vol. 45, pp. 519-535.
- Bartoli, G., M. Betti, and S. Giordano, 2013, “In Situ Static and Dynamic Investigations on the “Torre Grossa” Masonry Tower”, *Engineering Structures*, Vol. 52, pp. 718-733.
- Bathe, K.J., and E. L. Wilson, 1976, *Numerical Methods in Finite Element Analysis*, Englewood Cliffs, New Jersey: Prentice-Hall, Inc.
- Bayraktar, A., A. Şahin, D. M. Özcan and F. Yıldırım, 2010, “Numerical Damage Assessment of Hagia Sophia Bell Tower by Nonlinear FE Modeling”, *Applied Mathematical Modeling* Vol. 34, No. 1, pp. 92-121.
- Belmouden, Y. and P. Lestuzzi, 2009, “An Equivalent Frame Model for Seismic Analysis of Masonry and Reinforced Concrete Buildings”, *Construction and Building Materials*, Vol. 23, No. 1, pp. 40-53.
- Beyer K. and A. Dazio, 2012, “Quasi-Static Cyclic Tests on Masonry Spandrels”, *Earthquake Spectra*, Vol. 28, No. 3, pp. 907-929.

- Blondet, J. M., R. W. Clough and S. A. Maphin, 1980, *Evaluation of Shaking Table Test Program on Response Behavior of a Two Story Reinforced Concrete Frame*, Report No. UCB/EERC-80/42, EERC, Univ. of California, Berkeley, California.
- Blondet, J. M., R. L. Mayes and T. E. Kelly, 1990, "Out-of-plane Testing of Slender Hollow Clay Masonry Block Walls", *Proceedings of the Fifth North American Masonry Conference*, University of Illinois.
- Bloomfield, P., 2000, *Fourier analysis of Time Series: An Introduction*, New York: Wiley-Inter science.
- Boore, DM. 2009, "Comparing Stochastic Point-source and Finite-source Ground-motion Simulations: SMSIM and EXSIM", *Bulletin of the Seismological Society of America (BSSA)*, Vol. 99, No. 6, pp.3202-3216.
- Bosiljkov, V., M. Uranjek, R. Zarnić and V. Bokan-Bosiljkov, 2010, "An Integrated Diagnostic Approach for the Assessment of Historic Masonry Structures", *Journal of Cultural Heritage*, Vol. 11, No. 3, pp. 239-249.
- Brasile, S., R. Casciaro and G. Formica, 2007, "Multilevel Approach for Brick Masonry Walls Part II: On the Use of Equivalent Continua", *Computer Methods in Applied Mechanics and Engineering*, Vol. 196, No. 49, pp. 4801-4810.
- Brencich, A. and E. Sterpi, 2006, "Compressive Strength of Solid Clay Brick Masonry: Calibration of Experimental Tests and Theoretical Issues", *Proceedings of the International Conference on Structural Analysis of Historical Constructions*, New Delhi, India, Macmillan India Ltd., New Delhi, India, pp. 757-765.
- Burnett S., M. Gilbert, T. Molyneaux, A. Tyas, B. Hobbs and G. Beattie, 2007, "The Response of Masonry Joints to Dynamic Tensile Loading", *Materials and Structures*, Vol. 40, No. 5, pp. 517-527.

- Button, M. R. and R. L. Mayes, 1992, "Out-of-Plane Seismic Response of Reinforced Masonry Walls", *Journal of Structural Engineering, ASCE*, Vol. 118, No. 9, pp. 2495-2513.
- Cagnan, Z., 2012, "Numerical Models for the Seismic Assessment of St. Nicholas Cathedral, Cyprus", *Soil Dynamics and Earthquake Engineering*, Vol. 39, pp. 50-60.
- Calderini, C. and S. Lagomarsino, 2008, "A Continuum Model for In-Plane Anisotropic Inelastic Behavior of Masonry", *Journal of Structural Engineering, ASCE*, Vol.134, No. 2, pp. 209-220.
- Caliò, I., M. Marletta, and B. Pantò, 2008, "A Discrete Element Approach for the Evaluation of the Seismic Response of Masonry Buildings", *Proceedings of the Fourteenth World Conference on Earthquake Engineering*, October 12-17 2008, Beijing, China.
- Calvi G. M., R. K. Gregory and G. Maganes, 1996, "Testing of Masonry Structures for Seismic Assessment", *Earthquake Spectra*, Vol. 12, No. 1, pp. 145-162.
- Çamlıbel, N., 2000, *Geleneksel Yapılarda Stabilitenin İyileştirilmesi ve Temellerin Takviyesi*, Birsen Yayınevi, İstanbul.
- Candeias, P., A. C. Costa and E. Coelho, 2004, "Shaking Table Test of 1:3 Reduced Scale Models of Four Storey Unreinforced Masonry Buildings", *Proceedings of Thirteenth World Conference on Earthquake Engineering*, Vancouver, B.C., August 1-6, paper no. 2199, Canada.
- Candela, M., S. Cattari, S. Lagomarsino, M. Rossi, R. Fonti and E. Pagliuca, 2012, "In-Situ Test for the Shear Strength Evaluation of Masonry: the Case of a Building Hit by L'Aquila Earthquake", *Proceedings of the Fifteenth World Conference on Earthquake Engineering Lisbon, Portugal*.

- Casarin, F., M. Dalla Benetta, C. Modena, F. da Porto, M. R. Valluzi, L. Cantini, C. Tedeschi and P. Condoleo, 2013, "Structural Monitoring and Investigation Campaign in the Church of St. Giuseppe dei Minimi in L'Aquila, After the 6th of April 2009 Earthquake" *Nondestructive Testing of Materials and Structures RILEM Bookseries* 6, pp. 1187-1193.
- Casolo, S., G. Milani, G. Uva and C. Alessandri, 2013, "Comparative Seismic Vulnerability Analysis on Ten Masonry Towers in the Coastal Po Valley in Italy", *Engineering Structures*, Vol. 49, pp. 465-490.
- Casolo, S. and F. Peña, 2007, "Rigid Element Model for In-Plane Dynamics of Masonry Walls Considering Hysteretic Behavior and Damage", *Earthquake Engineering and Structural Dynamics*, Vol. 36, No. 8, pp. 1029-1048.
- Cerdeira, F., M. E. Vázquez, J. Collazo and E. Granada, 2011, "Applicability of Infrared Thermography to the Study of the Behavior of Stone Panels as Building Envelopes", *Energy and Buildings*, Vol. 43, No. 8, pp. 1845-1851.
- Chaimoon, K. and M. M. Attard, 2007, "Modeling of Unreinforced Masonry Walls under Shear and Compression", *Engineering Structures*, Vol. 29, No. 9, pp.2056-2068.
- Chaimoon, K. and M. M. Attard, 2009, "Experimental and Numerical Investigation of Masonry under Three-Point Bending (in-plane)", *Engineering Structures*, Vol. 31, No. 1, pp. 103-112.
- Clark, M.R., D. M. McCann and M. C. Forde, 2003, "Application of Infrared Thermography to the Non-Destructive Testing of Concrete and Masonry Bridges", *NDT&E International*, Vol. 36, No. 4, pp. 265-275.
- Colla, C., P. C. Das, D. McCann and M. C. Forde, 1997, "Sonic, Electromagnetic and Impulse Radar Investigation of Stone Masonry Bridges" *NDT&E International*, Vol. 30, No. 4, pp. 249-254.

- Concu, G., B. De Nicolo, C. Piga and V. Popescu, 2009, "Non-Destructive Testing of Stone Masonry using Acoustic Attenuation Tomography Imaging", in B.H.V. Topping, L.F. Costa Neves, R.C. Barros, (Editors), *Proceedings of the Twelfth International Conference on Civil, Structural and Environmental Engineering Computing*, Civil-Comp Press, Stirlingshire, Paper 155, UK.
- Çaktı, E., C. S. Oliveira, J. V. Lemos, Ö Saygılı, S. Görk and E. Zengin, 2013, "Earthquake Behavior of Historical Minarets in Istanbul", *Proceedings of the Fourth ECCOMAS Thematic Conference on Computational Methods in Structural Dynamics and Earthquake Engineering*, 12-14 June 2013, Kos Island, Greece.
- Çaktı, E., C. S. Oliveira, J. V. Lemos, Ö Saygılı, S. Görk and E. Zengin, 2014, Seismic Assessment of Historical Minarets in Istanbul, *in preparation*.
- D'Ambrisi, A., V. Mariani and M. Mezzi, 2012, "Seismic Assessment of a Historical Masonry Tower with Nonlinear Static and Dynamic Analyses Tuned on Ambient Vibration Tests", *Engineering Structures*, Vol. 36, pp. 210-219.
- Dawood, N., H. Marzouk, A. Hussein and N. Gillis, 2013, "Nondestructive Assessment of a Jetty Bridge Structure Using Impact-Echo and Shear-Wave Techniques." *Journal of Bridge Engineering*, Vol. 18, No. 8, pp. 801-809.
- DeJong, M.J. and C. Vibert, 2012, "Seismic Response of stone Masonry Spires: Computational and Experimental Modeling", *Engineering Structures*, Vol. 40, pp. 566-574.
- Doğangün, A., R. Acar, H. Sezen and R. Livaoğlu, 2008, "Investigation of Dynamic Response of Masonry Minaret Structures", *Bulletin of Earthquake Engineering*, Vol. 6, No. 3, pp. 505-517.
- Doğangün, A. and H. Sezen, 2012, "Seismic Vulnerability and Preservation of Historical Masonry Monumental Structures", *Earthquakes and Structures*, Vol. 3, No. 1, 83-95.

- Drysdale, R.G., A. A. Hamid and L. R. Baker, 1994, *Masonry Structures, Behavior and Design*, Prentice Hall, Englewood Cliffs, New Jersey, U.S.A.
- Durukal, E., S. Cimilli and M. Erdik, 2003, “Dynamic Response of Two Historical Monuments in İstanbul Deduced from the Recordings of Kocaeli and Düzce Earthquakes”, *Bulletin of the Seismological Society of America*, Vol. 93, No. 2, pp. 694-712.
- Ediz, Ö. and M. J. Ostwald, 2012, “The Süleymaniye Mosque: A Computational Fractal Analysis of Visual Complexity and Layering in Sinan's Masterwork”, *Architectural Research Quarterly*, Vol. 16 No. 02, 171-182.
- Eilouti, B., 2012, “Sinan and Palladio: Two Cultures and Nine Squares”, *International Journal of Architectural Heritage*, Vol. 6, No. 1, 1-18.
- Elwan, SH., 1996, *Seismic Response of Historical Masonry Minarets*, Ph.D. Dissertation, Faculty of Engineering, Ain Shams University, Cairo.
- Elwood, K. J. and J. P. Moehle, 2003, *Shaking Table Tests and Analytical Studies on the Gravity Load Collapse of Reinforced Concrete Frames*, PEER Report No. 2003/01, Pacific Earthquake Engineering Research Center, Univ. of California, Berkeley, California.
- Erdik, M., 2012, *Personal Communication*, Boğaziçi University, İstanbul, Turkey.
- ES 1999, *Methods of Test for Mortar for Masonry - Part 11: Determination of Flexural and Compressive Strength of Hardened Mortar*, European Standard EN 1015-11, 1999.
- Faella, G., G. Frunzio, M. Guadagnuolo, A. Donadio and L. Ferri, 2012, “The Church of the Nativity in Bethlehem: Non-Destructive Tests for the Structural Knowledge”, *Journal of Cultural Heritage*, Vol. 13, No. 4, pp. e27-e41.

- Gentry, T. A., 2012, "Identifying Non-Catastrophic Failures in Glazed Architectural Terra Cotta Masonry", *Proceedings of the Sixth Congress on Forensic Engineering*, San Francisco, California, United States, pp. 201-209.
- Foti, D., S.I. Chorro and M. F. Sabbà, 2012, "Dynamic Investigation of an Ancient Masonry Bell Tower with Operational Modal Analysis", *The Open Construction and Building Technology Journal*, Vol. 6, pp. 384-391.
- Gesualdo, A. and M. Monaco, 2011, "Seismic Retrofitting Techniques for Existing Masonry Buildings", *Journal of Civil Engineering and Architecture*, Vol. 5, No. 11, pp. 1011-1018.
- Giambanco, G. and L. Di Gatti, 1997, "A Cohesive Interface Model for the Structural Mechanics of Block Masonry", *Mechanics Research Communications*, Vol. 24, No. 5, pp. 503-512.
- Giambanco, G., S. Rizzo and R. Spallino, 2001, "Numerical Analysis of Masonry Structures via Interface Models", *Computer Methods in Applied Mechanics and Engineering*, Vol. 190, No. 50, pp. 6493-6511.
- Giordano, A., E. Mele and A. De Luca, 2002, "Modeling of Historical Masonry Structures: Comparison of Different Approaches through a Case Study", *Engineering Structures*, Vol. 24, No.4, pp. 1057-1069.
- Griffith, M. C., N. T. K. Lam, J. L. Wilson and K. Doherty, 2004, "Experimental Investigation of Unreinforced Brick Masonry Walls in Flexure", *Journal of Structural Engineering*, Vol. 130, No. 3, pp. 423-432.
- Gurlitt, C., 1999, *İstanbul'un Mimari Sanatı*, Translation: R. Kızıltan, Ankara.
- Hacıefendi, K. and B. Fahri, 2011, "Stochastic Dynamic Response of Masonry Minarets Subjected to Random Blast and Earthquake-Induced Ground Motions" *The Structural Design of Tall and Special Buildings*, Vol. 20, No. 6, pp. 669-678.

- Hamed, E. and O. Rabinovitch, 2008, "Nonlinear Dynamic Behavior of Unreinforced Masonry Walls Subjected to Out-of-Plane Loads", *Journal of Structural Engineering*, Vol. 134, No. 11, pp. 1743-1753.
- Hamrouche, R., G. Klysz, J. P. Balayssac, J. Rhazi and G. Ballivy, 2012, "Numerical Simulations and Laboratory Tests to Explore the Potential of Ground-Penetrating Radar (GPR) in Detecting Unfilled Joints in Brick Masonry Structures", *International Journal of Architectural Heritage: Conservation, Analysis, and Restoration*, Vol. 6, No. 6, pp. 648-664.
- Hendry, A.W., 1998, *Structural Masonry*, 2<sup>nd</sup> Edn. MacMillan Press LTD, London.
- Heyman, J., 1966, "The Stone Skeleton", *International Journal of Solids and Structures*, Vol. 2, No. 2, pp. 249-279.
- Idris J., M. Al Heib and T. Verdel, 2009, "Masonry Joints Mechanical Behavior Evolution in Built Tunnels", *Tunneling and Underground Space Technology*, Vol. 24, No. 6, pp. 617-626.
- Iiba, M., H. Mizuno, T. Goto and H. Kato, 1996, "Shaking Table Test on Seismic Performance of Confined Masonry Wall", *Proceedings of the Eleventh World Conference on Earthquake Engineering*, pp. 659.
- Indirli, M., B. Carpani, A. Martelli, M. G. Castellano, S. Infanti, G. Croci, M. Biritognolo, A. Bonci, A. Viskovic and S. Viani, 2000, "Experimental Tests on Masonry Structures Provided with Shape Memory Alloy Antiseismic Devices", *Proceedings of the Twelfth World Conference on Earthquake Engineering*, 2000, pp.1773.
- Islam, R., 2008, *Inventory of FRP Strengthening Methods in Masonry Structures*, M.S. Thesis, Technical University of Catalonia, Barcelona.
- Itasca International Incorporation, UDEC, Theory and Manual, 2000.

Itasca International Incorporation, 3DEC 4.1 Theory and Manual, 2013.

İspir, M., C. Demir, A. İlki and N. Kumbasar, 2010, “Material Characterization of the Historical Unreinforced Masonry Akaretler Row Houses in Istanbul” *Journal of Materials in Civil Engineering*, Vol. 22, No. 7, pp. 702-713.

Javed, M., 2009, *Seismic Risk Assessment of Unreinforced Brick Masonry Buildings System of Northern Pakistan*, Ph.D. Dissertation, N-W.F.P. University of Engineering and Technology, Peshawar, Pakistan.

Jeffs P.A., 2000, Core Consolidation of Heritage Structure Masonry Walls and Foundation Using Grouting Techniques – Canadian Case Study. *Proceedings of the Ninth Canad. Masonry Symposium 12*, 2000, 1-12, Canada.

Juha'sova', E., M. Hurak and Z. Zembaty, 2002, “Assessment of Seismic Resistance of Masonry Structures Including Boundary Conditions”, *Soil Dynamics and Earthquake Engineering*, Vol. 22, No. 9-12, pp. 1193-1197.

Kaya Y. and E. Şafak, 2013, “Real-Time Structural Health Monitoring and Damage Detection” *Proceedings of the 31st IMAC, A Conference on Structural Dynamics*, Hyatt Regency Orange County. Garden Grove, CA USA.

Kim, S. H., 1995, *A Study on the Optimal Design of Structure with the Application of Isolation Devices.*, Korea Power Engineering Co. Inc., Report, KOPEC/95-T-106.

Klingner, R.E., P. B. Shing, W. M. McGinley, D. I. McLean, H. Okail and S. Jo, 2011, “Seismic Performance Tests of Masonry and Masonry Veneer”, *Proceedings of the Eleventh NAMC*, Minneapolis mn USA.

Kouris, S.S. and M. K. K. Weber, 2011, “Numerical Analysis of Masonry Bell-Towers under Dynamic Loading” *Journal of Civil Engineering and Architecture*, Vol. 5, No. 8, pp. 715-722.

- Krause, M., C. Maierhofer, A. Gadei, C. Kohl and H. Wiggenhauser, 2003, "Improvement and Combination of Echo Methods for NDT of Concrete Elements", *Proceedings of the Second International RILEM Workshop on Life Prediction and Management of Concrete Structures*, 5-6 May 2003, Paris, France.
- Krstevska L., L. A. Tashkov, K. Gramatikov, F. M. Mazzolani and R. Landolfo, 2009, *Shaking Table Test of Mustafa Pasha Mosque Model in Reduced Scale*, Protection of Historical Buildings, PROHITECH 09 – Mazzolani (ed) Taylor and Francis Group, London, ISBN 978-0-415-55803-7.
- Kumar, S., Y. Itoh, K. Saizuka and T. Usami, 1997, "Pseudo Dynamic Testing of Scaled Models", *Journal of Structural Engineering*, pp. 524-526.
- Lagomarsino S., 1998, "A New Methodology for the Post-Earthquake Investigation of Ancient Churches", *Proceedings of the Eleventh European Conference on Earthquake Engineering (11th ECEE)*, Rotterdam.
- Langhaar, H., 1951, *Dimensional Analysis and Theory of Models*, New York: John Wiley.
- Largo, A. and R. Angiuli, 2013, *Thermographic Investigation of "leccese" Stone Masonry Structures, Nondestructive Testing of Materials and Structures*, RILEM Book series 6, pp 1137-1142.
- Laska, T., I. Tsimbal, S. Golubkov and Y. A. Petrova, 2013, "Practice of Using Virtual Reconstruction in the Restoration of Monumental Painting of the Church of the Transfiguration of Our Saviour on Neredita Hill", *Knowledge Visualization Currents*, pp. 147-164.
- Lemos, J.V., 2007, "Discrete Element Modeling of Masonry Structures", *International Journal of Architectural Heritage*, Vol. 1, No.1, pp. 190-213.

- Lemoni, H. and B. Christaras, 1999, "Classification of Soils Using in Situ Ultrasonic Velocity Techniques", *Proceedings of The Twelfth European Conference on Soil Mechanics and Geotechnical Engineering* (p. 393-400). June 7-10, 1999. Amsterdam, Netherlands.
- Li, C. S., S. S. E. Lam, M. Z. Zhang and Y. L. Wong, 2006, "Shaking Table Test of a 1:20 Scale High-Rise Building with a Transfer Plate System", *Journal of Structural Engineering*, Vol. 132, No. 11, pp. 1732-1744.
- Li, T., and S. Atamtürk, 2013, "Fidelity and Robustness of Detailed Micro, Simplified Micro, and Macro Modeling Techniques for a Masonry Dome", *Journal of Performance of Constructed Facilities*.
- Liu, M., Y. Cheng and X. Liu, 2011, "Shaking Table Test on Out-of-plane Stability of Infill Masonry Wall", *Transaction of Tianjin University*, Vol. 17, No. 2, pp. 125-131.
- Lofti, H.R. and B. P. Shing, 1994, "Interface Model Applied to Fracture of Masonry Structures", *Journal of Structural Engineering, ASCE*, Vol. 120, No.1, pp. 63-80.
- Lombillo, I., C. Thomas, L. Villegas, J. P. Fernández-Álvarez and J. Norambuena-Contreras, 2013, "Mechanical Characterization of Rubble Stone Masonry Walls Using Non and Minor Destructive Tests", *Construction and Building Materials*, Vol. 43, pp. 266-277.
- Lopez-Arce, P., J. Garcia-Guinea, M. Gracia and J. Obis, 2003, "Bricks in Historical Buildings of Toledo City: Characterization and Restoration", *Materials Characterization*, Vol. 50, pp. 59-68.
- Lourenço, P.B., 1994, *Analysis of Masonry Structures with Interface Elements, Theory and Applications*, TU-DELFT Report No. 03-21-22-0-01, Faculty of Civil Engineering, Delft Univ. of Technology, Delft, Netherlands.

- Lourenço, P.B., 1996, *Computational Strategies for Masonry Structures*, Ph.D. Dissertation, Delft University of Technology, Delft University Press.
- Lourenço, P.B., 1998, “Experimental and Numerical Issues in the Modeling of the Mechanical Behavior of Masonry”, *Proceedings of the II Structural Analysis of Historical Constructions (IISAHC)*, Barcelona.
- Lourenço, P.B., 2002, “Computations on Historic Masonry Structures”, *Structural Engineering, Mechanics and Materials*, John Wiley and Sons Ltd, Vol. 4, No. 3, pp. 301-319.
- Lourenço, P. B and J. G. Rots, 1997, “Multi surface Interface Model for Analysis of Masonry Structures”, *Journal of Engineering Mechanics*, Vol. 123, No. 7, pp. 660-668.
- Lubowiecka, I., J. Armesto, P. Arias and H. Lorenzo, 2009, “Historic Bridge Modeling Using Laser Scanning, Ground Penetrating Radar and Finite Element Methods in the Context of Structural Dynamics”, *Engineering Structures*, Vol. 31, No. 11, pp. 2667-2676.
- Luciano R. and E. Sacco, 1997, “Homogenization Technique and Damage Model for Old Masonry Material”, *International Journal of Solids and Structures*, Vol. 34, No. 4, pp. 3191-3208.
- Lu, X., Q. Zhou, X. Wu and W. Zhang, 1996, “Shaking Table Testing on Model Building Constructed in Moderate Seismic Region”, *Proceedings of the International Workshop on Earthquake Engineering for Regions of Moderate Seismicity*, Hong Kong, pp. 227-237.
- Macchi, G., 1997, “General methodology. The combined Use of Experimental and Numerical Techniques inside a Single Study”, *Proceedings of the Structural Analysis of Historical Constructions, CIMNE*, pp. 10-23, Barcelona.

- Maganes G. and G. M. Calvi, 1997, "In Plane Seismic Response of Brick Masonry Walls", *Earthquake Engineering and Structural Dynamics*, Vol. 26, No. 11, pp. 1091-1112.
- Mahin S.A., and P. B. Shing, 1989, "Pseudo Dynamic Test method-Current Status and Future Directions", *ASCE Journal of Structural Engineering*, Vol. 115, No. 8, pp. 2113-2128.
- McCann, D.M. and M. C. Forde, 2001, "Review of NDT Methods in the Assessment of Concrete and Masonry Structures", *NDT&E International*, Vol. 34, No. 2, pp. 71-84.
- Mele, T.V., J. McInerney, M. J. DeJong and P. Block, 2012, "Physical and Computational Discrete Modeling of Masonry Vault Collapse", *Proceedings of the SAHC 2012 Eight International Conference on Structural Analysis of Historical Constructions*, October 15-17 wroclaw Poland.
- Mendes, N., P. B. Lourenço and A. Campos-Costa, 2014, "Shaking Table Testing of an Existing Masonry Building: Assessment and Improvement of the Seismic Performance", *Earthquake Engineering Structural Dynamics*, Vol. 43, No. 2, pp. 247-266.
- Meola, C., 2007, "Infrared Thermography of Masonry Structures", *Infrared Physics and Technology*, Vol. 49, No. 3, pp. 228-233.
- Meola, C., R. D. Maio, N. Roberti and G. M. Carlomagno, 2005, "Application of Infrared Thermography and Geophysical Methods for Defect Detection in Architectural Structures", *Engineering Failure Analysis*, Vol. 12, No. 6, pp. 875-892.
- Michael P. and P. E. Schuller, 2003, "Nondestructive Testing and Damage Assessment of Masonry Structures", *Progress in Structural Engineering and Materials*, Vol. 5, No. 4, pp. 239-251.

- Milani, G., P. B. Lourenço and A. Tralli, 2006, "Homogenized Limit Analysis of Masonry Walls, Part I: Failure Surfaces; Part II: Structural Examples", *Computers and Structures*, Vol. 84, pp. 166-195.
- Miranda, L., L. Cantini, J. Guedes, L. Binda and A. Costa, 2013, "Applications of Sonic Tests to Masonry Elements: Influence of Joints on the Propagation Velocity of Elastic Waves." *Journal of Materials in Civil Engineering*, Vol. 25, No. 6, pp. 667-682.
- Mojsilovic', N., N. Kostic and J. Schwartz, 2013, "Modeling of the Behavior of Seismically Strengthened Masonry Walls Subjected to Cyclic In-Plane Shear", *Journal of Engineering Structures*, Vol. 56, pp. 1117-1129.
- Mortezaei, A., A. Kheyroddin and H. R. Ronagh, 2012, "Finite Element Analysis and Seismic Rehabilitation of a 1000-year-old Heritage Listed Tall Masonry Mosque", *The Structural Design of Tall and Special Buildings*, Vol. 21, No. 5, pp. 334-353.
- Müller-Wiener, W., 1977, *Bildlexikon Zur Topographie Istanbuls*, Deutsches Archäologisches Institute, Verlag Ernst Wasmuth Tübingen, (Translated by U. Sayin as Istanbul' un Tarihsel Topografyasi, Istanbul, 1998).
- Nacheman, R., J. Yu and K. Badheka, 2012, "Repair of a Landmark Building's Façade: 230 Park Avenue, New York, NY", *Proceedings of the Sixth Congress on Forensic Engineering*, San Francisco, California, United States, pp. 210-219.
- Nakagawa, T., T. Narafu, H. Imai, T. Hanazato, Q. Ali and C. Minowa, 2012, "Collapse Behavior of a Brick Masonry House Using a Shaking Table and Numerical Simulation Based on the Extended Distinct Element Method", *Bulletin of Earthquake Engineering*, Vol. 10, No. 1, pp. 269-283.
- Narine K. and S. N. Sinha, 1989, "Behavior of Masonry under Cyclic Compressive Loading", *Journal of Construction Engineering Management ASCE*, Vol. 115, No. 2, pp. 1432-1445.

- Nazir, S. and M. Dhanasekar, 2013, "Modeling the Failure of Thin Layered Mortar Joints in Masonry", *Engineering Structures*, Vol. 49, pp. 615-627.
- Oğuzmert, M., 2002, *Yığma Minarelerin Dinamik Davranışı*, M.S. Thesis, Istanbul Technical University, Istanbul.
- Oliveira, D.V.C., 2000, *Mechanical Characterization of Stone and Brick Masonry*, Report 00-DEC/E-4, University of Minho, Department of Civil Engineering, Portugal.
- Oliveira, C. S., E. Çaktı, D. Stengeland and M. Branco, 2012, "Minaret Behavior Under Earthquake Loading: The Case of Historical Istanbul" *Earthquake Engineering Structural Dynamics*, Vol. 41, No. 1, pp. 19-39.
- Olivito, R. S. and P. Stumpo, 2001, "Fracture Mechanics in the Characterization of Brick Masonry Structures", *International Journal of Materials and Structures*, Vol. 34, No. 4, pp. 217-223.
- Orbána, Z. and M. Gutermann, 2009, "Assessment of Masonry Arch Railway Bridges Using Non-Destructive In-Situ Testing Methods" *Engineering Structures*, Vol. 31, No. 10, pp. 2287-2298.
- Page, A.W., 1978, "Finite Element Model for Masonry", *Journal of the Structural Division, ASCE, 104(ST8), Proceeding Paper 13957*, pp. 1267-1285.
- Papayianni, I. and M. Stefanidou, 2001, "Porosity and Structure of Old Mortars", *Proceedings of the International Congress on Studies in Ancient Structures*, Yıldız Technical University, Istanbul, Turkey, pp. 509-517.
- Paquette, J. and M. Bruneau, 2004, "Pseudo Dynamic Testing of Unreinforced Masonry Building with Flexible Diaphragm" *Proceedings of the Thirteenth World Conference on Earthquake Engineering*, Vancouver, B.C., August 1-6, pp. 2609, Canada.

- Parisi, F., 2010, *Non-Linear Seismic Analysis of Masonry Buildings*, Ph.D. Dissertation, University of Naples Federico II, Italy.
- Pegon P., A. V. Pinto and M. Geradin, 2001, "Numerical Modelling of Stone-Block Monumental Structures", *Computer and Structures*, Vol. 79, No. 22, pp. 2165-2181.
- Pekgökgöz, R. K., M. A. Gürel, Z. Mammadov and F. Çili, 2013, "Dynamic Analysis of Vertically Post-Tensioned Masonry Minarets", *Journal of Earthquake Engineering*, Vol. 17, No. 4, pp. 560-589.
- Peña, F., P. B. Lourenço, N. Mendes and D. V. Oliveira, 2010, "Numerical Models for the Seismic Assessment of an Old Masonry Tower", *Engineering Structures*, Vol. 32, No. 5, pp. 1466-1478.
- Penna, A., M. Rota, A. Mouyiannou and G. Magenes, 2013, "Issues on the Use of Time-History Analysis for the Design and Assessment of Masonry Structures", *Proceedings of the COMPDYN 2013 Fourth ECCOMAS Thematic Conference on Computational Methods in Structural Dynamics and Earthquake Engineering*, 12-14 June 2013, Kos Island, Greece.
- Petrova, Y. A., I. V. Tsimbal, T. V. Laska and S. V. Golubkov, 2011, "Practice of Using Virtual Reconstruction in the Restoration of Monumental Painting of the Church of the Transfiguration of Our Saviour on Neredita Hill", *Proceedings of the Fifteenth International Conference on Information Visualization*, 13-15 July, pp. 389-394 London.
- Pietruszczak, S. and R. Ushaksaraei, 2003, "Description of Inelastic Behavior of Structural Masonry", *International Journal of Solids and Structures*, Vol. 40, pp. 4003-4019.
- Pineda, P., M. D. Robador and M. A. Gil-Martí, 2011, "Seismic Damage Propagation Prediction in Ancient Masonry Structures: an Application in the Non-Linear Range via Numerical Models", *The Open Construction and Building Technology Journal*, Vol. 5, No. 1, pp. 71-79.

- Pohle, F. and W. Jager, 2003, "Material Properties of Historical Masonry of the Frauenkirche and the Masonry Guideline for Reconstruction." *Construction and Building Materials*, Vol. 17, No. 8, pp. 651–667.
- Portioli, F., O. Mammana, R. Landolfo, F. M. Mazzolani, L. Krstevska, L. A. Tashkov and K. Gramatikov, 2011, "Seismic Retrofitting of Mustafa Pasha Mosque in Skopje: Finite Element Analysis", *Journal of Earthquake Engineering*, Vol. 15, No.4, pp. 620-639.
- Quiroz, A.P., 2011, *Seismic Vulnerability Reduction of Historical Masonry Towers by External Prestressing Devices*, Ph.D. Dissertation, Department of Architecture, Civil Engineering and Environmental Sciences University of Braunschweig – Institute of Technology and the Faculty of Engineering University of Florence.
- Raffaele, S., B. Adriana, L. Giovanni and P. Rocco, 2010, "Masonry Structure Diagnostics Via a Microwave Tomographic Approach", *Proceedings of the EGU General Assembly 2010*, Vienna, 2-7 May, pp. 14664, Austria.
- Rezaifar, O., M. Z. Kabir and A. Bakhshi, 2009, "Shaking Table Test of a 1:2.35 Scale 4-Story Building Constructed with a 3D Panel System", *Transaction A: Civil Engineering*, Vol. 16, No. 3, pp. 199.
- Ricamato M., 2007, *Numerical and Experimental Analysis of Masonry Arches Strengthened with FRP Materials*, Ph.D. Dissertation, University of Cassino, Cassino.
- Romano, A., 2005, *Modelling, Analysis and Testing of Masonry Structures*, Ph.D. Dissertation, University of Naples Federico II, Italy.
- Romaro, F., 2011, *A Study on Seismic Behavior of Masonry Towers*, Ph.D. Dissertation, University of Trento, Italy.

- Rossi, C., P. P. Rossi and E. Vio, 1996, "Monitoring system of St. Mark's Basilica in Venice. Analysis and interpretation of the data", *Proceedings of the International Conference*, October, Napoli, Italy.
- Rots, J.G., 1997, *Structural Masonry: An Experimental/ Numerical Basis for Practical Design Rules*, AA Taylor and Francis, 1.
- Russo, G., O. Bergamo, L. Damiani and D. Lugato, 2010, "Experimental Analysis of the Saint Andrea" Masonry Bell Tower in Venice. A New Method for the Determination of "Tower Global Young's Modulus E ", *Engineering Structures*, Vol. 32, No. 2, pp. 353-360.
- Sabnis, G. M., H. G. Harris and R. N. White, 1983, *Structural Modeling and Experimental Techniques*, Prentice-Hall, Inc., Englewood Cliffs, N.J.
- Sadri, A., 2003, "Application of Impact-Echo Technique in Diagnoses and Repair of Stone Masonry Structures", *NDT&E International*, Vol. 36, No. 4, pp. 195–202.
- Salmanpour, A., N. Mojsilović and J. Schwartz, 2013, "Experimental Study of the Deformation Capacity of Structural Masonry", *Proceedings of the Twelfth Canadian Masonry Symposium*, Vancouver, British June 2-5, Columbia.
- Salonikios T., C. Karakostas, V. Lekidis and A. Anthoine, 2003, "Comparative Inelastic Pushover Analysis of Masonry Frames", *Engineering structures*, Vol. 25, No. 12, pp.1515-1523.
- Sandoval, C., P. Roca, E. Bernat and L. Gil, 2011, "Testing and Numerical Modelling of Buckling Failure of Masonry Walls", *Construction and Building Materials*, Vol. 25, No. 12, pp. 4394–4402.
- Sansalone, M. J. and W. B. Streett, 1997, *Impact Echo, Non Destructive Evaluation of Concrete and Masonry*, Bulbrier Press, Ithaca, NY.

- Schriever W. R., 1980, "Full-scale Load Testing of Structures", *Proceedings of a Symposium, ASTM International*.
- Sedov, L. I., 1959, *Similarity and Dimensional Methods in Mechanics*, Academic Press, New York.
- Sezen, H., G. Y. Firat and M. A. Sözen, 2003, "Investigation of the Performance of Monumental Structures During the 1999 Kocaeli and Düzce Earthquakes", *Proceedings of the Fifth National Conference on Earthquake Engineering*, AE-020, Istanbul.
- Sezen, H., R. Acar, A. Doğangün and R. Livaoglu, 2008, "Dynamic Analysis and Seismic Performance of Reinforced Concrete Minarets", *Engineering Structures*, Vol. 30, No. 8, pp. 2253-2264.
- Sezen, H. and A. Doğangün, 2012, *Seismic Performance of Historical and Monumental Structures*, Earthquake Engineering, Prof. Halil Sezen (Ed.), ISBN: 978-953-51-0694-4, InTech, DOI: 10.5772/51338.
- Shing P. B. and S. A. Mahin, 1985, "Computational Aspects of a Seismic Performance Test Method Using On-Line Computer Control", *Earthquake Engineering and Structural Dynamics*, Vol. 13, No. 4, pp. 507-526.
- Sinha, B.P., 1978, "Simplified Ultimate Load Analysis of Laterally Loaded Model Orthotropic Brick Work Panels of Low Tensile Strength", *Structural Engineering*, Vol. 56B, No. 4, pp. 81-84.
- Solla, M., H. Lorenzo, F. I. Rial and A. Novo, 2012, "Ground-Penetrating Radar for the Structural Evaluation of Masonry Bridges: Results and Interpretational Tools", *Construction and Building Materials*, Vol. 29, pp. 458–465.

- Solla, M., H. Lorenzo, B. Riveiro and F. I. Rial, 2011, "Non-Destructive Methodologies in the Assessment of the Masonry Arch Bridge of Traba, Spain", *Engineering Failure Analysis*, Vol. 18, No. 3, pp. 828–835.
- Solla, M., B. Riveiro, H. Lorenzo and J. Armesto, 2014, "Ancient Stone Bridge Surveying by Ground-Penetrating Radar and Numerical Modeling Methods." *Journal of Bridge Engineering*, Vol.19, No.1, pp. 110–119.
- Spada A, G. Giambanco and P. Rizzo, 2009, "Damage and Plasticity at the Interfaces in Composite Materials and Structures", *Computer Methods in Applied Mechanics and Engineering*, Vol. 198, No. 49-52, pp. 3884–901.
- Sugo, H.O., A. W. Page and S. J. Lawrence, 1996, "Influence of the Macro and Micro Constituents of air Entrained Mortars on Masonry Bond Strength", *Proceedings of the Seventh North American Masonry Conference*, Notre Dame, Indiana. Vol. 1, pp. 230-241.
- Sulaeman, A., 2010, *The Use of Lightweight Concrete Piles For Deep Foundation on Soft Soils*, Ph.D. Dissertation, Faculty of Civil and Environmental Engineering University Tun Hussein Onn Malaysia.
- Sutcliffe D.J., H. S. Yu and A. W. Page, 2001, "Lower Bound Limit Analysis of Unreinforced Masonry Shear Walls", *Computers and Structures*, Vol. 79, No. 14, pp. 1295-1312.
- Syrmankezis C.A. and P. G. Asteris, 2001, "Masonry Failure Criterion under Biaxial Stress State", *Journal of Materials in Civil Engineering*, Vol. 13, No. 1, pp. 58-64.
- Şen, B., 2006, *Modeling and Analysis of the Historical Masonry Structures*, M.S. Thesis, Boğaziçi University, Istanbul, Turkey.
- Tabeshpour, M.R., 2012, "Nonlinear Dynamic Analysis of Chimney-Like Towers" *Asian Journal of Civil Engineering (Building and Housing)*, Vol. 13, No. 1, pp. 97-112.

- Takanashi, T., 1974, "Seismic Failure Analysis of Structures by Computer-pulsator on-line System", *Bulletin of Earthquake Resistant Structure Research Center*, University of Tokyo, Vol. 26, No. 11, pp. 13-25.
- Takanashi K. and M. Nakashima, 1987, "Japanese Activities on On-line Testing", *ASCE Journal of Engineering Mechanics*, Vol. 113, No. 7, pp. 1014-1031.
- Tan, X. J. and B. Wu, 2011, "Substructure Pseudo-Dynamic Testing of a Full-Scale Confined Masonry Building", *Advanced Materials Research*, Vol. 250, pp. 2566-2570
- Tashkov, L.A., L. S. Krstevska, E. Şafak, E. Çaktı, A. Edinçliler and M. Erdik, 2012, "Comparative Study of Large and Medium Scale Mosque Models Tested on Seismic Shaking Table" *Proceedings of the Fifteenth World Conference on Earthquake Engineering*, Lisbon, Portugal.
- Tahskov, L. A., 2012, *Personal Communication*, University of Ss. Cyril and Methodius, Skopje.
- Tavukçuoğlu, A., S. Akevren and E. Grinzato, 2010, "In Situ Examination of Structural Cracks at Historic Masonry Structures by Quantitative Infrared Thermography and Ultrasonic Testing", *Journal of Modern Optics*, Vol. 57, No. 18, pp. 1779-1789.
- Theodossopoulos, D. and B. Sinha, 2013, "A Review of Analytical Methods in the Current Design Processes and Assessment of Performance of Masonry Structures", *Construction and Building Materials*, Vol. 41, pp. 990–1001.
- Tomazevic, M. and M. Gams, 2012, "Shaking Table Study and Modeling of Seismic Behavior of Confined AAC Masonry Buildings", *Bulletin of Earthquake Engineering*, Vol. 10, No. 3, pp. 863–893.
- Tomzevic, M., 2000, *Shaking Table Tests of Small-Scale Model of Masonry Building: Advantages and Disadvantages*, Munchner Massivbau-Seminar.

- Trujillo Leon F. R., 2007, *Seismic Response and Rehabilitation of Historic Masonry Buildings*, M.S. Thesis, University of Sheffield, Dept. of Civil Structural Engineering.
- Türk, A. M. and C. Coşgun, 2010, “The Determination of Seismic Behavior and Retrofit of Historical Masonry Minaret with FRP”, *Proceedings of the Eight International Masonry Conference*, Vol.148, pp.2029-2038, Dresden.
- Ünay, A., İ., 1997, *A Method for the Evaluation of the Ultimate Safety of Historical Masonry Structures*, Ph.D. Dissertation, METU, Ankara.
- Ünay, A. İ., 2002, *Tarihi Yapıların Depreme Dayanımı*, ODTÜ Mimarlık Fakültesi, Ankara.
- Vinzileou, E., A. R. Skoura, G. Plesu, D. Taranu, I. D. Covatariu and U. Gradinari, 2011, “Strengthening and Rehabilitation Conventional Methods for Masonry Structures”, *Bulletin of the Polytechnic Institute of Iasi*, Vol. 61, No. 4, pp. 165-176.
- Wei, H., H. Minggang and H. Qun, 1999, “Quasi-Static Testing of Composite Masonry Construction”, *Building Research And Information*, Vol. 27, No. 2, pp. 120–123.
- Wu, C., H. Hao and Y. Lu, 2005, “Dynamic Response and Damage Analysis of Masonry Structures and Masonry Infilled RC Frames to Blast Ground Motion.” *Engineering Structures*, Vol. 27, No. 3, pp. 323–333.
- Xianguo, Y., J. Jiaru and L. Kangning, 2004, “Shaking Table Test and Dynamic Response Prediction on an Earthquake-Damaged RC Building”, *Earthquake Engineering and Engineering Vibration*, Vol.3, No.2, pp. 205-214.
- Yang, G., 2010, *Dynamic Analyses of a Masonry Building Tested in a Shaking Table*, M.S. Thesis, University of Minho, Portugal.

- Yükçü, S., L. D. Y. İçerli and L. C. Yükçü, 2007, "Construction of Süleymaniye Mosque In Istanbul and Cost Accounting (1550-1557)", *Proceedings of the Balkan Countries 1st International Conference on Accounting and Auditing*, 8-9 March, Edirne.
- Zhang, M., 1997, "Study on Similitude Laws for Shaking Table Test," *Earthquake Engineering and Engineering Vibration*, Vol. 17, No. 2, pp. 52-58.
- Zhuge, Y., D. Thambiratnam and J. Corderoy, 1998, "Nonlinear Dynamic Analysis of Unreinforced Masonry", *Journal of Structural Engineering*, Vol. 124, No. 3, pp. 270-277.

## **APPENDIX A: COMPARISON WITH EXPERIMENTAL DATA AND DISTINCT ELEMENT MODEL**

In this appendix, comparisons of experimental and analytical velocities and Fourier amplitude spectra along the minaret and on the body of the model are presented. The comparisons are provided for 10%, 30%, 50%, 70%, 100%, 130%, 150%, 160%, 220% and 250% Montenegro. In Figure A1 measurement locations on the minaret of the shake table model and corresponding points on the numerical model are shown. In Figure A2 measurement locations on the body of the shake table model and corresponding points on the numerical model are indicated. Comparisons for the minaret are presented in Figures A3 – A.22. Comparisons for the body can be found in Figures A23 – A42.

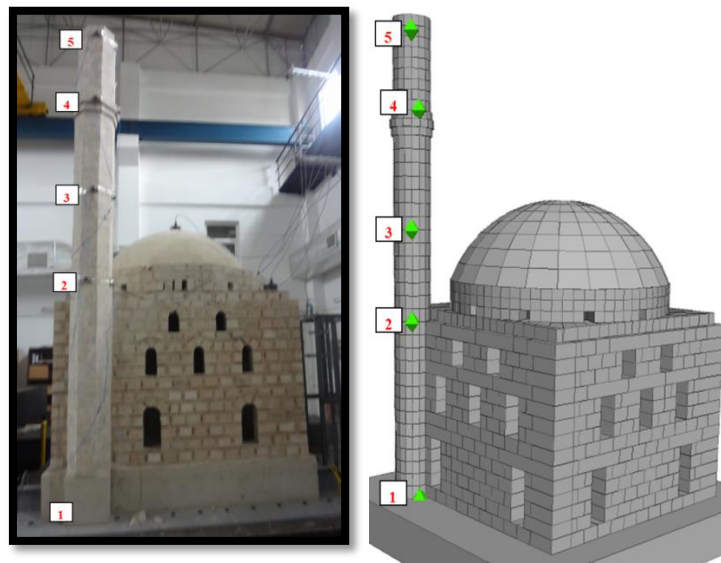


**Figure A1.** Images of measurement locations on the minaret of the shake table model and corresponding points on the numerical model.

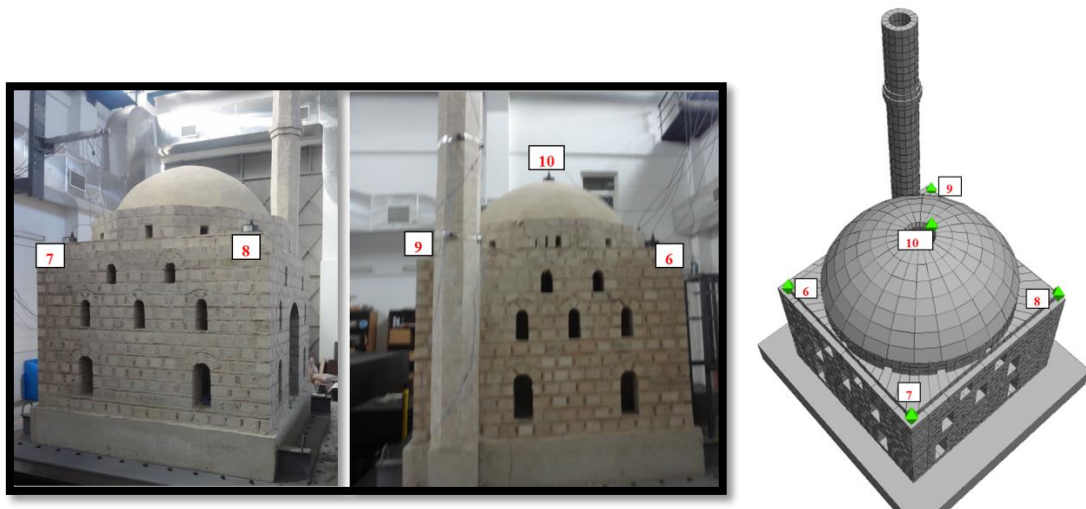


**Figure A2.** Images of measurement locations on the body of the shake table model and corresponding points on the numerical model.

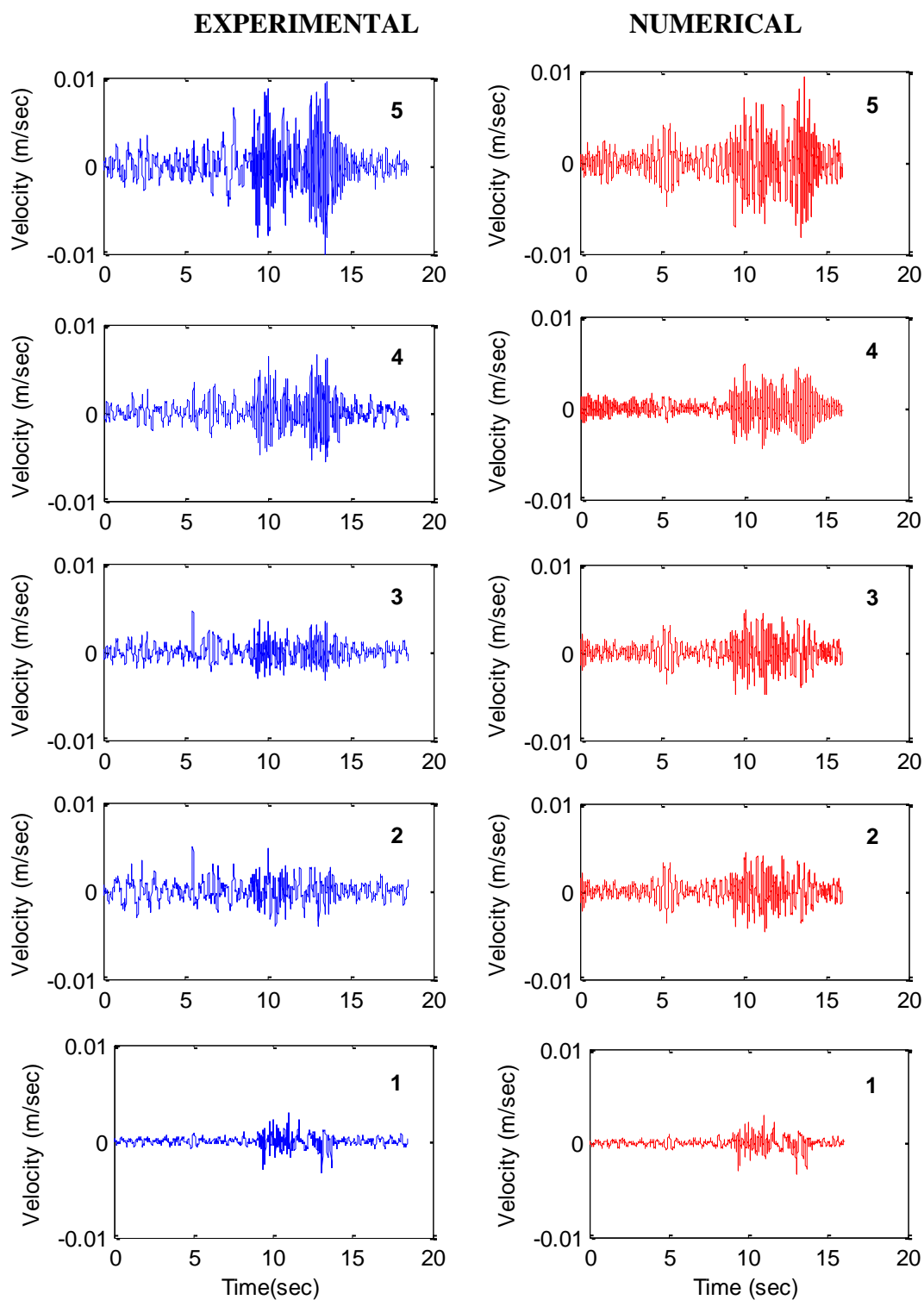


**Figure A3.** Comparisons of experimental and analytical velocities along the minaret under 10% Montenegro earthquake loading. 1, 2, 3, 4, 5 indicate the locations of accelerometers at 0.35m, 1.75m, 2.45m, 3.25m, 3.90m height of the minaret respectively. Refer to Figure A1 for the measurement locations on the minaret and corresponding points on the numerical model.

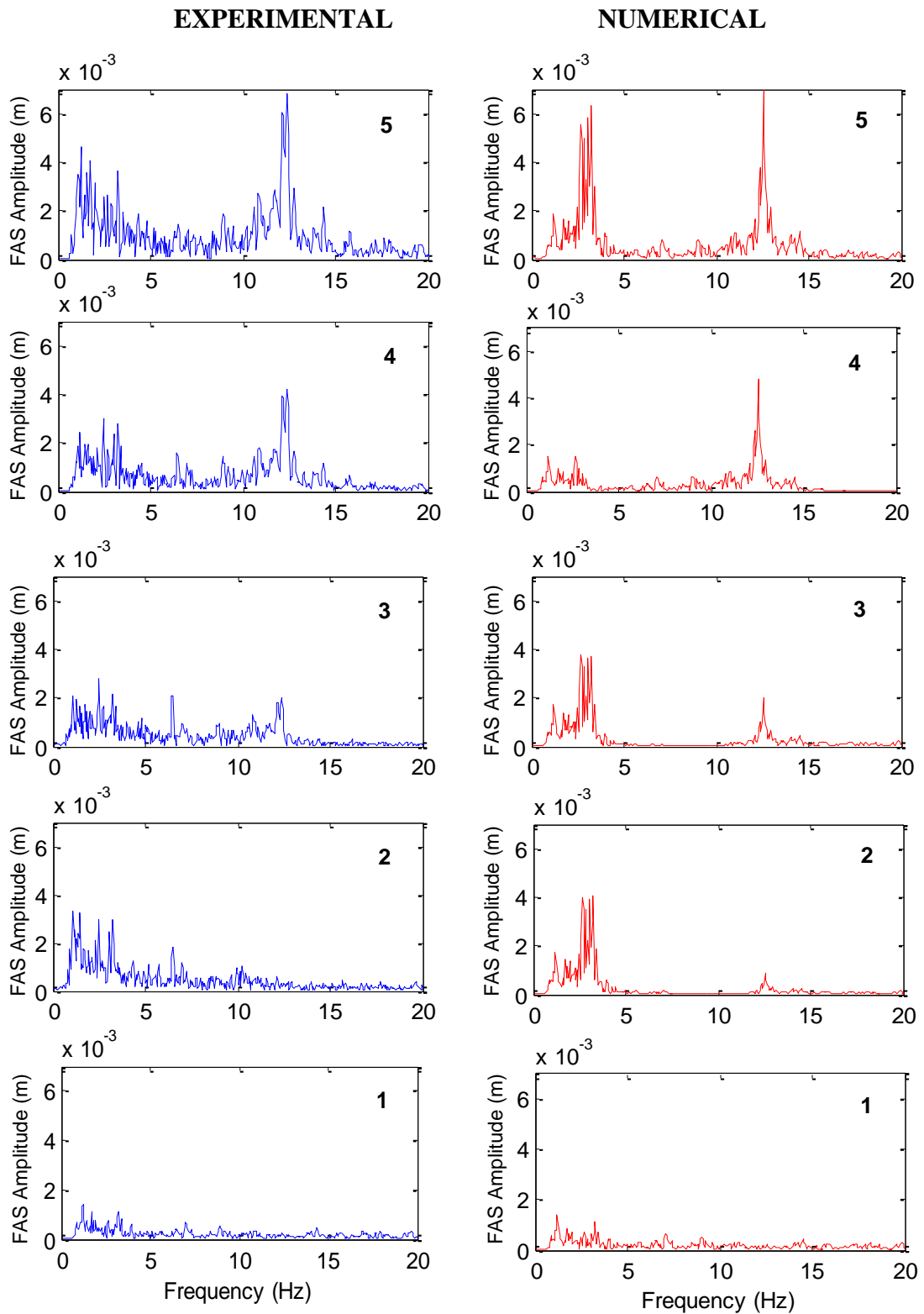


**Figure A4.** Comparisons of experimental and numerical FAS amplitude along the minaret under 10% Montenegro earthquake loading. 1, 2, 3, 4, 5 indicate the measurement locations. Refer to Figure A1 for the measurement locations on the minaret and corresponding points on the numerical model.

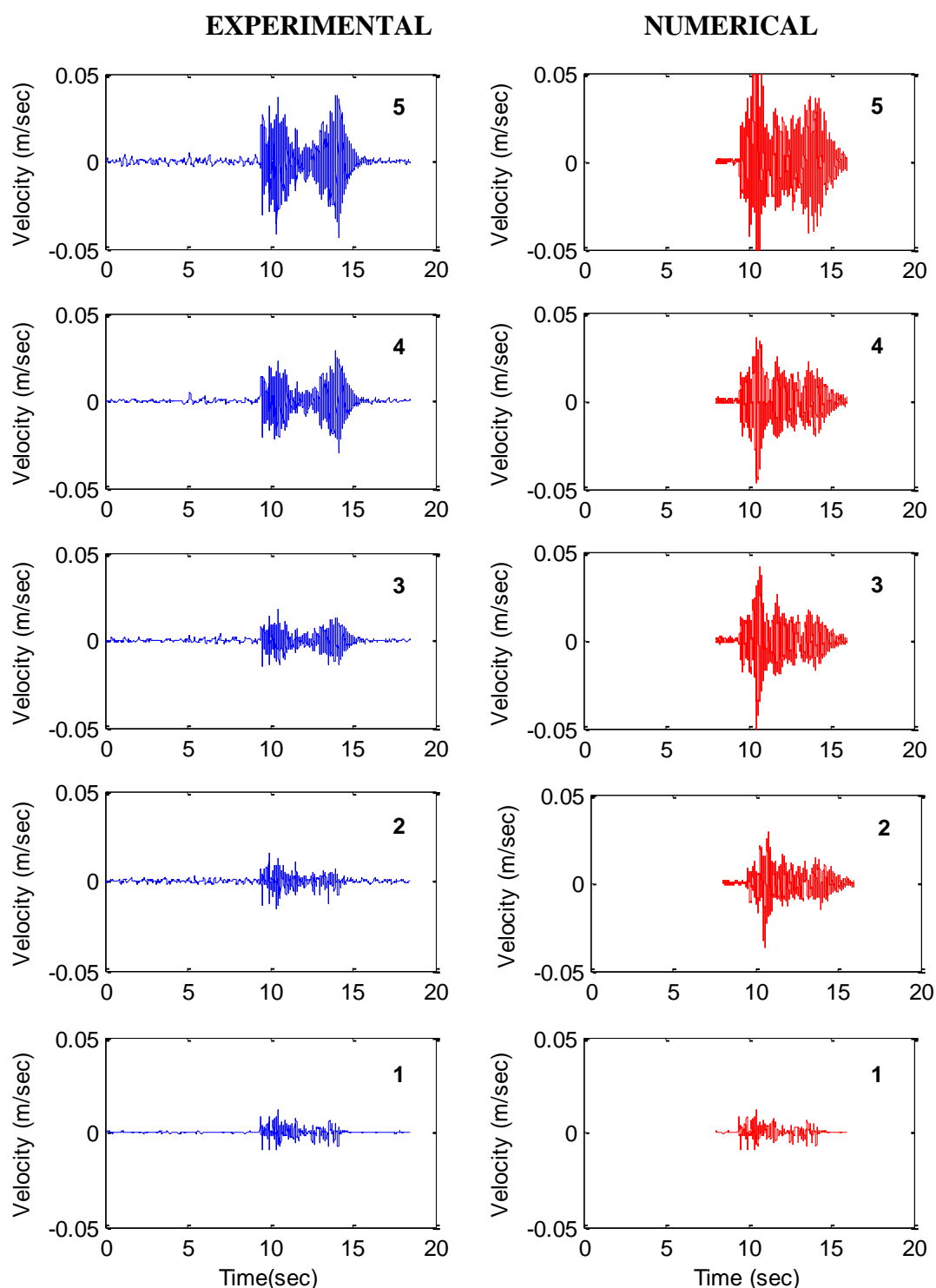


**Figure A5.** Comparisons of experimental and analytical velocities along the minaret under 30% Montenegro earthquake loading. 1, 2, 3, 4, 5 indicate the locations of accelerometers at 0.35m, 1.75m, 2.45m, 3.25m, 3.90m height of the minaret respectively. Refer to Figure A1 for the measurement locations on the minaret and corresponding points on the numerical model.

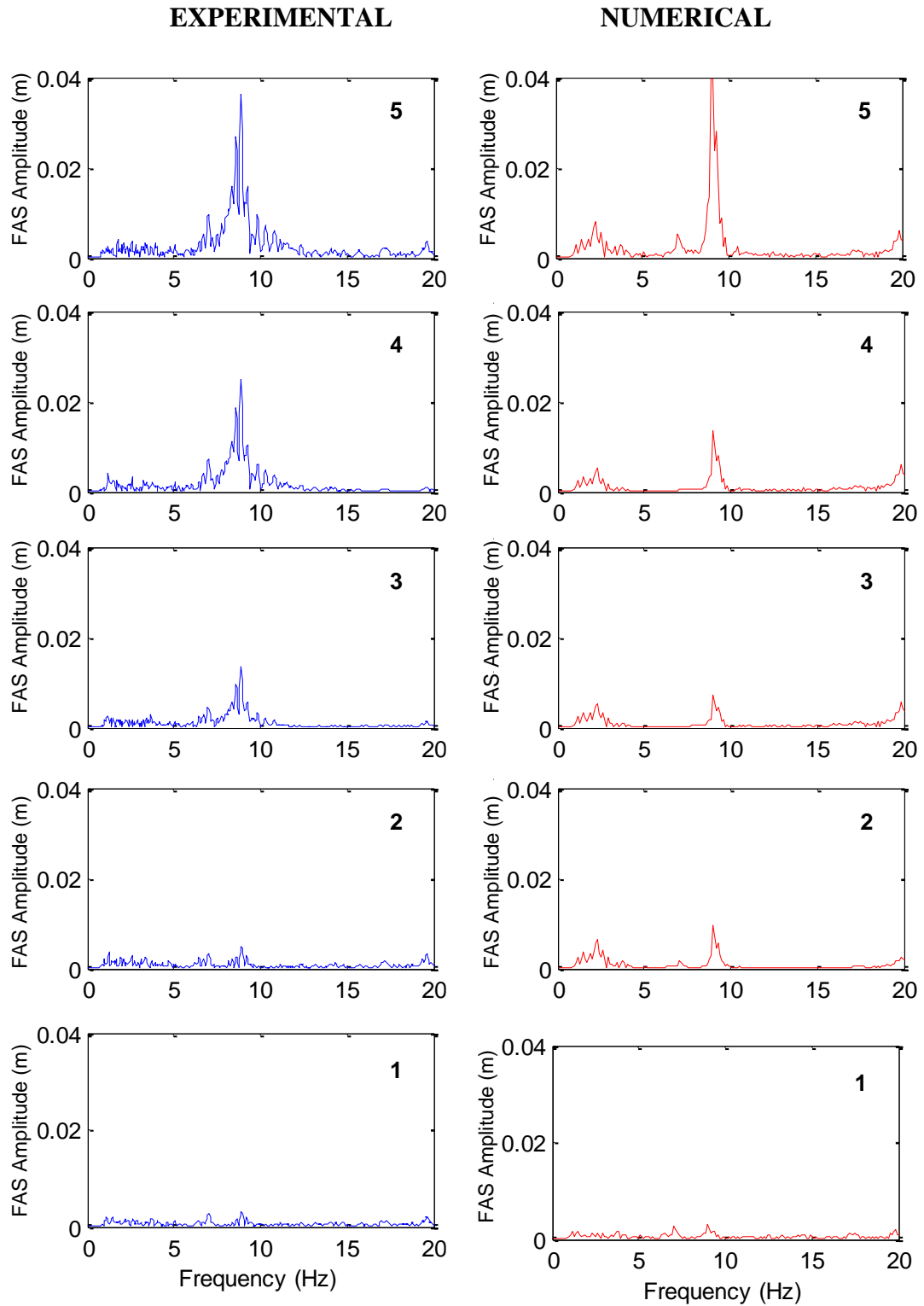


**Figure A6.** Comparisons of experimental and numerical FAS amplitude along the minaret under 30% Montenegro earthquake loading. 1, 2, 3, 4, 5 indicate the measurement locations. Refer to Figure A1 for the measurement locations on the minaret and corresponding points on the numerical model.

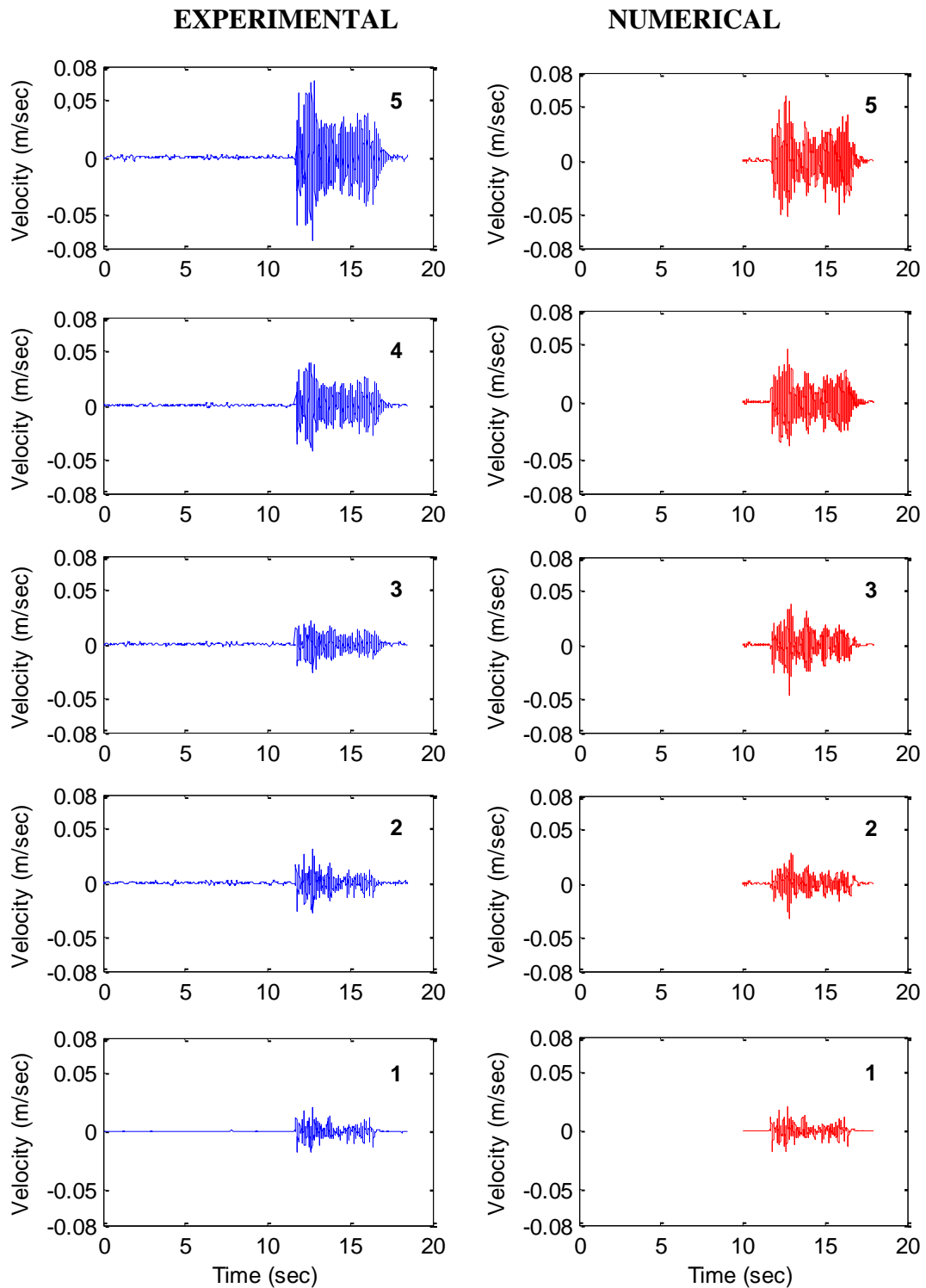


**Figure A7.** Comparisons of experimental and analytical velocities along the minaret under 50% Montenegro earthquake loading. 1, 2, 3, 4, 5 indicate the locations of accelerometers at 0.35m, 1.75m, 2.45m, 3.25m, 3.90m height of the minaret respectively. Refer to Figure A1 for the measurement locations on the minaret and corresponding points on the numerical model.

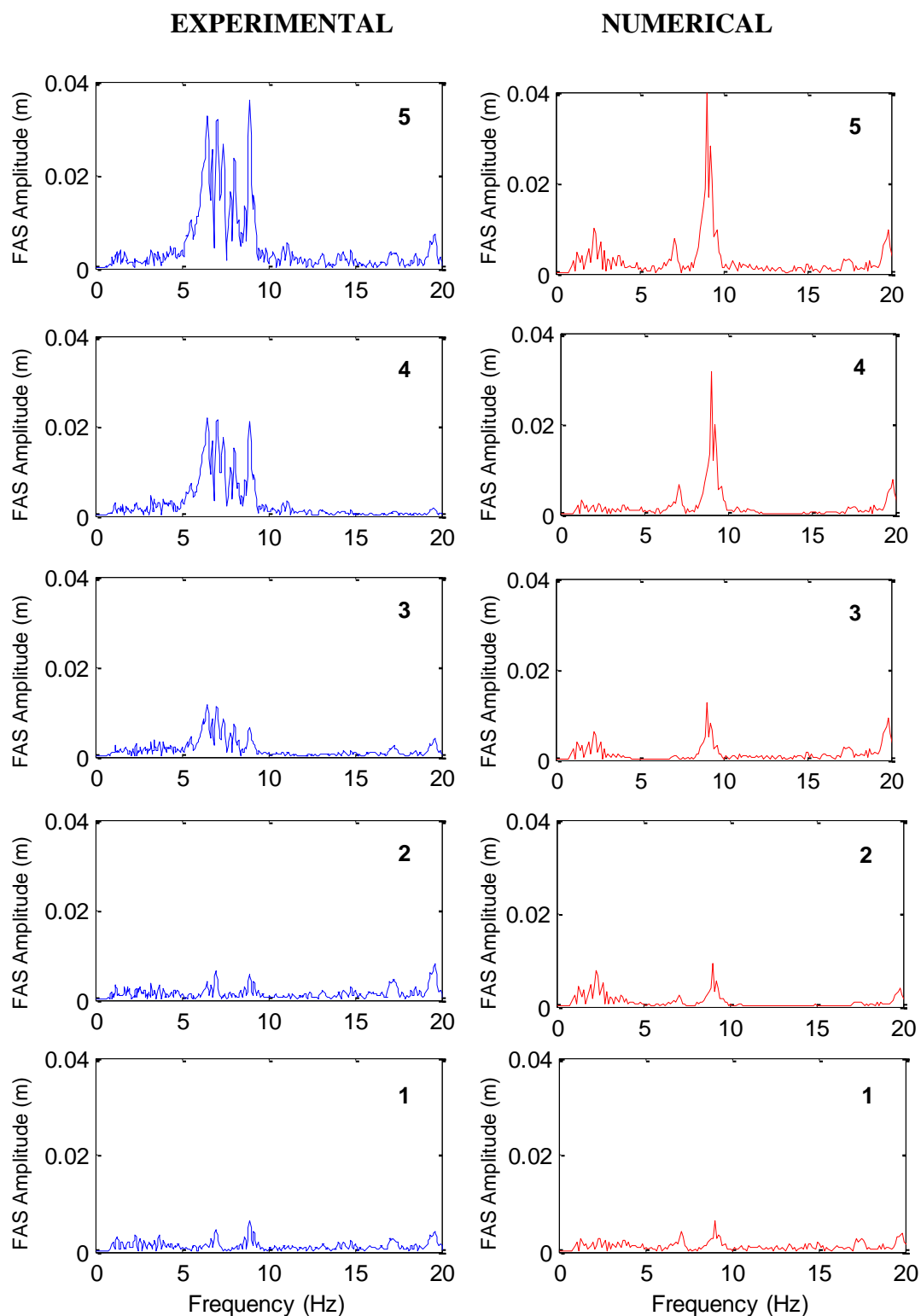


**Figure A8.** Comparisons of experimental and numerical FAS amplitude along the minaret under 50% Montenegro earthquake loading. 1, 2, 3, 4, 5 indicate the measurement locations. Refer to Figure A1 for the measurement locations on the minaret and corresponding points on the numerical model.

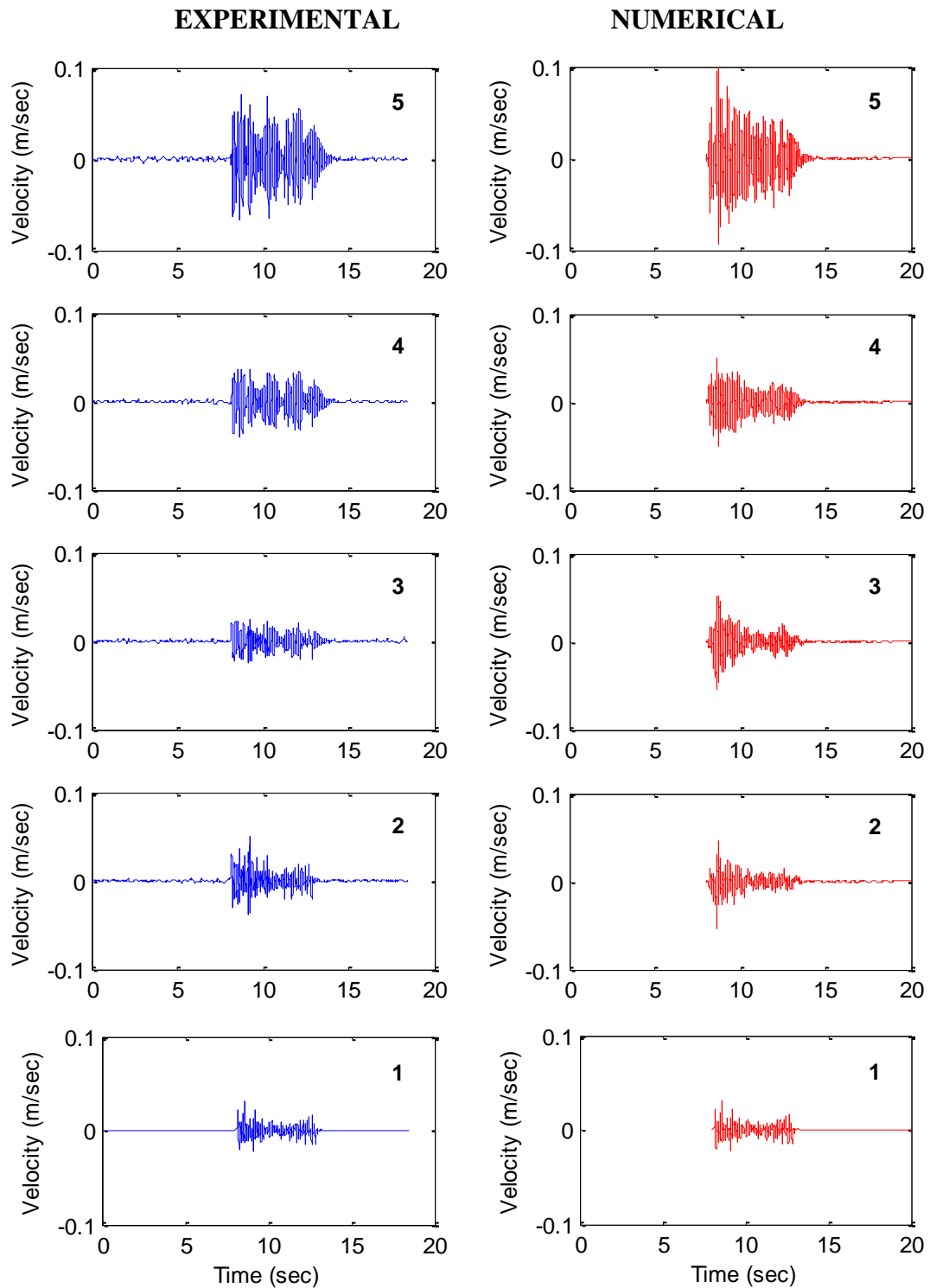


**Figure A9.** Comparisons of experimental and analytical velocities along the minaret under 70% Montenegro earthquake loading. 1, 2, 3, 4, 5 indicate the locations of accelerometers at 0.35m, 1.75m, 2.45m, 3.25m, 3.90m height of the minaret respectively. Refer to Figure A1 for the measurement locations on the minaret and corresponding points on the numerical model.

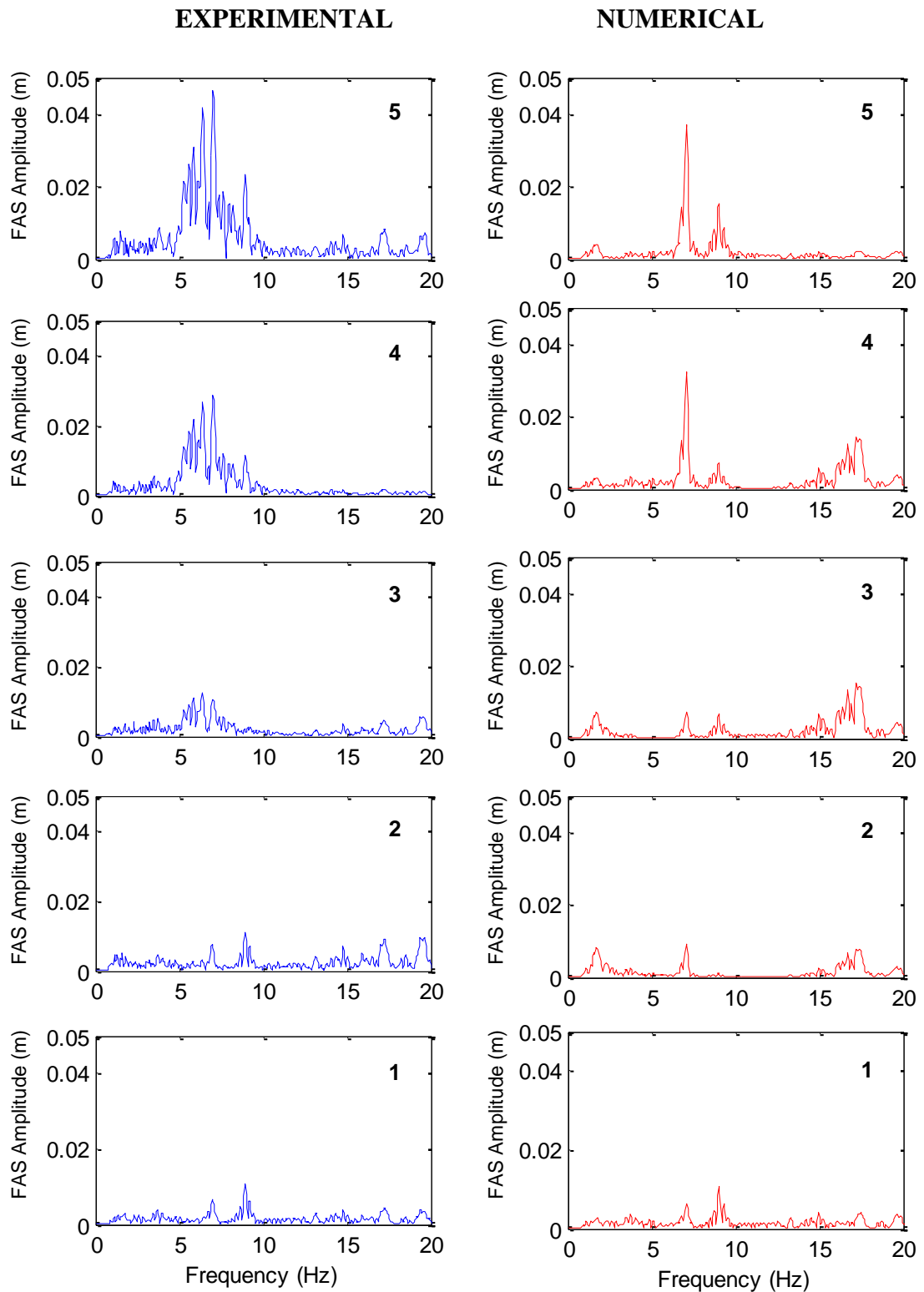


**Figure A10.** Comparisons of experimental and numerical FAS amplitude along the minaret under 70% Montenegro earthquake loading. 1, 2, 3, 4, 5 indicate the measurement locations. Refer to Figure A1 for the measurement locations on the minaret and corresponding points on the numerical model.

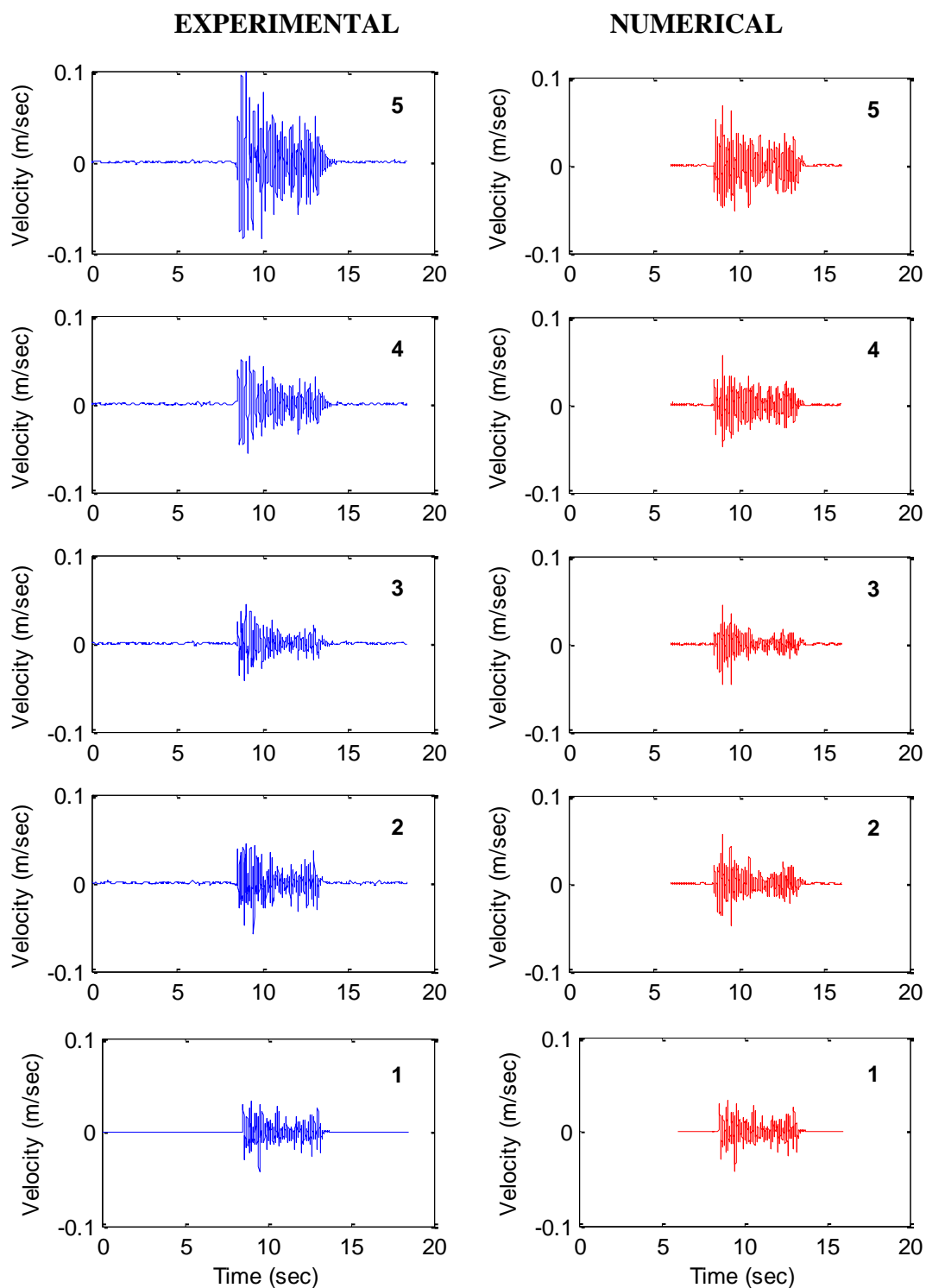


**Figure A11.** Comparisons of experimental and analytical velocities along the minaret under 100% Montenegro earthquake loading. 1, 2, 3, 4, 5 indicate the locations of accelerometers at 0.35m, 1.75m, 2.45m, 3.25m, 3.90m height of the minaret respectively. Refer to Figure A1 for the measurement locations on the minaret and corresponding points on the numerical model.

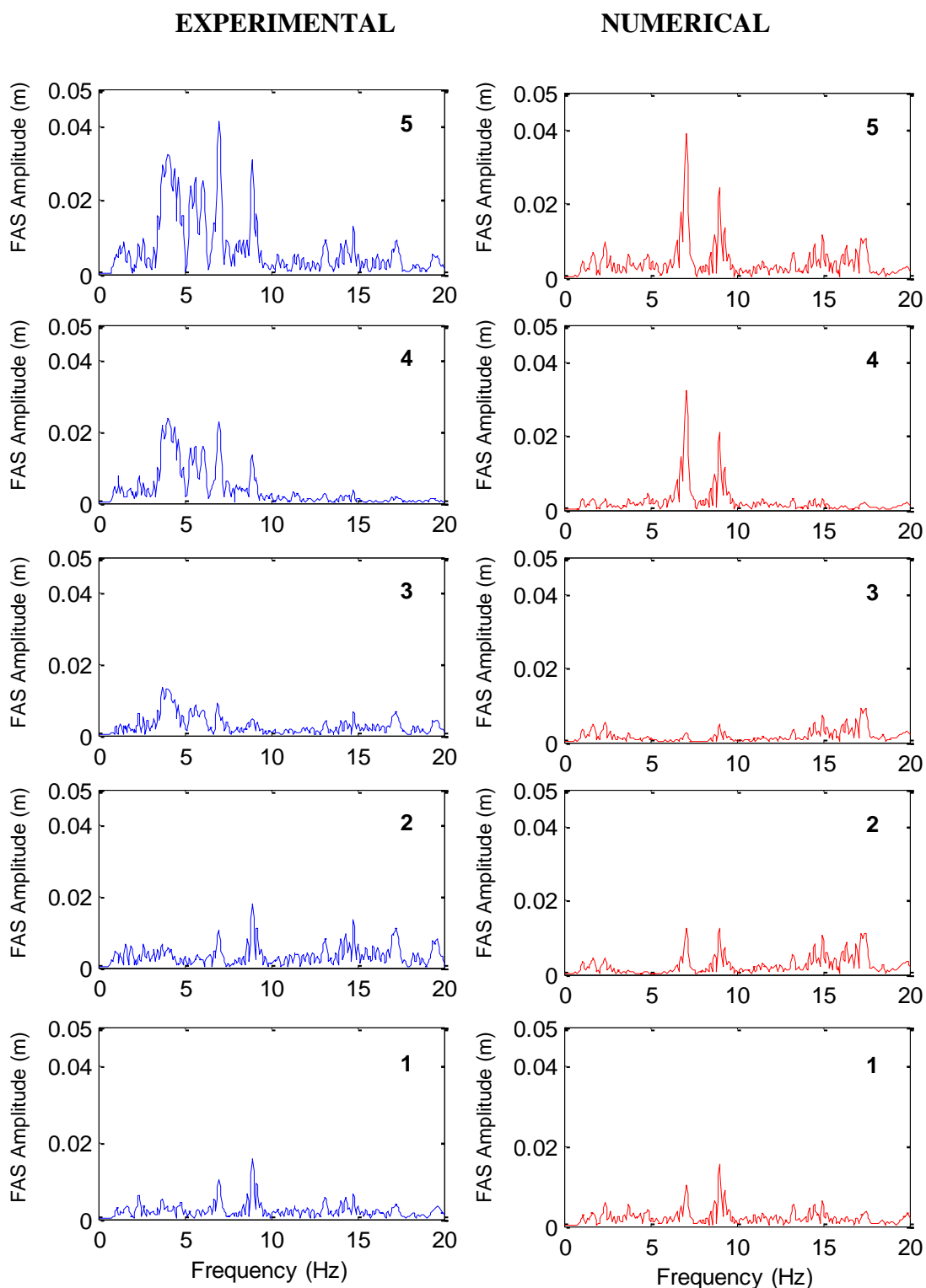


**Figure A12.** Comparisons of experimental and numerical FAS amplitude along the minaret under 100% Montenegro earthquake loading. 1, 2, 3, 4, 5 indicate the measurement locations. Refer to Figure A1 for the measurement locations on the minaret and corresponding points on the numerical model.

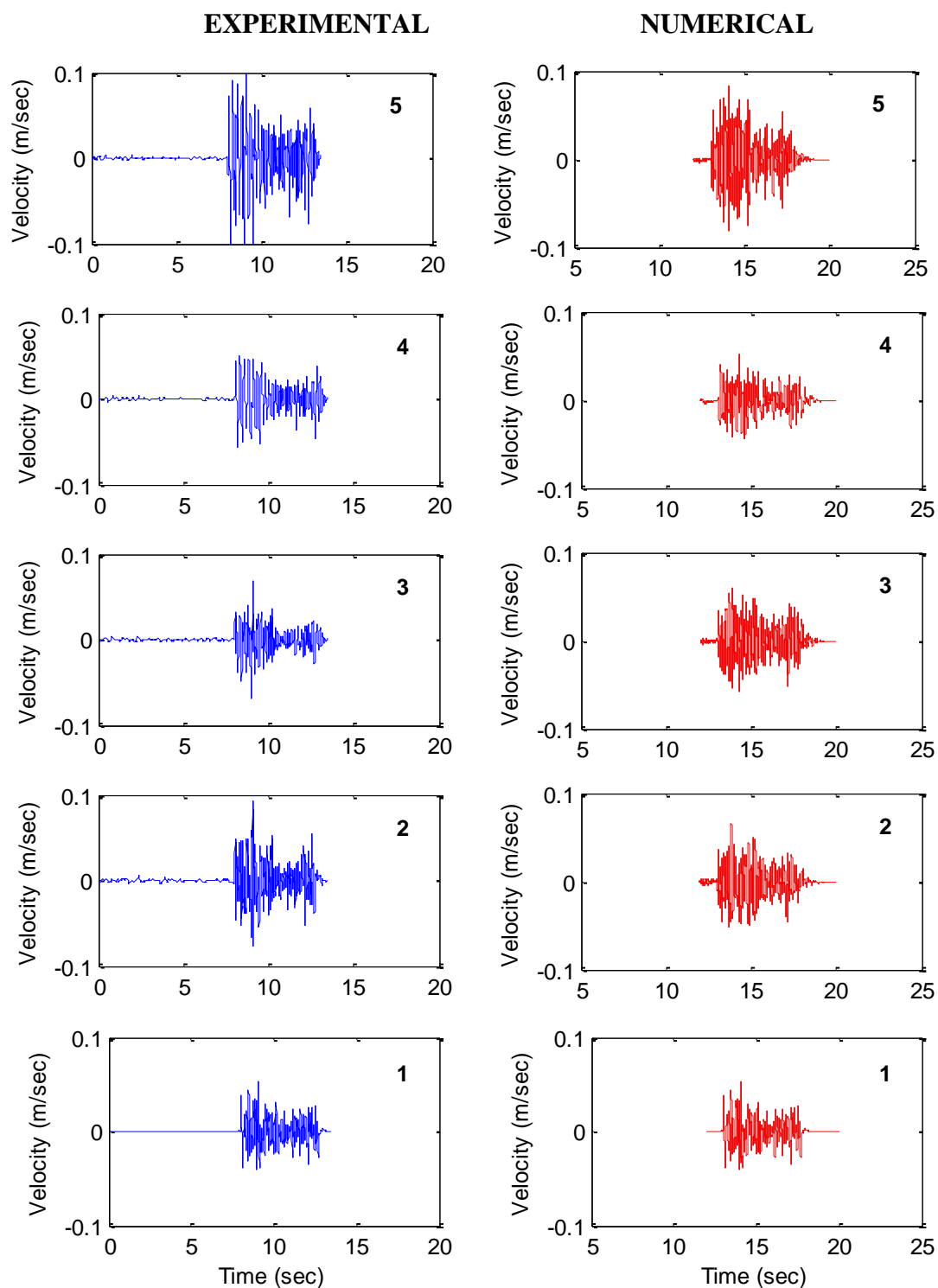


**Figure A13.** Comparisons of experimental and analytical velocities along the minaret under 130% Montenegro earthquake loading. 1, 2, 3, 4, 5 indicate the locations of accelerometers at 0.35m, 1.75m, 2.45m, 3.25m, 3.90m height of the minaret respectively. Refer to Figure A1 for the measurement locations on the minaret and corresponding points on the numerical model.

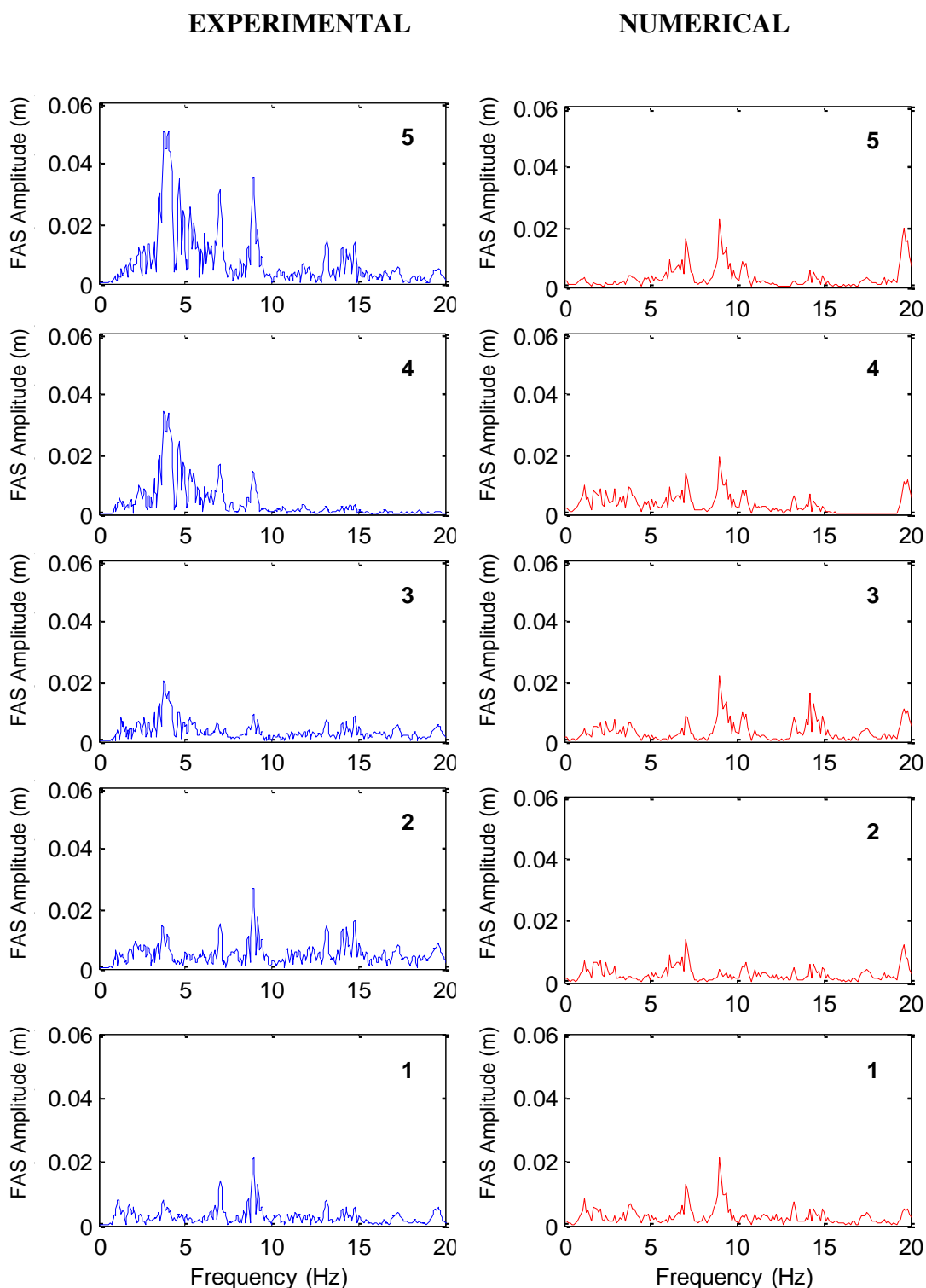


**Figure A14.** Comparisons of experimental and numerical FAS amplitude along the minaret under 130% Montenegro earthquake loading. 1, 2, 3, 4, 5 indicate the measurement locations. Refer to Figure A1 for the measurement locations on the minaret and corresponding points on the numerical model.

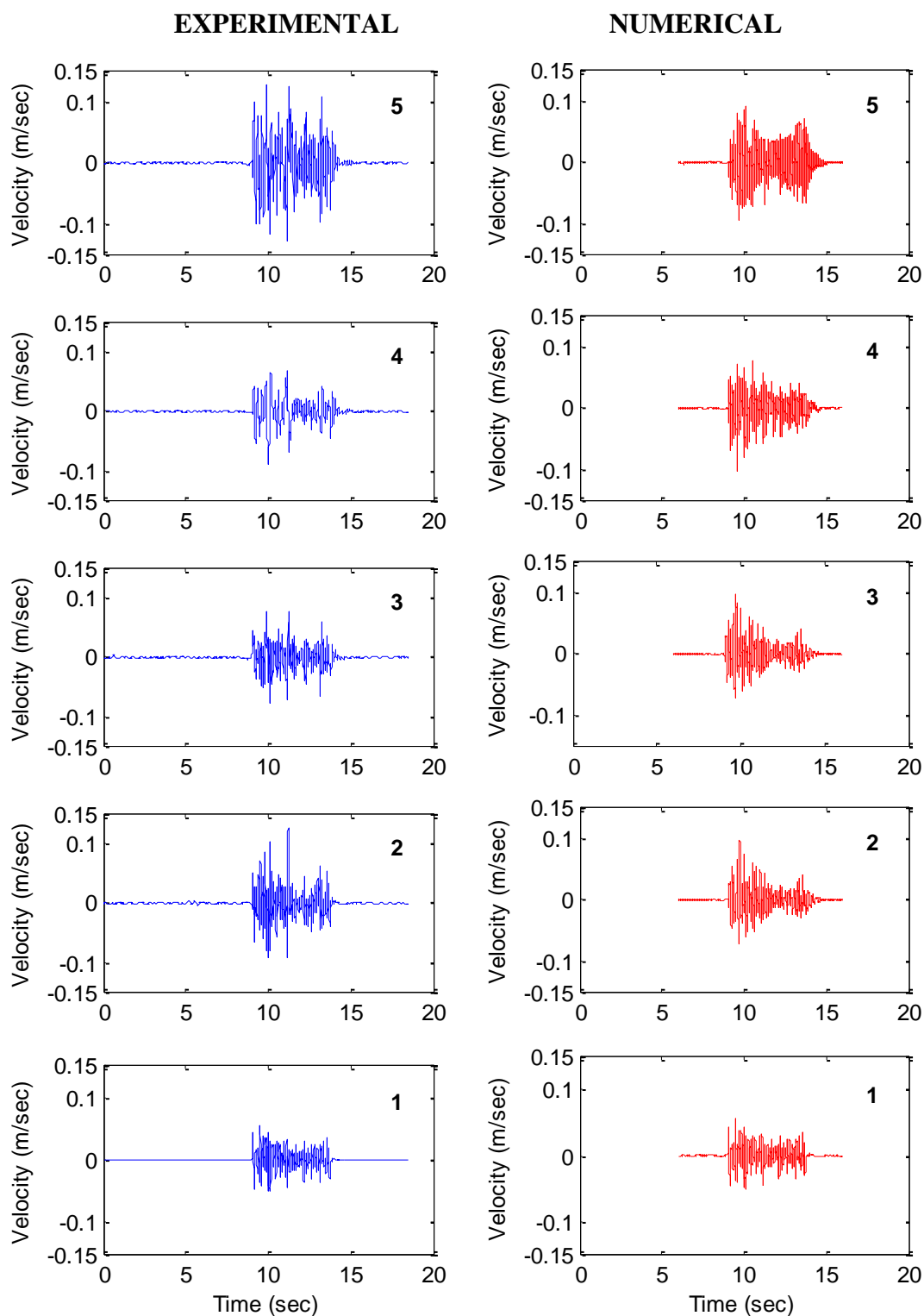


**Figure A15.** Comparisons of experimental and analytical velocities along the minaret under 150% Montenegro earthquake loading. 1, 2, 3, 4, 5 indicate the locations of accelerometers at 0.35m, 1.75m, 2.45m, 3.25m, 3.90m height of the minaret respectively. Refer to Figure A1 for the measurement locations on the minaret and corresponding points on the numerical model.

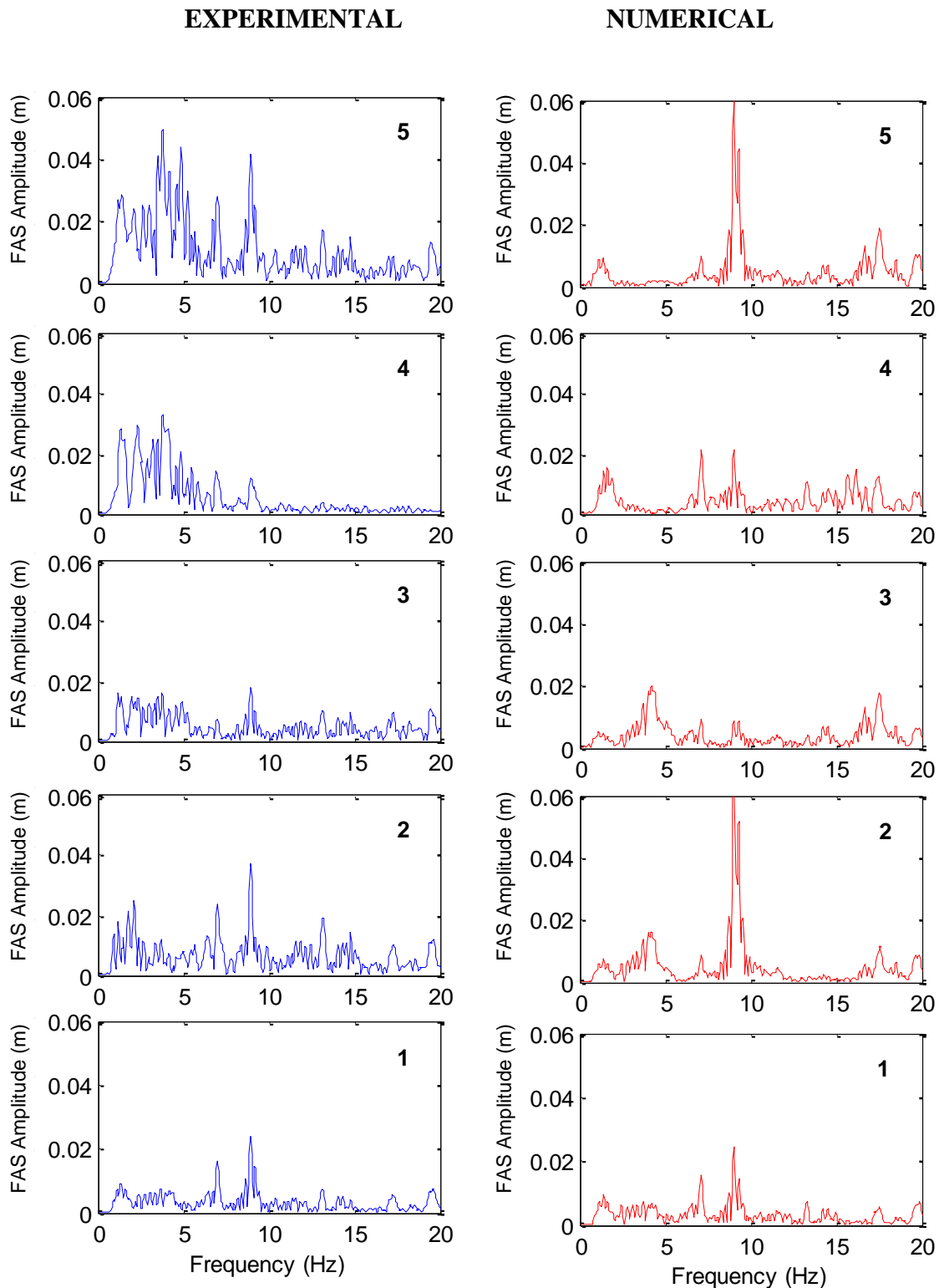


**Figure A16.** Comparisons of experimental and numerical FAS amplitude along the minaret under 150% Montenegro earthquake loading. 1, 2, 3, 4, 5 indicate the measurement locations. Refer to Figure A1 for the measurement locations on the minaret and corresponding points on the numerical model.

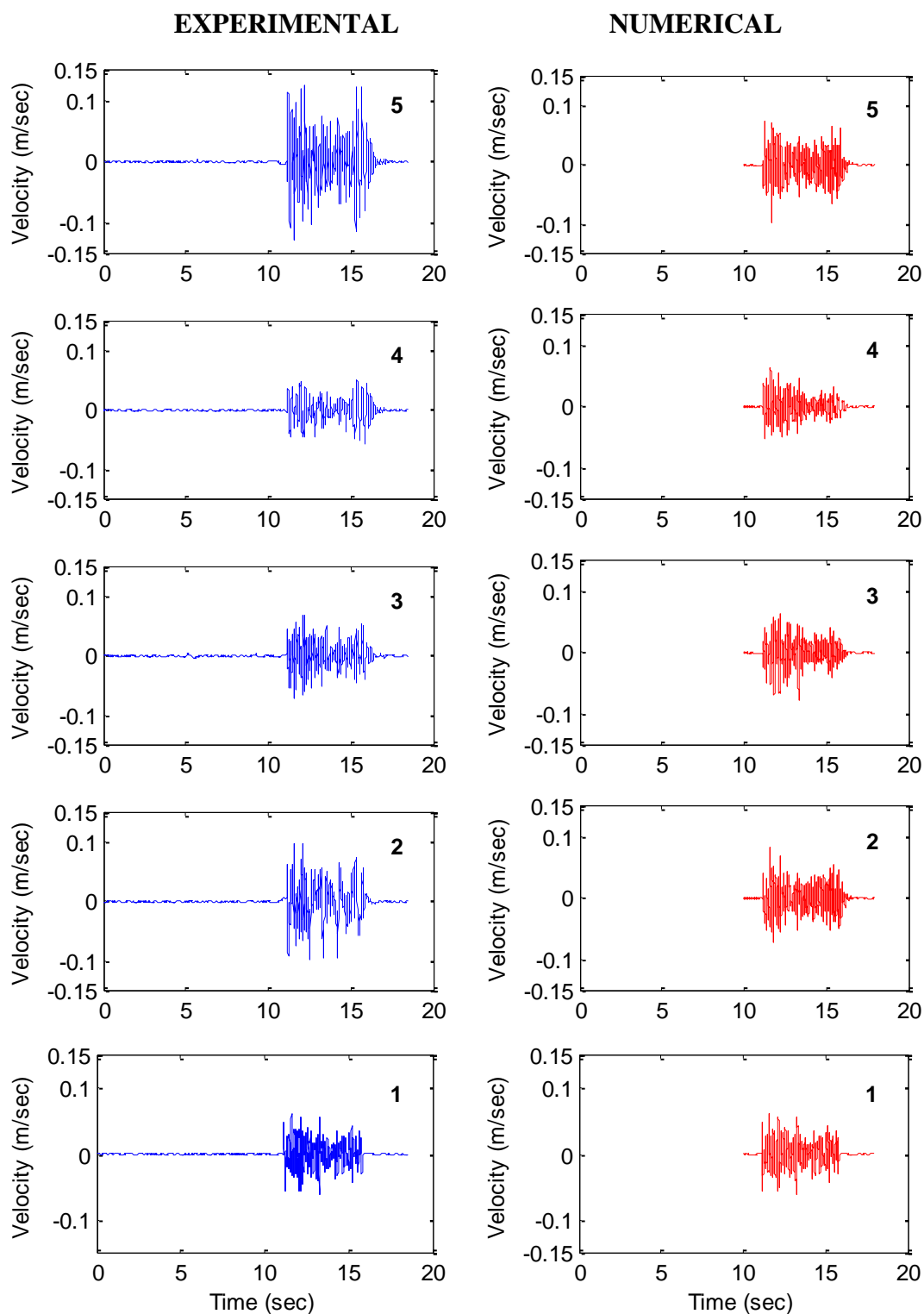


**Figure A17.** Comparisons of experimental and analytical velocities along the minaret under 160% Montenegro earthquake loading. 1, 2, 3, 4, 5 indicate the locations of accelerometers at 0.35m, 1.75m, 2.45m, 3.25m, 3.90m height of the minaret respectively. Refer to Figure A1 for the measurement locations on the minaret and corresponding points on the numerical model.

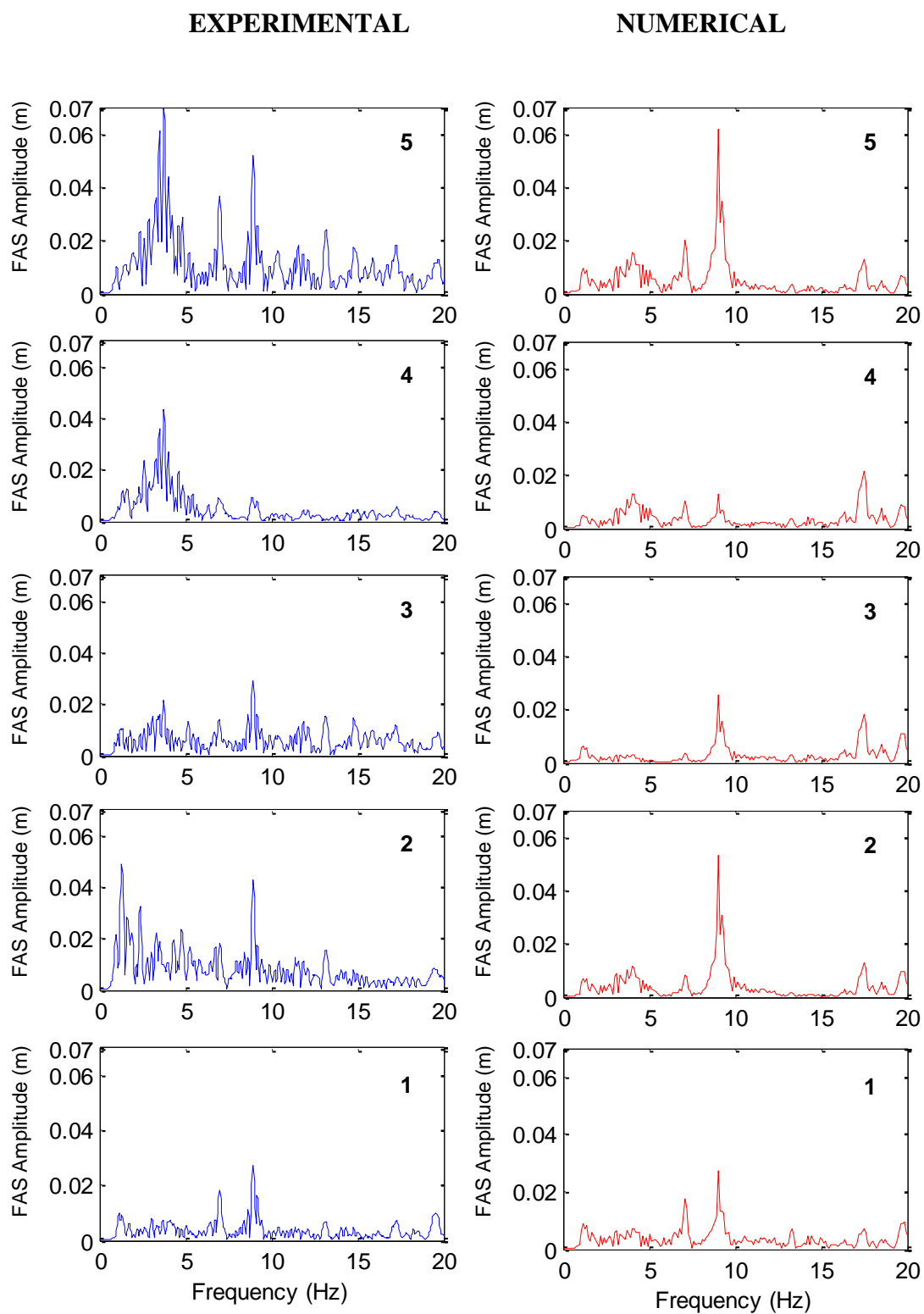


**Figure A18.** Comparisons of experimental and numerical FAS amplitude along the minaret under 160% Montenegro earthquake loading. 1, 2, 3, 4, 5 indicate the measurement locations. Refer to Figure A1 for the measurement locations on the minaret and corresponding points on the numerical model.

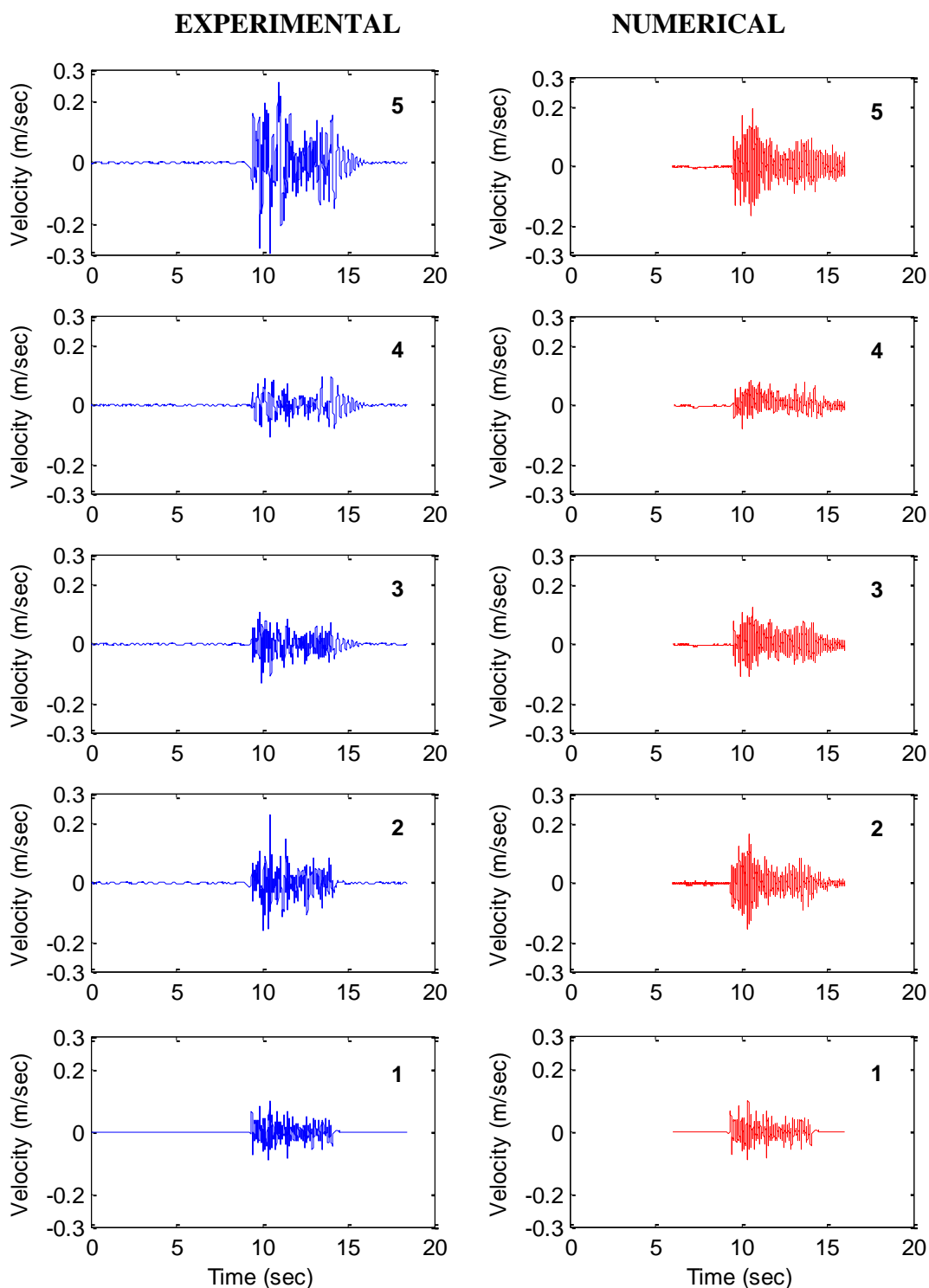


**Figure A19.** Comparisons of experimental and analytical velocities along the minaret under 220% Montenegro earthquake loading. 1, 2, 3, 4, 5 indicate the locations of accelerometers at 0.35m, 1.75m, 2.45m, 3.25m, 3.90m height of the minaret respectively. Refer to Figure A1 for the measurement locations on the minaret and corresponding points on the numerical model.

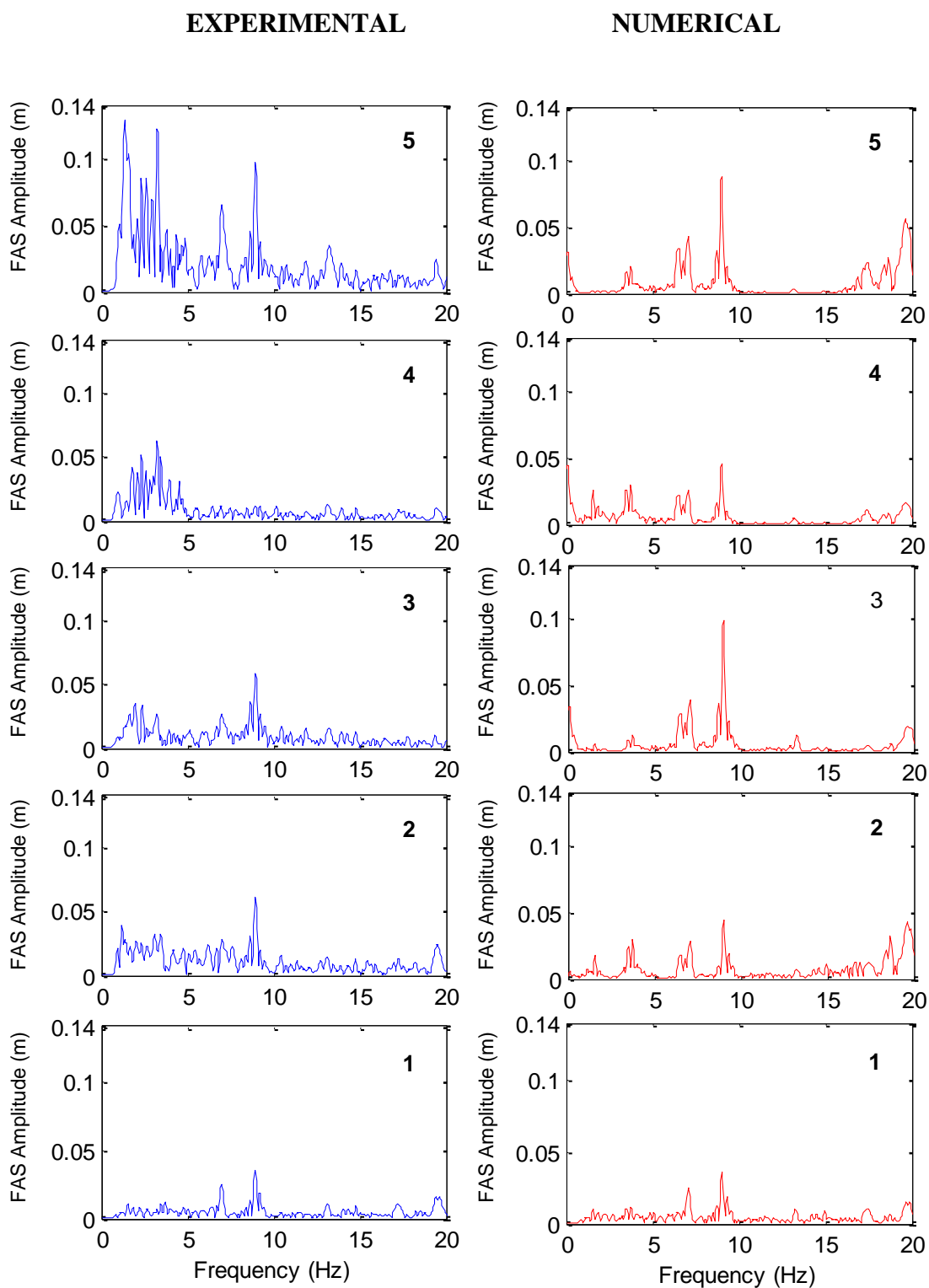


**Figure A20.** Comparisons of experimental and numerical FAS amplitude along the minaret under 220% Montenegro earthquake loading. 1, 2, 3, 4, 5 indicate the measurement locations. Refer to Figure A1 for the measurement locations on the minaret and corresponding points on the numerical model.

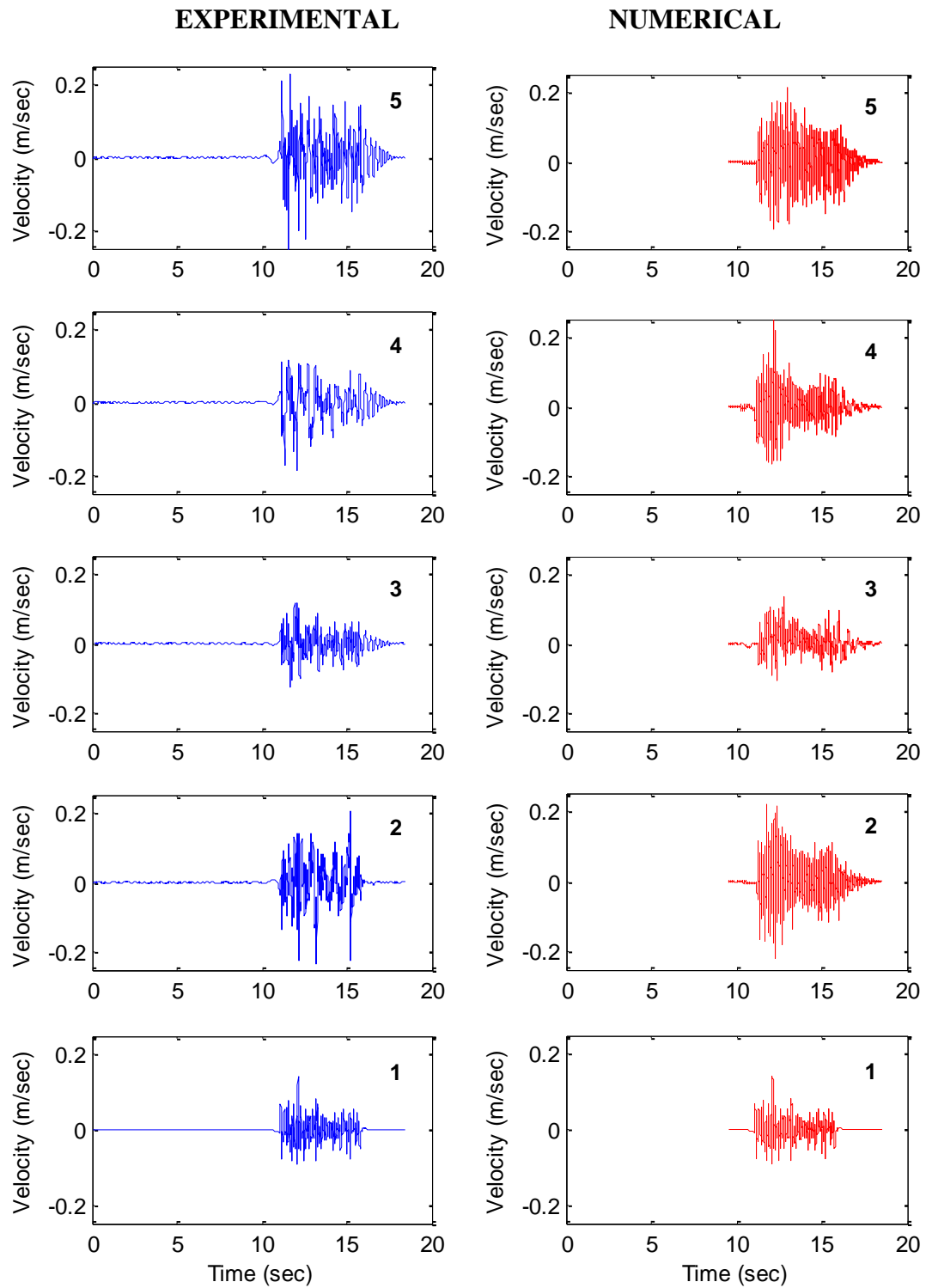


**Figure A21.** Comparisons of experimental and analytical velocities along the minaret under 250% Montenegro earthquake loading. 1, 2, 3, 4, 5 indicate the locations of accelerometers at 0.35m, 1.75m, 2.45m, 3.25m, 3.90m height of the minaret respectively. Refer to Figure A1 for the measurement locations on the minaret and corresponding points on the numerical model.

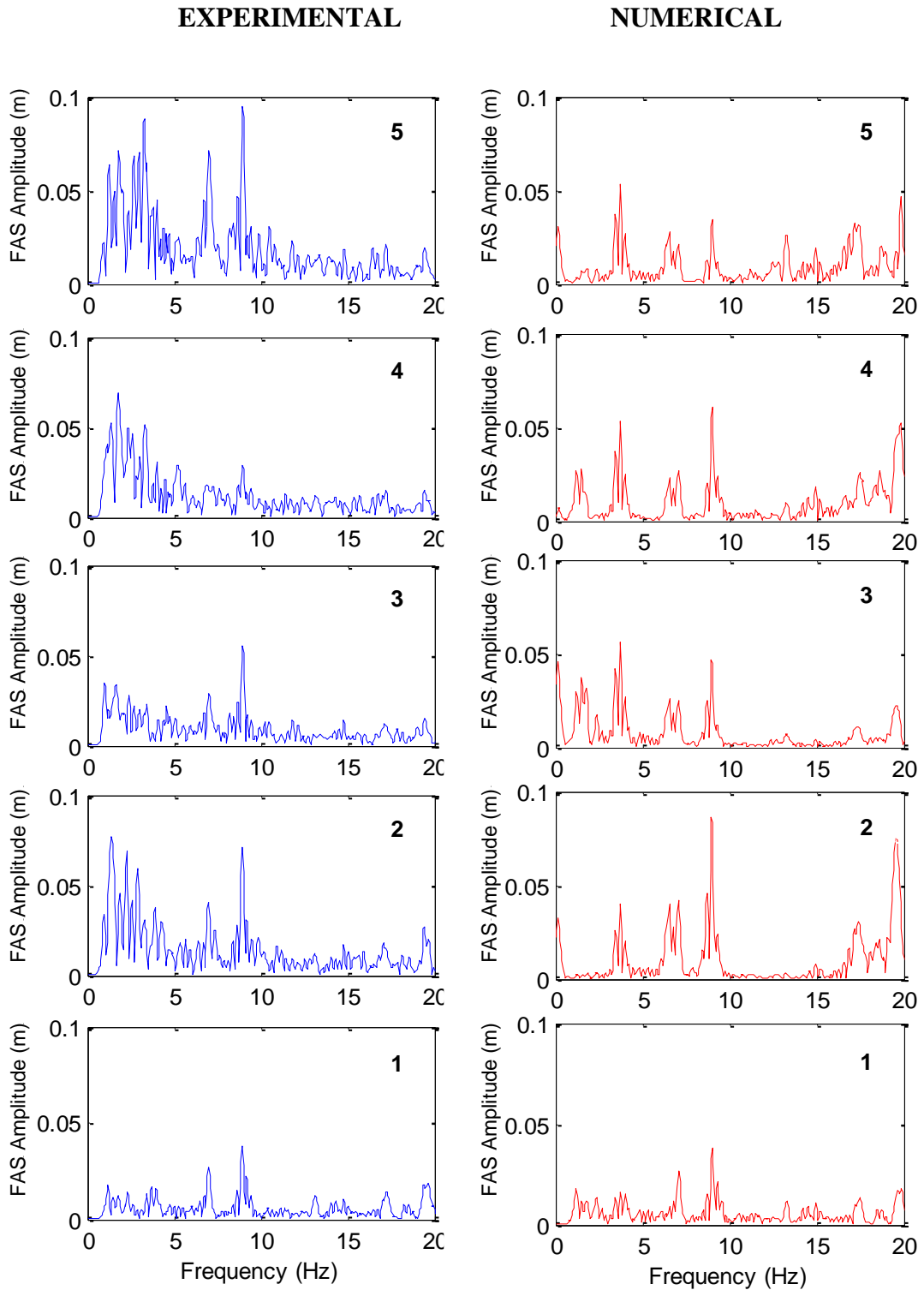


**Figure A22.** Comparisons of experimental and numerical FAS amplitude along the minaret under 250% Montenegro earthquake loading. 1, 2, 3, 4, 5 indicate the measurement locations. Refer to Figure A1 for the measurement locations on the minaret and corresponding points on the numerical model.

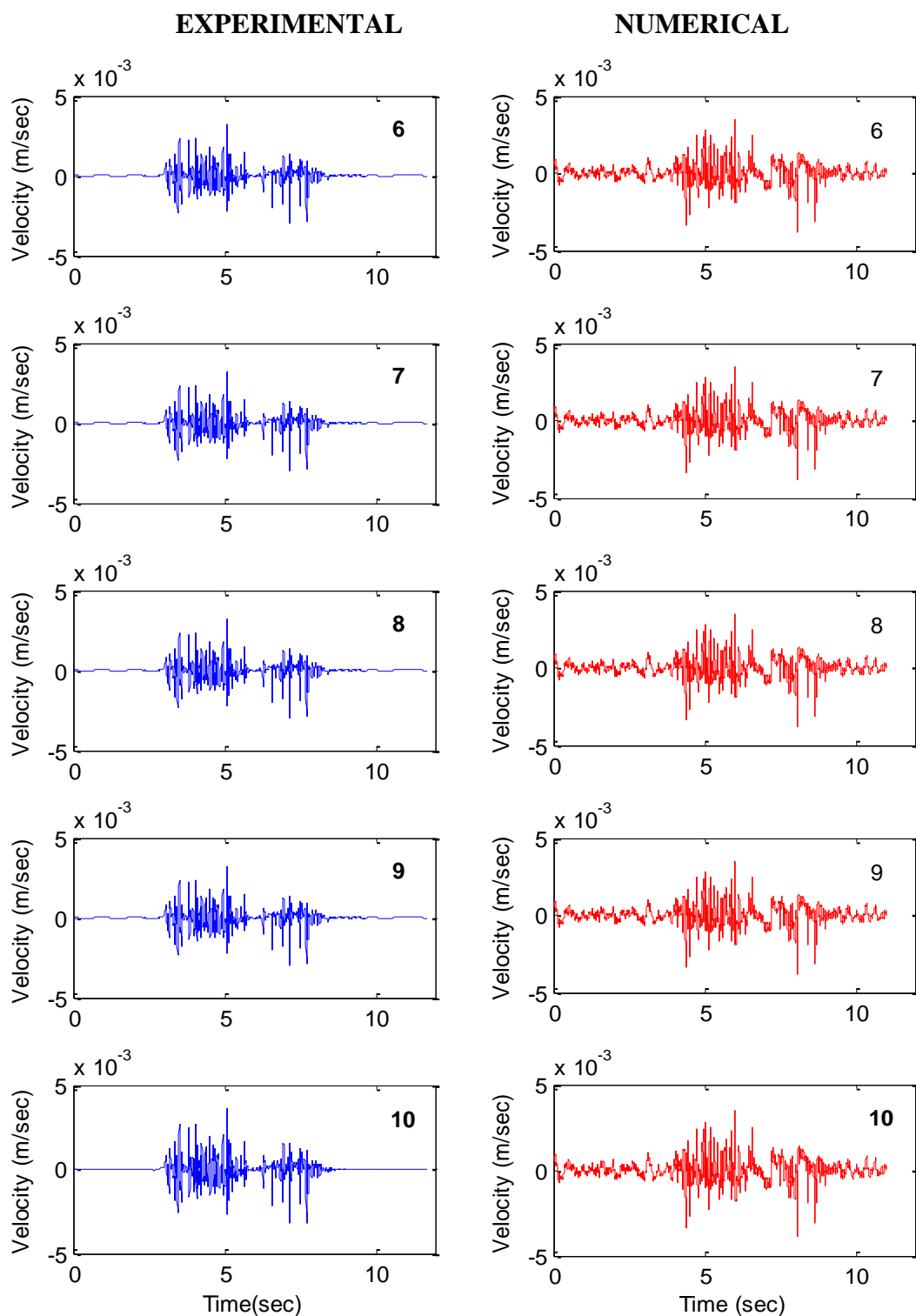


**Figure A23.** Comparisons of experimental and analytical velocities on the body of mosque model under 10% Montenegro earthquake loading. 10, 9, 8, 7 and 6 indicate the locations of accelerometers on the top of the dome and 4 at the four top corners of the body respectively. Refer to Figure A2 for the measurement locations on the minaret and corresponding points on the numerical model.

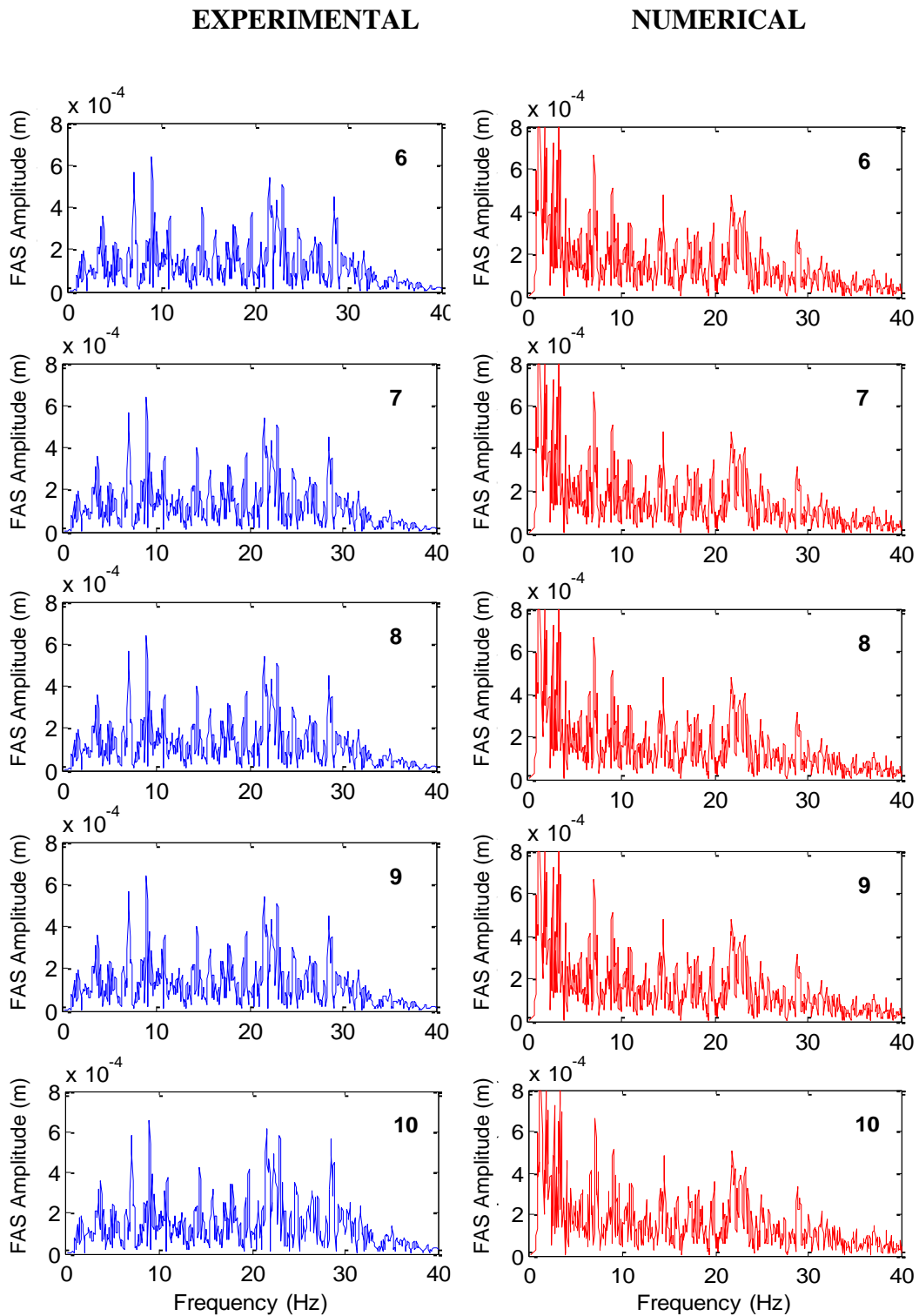


**Figure A24.** Comparisons of experimental and numerical FAS amplitude on the body of mosque model under 10% Montenegro earthquake loading. 10, 9, 8, 7 and 6 indicate the locations of accelerometers on the top of the dome and 4 at the four top corners of the body respectively. Refer to Figure A2 for the measurement locations on the minaret and corresponding points on the numerical model.

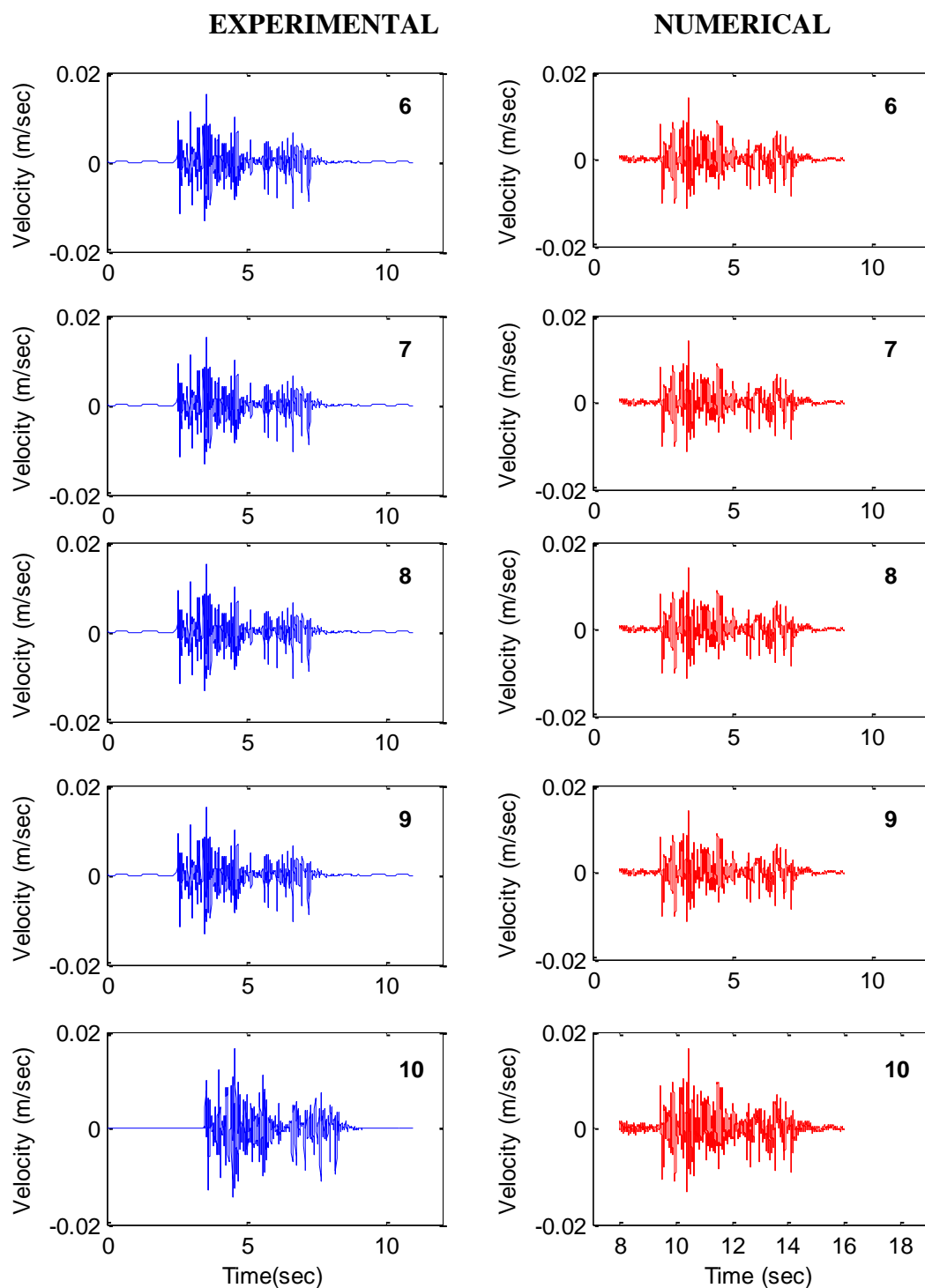


**Figure A25.** Comparisons of experimental and analytical velocities on the body of mosque model under 30% Montenegro earthquake loading. 10, 9, 8, 7 and 6 indicate the locations of accelerometers on the top of the dome and 4 at the four top corners of the body respectively. Refer to Figure A2 for the measurement locations on the minaret and corresponding points on the numerical model.

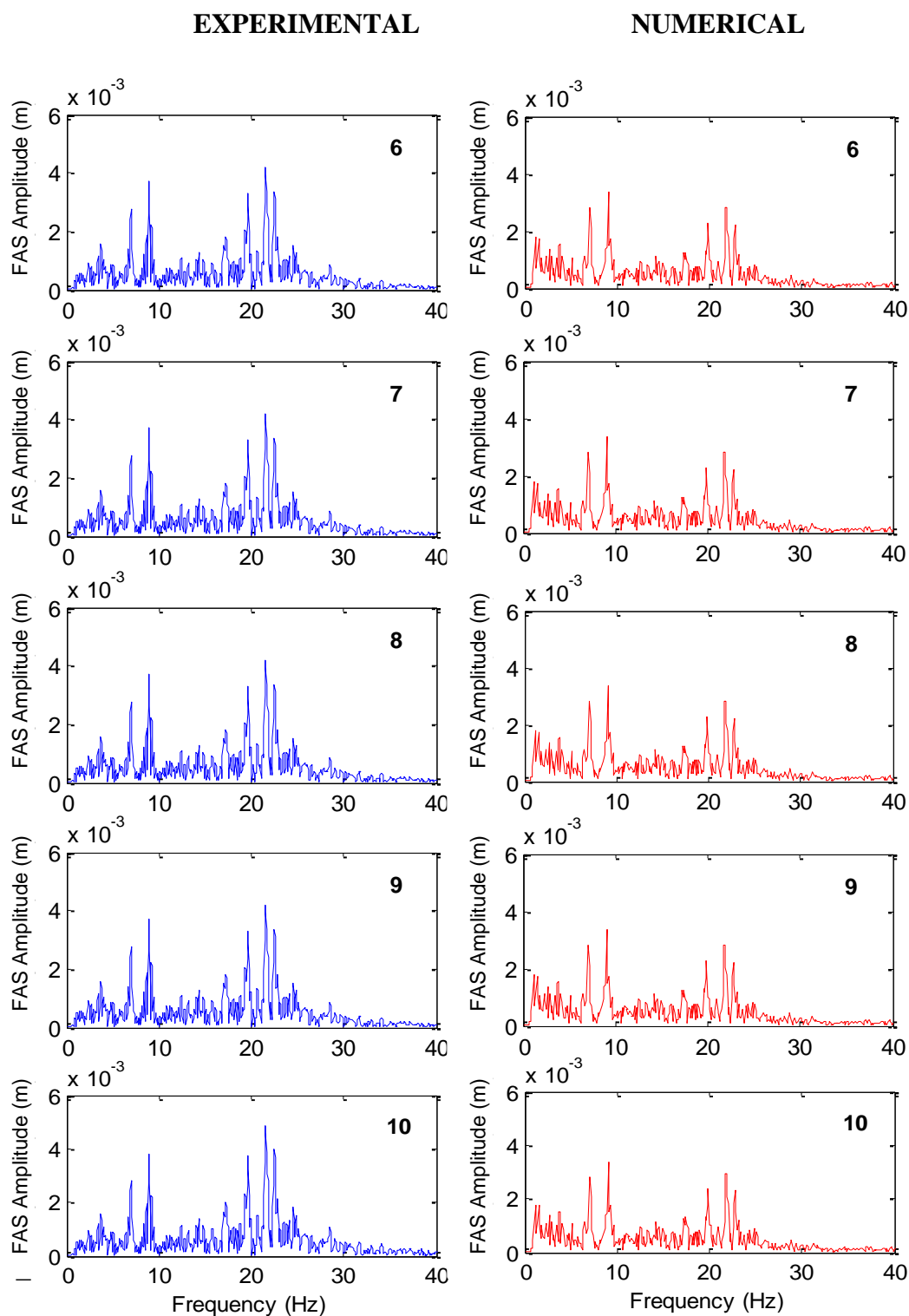


**Figure A26.** Comparisons of experimental and numerical FAS amplitude on the body of mosque model under 30% Montenegro earthquake loading. 10, 9, 8, 7 and 6 indicate the locations of accelerometers on the top of the dome and 4 at the four top corners of the body respectively. Refer to Figure A2 for the measurement locations on the minaret and corresponding points on the numerical model.

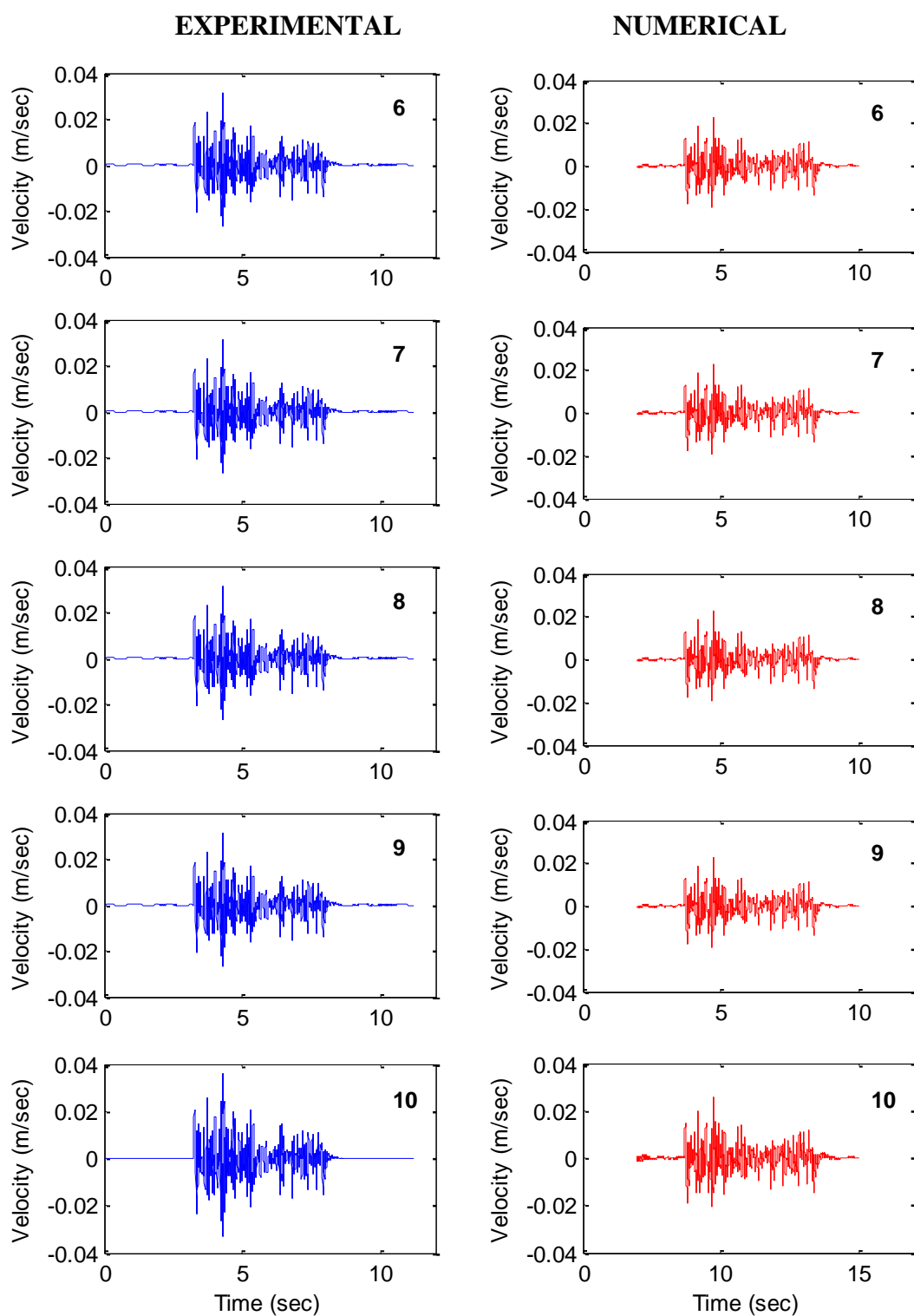


**Figure A27.** Comparisons of experimental and analytical velocities on the body of mosque model under 50% Montenegro earthquake loading. 10, 9, 8, 7 and 6 indicate the locations of accelerometers on the top of the dome and 4 at the four top corners of the body respectively. Refer to Figure A2 for the measurement locations on the minaret and corresponding points on the numerical model.

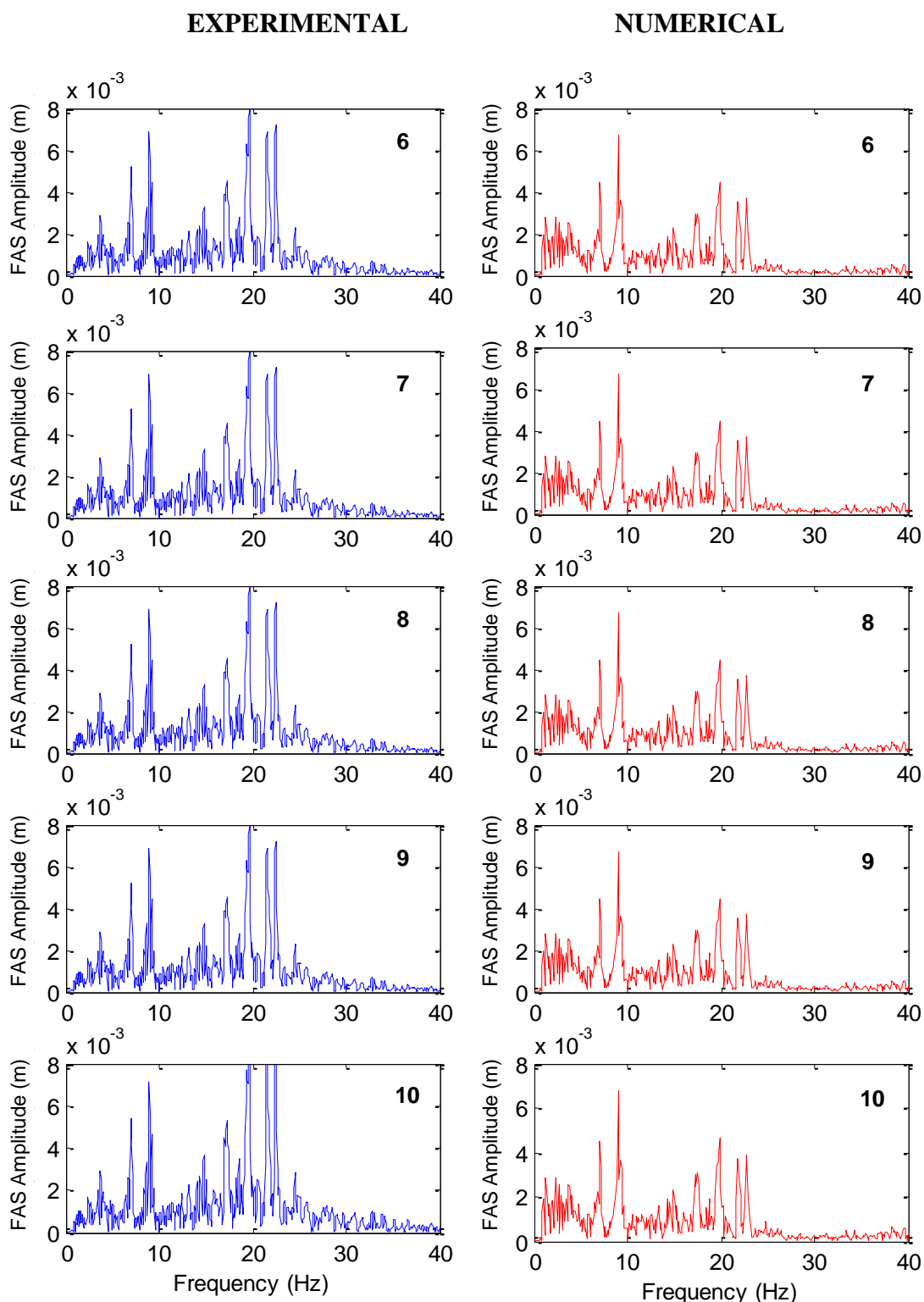


**Figure A28.** Comparisons of experimental and numerical FAS amplitude on the body of mosque model under 50% Montenegro earthquake loading. 10, 9, 8, 7 and 6 indicate the locations of accelerometers on the top of the dome and 4 at the four top corners of the body respectively. Refer to Figure A2 for the measurement locations on the minaret and corresponding points on the numerical model.

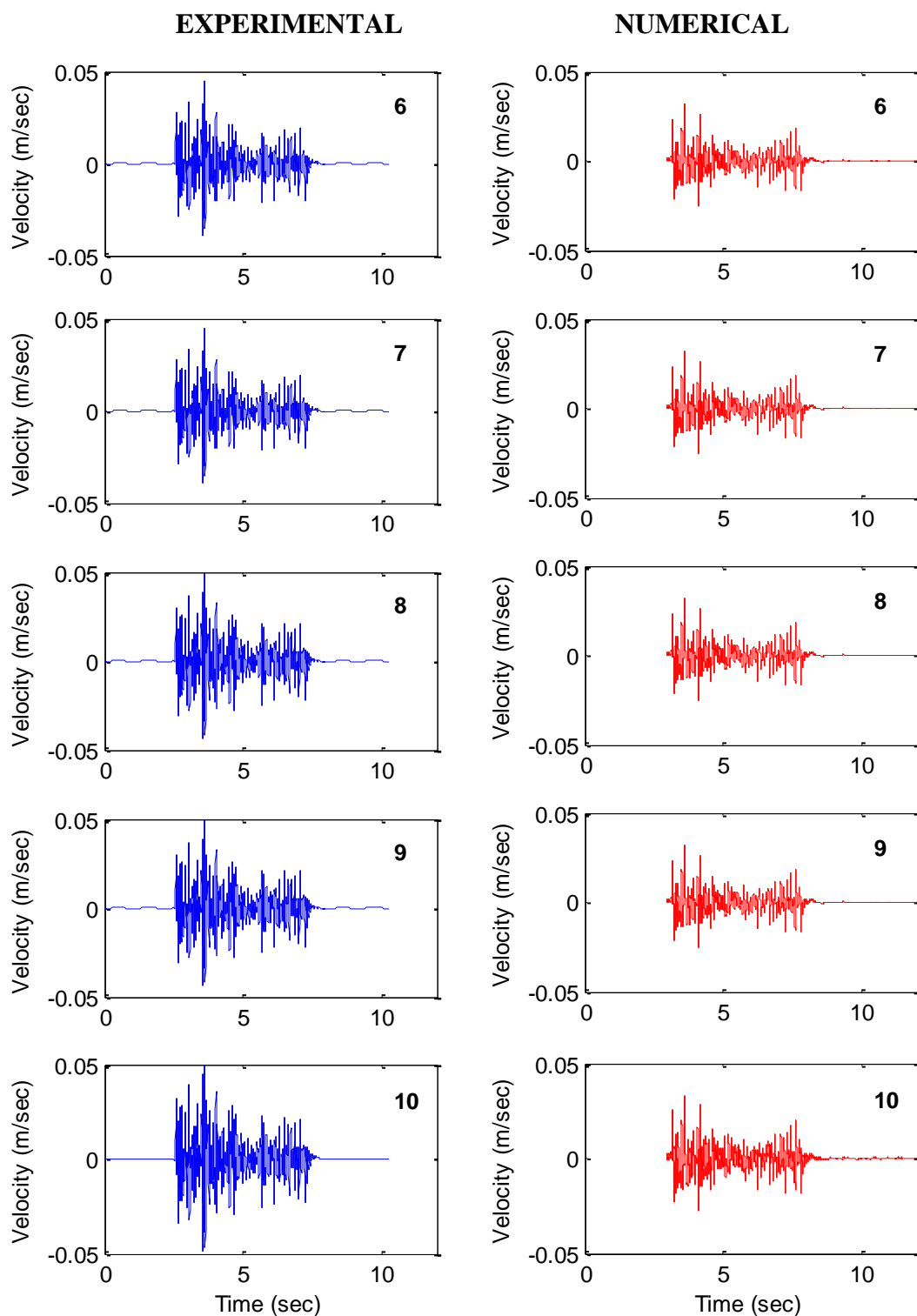


**Figure A29.** Comparisons of experimental and analytical velocities on the body of mosque model under 70% Montenegro earthquake loading. 10, 9, 8, 7 and 6 indicate the locations of accelerometers on the top of the dome and 4 at the four top corners of the body respectively. Refer to Figure A2 for the measurement locations on the minaret and corresponding points on the numerical model.

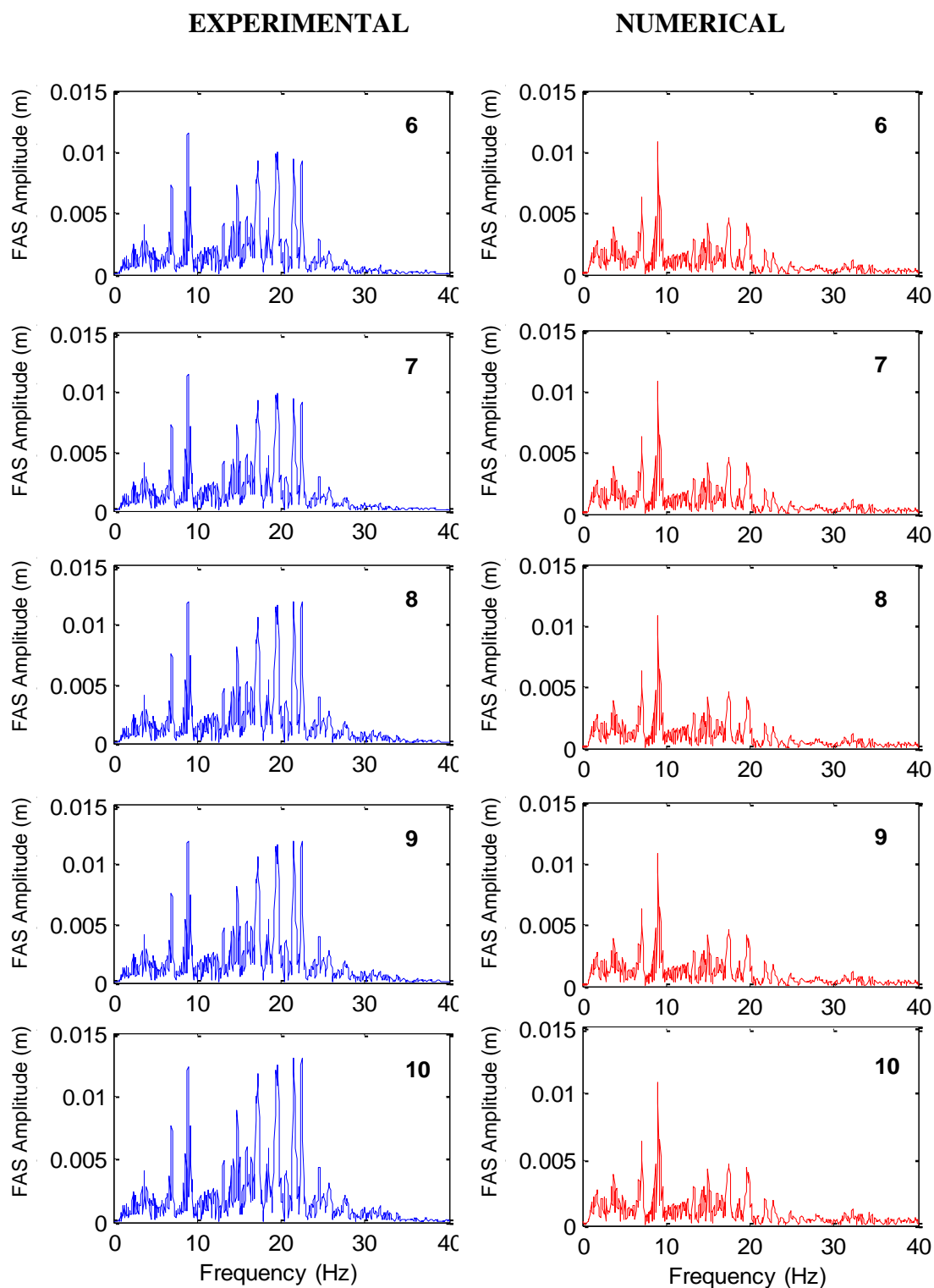


**Figure A30.** Comparisons of experimental and numerical FAS amplitude on the body of mosque model under 70% Montenegro earthquake loading. 10, 9, 8, 7 and 6 indicate the locations of accelerometers on the top of the dome and 4 at the four top corners of the body respectively. Refer to Figure A2 for the measurement locations on the minaret and corresponding points on the numerical model.



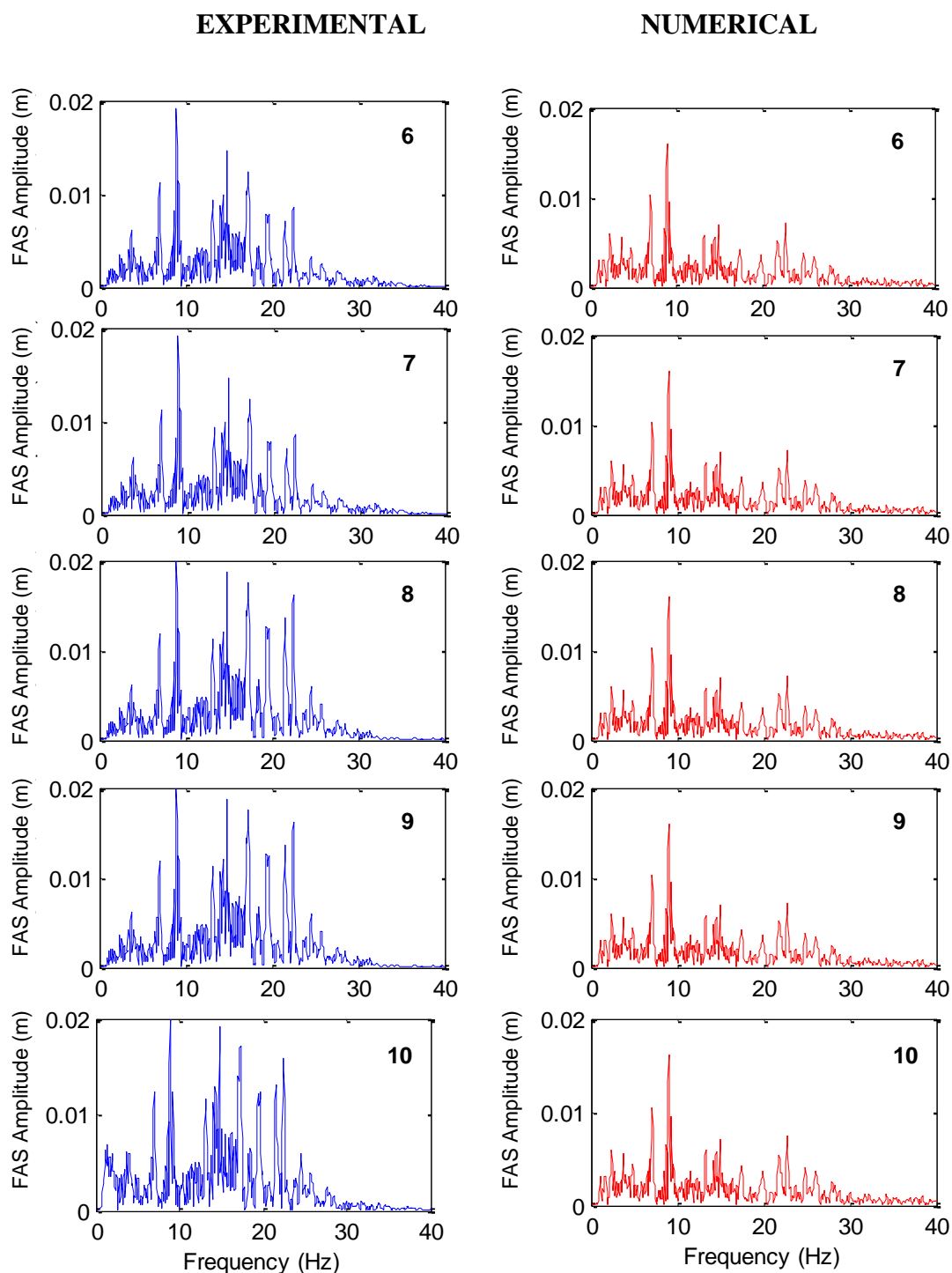


**Figure A32.** Comparisons of experimental and numerical FAS amplitude on the body of mosque model under 100% Montenegro earthquake loading. 10, 9, 8, 7 and 6 indicate the locations of accelerometers on the top of the dome and 4 at the four top corners of the body respectively. Refer to Figure A2 for the measurement locations on the minaret and corresponding points on the numerical model.

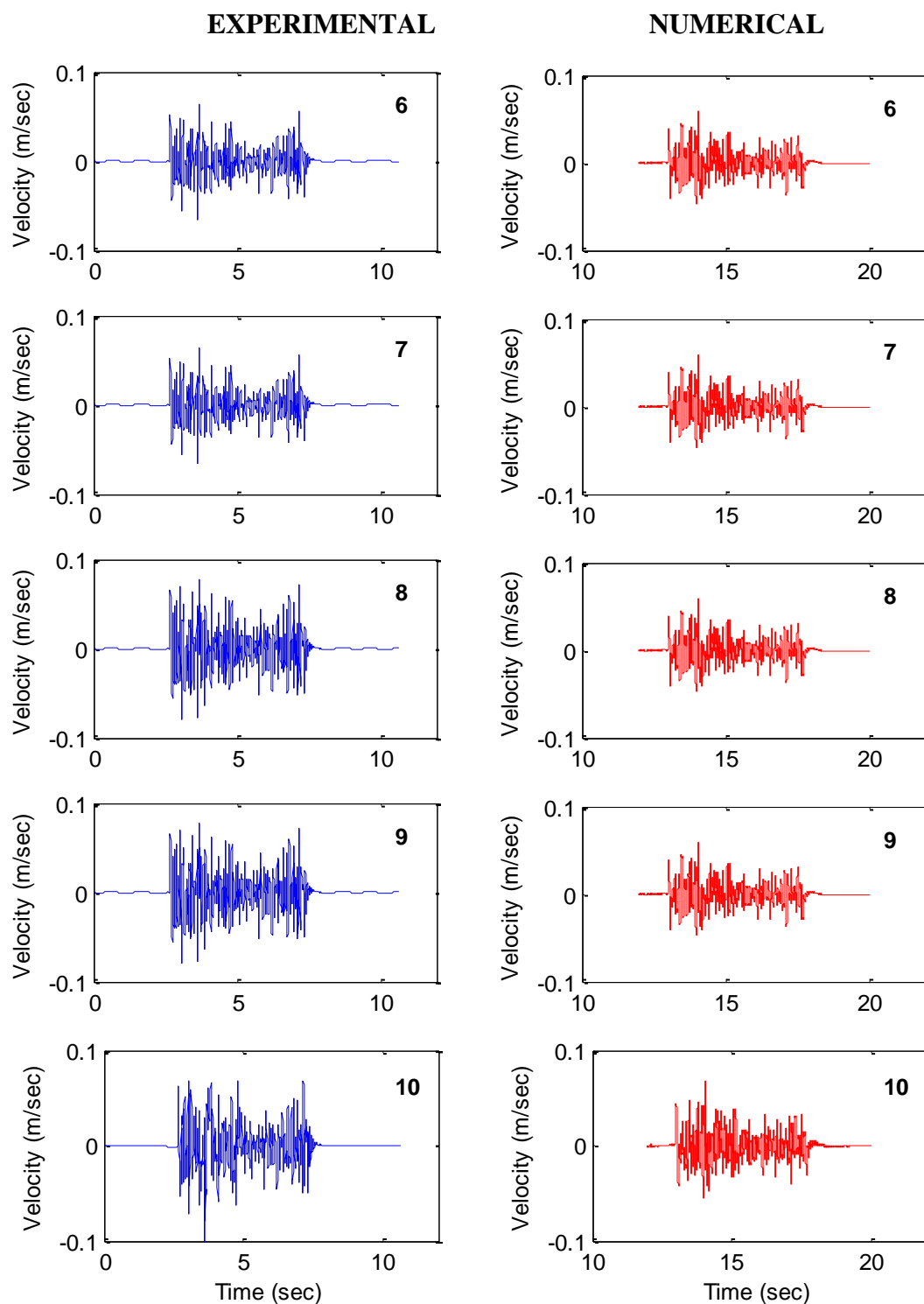


**Figure A33.** Comparisons of experimental and analytical velocities on the body of mosque model under 130% Montenegro earthquake loading. 10, 9, 8, 7 and 6 indicate the locations of accelerometers on the top of the dome and 4 at the four top corners of the body respectively. Refer to Figure A2 for the measurement locations on the minaret and corresponding points on the numerical model.

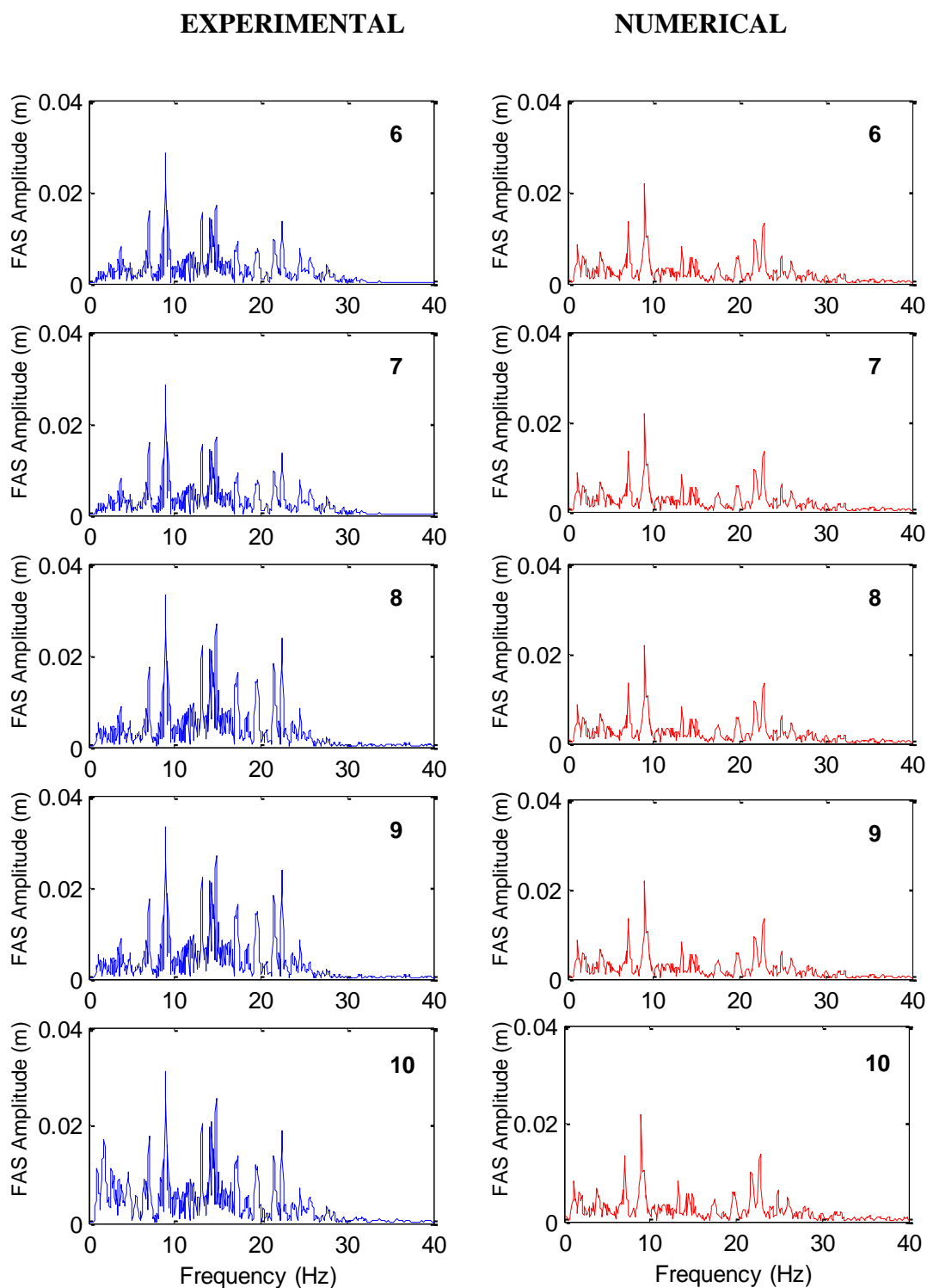


**Figure A34.** Comparisons of experimental and numerical FAS amplitude on the body of mosque model under 130% Montenegro earthquake loading. 10, 9, 8, 7 and 6 indicate the locations of accelerometers on the top of the dome and 4 at the four top corners of the body respectively. Refer to Figure A2 for the measurement locations on the minaret and corresponding points on the numerical model.



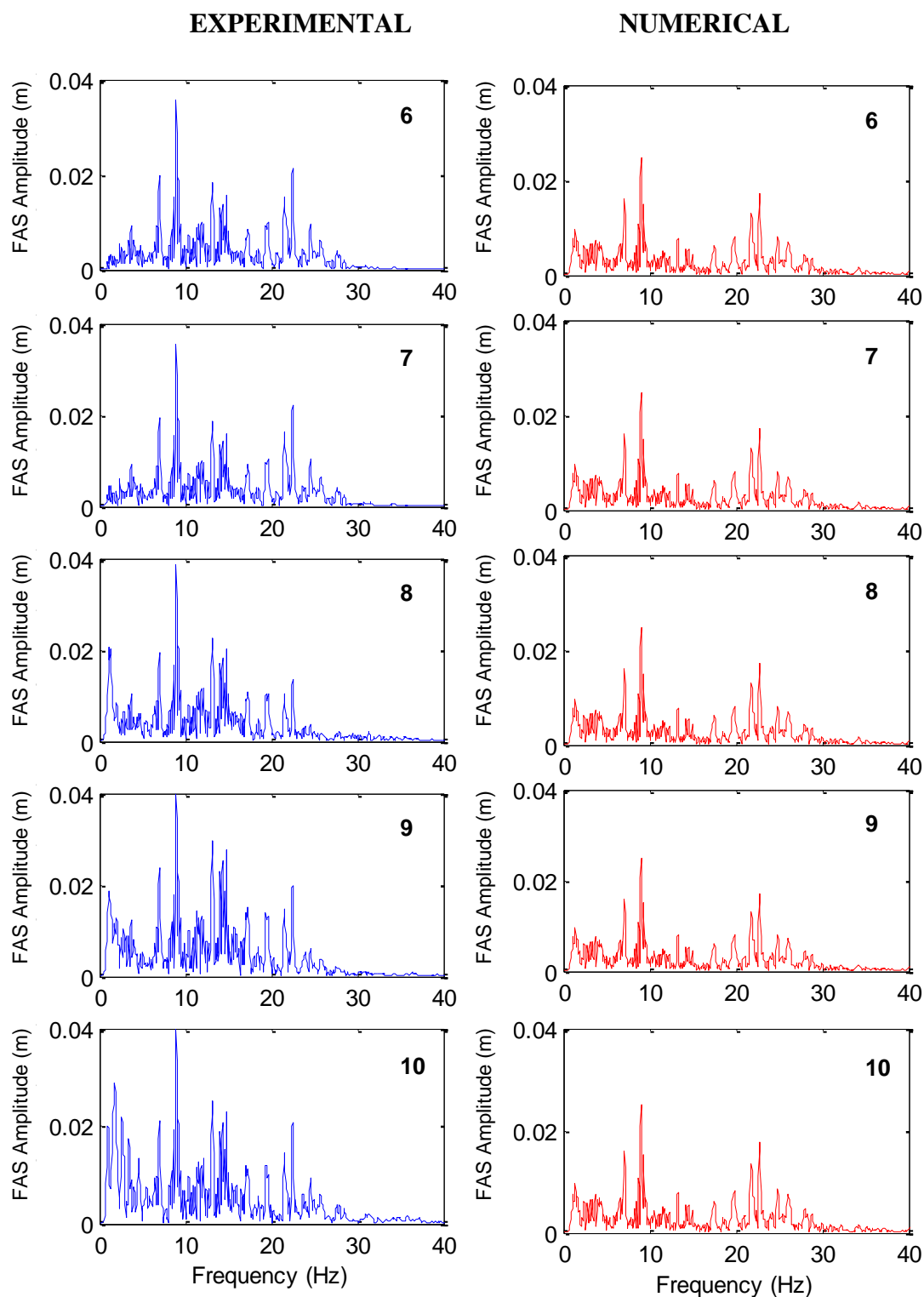


**Figure A36.** Comparisons of experimental and numerical FAS amplitude on the body of mosque model under 150% Montenegro earthquake loading. 10, 9, 8, 7 and 6 indicate the locations of accelerometers on the top of the dome and 4 at the four top corners of the body respectively. Refer to Figure A2 for the measurement locations on the minaret and corresponding points on the numerical model.

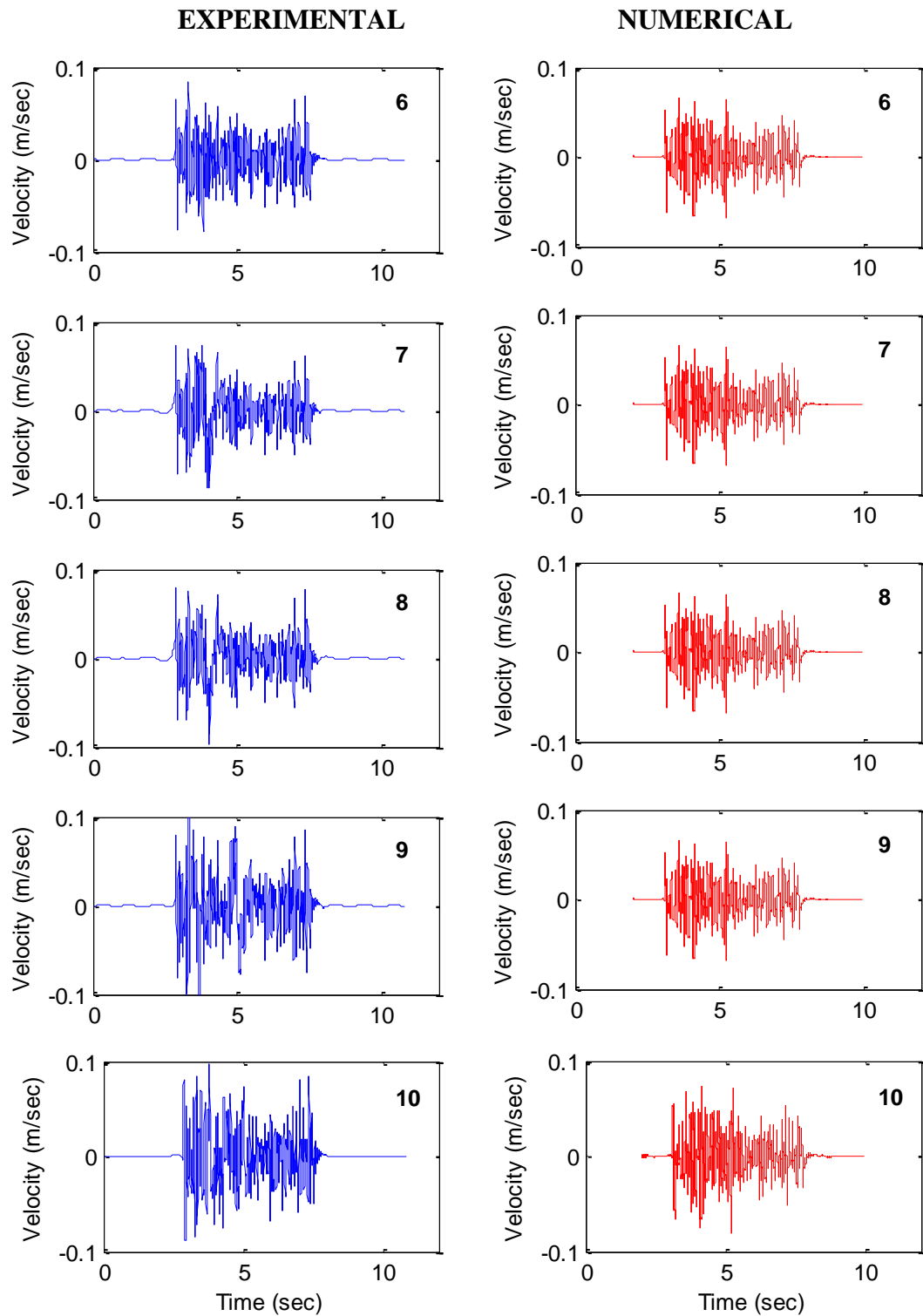


**Figure A37.** Comparisons of experimental and analytical velocities on the body of mosque model under 160% Montenegro earthquake loading. 10, 9, 8, 7 and 6 indicate the locations of accelerometers on the top of the dome and 4 at the four top corners of the body respectively. Refer to Figure A2 for the measurement locations on the minaret and corresponding points on the numerical model.

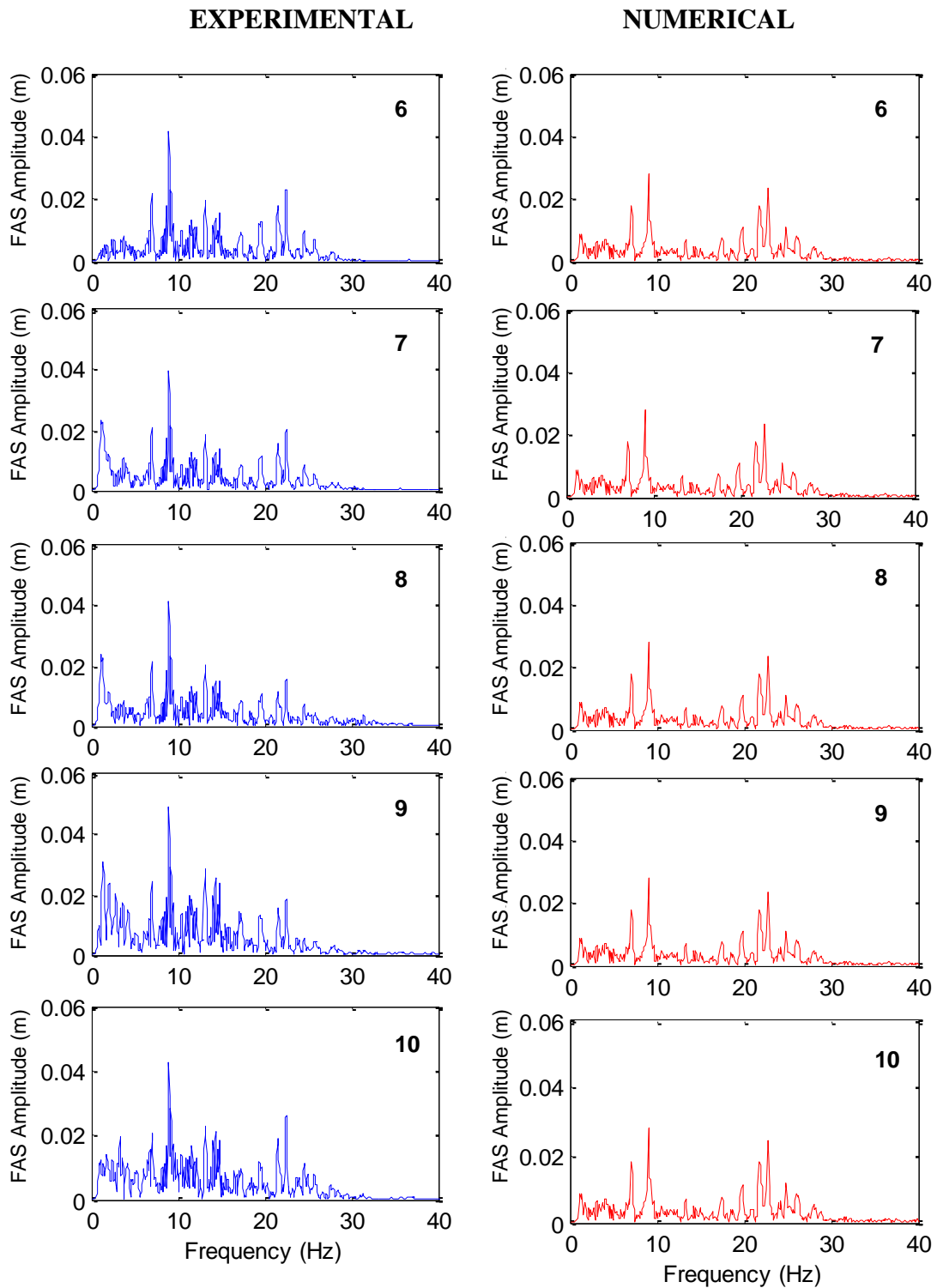


**Figure A38.** Comparisons of experimental and numerical FAS amplitude on the body of mosque model under 160% Montenegro earthquake loading. 10, 9, 8, 7 and 6 indicate the locations of accelerometers on the top of the dome and 4 at the four top corners of the body respectively. Refer to Figure A2 for the measurement locations on the minaret and corresponding points on the numerical model.



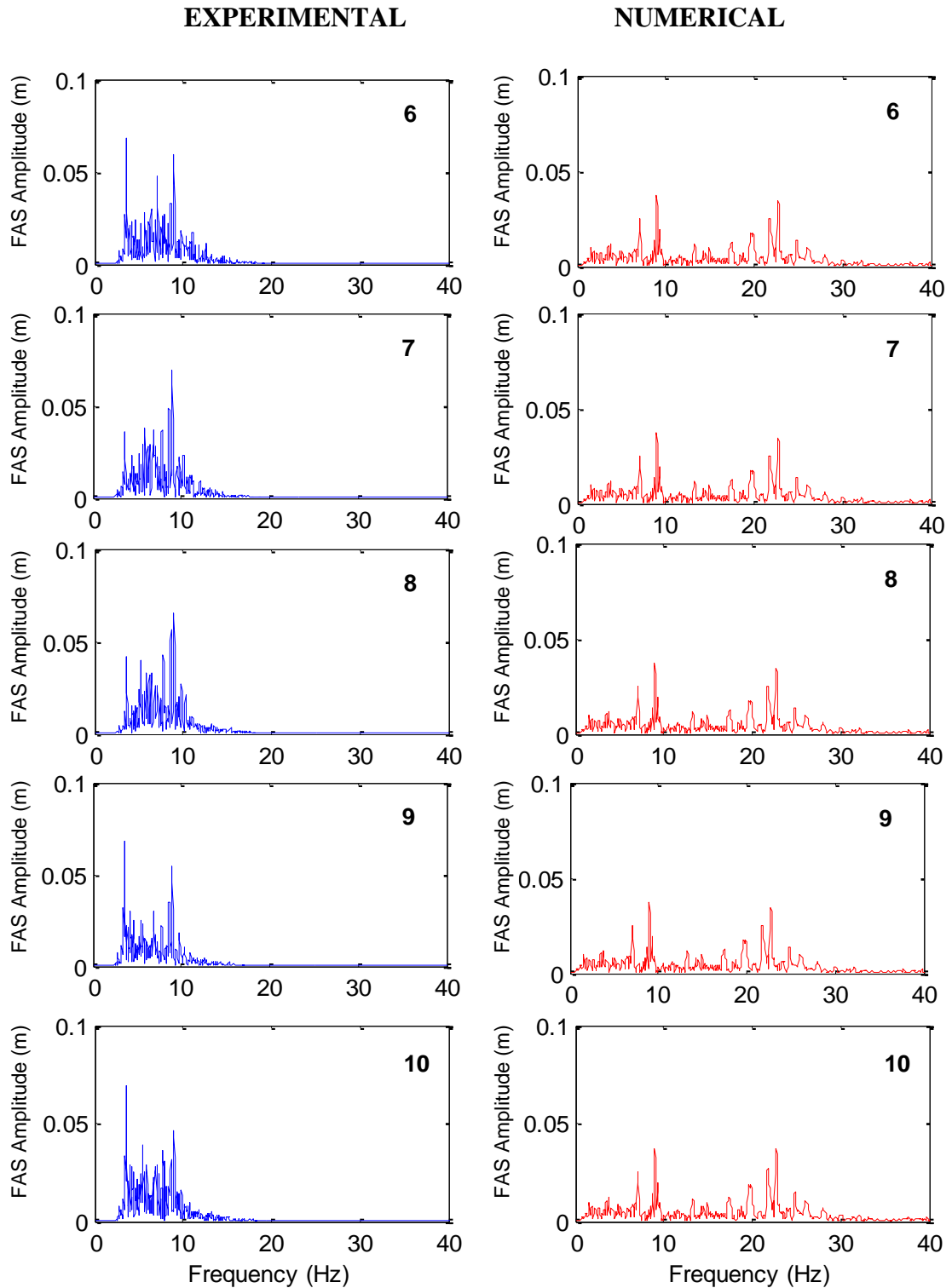


**Figure A40.** Comparisons of experimental and numerical FAS amplitude on the body of mosque model under 220% Montenegro earthquake loading. 10, 9, 8, 7 and 6 indicate the locations of accelerometers on the top of the dome and 4 at the four top corners of the body respectively. Refer to Figure A2 for the measurement locations on the minaret and corresponding points on the numerical model..

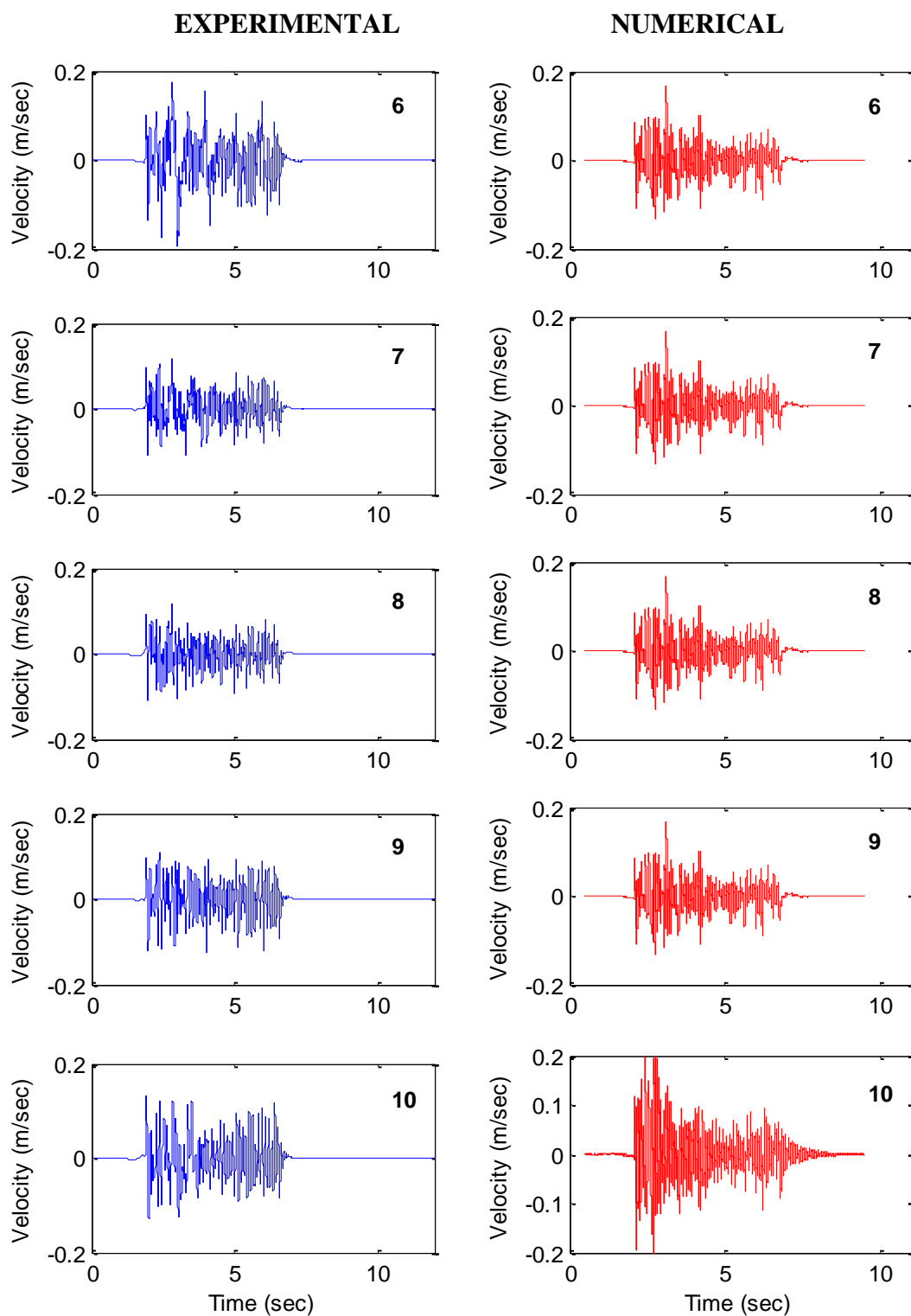


**Figure A41.** Comparisons of experimental and analytical velocities on the body of mosque model under 250% Montenegro earthquake loading. 10, 9, 8, 7 and 6 indicate the locations of accelerometers on the top of the dome and 4 at the four top corners of the body respectively. Refer to Figure A2 for the measurement locations on the minaret and corresponding points on the numerical model.

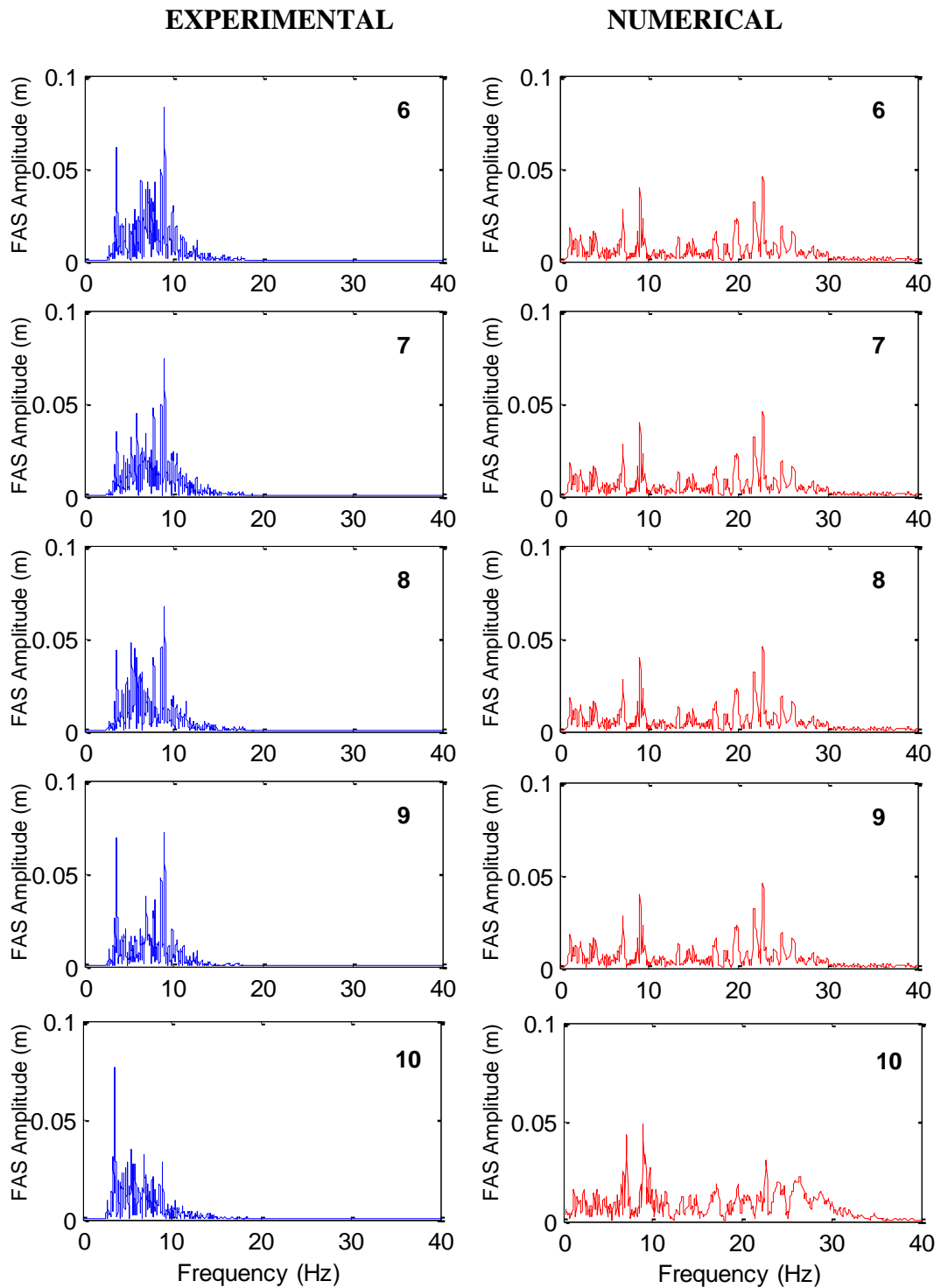


**Figure A42.** Comparisons of experimental and numerical FAS amplitude on the body of mosque model under 250% Montenegro earthquake loading. 10, 9, 8, 7 and 6 indicate the locations of accelerometers on the top of the dome and 4 at the four top corners of the body respectively. Refer to Figure A2 for the measurement locations on the minaret and corresponding points on the numerical model.

## **APPENDIX B: COMPARISON WITH EXPERIMENTAL DATA AND DISTINCT ELEMENT MODEL WITH FRP STRENGTHENING**

In this appendix, comparisons of experimental and analytical velocities and Fourier amplitude spectra along the minaret and on the body of the model are presented. The comparisons are provided for 60%, 160%, 190%, 210%, 230%, 250% and 325% Montenegro. In Figure B1 measurement locations on the minaret of the shake table model and corresponding points on the numerical model are shown. Comparisons for the minaret are presented in Figures B2 – B15.

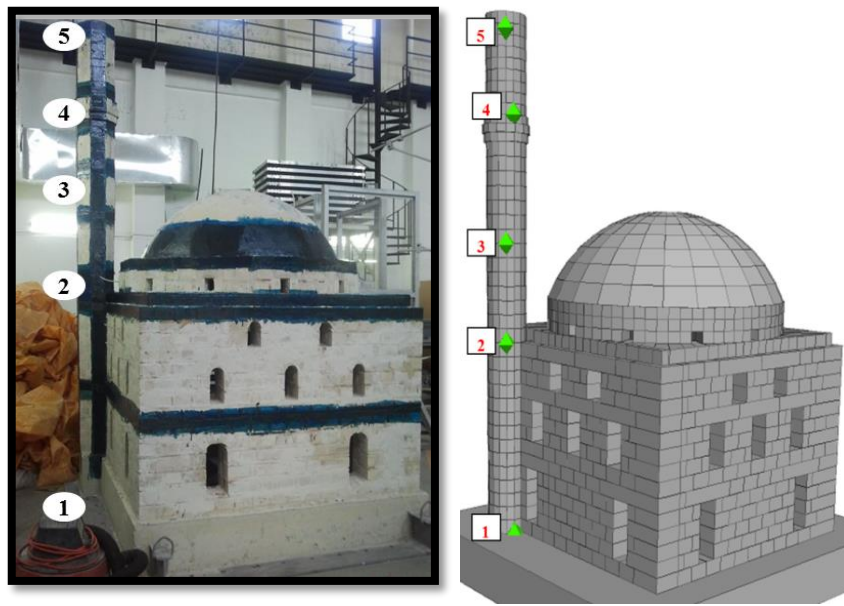


**Figure B1.** Images of measurement locations on the minaret of the shake table model and corresponding points on the numerical model.

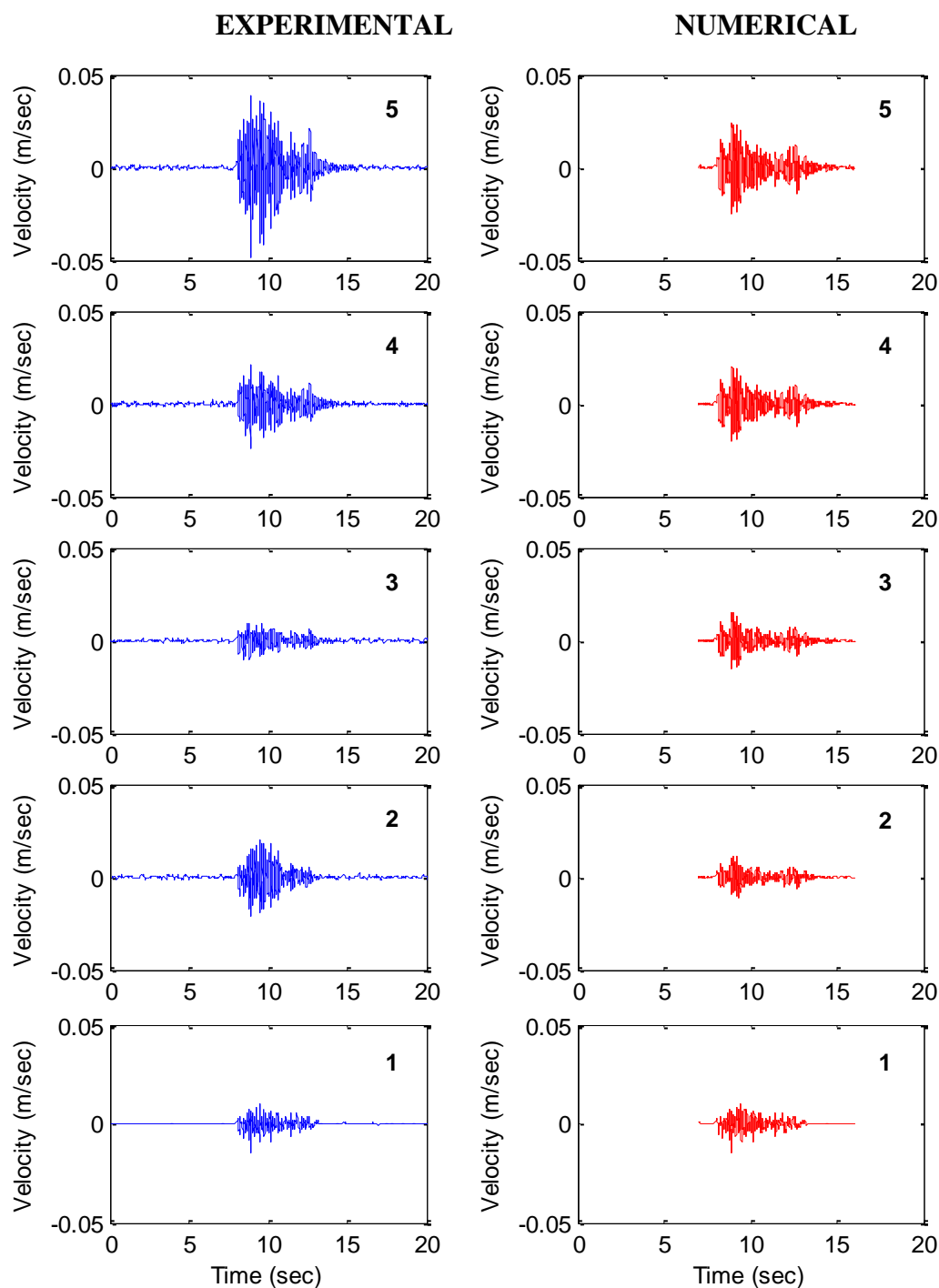


**Figure B2.** Comparisons of experimental and analytical velocities along the minaret under 60% Montenegro earthquake loading. 1, 2, 3, 4, 5 indicate the locations of accelerometers at 0.35m, 1.75m, 2.45m, 3.25m, 3.90m height of the minaret respectively. Refer to Figure B1 for the measurement locations on the minaret and corresponding points on the numerical model.

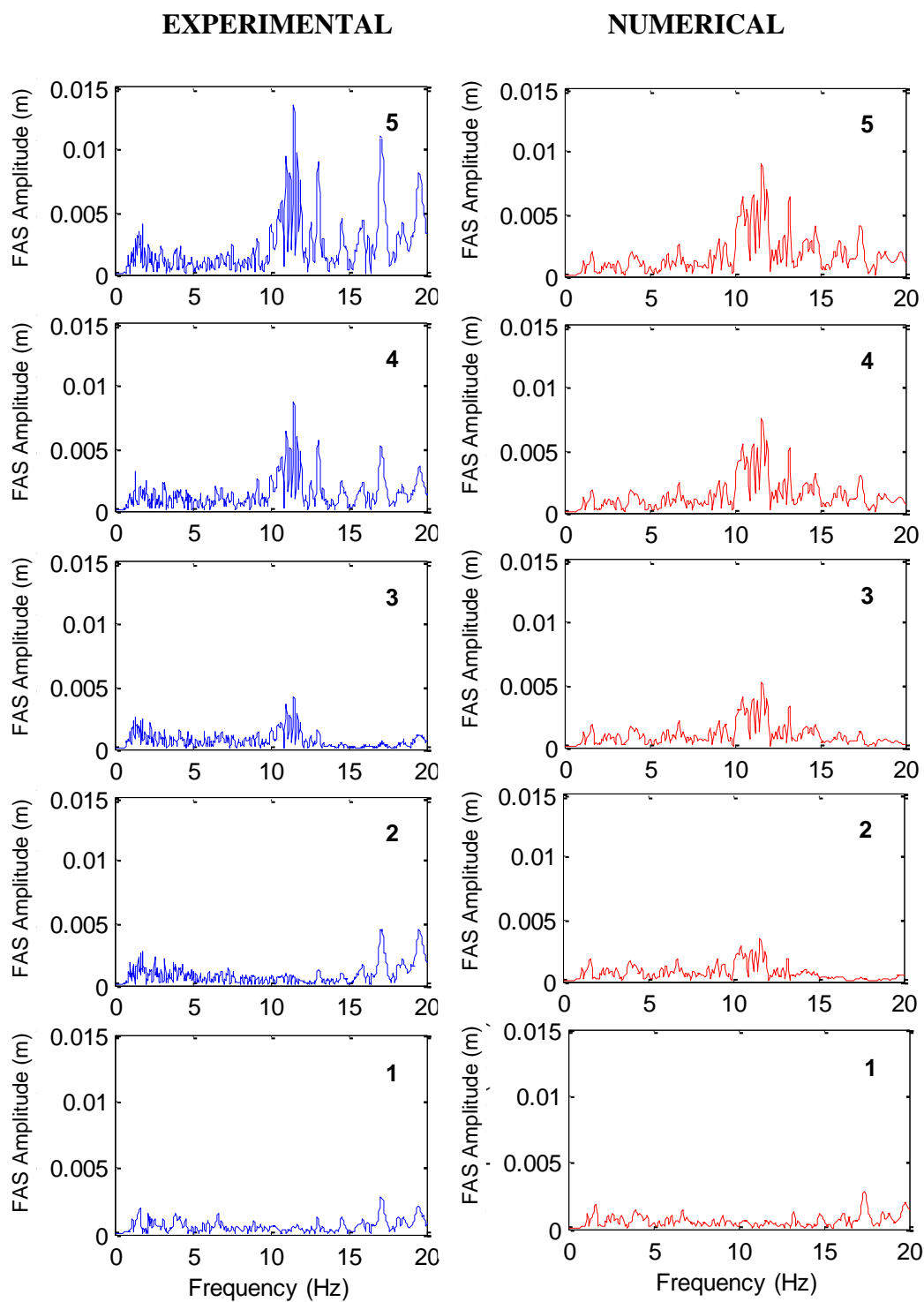


**Figure B3.** Comparisons of experimental and numerical FAS amplitude along the minaret under 60% Montenegro earthquake loading. 1, 2, 3, 4, 5 indicate the measurement locations. Refer to Figure B1 for the measurement locations on the minaret and corresponding points on the numerical model.

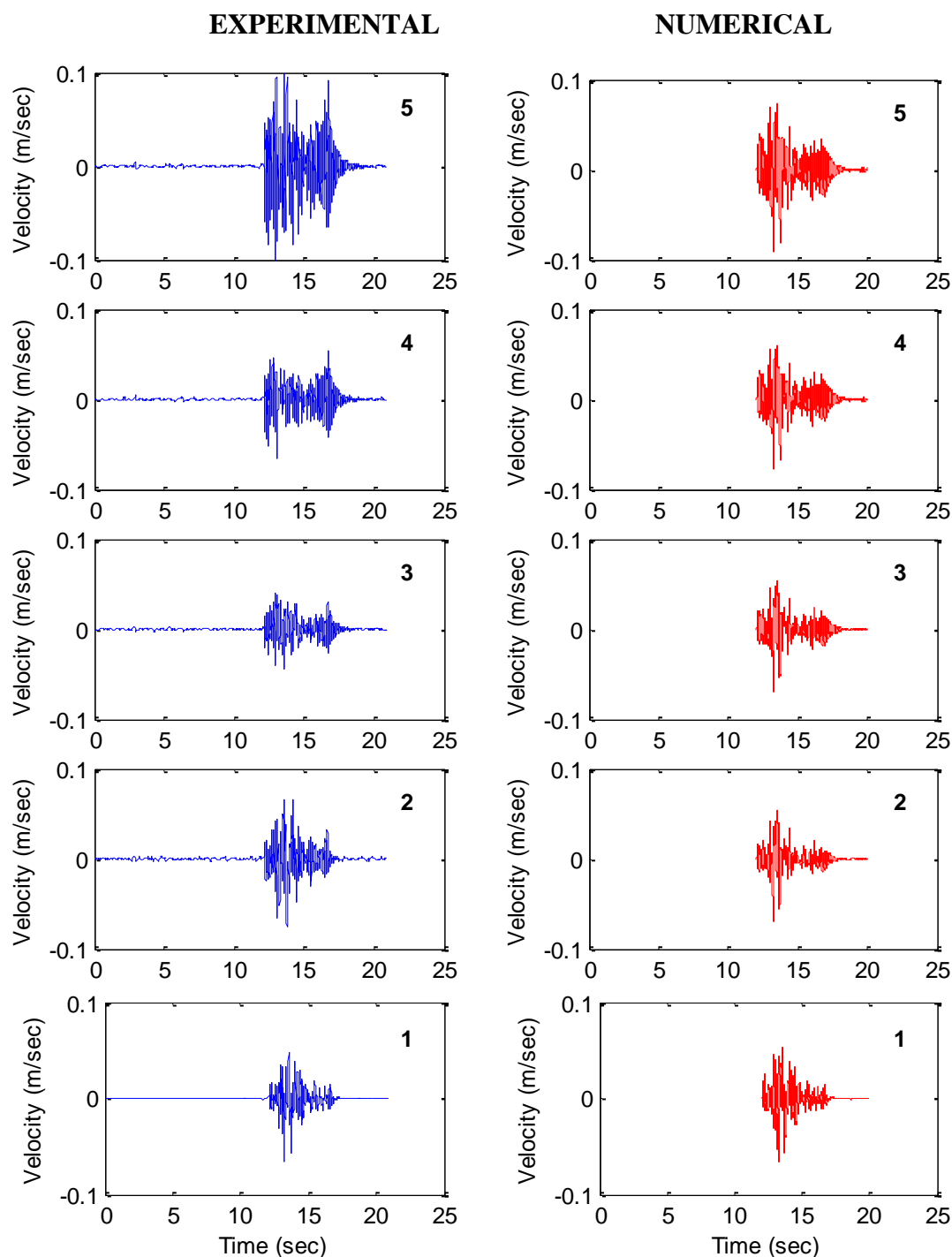


**Figure B4.** Comparisons of experimental and analytical velocities along the minaret under 160% Montenegro earthquake loading. 1, 2, 3, 4, 5 indicate the locations of accelerometers at 0.35m, 1.75m, 2.45m, 3.25m, 3.90m height of the minaret respectively. Refer to Figure B1 for the measurement locations on the minaret and corresponding points on the numerical model.

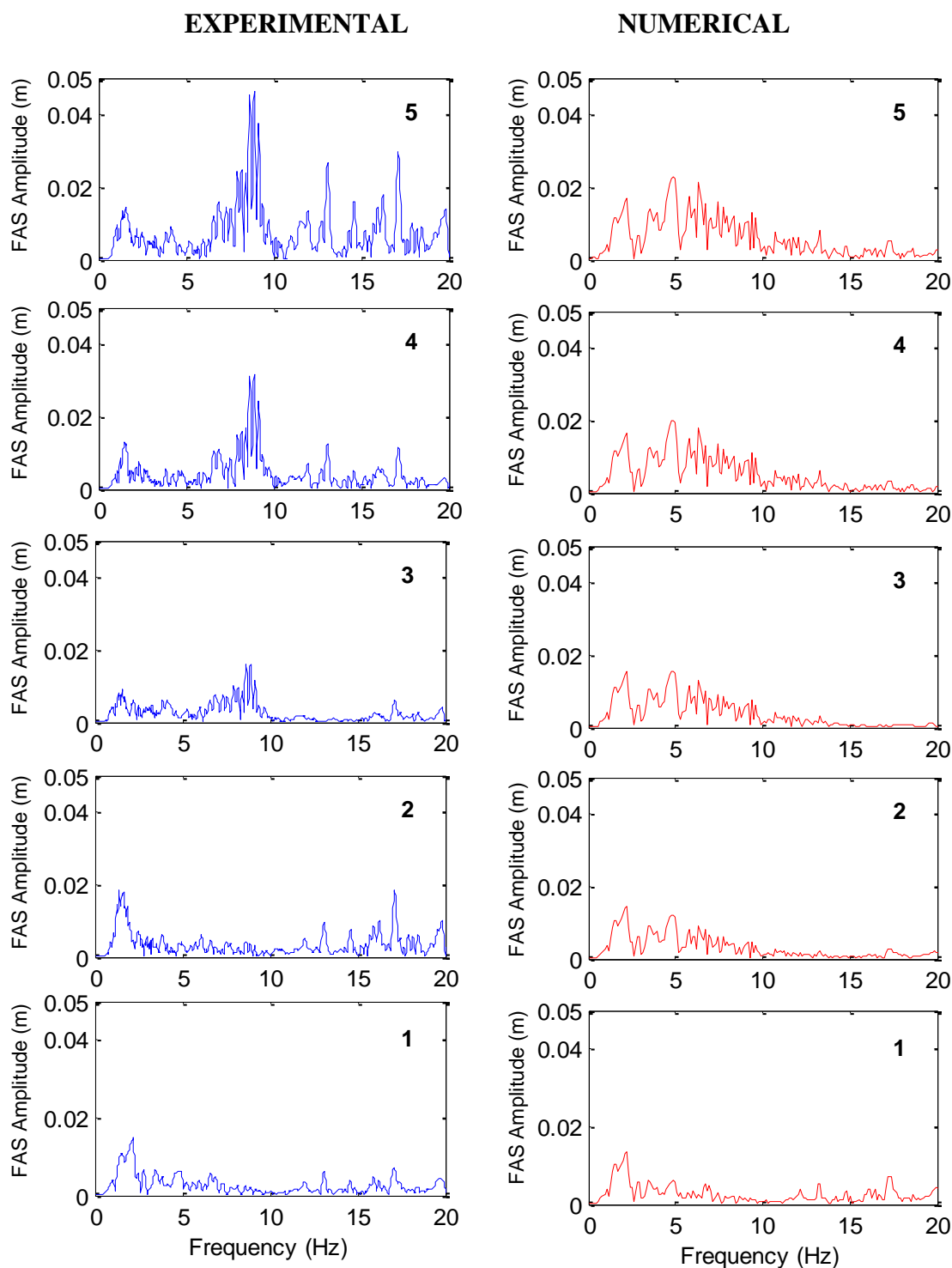


**Figure B5.** Comparisons of experimental and numerical FAS amplitude along the minaret under 160% Montenegro earthquake loading. 1, 2, 3, 4, 5 indicate the measurement locations. Refer to Figure B1 for the measurement locations on the minaret and corresponding points on the numerical model.

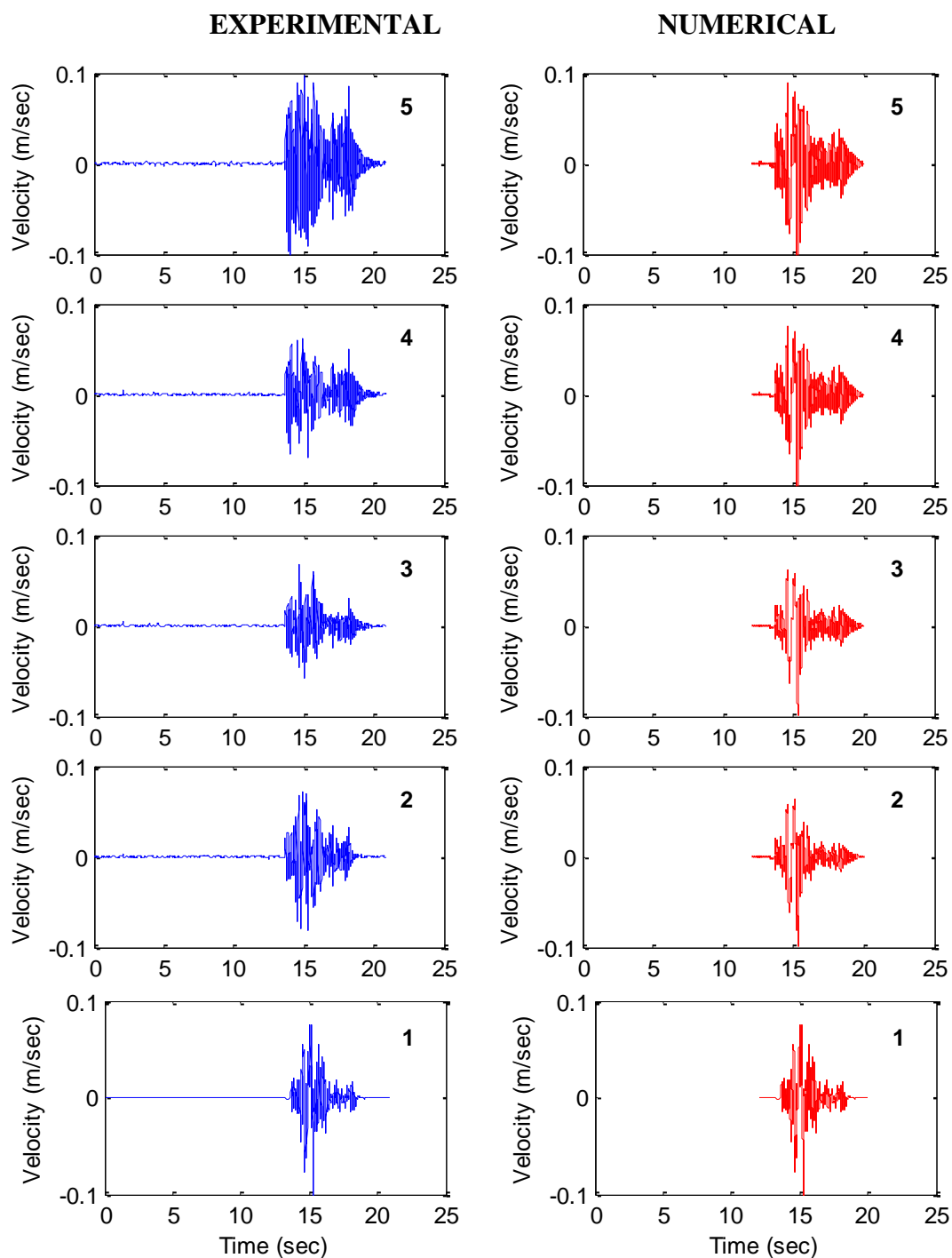


**Figure B6.** Comparisons of experimental and analytical velocities along the minaret under 190% Montenegro earthquake loading. 1, 2, 3, 4, 5 indicate the locations of accelerometers at 0.35m, 1.75m, 2.45m, 3.25m, 3.90m height of the minaret respectively. Refer to Figure B1 for the measurement locations on the minaret and corresponding points on the numerical model.

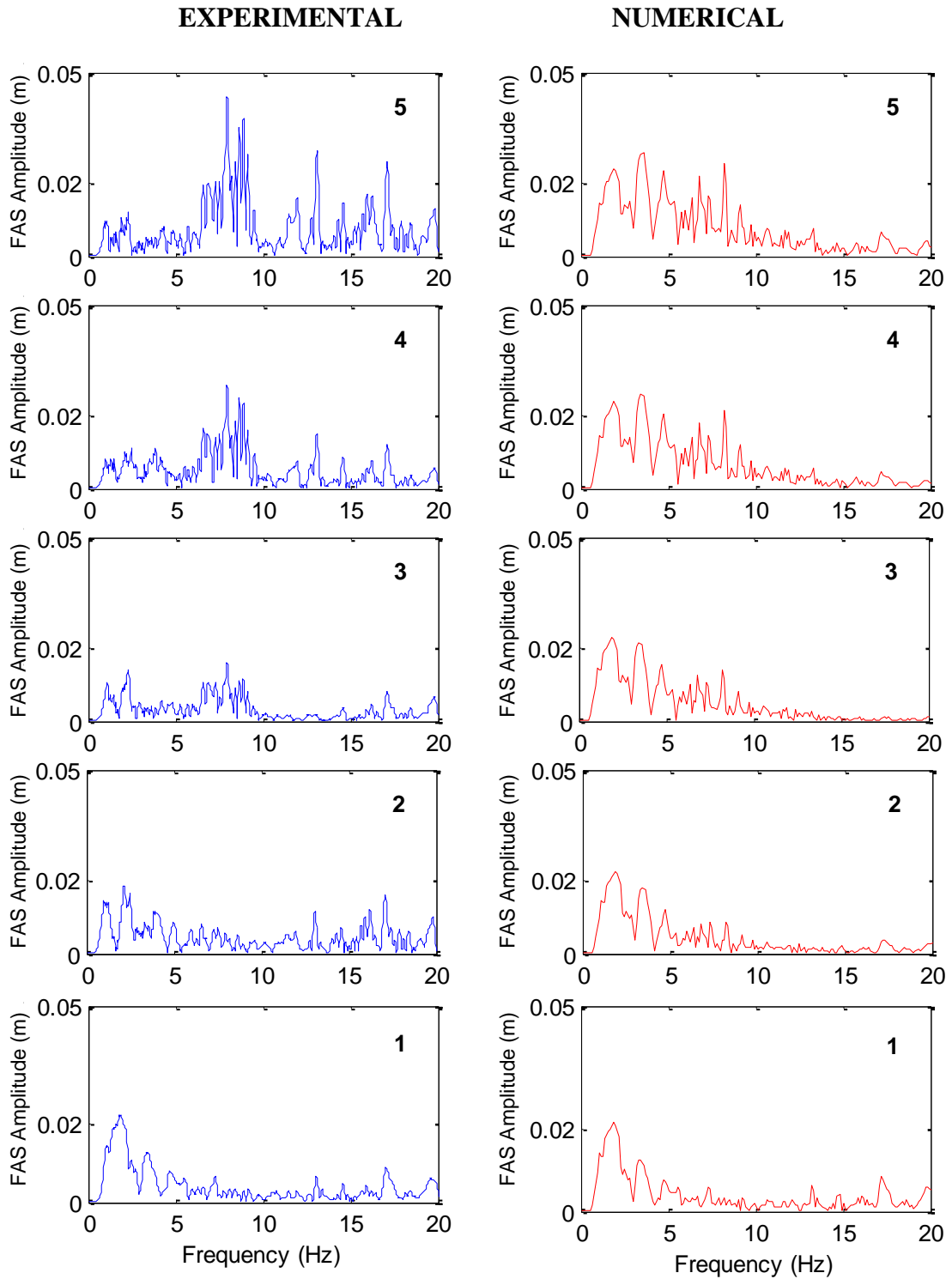


**Figure B7.** Comparisons of experimental and numerical FAS amplitude along the minaret under 190% Montenegro earthquake loading. 1, 2, 3, 4, 5 indicate the measurement locations. Refer to Figure B1 for the measurement locations on the minaret and corresponding points on the numerical model.

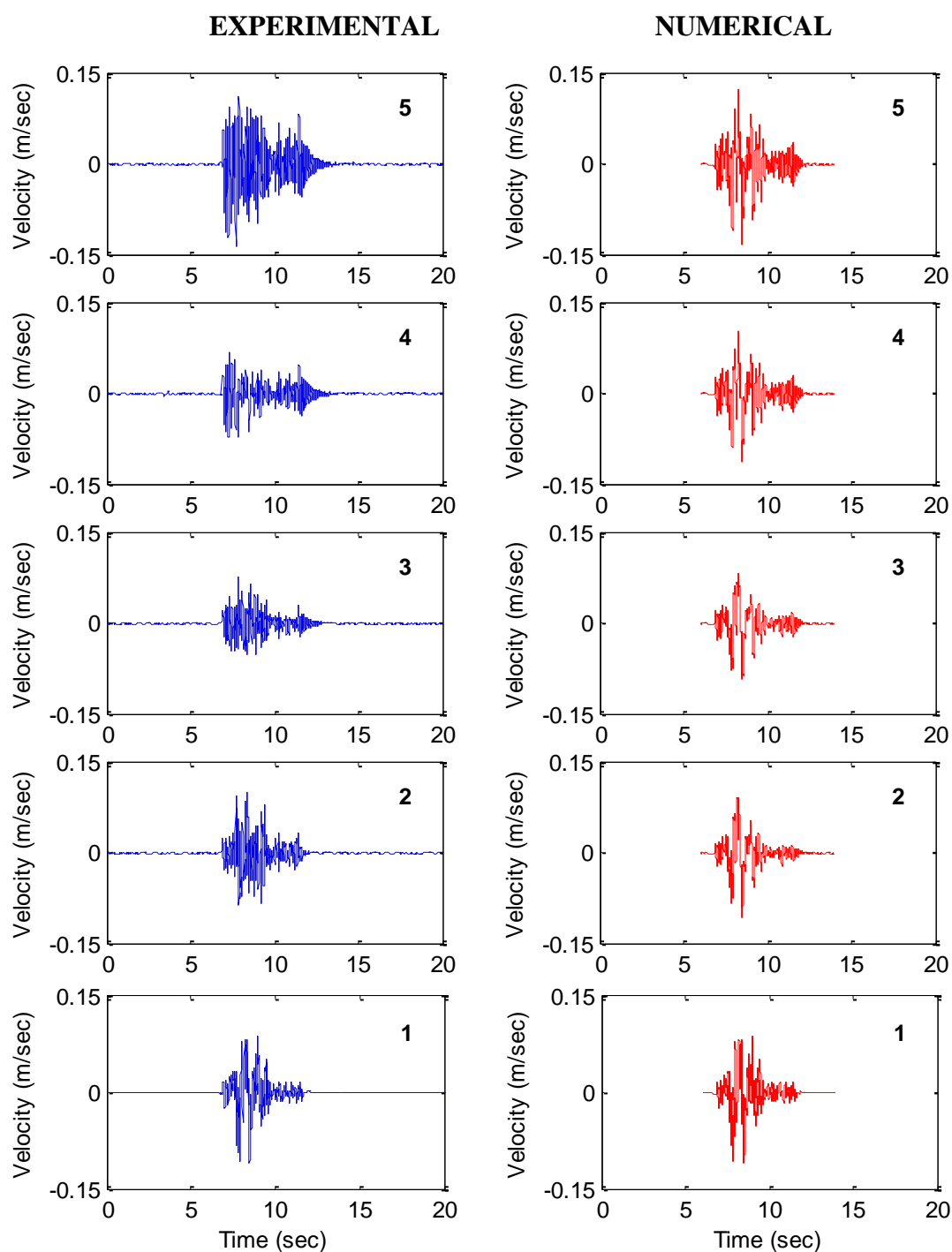


**Figure B8.** Comparisons of experimental and analytical velocities along the minaret under 210% Montenegro earthquake loading. 1, 2, 3, 4, 5 indicate the locations of accelerometers at 0.35m, 1.75m, 2.45m, 3.25m, 3.90m height of the minaret respectively. Refer to Figure B1 for the measurement locations on the minaret and corresponding points on the numerical model.

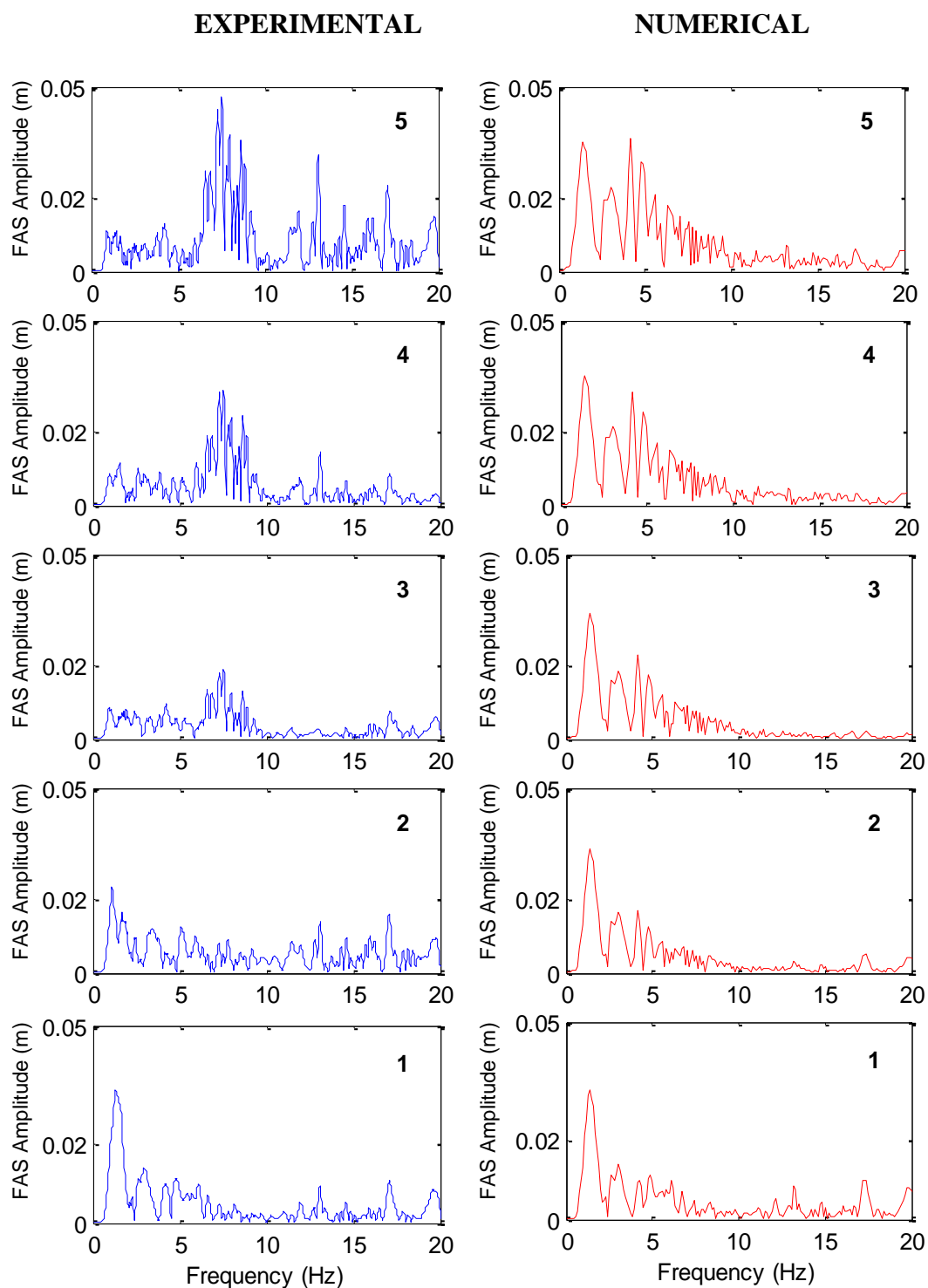


**Figure B9.** Comparisons of experimental and numerical FAS amplitude along the minaret under 210% Montenegro earthquake loading. 1, 2, 3, 4, 5 indicate the measurement locations. Refer to Figure B1 for the measurement locations on the minaret and corresponding points on the numerical model.

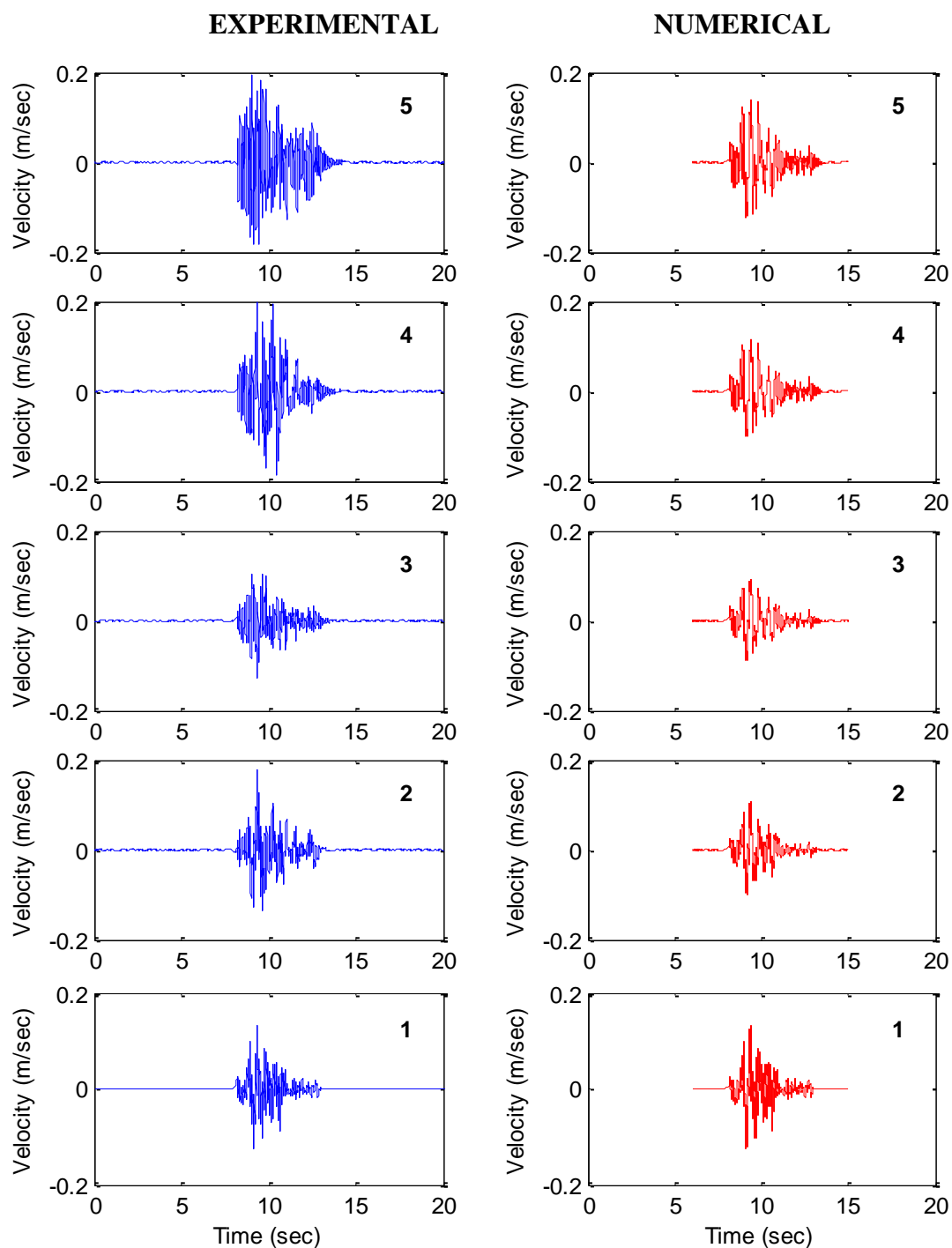


**Figure B10.** Comparisons of experimental and analytical velocities along the minaret under 230% Montenegro earthquake loading. 1, 2, 3, 4, 5 indicate the locations of accelerometers at 0.35m, 1.75m, 2.45m, 3.25m, 3.90m height of the minaret respectively. Refer to Figure B1 for the measurement locations on the minaret and corresponding points on the numerical model.

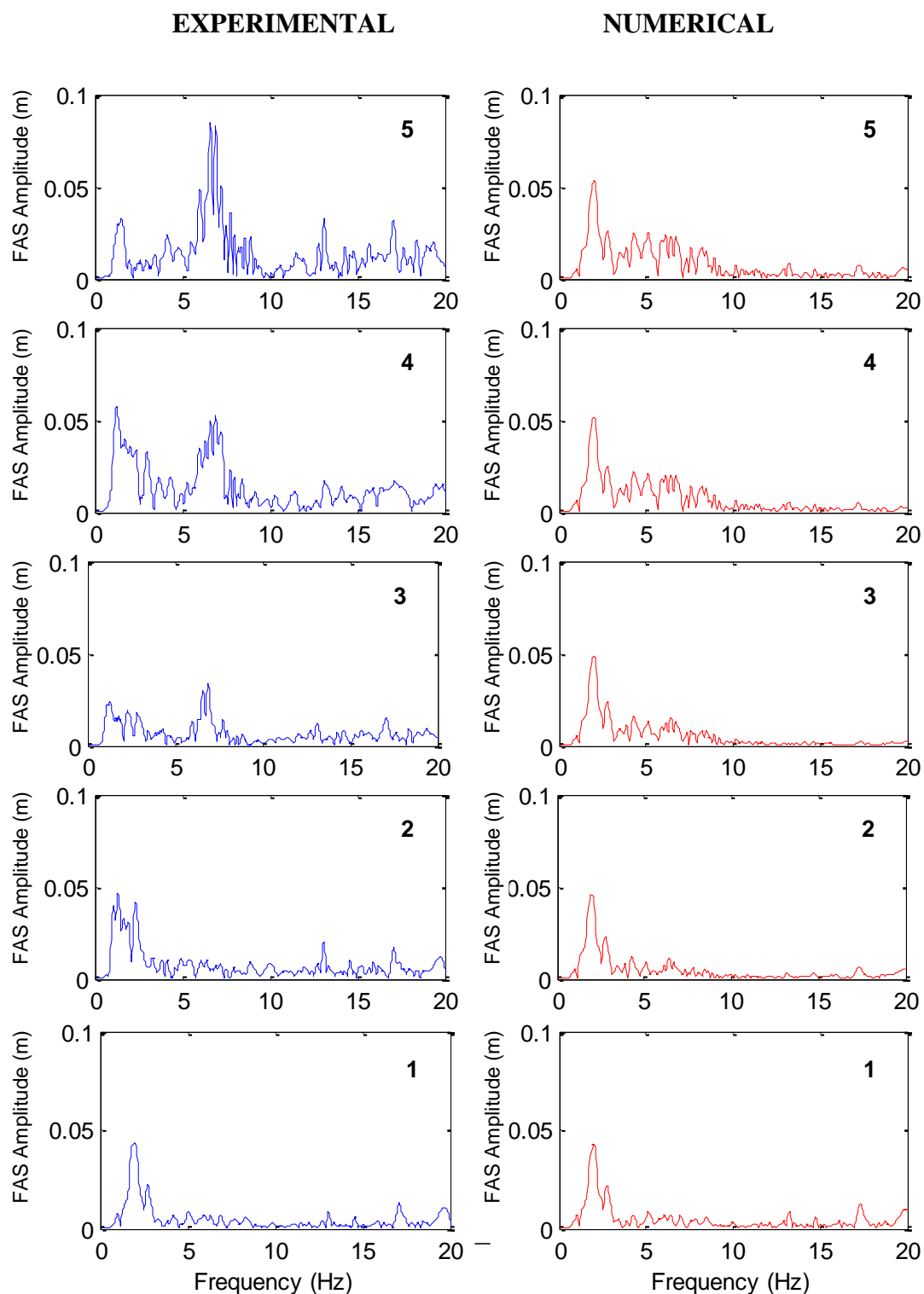


**Figure B11.** Comparisons of experimental and numerical FAS amplitude along the minaret under 230% Montenegro earthquake loading. 1, 2, 3, 4, 5 indicate the measurement locations. Refer to Figure B1 for the measurement locations on the minaret and corresponding points on the numerical model.

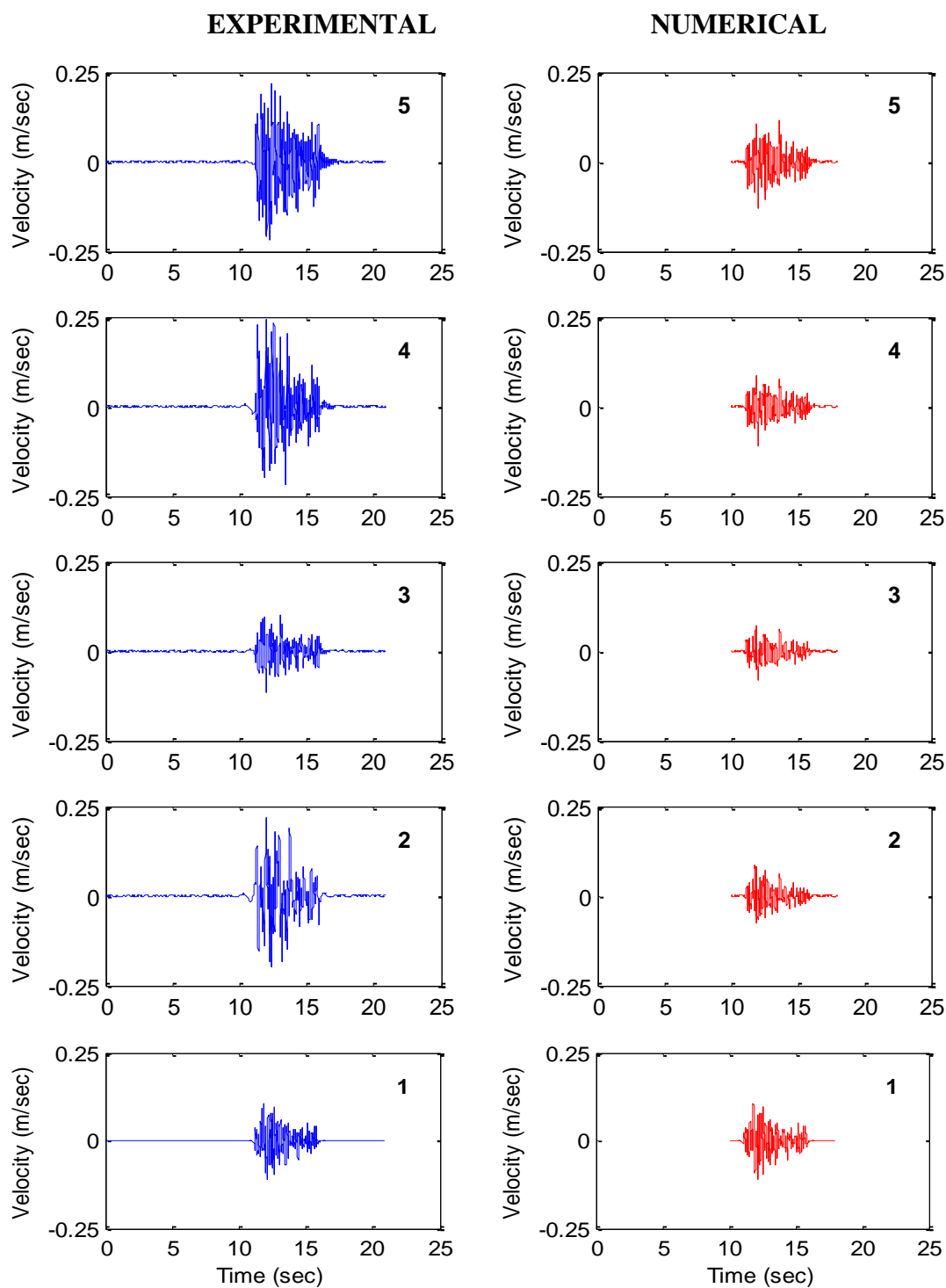


**Figure B12.** Comparisons of experimental and analytical velocities along the minaret under 250% Montenegro earthquake loading. 1, 2, 3, 4, 5 indicate the locations of accelerometers at 0.35m, 1.75m, 2.45m, 3.25m, 3.90m height of the minaret respectively. Refer to Figure B1 for the measurement locations on the minaret and corresponding points on the numerical model.

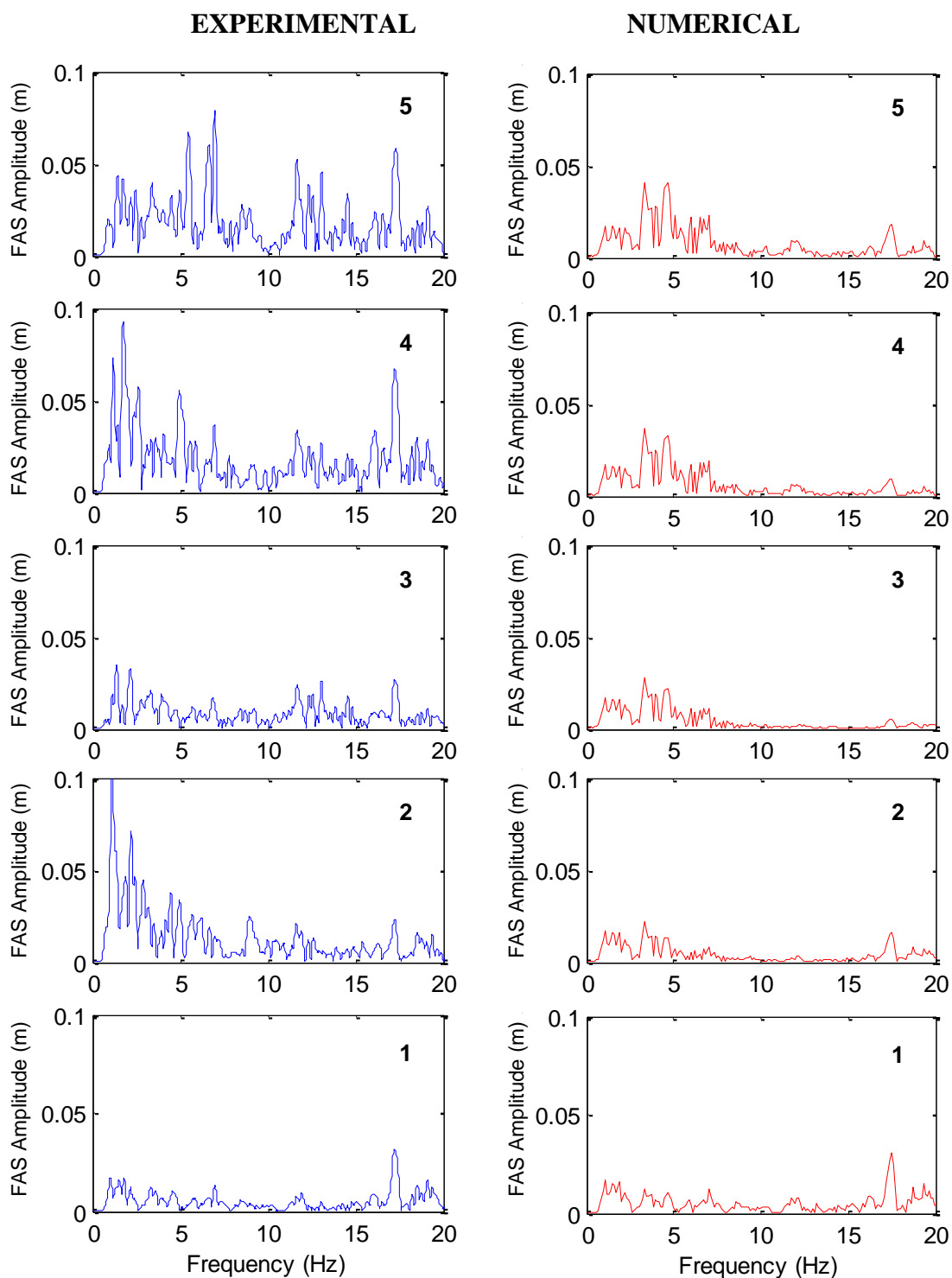


**Figure B13.** Comparisons of experimental and numerical FAS amplitude along the minaret under 250% Montenegro earthquake loading. 1, 2, 3, 4, 5 indicate the measurement locations. Refer to Figure B1 for the measurement locations on the minaret and corresponding points on the numerical model.

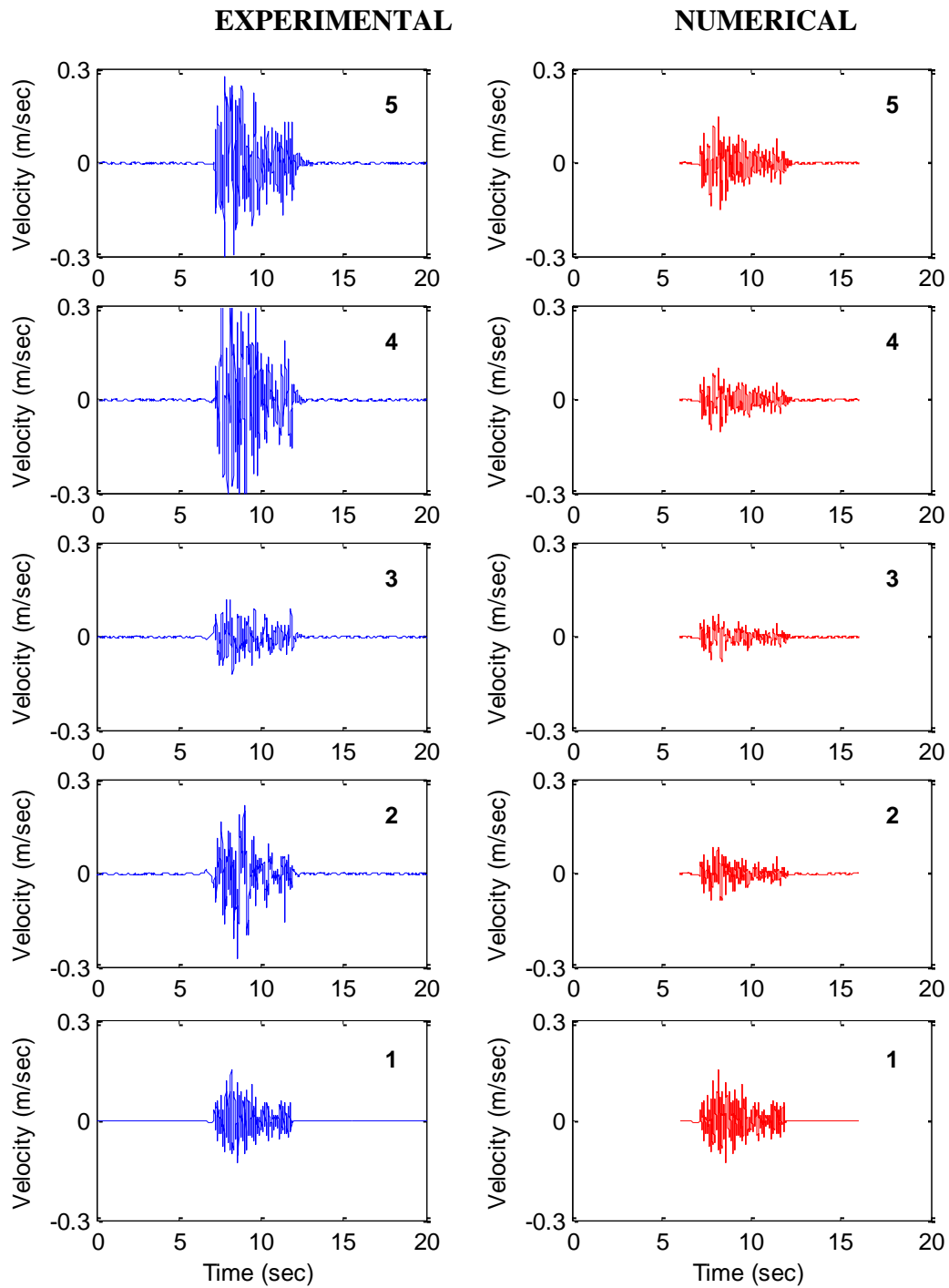


**Figure B14.** Comparisons of experimental and analytical velocities along the minaret under 325% Montenegro earthquake loading. 1, 2, 3, 4, 5 indicate the locations of accelerometers at 0.35m, 1.75m, 2.45m, 3.25m, 3.90m height of the minaret respectively. Refer to Figure B1 for the measurement locations on the minaret and corresponding points on the numerical model.

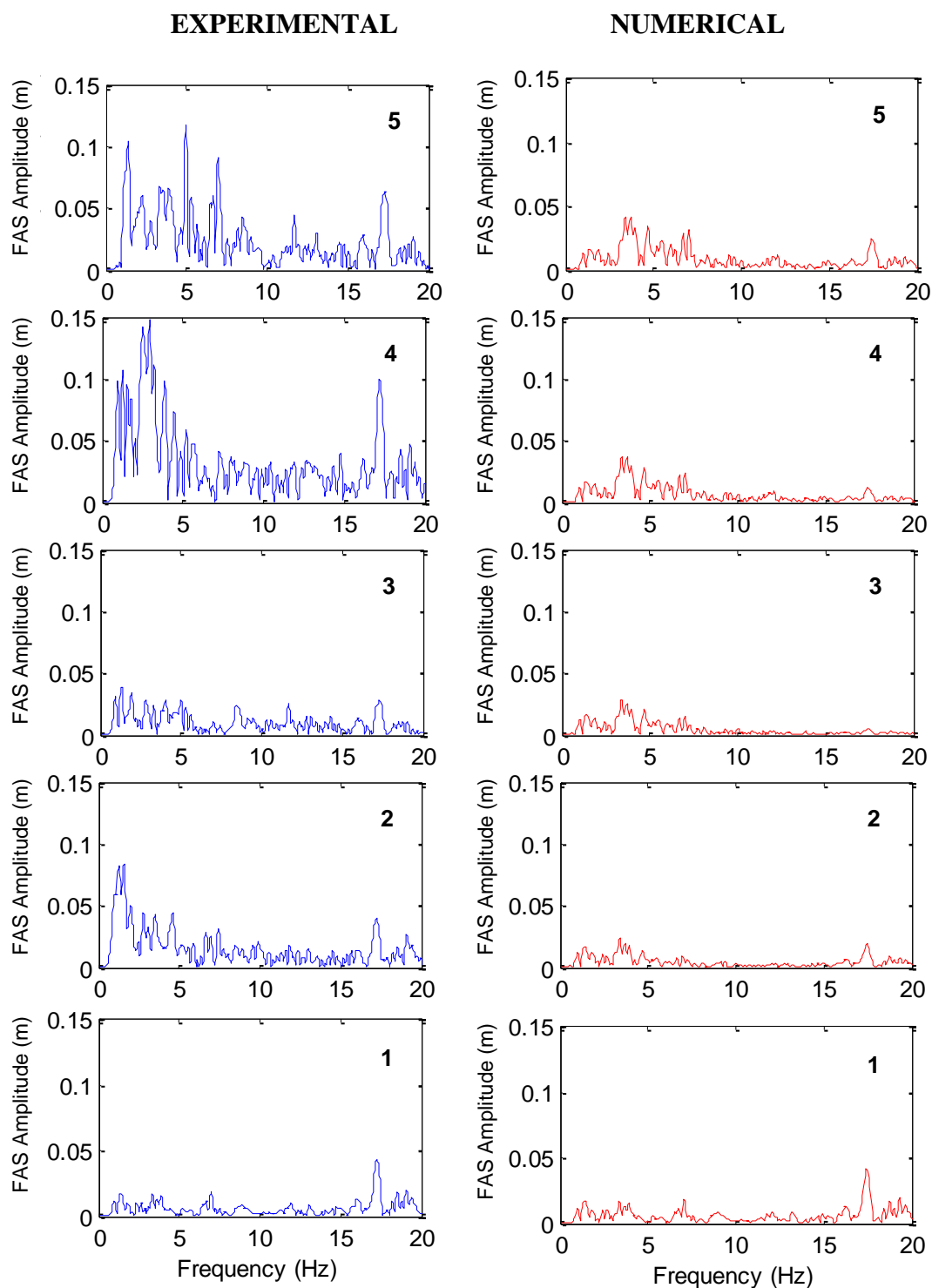


**Figure B15.** Comparisons of experimental and numerical FAS amplitude along the minaret under 325% Montenegro earthquake loading. 1, 2, 3, 4, 5 indicate the measurement locations. Refer to Figure B1 for the measurement locations on the minaret and corresponding points on the numerical model.